The Dissertation Committee for Ching-Hsiang Chen Certifies that this is the approved version of the following dissertation:

Performance of Suction Caissons with a Small Aspect Ratio

Committee:

Robert B. Gilbert, Supervisor

Charles Aubeny

Chadi El Mohtar

John L. Tassoulas

Jorge G. Zornberg

Performance of Suction Caissons with a Small Aspect Ratio

by

Ching-Hsiang Chen, B.S., M.S.

Dissertation

Presented to the Faculty of the Graduate School of

The University of Texas at Austin

in Partial Fulfillment

of the Requirements

for the Degree of

Doctor of Philosophy

The University of Texas at Austin

December 2013

Dedication

To my family

Acknowledgements

I would like to express my gratitude to my advisor, Dr. Bob Gilbert, for his guidance and encouragement. He exposed me to various research projects and provided me the opportunity to work with different people through my study at UT. I would like to thank my committee members, Drs. Chuck Aubeny, John Tassoulas, Chadi El Mohtar, and Jorge Zornberg, for their valuable comments and support.

Special thanks to Horton Wison Deepwater for supporting this research project. I also appreciate the help from Dr. Adam Saleh of SOLQUEST Engineering, Dr. Lyle Finn and Mr. Brian Kuehner of Horton Wisson Deepwater for setting up the test program.

I would like to thank Hande Gerkus, Matteo Sottile, and Jani Vilkki for their hard work on the scale model tests. I would not be able to finish the testing without them. I appreciate Federico Castro, Michael Plaisted, and Jeremiah Fasl for helping me set up the instrumentation in the laboratory.

I also want to thank all the professors, staff, and fellow graduate students in the Department of Civil, Architectural and Environmental Engineering for making my study at UT a wonderful experience.

Finally, I would like to express my gratitude to my parents for their continuous support. I am grateful to my lovely wife for her patience, encouragement, and support. I also want to thank my son for bringing lots of joy into my life.

Ching-Hsiang Chen

The University of Texas at Austin

December 2013

Performance of Suction Caissons with a Small Aspect Ratio

Ching-Hsiang Chen, Ph.D.

The University of Texas at Austin, 2013

Supervisor: Robert B. Gilbert

Suction caissons with a smaller aspect (length to diameter) ratio are increasingly used for supporting offshore structures, such as wind turbines and oil and gas production facilities. The design of these stubbier foundations is usually governed by lateral loads from wind, waves, or currents. It is desired to have more physical understanding of the behavior of less slender suction caissons under cyclic lateral loading condition and to have robust design tools for analyzing these laterally loaded caissons.

In this study, one-g model tests with 1:25 and 1:50 suction can foundation scale models with an aspect ratio of one are conducted in five different soil profiles: normally consolidated clay, overconsolidated clay, loose siliceous sand, cemented siliceous sand, and cemented calcareous sand. This test program involves monitoring settlements, lateral displacements (walking), tilt, lateral load and pore water pressures in the suction can during two-way cyclic lateral loading at one, three and five degrees of rotation. The model foundations are monitored during installation, axial load tests, and pullout tests.

In one and two-degree (±0.5 and ±1 degree) rotation tests, the suction can does not have significant walking or settlement in all the five soil profiles after 1000 load cycles. However, more significant walking or settlement may occur at extreme conditions such as the 5-degree (±2.5 degrees) rotation tests. Gaps between the foundation wall and

the soil may also form in these extreme conditions in overconsolidated clay, cemented siliceous sand, and cemented calcareous sand.

Plastic limit analysis, finite element analysis, and finite difference analysis are used to evaluate the laterally loaded suction can in clay. The plastic limit analysis originally developed for more slender suction caissons appears to predict a lateral capacity close to the measured short-term static capacity of the caisson with an aspect ratio of one when undisturbed undrained shear strength of soil is used. However, this plastic limit model underestimates the long-term cyclic lateral load capacity of the caisson when the remolded undrained shear strength was used. The finite element model developed in this study can simulate the development and effect of a gap between the foundation and surrounding soil as observed in the experiments in overconsolidated clay. The lateral load-displacement response predicted by this finite element model matches well with the experimental data. Finally, finite difference analysis for a rigid caisson with lateral and rotational springs was developed by fitting the lateral load-displacement response of the suction can in clay. The calibrated p-y curves for rigid caisson are significantly stiffer and have higher ultimate resistance than the p-y curves recommended by API which is consistent with other studies. This finite difference model provides an efficient approach to analyze a laterally loaded caisson with a small aspect ratio in clay.

Table of Contents

List of Tables

List of Figures

Chapter 1: Introduction

1.1 BACKGROUND

Suction caissons have been commonly used for supporting fixed offshore platforms, subsea structures, or mooring floating structures. The capacity of suction caisson has been examined using scale model tests in a number of studies (eg. Fuglsang and Steensen-Bach 1991, Renzi et al. 1991, Clukey and Morrison 1995, Watson and Randolph 1997, El-Gharbawy 1998, Allersma et al. 1999, Luke 2002, Cao 2003, Raines and Garnier 2004, El-Sherbiny 2005, and Zhang et al. 2007). Other studies evaluate the suction caisson capacity by numerical analyses and upper bound plasticity methods (Zdravkovic et al. 2001, Templeton 2002, Sparrevik 2002, Cao 2003, Maniar et al. 2003, Randolph and Puzrin 2003, Clukey et al 2004, Tran et al. 2005, Aubeny and Murff 2005, Zhang et al. 2008, Vásquez et al. 2010). Most of these studies focus on suction caissons with an aspect ratio (length to diameter ratio) of 3 to 10, which is commonly used in the industry.

Recently, suction caissons with a smaller aspect ratio (usually less than one) are considered as an economical alternative for supporting offshore wind turbines (see Figure 1.1), met mast (see Figure 1.2), and compliant structures such as a buoyant tower (see Figure 1.3) in shallower water. Suction caissons become attractive in these applications because the suction installation process (see Figure 1.4) minimizes the heavy equipment required for driven piles or other foundations. The design of these stubbier foundations is usually governed by lateral loads from wind, waves, and/or currents. However, whether the conventional limit equilibrium methods and the deflection models derived for more slender suction caissons and piles can be used for stubbier suction caissons is in question.

Therefore, it is desired to have more physical understanding of the behavior of stubby suction caissons under lateral loads, especially cyclic lateral loads.

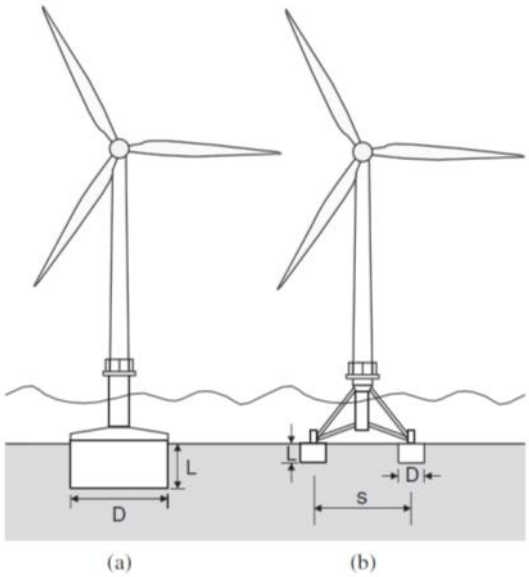

Figure 1.1: Suction Caissons for Offshore Wind Turbines: (a) Monopod and (b) Tripod/Tetrapod. (Houlsby et al. 2005a)

Figure 1.2: Suction Caisson for Met Mast Installed at Horn Rev 3 Offshore Wind Farm, Denmark (LeBlanc 2009).

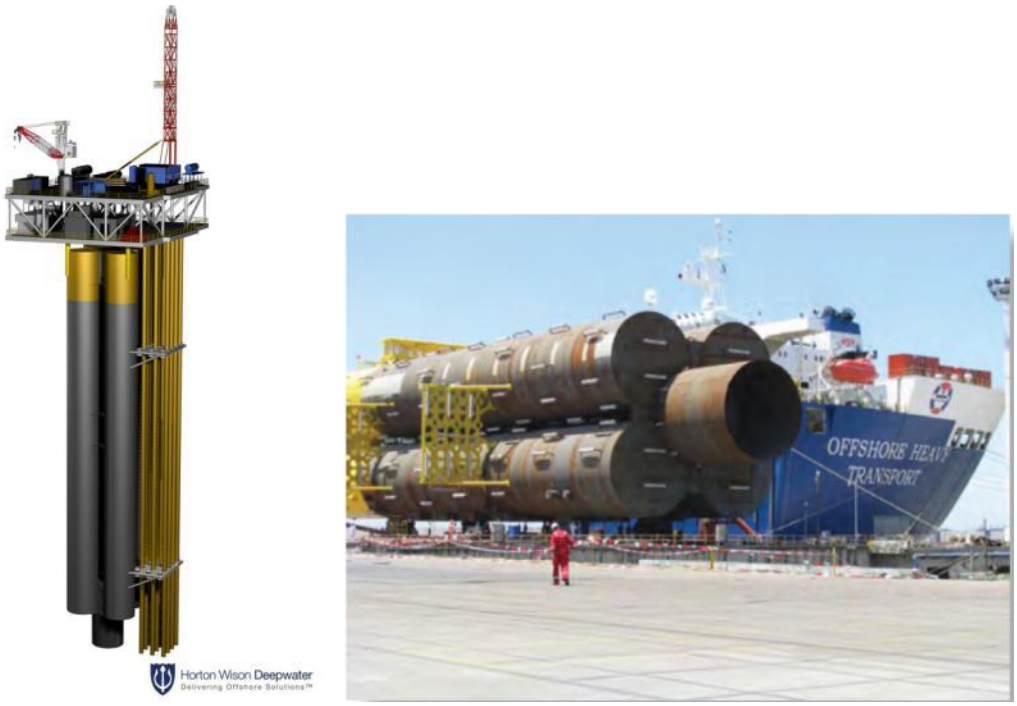

Figure 1.3: Buoyant Tower and Suction Can (Horton Wison Deepwater 2013 and GMC 2013)

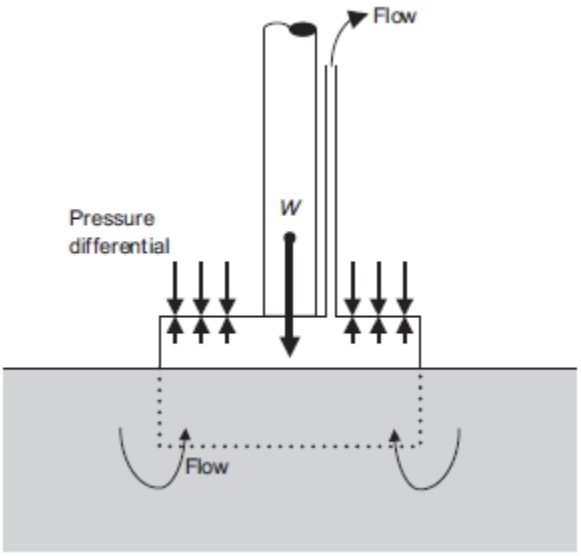

Figure 1.4: Suction Caisson Installation (Houlsby 2005b)

Some recent studies evaluate the capacity of suction caisson with a smaller aspect ratio using scale model tests (Houlsby et al. 2005a, Houlsby et al. 2005b, Houlsby et al. 2006, Kelly et al. 2006, Zhu et al. 2013), numerical methods (Zhan and Liu 2010, Hung and Kim 2012), or plasticity theory (Lam 2005, Zhang et al. 2010). However, most of these studies focus on the capacity of stubby suction caissons in loose sand and limited tests in clay. In addition, the rotational stiffness of suction caissons with a small aspect ratio in soils is crucial to predict the lateral deflection under cyclic environmental loads. Therefore, it is also desired to examine the performance of these foundations in various different soils under working cyclic lateral loads in addition to ultimate capacity.

1.2 MOTIVATION

The motivation of this research is to evaluate performance of the suction can foundation, which is a suction caisson with an aspect ratio of one, for a buoyant tower system for oil and gas production. A Buoyant Tower is a compliant structure that is viable for water depths ranging from 50 to 250 m. The tower (see Figure 1.3) is designed as a rigid, buoyant column with a suction can foundation (SCF) at its base that rotates in the soil to act as a hinge while the buoyant tower sways back and forth in response to environmental loads (Finn and Hegler 2013). Therefore, it is crucial to examine the long-term lateral, vertical, and rotational stiffness of the suction can foundation. Although this research aims to test the performance of the suction can/buoyant tower system, the results in this study may be applicable to foundations with similar aspect ratio used for offshore wind turbines and other applications subjected to significant cyclic lateral loads.

1.3 OBJECTIVES

The goal of this research is to study the performance of a laterally loaded suction caisson with a small length to diameter ratio. Scale model tests are conducted to address the following objectives:

- Provide physical understanding of the performance of a suction can foundation under different loading conditions including installation, cyclic environment loads, compressive axial loadings, and pullout.
- Evaluate the performance of a suction can foundation in various soil profiles.
- Determine the rotational stiffness of a suction can foundation under cyclic lateral loads.
- Evaluate the long-term lateral and vertical displacements of a suction can foundation under cyclic lateral loads.

1.4 METHODOLOGY

In order to study the performance of the suction can foundation, one-g model tests using one-foot diameter and six-inch diameter scale models are performed in five different soil profiles in the laboratory at The University of Texas at Austin. These five soil profiles includes: normally consolidated clay, overconsolidated clay, loose silica sand, cemented silica sand, and cemented calcareous sand. The scale model tests in each soil profiles include:

- Installation
- Cyclic lateral load tests
- Pore water pressure dissipation between tests
- Hydraulic lifting after excessive settlements
- Axial load tests

- Compressive ultimate axial capacity tests in clays or proof load tests in sands
- Pullout

The test program involves monitoring settlements, lateral displacements (walking), tilt, lateral load and pore water pressures in the suction can during two-way displacement controlled, cyclic lateral loading at one, three and five degrees of rotation. The model foundations are also monitored during installation, axial load tests, and pullout tests.

Since cyclic lateral loading is one of the most important aspects for the design of suction caissons with a small aspect ratio, more detailed analyses on cyclic loading tests are conducted in this study. These analyses focus on caisson behaviors in normally consolidated and overconsolidated clays because they are two common soil profiles in offshore environments. In this study, the backbone curves of cyclic lateral load-displacement relationships in clay were further evaluated with plastic limit analyses and finite element analyses. In addition, a rigid caisson p-y analysis model was constructed base on the cyclic lateral load test results.

1.5 STRUCTURE OF THE DISSERTATION

This dissertation includes 12 chapters. Contents of each chapter are summarized below:

- Chapter 1: Introduction presents the background, motivation, objective, and methodology of this study.
- Chapter 2: Literature Review presents the common practice of suction caisson design, findings of previous research on suction caisson behavior, p-y analysis of flexible piles, and resent studies on suction caissons with small aspect ratios.

- Chapter 3: Soil Test Beds presents the normally consolidated clay, overconsolidated clay, loose siliceous sand, cemented siliceous sand, and cemented calcareous sand test beds that were used in this study.
- Chapter 4: Suction Can Foundation Scale Models presents the 6-inch and 12-inch diameter suction can scale model used in this study.
- Chapter 5: Test Facility and Instrumentation presents the test facility and instrumentation used for the scale model tests.
- Chapter 6: Tests in Normally Consolidated Clay Test Bed presents the test procedure and results of suction can scale model tests in normally consolidated clay.
- Chapter 7: Tests in Overconsolidated Clay Test Bed presents the test procedure and results of suction can scale model tests in overconsolidated clay.
- Chapter 8: Tests in Loose Siliceous Sand Test Bed presents the test procedure and results of suction can scale model tests in loose siliceous sand.
- Chapter 9: Tests in Cemented Siliceous Sand Test Bed presents the test procedure and results of suction can scale model tests in cemented siliceous sand.
- Chapter 10: Tests in Cemented Calcareous Sand Test Bed presents the test procedure and results of suction can scale model tests in cemented calcareous sand.
- Chapter 11: Analysis of Cyclic Lateral Load Tests in Clay presents analyses on the cyclic lateral load-displacement relationships, plastic limit analyses, finite element analyses, and the construction of a rigid caisson p-y analysis model.
- Chapter 12: Conclusions summarizes the findings of this dissertation.

Chapter 2: Literature Review

Suction caissons have been used to support fixed offshore structures and also to keep floating structures in station for more than 20 years. Performance of suction caissons for these applications has been evaluated in various studies. Recently, suction caissons with aspect ratio less than one have been consider as an economical alternative to offshore wind turbines and compliant structures such as the buoyant tower. The cyclic lateral capacity or moment resistance against wind, wave, and current loads become more important for these new applications because of relatively low axial load from the structures.

The common practice for installation, axial capacity, and lateral capacity analyses for more slender caissons in clay is reviewed in Section 2.1. Finding and recommendations from research on suction caisson analysis are also presented. In section 2.2, the p-y curves for soft clay proposed by Matlock (1970) and recommended by API were presented along with suggested revisions from related research. Finally, more recent studies on suction caissons with aspect ratio less than one are summarized in Section 2.3.

2.1 Analysis of Suction Caissons in Clay

This section summarizes the approaches recommended by American Petroleum Institute (API) for installation (penetration), axial capacity, and lateral capacity analyses of suction caissons. Some results and recommendations from research on suction caisson analysis are also presented.

2.1.1 Penetration Analysis of Suction Caisson

Suction caissons are usually installed by penetrating into the soil to a certain depth by self weight to create a seal between the soil and the wall then followed by applying underpressure (suction) in the caisson to reach the designed penetration. It is important to predict the self-weight penetration depth, the required suction to install the caisson, and the allowable suction to prevent soil plug failure (Huang et al., 2003).

The penetration resistance during suction caisson installation in clay can be estimated using the α method based on limit equilibrium analysis recommended by the American Petroleum Institute (API RP 2SK, A 2008). Without protuberance (such as stiffeners), the penetration resistance of a suction caisson is calculated as the sum of two components: 1) side shear acting on the inner and outer wall and 2) the end bearing on the tip of the wall. Therefore, the total penetration resistance can be obtained by Equation 2.1.

$$Q_{total} = Q_{side} + Q_{tip} \quad \text{(Equation 2.1)}$$

$$Q_{side} = A_{wall} \left(\alpha_{ins} \, Su_{DSS}\right)_{AVE}$$

$$Q_{tip} = \left(N_c \, Su_{tip}^{AVE} + \gamma' z\right) A_{tip}$$

where

Q_{total} = total penetration resistance,

Q_{side} = resistance along the side of the wall,

Q_{tip} = resistance at the tip,

A_{wall} = sum of inside and outside wall area embedded into soil,

α_{ins} = adhesion factor during installation,

Su_{DSS} = direct simple shear strength,

$(\alpha_{ins} \, Su_{DSS})_{AVE}$ = average side friction from mudline to depth z,

N_c = bearing capacity factor,

Su_{tip}^{AVE} = average of triaxial compression, triaxial extension, and DSS undrained shear strength at tip,

γ' = submerged unit weight of soil,

z = tip penetration depth.

The bearing capacity factor for the wall tip, N_c, is usually assume to be 7.5, which is the same as a deeply embedded strip footing because the anchor wall thickness is usually small compared to the anchor diameter and the embedment depth. The adhesion factor during installation, α_{ins}, is often taken as the inverse of soil sensitivity. The value of α_{ins} typically ranges from 0.2 to 0.5 for Gulf of Mexico deepwater clay. However, Dendani and Colliat (2002) reported that using the inverse of soil sensitivity for α_{ins} (ranged from 0.2 to 0.45) overestimates the installation resistance according to the field measurements of 25 suction caissons installed offshore West Africa. This implies that the α_{ins} can be lower than the inverse of sensitivity. The calculated penetration resistance agreed well with the measured resistance if α_{ins} of 0.25 was used for the non-painted part and 0.08 was used for the painted part. Huang et al. (2003) supported the reported α_{ins} values of 0.25 to 0.3 and 0.08 for painted areas of the caisson and also suggested that α_{ins} can be lower than the inverse of the sensitivity.

The required underpressure (or suction) to install the suction caisson can be calculated according to API RP 2SK (A 2008):

$$\Delta U_{req} = \frac{Q_{total} - W'}{A_{in}} \qquad \text{(Equation 2.2)}$$

where

W' = submerged weight during installation,

A_{in} = cross-section area where underpressure is applied.

If the applied underpressure is greater than a critical value, ΔU_{crit}, the soil plug failure (a general reverse bearing failure at the anchor tip and large soil heave within the anchor) may occur during installation. The can be calculated by using Equation 2.3 recommended by API RP 2SK (A 2008).

$$\Delta U_{crit} = N_c \, Su_{tip}^{AVE} + \frac{A_{inside} \, (\alpha_{ins} \, Su_{DSS})_{AVE}}{A_{in}} \qquad \text{(Equation 2.3)}$$

where

A_{inside} = inner wall area.

The allowable underpressure that can be applied to the suction caisson is then calculated as the critical underpressure divided by a factor of safety of 1.5.

2.1.2 Axial Capacity of Suction Caisson

The α method for piles in clay based on limit equilibrium analysis recommended by API has been used to evaluate the axial capacity of suction caissons in clay (El-Sherbiny, 2005). If the top cap is sealed, the axial capacity is assume to be the sum of friction on the exterior side wall and end-bearing at the tip (or reverse end bearing depending whether the caisson is loaded in tension or compression). Therefore, the axial capacity due to soil resistance, *R*, can be calculated by Equation 2.4 (API RP 2GEO, 2011).

$$R = Q_f + Q_p = f(z) \, A_s + q \, A_p \qquad \text{(Equation 2.4)}$$

where

Q_f = side friction resistance,

Q_p = end bearing,

$f(z)$ = unit side shear,

A_s = side surface area of caisson,

q = unit end bearing,

A_p = gross end area of the caisson,

z = depth below seafloor.

The unit side shear, $f(z)$, in the equation above can be expressed as a function of depth in Equation 2.5.

$$f(z) = \alpha\, s_u \qquad \text{(Equation 2.5)}$$

where

α = dimensionless side friction factor,

s_u = undrained shear strength at the depth in question

The dimensionless side friction factor, α, depends on the ratio of undrained shear strength to effective stress (Ψ or c/p ratio) and can be expressed as Equation 2.6.

$$\alpha = 0.5\Psi^{-0.5} \quad \text{for } \Psi \leq 1.0 \qquad \text{(Equation 2.6)}$$

$$\alpha = 0.5\Psi^{-0.25} \quad \text{for } \Psi > 1.0$$

with the constraint that $\alpha \leq 1.0$

where

$\Psi = \frac{s_u}{p'_0(z)}$,

$p'_0(z) =$ effective vertical stress at depth z.

The unit end bearing in Equation 2.4 can be expressed as a function of the undrained shear strength as Equation 2.7.

$$q = N_c \, s_{u,tip} \qquad \text{(Equation 2.7)}$$

where

N_c = end bearing factor,

$s_{u,tip}$ = undrained shear strength of soil at the tip of caisson.

This limit equilibrium approach recommended by API accounts for only the capacity from soil resistance and does not consider the weight of the caisson, weight of the soil plug, and water pressure acting down on the top cap, and the total stress acting up at the tip of the caisson. The sum of these additional forces is equal to the submerged weight of the caisson in soil (El-Sherbiny, 2005).

API recommended using 9.0 for end bearing factor, N_c, in Equation 2.7 based on the bearing capacity factor of deeply embedded square and circular foundation suggested by Skempton (1951). The α value, according to Equation 2.6, equals to one for normally consolidated clay with Ψ = 0.25. However, several studies suggested that a lower side friction factor should be used for suction installed caissons because suction installation reduces the stresses acting on the outer wall of the caisson and soil moves to inside of the caisson (Andersen and Jostad, 1999 and 2004). The reported side friction factors ranges between 0.25 and 0.8, accompanied by a range of end-bearing factors varying between 6 and 16 based on various experiments and field measurements (Clukey et al 2004, El-Sherbiny 2005). However, most of these studies did not separate measurements of side friction and end bearing. Therefore, the values of N_c and α are subjective to the assumptions made in these studies and also the uncertainty of the soil plug weight (Luke et al., 2005). El-Sherbiny (2005) conducted pullout tests of prototype suction caissons in normally consolidated clay using a double-walled caisson which provides separate measurements of side shear and end bearing. El-Sherbiny concludes that α and N_c are 0.8

and 15, respectively, for the suction caisson pulled out rapidly with a sealed top cap. In addition, there is no difference in axial capacity between caissons installed using deadweight or suction.

2.1.3 Lateral Capacity of Suction Caisson

API RP 2SK (A 2008) recommends using finite element method, limit equilibrium or plastic limit analyses for holding capacity design of suction caissons. For suction caissons subjected to mainly horizontal loads, beam-column analyses (or p-y analyses) described in API RP 2A (now API RP 2GEO) can be used with modifications that account for the larger caisson diameter. Details on the p-y analyses are presented in Section 2.3.

Finite element method is the most rigorous and general approach to evaluate the lateral capacity of suction caissons. If an appropriate constitutive model is used, the critical failure mechanism can be found without prior assumptions that are required for plastic limit analysis. In addition, finite element models can simulate the caisson with combined axial-lateral loading condition and other complicated geometry or soil conditions. However, finite element analyses require knowledge of advanced numerical analysis and significant amount of time to set up and implement the model (API RP 2SK, A 2008). Several finite element analyses have shown good agreements with measured capacities such as those presented by Sukumaran et al (1999); Deng and Carter (2002), Templeton (2002), Cao et al. (2003); Maniar et al. (2003), Barari and Ibsen (2012), and Templeton (2012). More complicated and computationally intensive finite element analyses included the installation phase of suction caissons and considered soil disturbance during installation and post installation reconsolidation (Maniar and Tassoulas, 2002, Vásquez et al, 2010). However, the good agreements with other

analyses assuming the caisson is “wished-in-place” suggest that finite element model with wished-in-place caisson might be sufficient (El-Sherbiny, 2005).

One alternative to finite element analysis is the plastic limit analysis, which is comparatively less computationally expensive and easier to use. However, it requires assumptions of failure mechanism and may not be suitable for all types of suction caissons, which may have dramatic differences in geometry and loading conditions. Murff and Hamilton (1993) developed an upper-bound plasticity model for laterally loaded piles by assuming a combined three-dimensional failure mechanism: a conical soil wedge moving upward near the surface and a plane strain flow-around failure at depth as shown in Figure 2.1 (a). For piles or caissons with a small aspect ratio, an additional resistance from the end spherical soil cap was included to account for end resistance of large diameter caissons. This model was later adopted for use in suction caisson design. Aubeny et al. (2001) further simplified this model base on the empirical model that Murff and Hamilton (1993) proposed by formulating the lateral bearing factor, N_p, as a function of depth as shown in Figure 2.1 (b). N_p is reduced to lower values at shallow depths to account for the reduced soil resistance due to conical soil wedge in this simplified model. Aubeny et al. (2003) modified this model to accommodate inclined loading conditions. For the case of purely axial loading, the formulation of the model reduces to the α-method while, for the case of pure lateral loading, the formulation reduces to the lateral loaded caisson analysis as stated previously. The interaction between the axial and lateral resistances for inclined loadings was estimated based on finite element simulations (Aubeny et al., 2003). This simplified plastic limit model was implemented in a spreadsheet based program, FALL16, to find the critical lateral load by optimizing the center of rotation.

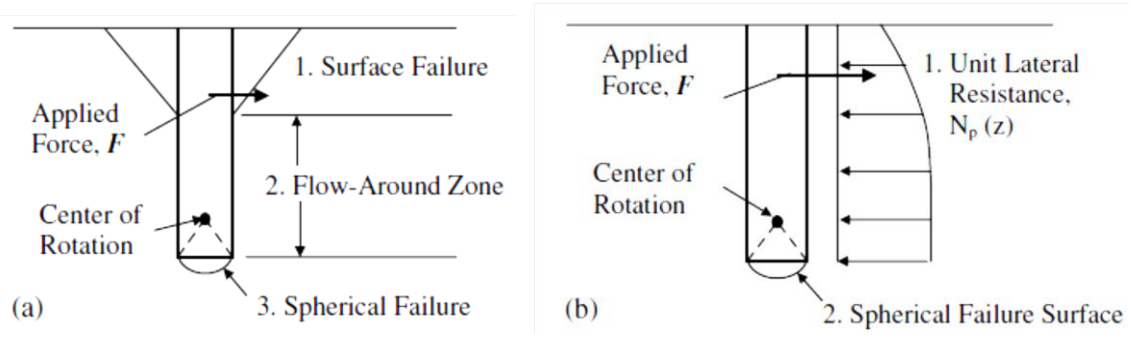

Figure 2.1: Failure Mechanisms of Suction Caissons: (a) three-dimensional failure mechanism proposed by Murff and Hamilton (1993), and (b) simplified analysis by Aubeny et al. (2001). (after Aubeny et al. 2003)

Randoph and House (2002) and Aubeny et al. (2003) reported that the simplified plastic limit model over predicts capacity for short suction caissons (L/D = 2) comparing to finite element analyses while good agreements were found for aspect ratios greater than six. Centrifuge tests on suction caissons under inclined loading indicated that the simplified plastic limit model may slightly over predict or under predict the capacity depending on the load inclination (Cluckey et al., 2003). In general, the available data suggest that the plasticity model works better for more slender suction caissons. However, current designs for offshore laterally loaded suction caissons still depends heavily on finite element analyses in spite of its complexity (El-Sherbiny, 2005).

2.2 P-Y CURVES FOR FLEXIBLE PILES IN CLAY

API RP 2SK (A 2008) recommended that if the suction caisson is subjected to primarily lateral loads, beam-column analyses (or p-y analyses) described in API RP 2A (now API RP 2GEO) can be used with modifications that account for the larger caisson diameter. The p-y analyses described in API and its background are presented in this section. Some studies and discussions on the p-y curves recommended by API are also presented.

The behavior of a laterally loaded flexible pile can be expressed in the form of the differential equation as shown in Equation 2.8 based on the analysis of a beam on elastic foundation. The soil resistance, p, can be expressed as a function of y. The p versus y relationship is often referred to p-y curve. If the pile properties and boundary conditions are known, Equation 2.8 can be solved by discretizing the pile using finite difference method with discrete translational springs to represent the soil resistance as a foundation of y (Reese et al., 1975). In this formulation, the analysis of laterally loaded flexible piles becomes a soil-structure interaction problem.

$$EI\frac{d^4y}{dz^4} = p \qquad \text{(Equation 2.8)}$$

where

y = pile deflection,

z = depth,

EI = flexural stiffness of pile,

p = soil resistance per unit length of pile.

2.2.1 P-y Curves in Soft Clay (Matlock, 1970)

Matlock (1970) developed p-y curves for static and cyclic loading conditions in soft clay (see Figure 2.2) based on field tests of laterally loaded 12.75-inch diameter piles along with laboratory tests. Matlock suggested that the ultimate soil resistance per unit length of pile, p_u, can be expressed by Equation 2.9.

$$p_u = N_p s_u D \qquad \text{(Equation 2.9)}$$

where

N_p = bearing capacity factor for laterally loaded pile (dimensionless) = 9,

s_u = undrained shear strength of soil,

D = pile diameter.

The value of bearing capacity factor, N_p, at depth where only the flow-around failure occurs is assumed to be 9. At shallower depths where the upward soil wedge forms due to lower overburden pressures, the reduced N_p is given by Equation 2.10. The dimensionless constant, *J*, ranged from 0.25 to 0.5 according to the experiments conducted by Matlock (1970). The critical depth, z_R, where N_p becomes 9 can be calculated by Equation 2.11.

$$N_p = 3 + \frac{\gamma' z}{s_u} + J\frac{z}{D} \qquad \text{(Equation 2.10)}$$

where

γ' = submerged unit weight of soil,

z = depth,

J = dimensionless constant depending on clay type.

$$z_R = \frac{6d}{\frac{\gamma' d}{s_u} + J} \qquad \text{(Equation 2.11)}$$

The pile deflection, y_{50}, corresponding to that half of the ultimate soil resistance is mobilized can be approximated by Equation 2.12.

$$y_{50} = 2.5\varepsilon_{50}D \qquad \text{(Equation 2.12)}$$

In the above equation, ε_{50} is the axial strain corresponds to half of the ultimate shear strength of the soil which can be obtained by laboratory tests of clay. It typically ranges from 0.005 to 0.02 with brittle or stiff clay close to the low end and soft clay close to the high end of this range (Matlock, 1970).

For short time static loading condition, Matlock (1970) expressed the p-y curves in a non-dimensional form as shown in Equation 2.13 and Figure 2.2 (a).

$$\frac{p}{p_u} = 0.5\left(\frac{y}{y_{50}}\right)^{1/3} \leq 1.0 \quad , for\ static\ loading \qquad \text{(Equation 2.13)}$$

For cyclic loading condition, the soil resistance decreases due to cyclic deterioration. The maximum soil resistance is limited to 0.72 p_u and followed by a softening behavior that can be expressed as Equation 2.14 and shown in Figure 2.2 (b) (Matlock 1970).

$$\frac{p}{p_u} = 0.72\left(\frac{z}{z_R}\right) \qquad \text{(Equation 2.14)}$$

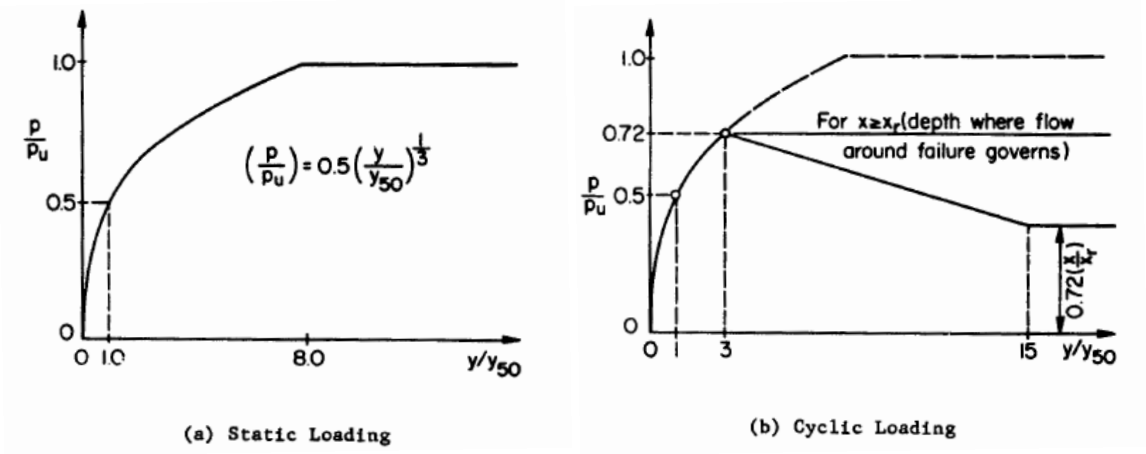

Figure 2.2: Matlock's P-y Curves in Soft Clays (Matlock, 1970)

Finally, a family of p-y curves can be constructed along the length of the pile with higher ultimate soil resistance at greater depth as the example for short-time static loading shown in Figure 2.3. Matlock's p-y curves for soft clays ($s_u \leq 2{,}000$ psf) were later adopted by API RP 2A (now API RP 2GEO).

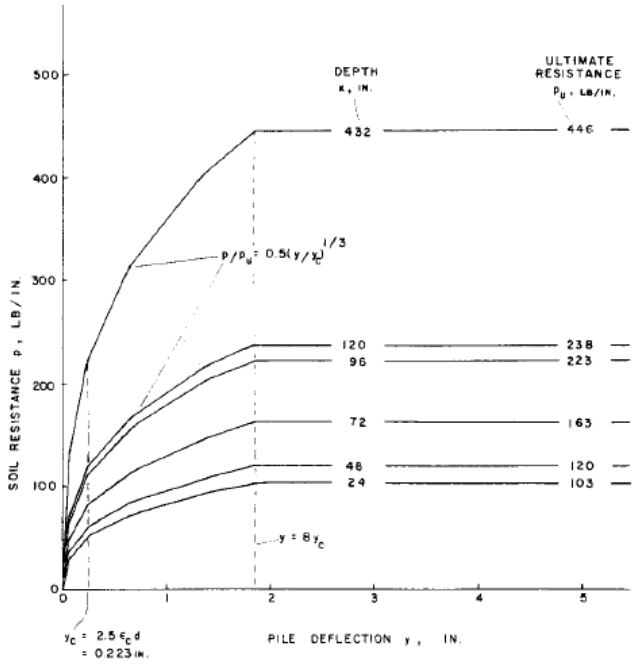

Figure 2.3: Family of p-y Curves in Soft Clays for Static Loading (Matlock, 1970)

2.2.2 Discussions on Matlock's p-y Curves

Stevens and Audibert (1979) reported that the predicted pile deflections using Matlock's p-y curves were significantly greater than the measured deflections in lateral pile load tests. Meanwhile, the maximum bending moments in the piles were underestimated. The comparisons were based on lateral load tests on pile up to 59 inches in diameter in soft to medium clay. Based on lateral pile load tests, Stevens and Audibert (1979) suggested using a nonlinear relationship between y_{50} and pile diameter as shown in Equation 2.15, which provides a smaller y_{50} for larger diameter piles. Note that both y_{50} and D are in inches in Equation 2.15 and this equation yields the same result as Equation 2.12 by Matlock (1970) when D = 12.75 inches.

$$y_{50} = 8.9\varepsilon_{50}D^{0.5} \qquad \text{(Equation 2.15)}$$

Stevens and Audibert (1979) also reported that the soil resistance at shallower depth was underestimated using the reduced N_p in Equation 2.10. Stevens and Audibert (1979) proposed to use the N_p versus normalized depth (z/D) relationship as shown in Figure 2.4 and use 12 for N_p at depth instead of 9 suggested by Matlock (1970). N_p = 12 at depth is also closer to the value of 11 proposed by Reese et al. (1975) for stiff clay.

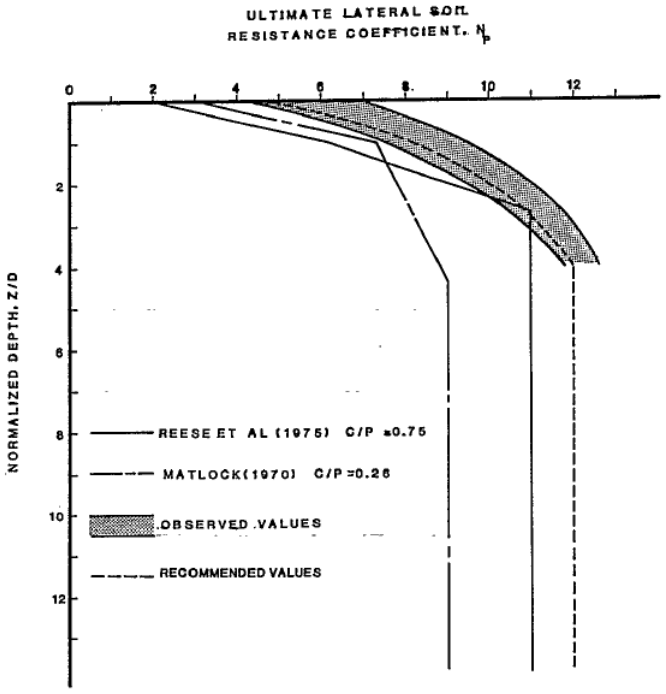

Figure 2.4: N_p versus Normalized Depth Proposed by Stevens and Audibert (1979) (after Stevens and Audibert, 1979)

Randolph and Houlsby (1984) obtained the analytical flow-around N_p of 9.14 for smooth pile (α = 0) and 11.94 for rough pile (α = 1) based on plain strain plasticity theory. Murff and Hamilton (1993) also found that the N_p profile proposed by Matlock underestimated the N_p from the centrifuge tests of laterally loaded piles as shown in Figure 2.5. Murff and Hamilton (1993) proposed using N_p = 12 for flow-around failure of rough piles. This value is consistent with the rough pile solution by Randolph and

Houlsby (1984) and close to the N_p of 11 by centrifuge tests. Murff and Hamilton (1993) also suggested that the flow-around N_p should occur at a much shallower depth than that proposed by Matlock (1970) with $J = 0.5$ in Equation 2.10. Reese et al. suggested using $J = 2.83$ for piles in stiff clay and the N_p profile proposed by Stevens and Audibert (1979) also suggested that J should be greater than 0.5. Jeanjean (2009) concluded that the p-y curves recommended by API and Matlock (1970) underestimate both the soil stiffness and ultimate soil resistance based on finite element analyses and centrifuge tests to re-evaluate the p-y curves recommended in API. Jeanjean (2009) reported N_p of 12.7 and 13.4 at depth obtained from finite element analyses and centrifuge test results, respectively. According to the studies on p-y curves, Matlock's (API) p-y curves seem to underestimate the soil stiffness and the ultimate soil resistance. Consequently, pile deflections of may be overestimated if Matlock's (API) p-y curves are used in analyses.

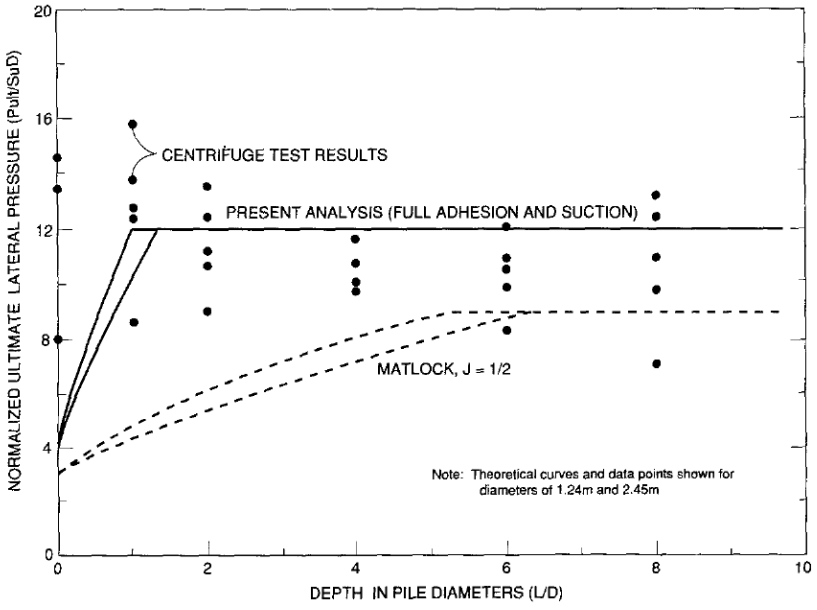

Figure 2.5: N_p versus Normalized Depth Proposed by Murff and Hamilton (1993) (after Murff and Hamilton, 1993)

2.3 STUDIES ON SUCTION CAISSONS WITH A SMALL ASPECT RATIO

Suction caissons with a small aspect ratio have been getting more attention recently because of its potential use for offshore wind turbines. The EPSRC/DTI joint industry project as well as other studies on suction caissons in clay, sand, and slit are summarized in this section.

2.3.1 EPSRC/DTI Joint Industry Project

A three-year joint industry project completed in 2005, which aimed to develop design guildlines of suction caissons for offshore wind turbines, was coordinated and conducted by Oxford University along with industry partners. In this project, a series of intermediate scale field tests along with small scale 1-g laboratory tests were conducted for suction caissons with an aspect ratio of 0.5 or 0.67 in both clay and sand. The experiment program included tests directed towards the design of both the monopod and the tetrapod (see Figure 1.1). The tests for monopod caisson focused on its cyclic moment resistance because monopod caisson resists overturning moments by its rotational resistance in the soil directly. However, the tests for tetrapod caissons focused on the cyclic, nearly vertical loading condition because tetrapod caissons resist overturning by primarily the push-pull action resistance (axial resistance) of individual caisson (Houlsby et al. 2005a, Houlsby et al. 2005b, Byrne and Houlsby 2006, and Kelly et al. 2006). Some of the important findings from these experiments are summarized in this section.

Intermediate scale suction caisson tests in clay were performed at the Bothkennar test site in Scotland (Houlsby et al. 2005b). A 3-meter (10-ft) diameter, 1.5-meter (5-ft) long suction caisson (L/D = 0.5) with 8-mm thick wall was used for the cyclic moment resistance tests (relevant to a monopod) while a 1.5-meter diameter, 1-meter long suction caisson (L/D = 0.67) was used for cyclic vertical load tests (relevant to a tetrapod). The

silty clay in the test pit has an undrained shear strength of 11.43 kPa (239 psf) at surface and a gradient of 1.9 kPa/m (12.1 psf/ft). The undrained shear strength of soil was estimated based on the undrained triaxial tests reported by Nash et al. (1992). The bulk density is approximately 1680 kg/m^3 (or a total unit weight of 105 pcf). Throughout the test period, the test bit was flooded with 0.25 m deep of water.

The suction caissons were installed under their own weight and followed by using suction to reach full penetration. The test equipment layout at the Bothkennar clay site is shown in Figure 2.6. All the field load tests were load controlled tests by applying specified load on the caissons. Six draw-wire displacement transducers were used to measure all the six degrees of freedom of caisson movements. The 1.5-meter diameter caisson (on the left in Figure 2.6a), a fixed vertical was applied by a hydraulic jack and the cyclic inclined loading (inclined at 2:1) was then applied using a second hydraulic jack. At the end of the tests, the caisson was pulled out by the vertical hydraulic after the inclined hydraulic jack was removed (Houlsby et al. 2005b).

For the 3-meter diameter caisson, the moment resistance tests consist of two parts: 1) small-amplitude, higher frequency cyclic horizontal loads applied at 4.23 m above the cap of the caisson using a structural eccentric mass vibrator (SEMV) as shown in Figure 2.6(b), and 2) large-amplitude, low-frequency (quasi-static) cyclic horizontal loads applied by a hydraulic jack as shown in Figure 2.6(a). The small-amplitude tests were to evaluate the moment resistance of the caisson subject to the vibration from the wind turbine rotor and blades. The large-amplitude tests were to assess the moment resistance under extreme wind, wave, and current loading conditions. The load amplitude was steadily increase with cycles until large movements (>200 mm) occurred (Houlsby et al. 2005b).

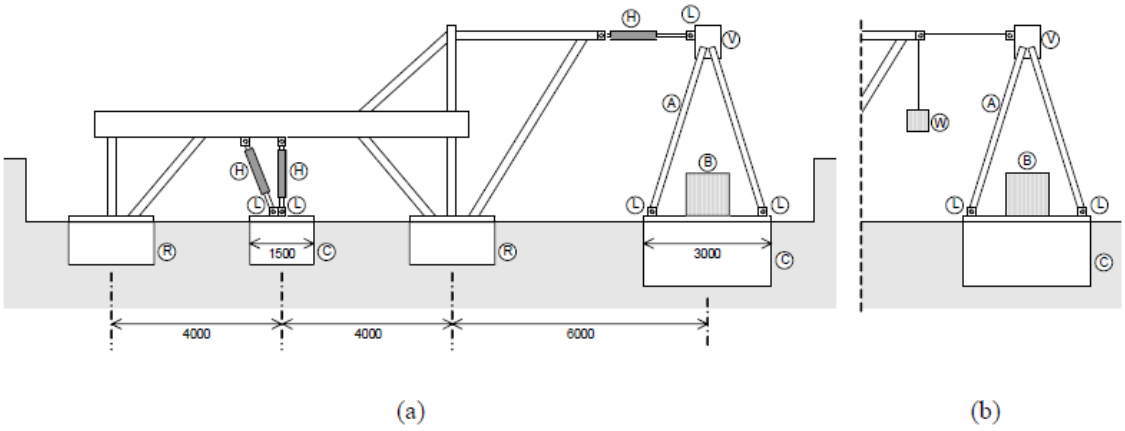

Figure 2.6: Bothkennar Field Test Equipment for 3-m and 1.5-m Suction Caisson: (a) Jacking Tests (b) SEMV tests (Houlsby et al, 2005b).

From the large-amplitude cyclic horizontal loading test results, Houlsby et al. (2005b) reported that the hysteresis increases with increasing load amplitude (see Figure 2.7a). In addition, the hysteresis loop of the largest loading cycle in Figure 2.7a shows a narrower "waist" because of the gap between the caisson and the soil. The initial stiffness and resistance was low because of the gap; however, the stiffness and resistance increased as the gap was close by further loading. Houlsby et al. (2005b) also points out that the stiffness degradation occurs over several cycles of constant amplitude loading (see Figure 2.7b). However, the stiffness degradation appears to be gradually stabilizing with cycles. This observation is consistent with the field test of laterally loaded piles in clay conducted by Matlock (1970) that the cyclic load-displacement hysteresis loop for a given lateral displacement tends to stabilized within 100 cycles.

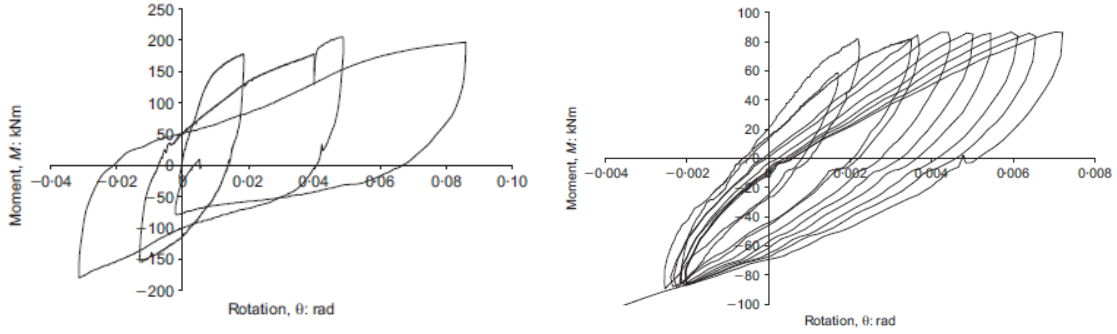

(a) Increasing Load Amplitude (b) Constant Load Amplitude

Figure 2.7: Moment-Rotation Curves for 3-m Caisson in Clay (Houlsby et al, 2005).

A series of suction caisson field tests similar to those conducted at Bothkennar clay test site were performed at Luce Bay test site in sand (Houlsby et al. 2006). The sand test pit was prepared by placing selected fill in 250-mm-thick layers and compacted by wheeled loader. The fill material consisted of 85% fine to medium-grained silica sand, 15% fine to coarse-grained gravel with the occasional cobble and peat inclusion. The sand is poorly graded with grain size of 0.3 to 0.4 mm. The estimated relative density of the sand test pit was 80-85%. The test pit was flooded with 150 mm deep of water throughout the test period.

For the horizontal quasi-static cyclic load tests with increasing amplitude with cycles, Houlsby et al. (2006) reported that the moment-rotation response of suction caisson in sand was stiff with no significant hysteresis under small load amplitudes. For larger amplitudes, the stiffness of the response decreases and hysteresis increases with increasing load amplitude as shown in Figure 2.8a. At very large amplitudes, the hysteresis loops have a “waisted” shape showing a gapping response similar to the tests at the clay site. For the horizontal cyclic load test, packets of 10-cycles of constant moment amplitudes of 42 kNm, 85 kNm, 169 kNm, and 254 kNm were applied on the caisson as

shown in Figure 2.8b. The moment–rotation hysteresis loop for each packet of cycles tends to reach a steady state by the end of the packet (Houlsby et al. 2006).

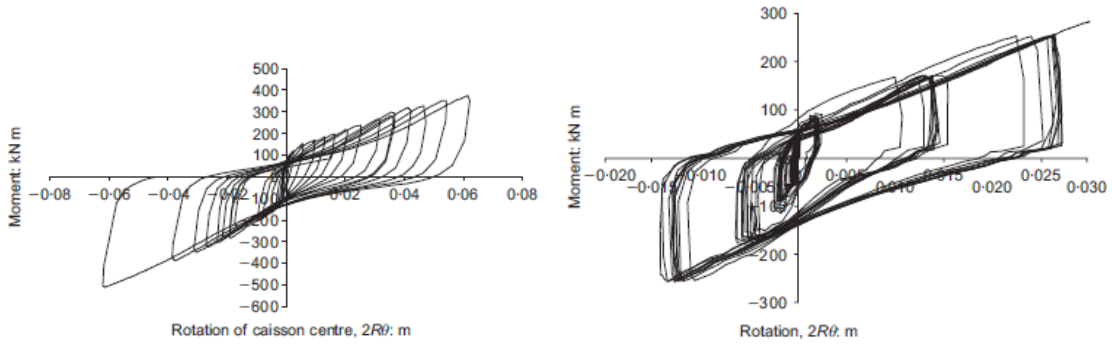

(a) Increasing Load Amplitude (b) Constant Load Amplitude

Figure 2.8: Moment-Rotation Curves for 3-m Caisson in Sand (Houlsby et al, 2006).

Small scale laboratory tests applying vertical and moment loads to suction caissons in sand and clay were also conducted to simulate the Bothkennar and Luce Bay field tests (Kelly et al. 2006). In the laboratory, model suction caissons with diameters of 0.15 m and 0.2 m for vertical load tests. Moment load tests were conducted using 0.2 m and 0.3 m diameter caissons in sand while 0.2 m diameter caissons were used in clay. The loads applied to the small scale caissons in the laboratory were scaled from those in the field tests. The test results in the laboratory and in the field were compared in non-dimensional form. The non-dimensional laboratory moment loading test results were similar to the field data in most cases. The laboratory test results were used to calibrate a strain-hardening plasticity model, and field test data were used to validate the model (Houlsby et al. 2005, Lam 2005, Cassidy et al. 2006, and Kelly et al. 2006).

2.3.2 Suction Caissons with Small Aspect Ratio in Clay

Bransby and Yun (2009) studied the behavior of skirted strip foundation under undrained combined vertical, horizontal, and moment loading conditions using plain strain finite element analyses and upper-bound plasticity analyses. For strip foundation with aspect ratio (emebedment to width ratio) equal to one, the capacity and failure mechanism of the skirted foundation is almost identical as the solid foundation (see figure 2.9). However, when the aspect ratio is equal to 0.2, the moment resistance of the skirted strip foundation may be significantly less than its solid counterpart because of the internal scoop failure mechanism in the soil plug (Figure 2.10).

Figure 2.9: Failure Mechanism of Strip Foundation with Aspect Ratio of One (Bransby and Yun, 2009).

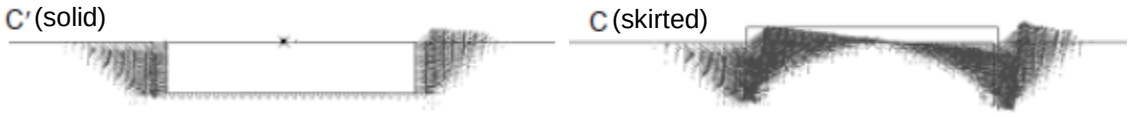

Figure 2.10: Failure Mechanism of Strip Foundation with Aspect Ratio of 0.2 (Bransby and Yun, 2009).

Barari and Ibsen (2012) conducted moment loading tests on 30 cm diameter suction caissons in clay. The aspect ratio of the suction caissons used in the experiments ranged from 0.25 to 1.0. The moments were applied by horizontal loads acting at a given

height, varying from 11 to 261 cm, on an extended vertical arm fixed on top of the caissons. The results were compared with a plain strain finite element model. Barari and Ibsen (2012) reached a similar conclusion as Bransby and Yun (2009) that suction caissons with an aspect ratio less than one may have less moment capacity than equivalent solid caissons due to the internal scoop failure mechanism developing within the soil plug. However, the analyses conducted by both Bransby and Yun (2009) and Barari and Ibsen (2012) were base on plain strain condition while it is a three-dimensional problem for the commonly used cylindrical suction caissons.

Hung and Kim (2012) evaluated the undrained capacity of suction caissons in clay using three-dimensional finite element analyses. Suction caissons with aspect ratios ranged from 0 to 1 were used in the finite element model. For lateral capacity analyses, a pure sliding failure mechanism was observed for suction caissons with an aspect ratio less than 0.5 while with a larger aspect ratio, the rotational behavior became significant with aspect ratio (see Figure 2.11).

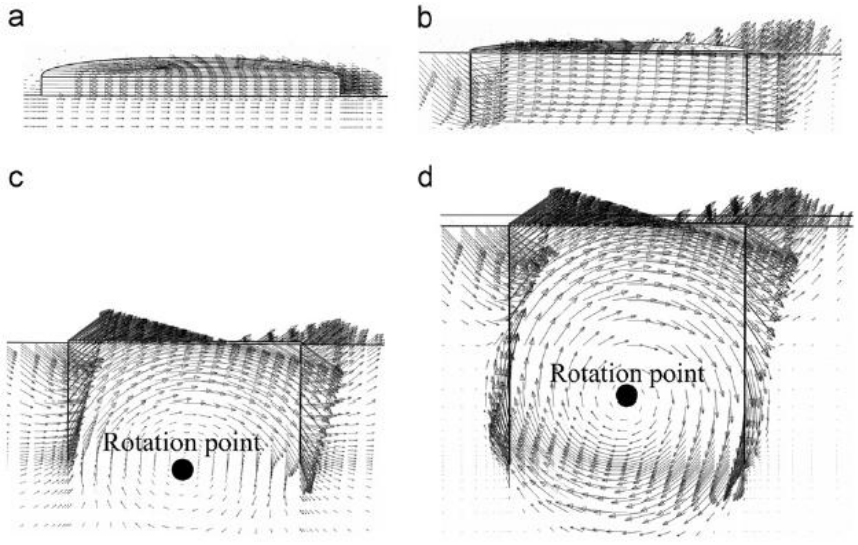

Figure 2.11: Failure Mechanism of Laterally Loaded Suction Caisson: (a) L/D = 0, (b) L/D = 0.25, (c) L/D = 0.5, and (d) L/D = 1 (Hung and Kim, 2012).

2.3.3 Suction Caissons with Small Aspect Ratio in Sand and Silt

Byrne and Houlsby (2004) performed cyclic combined loading tests on a 150 mm diameter, 50 mm long suction caisson in sand. The sand was saturated with silicon oil in the laboratory tests so that partial drainage rates are comparable to the field condition. Large moment and horizontal loads may be applied to the foundation as well as vertical loads. It was found that the loading rate had little effect on the load-displacement behavior for the experiments.

In order to evaluate the long-tem cyclic loading response of suction caisson in sand, Zhu et al. (2013) conducted 10,000-cycle loading tests on a 0.2 m diameter, 0.1 m long suction caisson in loose, silty, dry sand. The cyclic lateral load was applied through a vibrating motor with a cyclic load period of 9.3 second acting at a given height above the cap of the caisson. The moment-rotation curves in packets of 10 cycles during one of the tests are shown in Figure 2.12. The displacement of the first cycle was much larger than those of the following cycles. The accumulated cyclic rotation increased with the number of cycles, but at a decreasing rate with the cycle number. According to the test results, Zhu et al. (2013) proposed an empirical equation to predict the long-term accumulated rotation of the suction caisson.

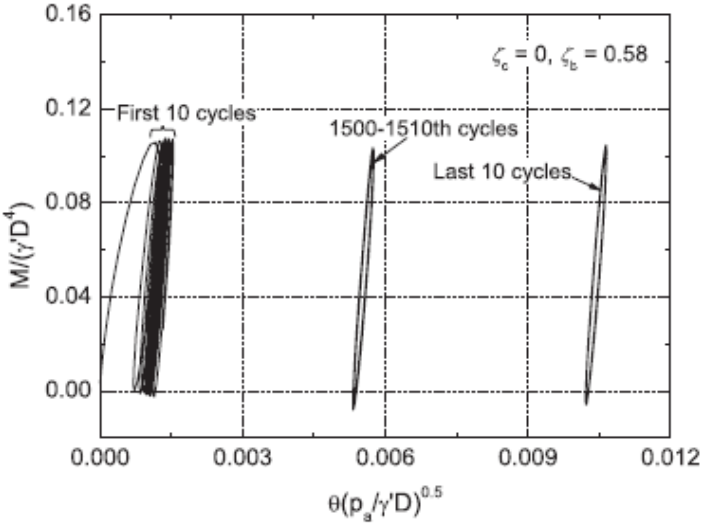

Figure 2.12: Moment-Rotation Curves in Packets of 10 Cycles during 10,000 Cycles (Zhu et al., 2013).

Zhu et al. (2011) conducted monotonic lateral loading tests of 1-meter (3.3-ft) diameter suction caisson with aspect ratio of 0.5 in a silt test bed. The lateral load was applied on an extended arm at 1.0, 1.5, or 2.6 meter above the cap of the caisson. The results showed that the center of rotation at failure was located at 0.8 caisson length below the cap.

2.4 SUMMARY FOR LITERATURE REVIEW

This chapter summarizes the common practice and research on analyses of suction caissons in clay, the p-y curves for soft clay recommended by API along with suggested revisions from related research, and recent studies on suction caissons with aspect ratio less than one.

For calculating suction caisson penetration resistance, API RP 2SK recommends using a bearing capacity factor, N_c, of 7.5 for the wall tip area and an adhesion factor,

α_{ins}, equal to the inverse of soil sensitivity. The value of α_{ins} typically ranges from 0.2 to 0.5 for Gulf of Mexico deepwater clay. However, previous studies showed that the α_{ins} can be lower than the inverse of sensitivity and suggested using α_{ins} values of 0.25 to 0.3 for unpainted areas and 0.08 for painted areas of the caisson (Dendani and Colliat 2002, Huang et al. 2003).

For axial capacity analysis of suction caissons in clay, API RP 2SK recommends using a end bearing factor, N_c, of 9 and a side friction factor, α, that depends on the ratio of undrained shear strength to effective stress (Ψ or c/p ratio). The α value equals to one for normally consolidated clay with Ψ = 0.25. However, several studies suggested that a lower side friction factor should be used for suction installed caissons (Andersen and Jostad, 1999 and 2004). However, most of these studies did not separate measurements of side friction and end bearing. Therefore, the values of N_c and α are subjective to the assumptions made in these studies and also the uncertainty of the soil plug weight (Luke et al., 2005). El-Sherbiny reported that α and N_c are 0.8 and 15, respectively, for the suction caisson pulled out rapidly with a sealed top cap according to separate measurements of side shear and end bearing. In addition, there is no difference in axial capacity between caissons installed using deadweight or suction.

API RP 2SK (A 2008) recommends using finite element method, limit equilibrium or plastic limit analyses for holding capacity design of suction caissons. For suction caissons subjected to mainly horizontal loads, beam-column analyses (or p-y analyses) described in can be used with modifications that account for the larger caisson diameter. Finite element method is the most rigorous and general approach to evaluate the lateral capacity of suction caissons. If an appropriate constitutive model is used, the critical failure mechanism can be found without prior assumptions that are required for plastic limit analysis. However, finite element analyses require knowledge of advanced

numerical analysis and significant amount of time to set up and implement the model. One alternative to finite element analysis is the plastic limit analysis, which is comparatively less computationally expensive and easier to use. However, it requires assumptions of failure mechanism and may not be suitable for all types of suction caissons. The development of the simplified plastic limit analysis of suction caisson by Aubeny et al. (2003) was summarized. Available data suggest that the plasticity model matches better with finite element analyses and test data for more slender ($L/D \geq 6$) suction caissons (Randoph and House 2002, Aubeny et al. 2003, Cluckey et al. 2003).

Matlock (1970) developed a family of p-y curves that represent the soil resistance versus pile deflection relationships as a function of depth base on field pile load tests and laboratory tests. These p-y curves were later adopted by API RP 2A (now API RP 2GEO). Studies on p-y curves showed that the predicted pile deflections using API p-y curves were significantly greater than the measured deflections in lateral pile load tests and the soil resistance at shallower depth was underestimated. A flow-around bearing capacity factor, N_p, of around 12 was suggested by related studies instead of 9 suggested by API (Stevens and Audibert 1979, Randolph and Houlsby 1984, Murff and Hamilton 1993, Aubeny et al. 2003, Jeanjean 2009).

Suction caissons with a small aspect ratio have been getting more attention recently because of its potential use for offshore wind turbines. The EPSRC/DTI joint industry project aimed to provide design guidance to suction caisson for offshore wind turbines is summarized in this chapter. Intermediate scale field tests and small scale laboratory tests were conducted both in clay and sand using suction caissons with an aspect ratio of 0.5 or 0.66 (Houlsby 2005a, Houlsby 2005b, Houlsby 2006, Kelly 2006). From the large-amplitude cyclic horizontal loading tests at clay test site, Houlsby et al. (2005b) reported that the hysteresis increases with increasing load amplitude. However,

for the field tests in sand, Houlsby et al. (2006) reported that the cyclic moment-rotation response of suction caisson in sand was stiff with no significant hysteresis under small load amplitudes, while for larger amplitudes, the stiffness of the response decreases and hysteresis increases with increasing load amplitude. For both the field tests in clay and sand, the hysteresis loop of the largest loading cycle shows a narrower "waist" because of the gap between the caisson and the soil. Houlsby et al. (2005b, 2006) also reported that the stiffness degradation occurs over several cycles of constant amplitude loading. However, the stiffness degradation appears to be gradually stabilizing with cycles. This observation is consistent with the field test of laterally loaded piles in clay conducted by Matlock (1970) that the cyclic load-displacement hysteresis loop for a given lateral displacement tends to stabilized within 100 cycles. Kelly et al. (2006) compared the test results in the laboratory and in the field in non-dimensional form and the cyclic moment-rotation were similar for the two sets tests in different scales.

Other studies on suction caissons in clay, sand, and slit are summarized in the last section of this chapter. Plain strain finite element analyses conducted by Bransby and Yun (2009) and Barari and Ibsen (2012) show that, with an aspect ratio less than one, the moment resistance of the skirted strip foundation may be significantly less than its solid counterpart because of the internal scoop failure mechanism in the soil plug. Hung and Kim (2012) evaluated the undrained capacity of suction caissons in clay using three-dimensional finite element analyses. A pure sliding failure mechanism was observed for suction caissons with an aspect ratio less than 0.5 while with a larger aspect ratio, the rotational behavior became significant with aspect ratio. Byrne and Houlsby (2004) performed cyclic combined loading tests small scale suction caisson in sand and found that the loading rate had little effect on the load-displacement behavior. Zhu et al. (2013) conducted 10,000-cycle loading tests on suction caisson with an aspect ratio of 0.5 in

loose, silty, dry sand to evaluate its long-tem cyclic loading response in sand. The accumulated cyclic rotation increased with the number of cycles, but at a decreasing rate with the cycle number. According to the test results, Zhu et al. (2013) proposed an empirical equation to predict the long-term accumulated rotation of the suction caisson.

Chapter 3: Soil Test Beds

In this study, suction can foundation scale model tests were conducted in five soil test beds:

- Normally Consolidated Clay Test Bed
- Overconsolidated Clay Test Bed
- Loose Silica Sand Test Bed
- Cemented Silica Sand Test Bed
- Cemented Calcareous Sand Test Bed.

The preparation and characteristics of the five test beds are presented in the following sections. Note that the one-g model foundation tests in uncemented sands are much more difficult than in clays because of the difficulty in scaling the drained behavior. Uncemented dense sands dilate much more severely in the model tests than in the field because of its low confining pressure in the scaled model tests. Therefore, the sand behavior in model tests may not be representative for those in the field. This challenge of excessive dilation of sands in scale model tests is addressed in different ways in this study: one is to reduce the density of the sand used in the scale model tests compared to that in the field and the other is to cement the sand particles. Using either of these treatments, the volume change behavior of the sand (contractive/dilative) in the model test will be more representative of that at the field scale over the depth of the foundation.

3.1 Normally Consolidated Clay Test Bed

The normally consolidated clay test bed used for this study was one of the two test beds construed in two metal tanks (see Tank 1 in Figure 3.1). These two tanks are 8 ft

long, 4 ft wide, and 6 ft high. Approximately 3 ft deep of kaolinite was placed in this test bed. Kaolinite is chosen for constructing the test beds because of its workability, high coefficient of consolidation, and low compressibility.

The normally consolidated clay test bed that is currently being used was prepared by placing and mixing the kaolinite in layers with the water content profile that creates a linearly increasing undrained shear strength with depth. The kaolinite was mixed to the water contents according to the water content and undrained shear strength relationships in Figure 3.2 such that the kaolinite has a lower water content (approximately 90%) at the bottom of the tank and a higher water content (approximately 140%) near the surface. These water content and undrained shear strength relationships were established according to previous experience of creating normally consolidated clay deposit from the consolidation of the kaolinite slurry by its own weight (Lee 2008). Mixing and placing the kaolinite in this approach can save significant time for waiting the clay to consolidate by its own weight (reduce from up to 15 months to 2 weeks). The sensitivity of the clay is 1.5 if left undisturbed for 3 to 4 months and it can go up to 2.1 if left undisturbed for a longer period.

Figure 3.1: Metal Tanks that Contain Normally Consolidated Clay (El-Sherbiny 2005)

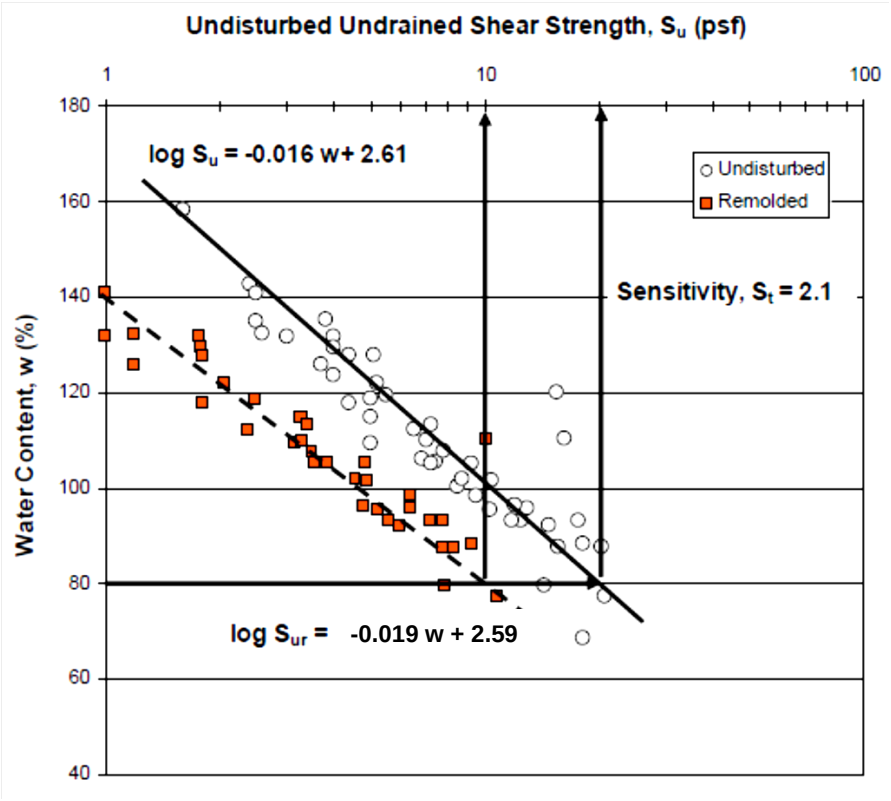

Figure 3.2: Water Content versus Undrained Shear Strength of the Kaolinite (Lee 2008)

T-bar tests were used to measure the undrained shear strength of the clay test beds at The University of Texas at Austin. The T-bar is an acrylic rod that is 1 inch in diameter by 4 inches long (see Figure 3.3). The acrylic rod was mounted transversely on a 3/8 in (9.5 mm) brass insertion rod. A stack of weights sat on top of the insert rod so it could be pushed down into the soil bed.

Figure 3.3: T-bar and Brass Insertion Rod (Gilbert et al. 2012)

The penetration rate is controlled by an actuator at approximately 0.8 in/sec (20 mm/s) to represent an undrained loading condition. The insertion resistance is measured using a 100-lb capacity load cell attached at the top of the insertion rod. A separate penetration of the insertion rod was used to the measure the friction and bearing of the insertion rod. The undrained shear strength, Su, was calculated using the following equation (Gilbert et al. 2012 and El-Sherbiny 2005):

$$s_u = \frac{(F_{total} - F_{rod})}{N_c \times A} \qquad \text{(Equation 3.1)}$$

Where F_{total} = total measured resistance during T-bar insertion,
F_{rod} = measured resistance during separate penetration of the insertion rod
A = projected area of the T-bar (4 in^2 = 2580 mm^2)
N_c = bearing capacity factor = 10.5, which is the convention in practice (Stewart and Randolph 1994)

Figures 3.4 to 3.6 show the undrained shear strength profile measured in the normally consolidated clay test bed according to recent T-bar tests. The T-bar tests were conducted within 12 inches from the scale model foundation on September 27, 2011, July 16, 2012, and December 7, 2012, respectively. On each of the three days, the T-bar was repeatedly inserted and pulled out for six cycles to measure the undisturbed and remolded undrained shear strength. The differences in the measured undrained shear strength profile can attribute to the consolidation, disturbance due to the tests, and the spatial variation of the soil strength in the tank. Figure 3.7 shows all of the above mentioned undrained shear strength profiles measured by T-bar. The undrained shear strength at mudline was approximately 0 psf. The gradient of undisturbed undrained shear strength profile is estimated to be 14 psf/ft. The measured undrained shear strength gradient decreased to 7 psf/ft after remolding the soil by penetrating and pulling out the T-bar for 6 cycles.

Figure 3.8 shows the estimated c/p ratio (undrained shear strength to effective overburden stress ratio) profile in the normally consolidated clay test bed. The c/p ratio ranges between 0.22 and 0.29 at a depth greater than 6 inches. This c/p ratio profile was estimated according to the unit weight of soil along the depth in this soil test bed reported by Lee (2008).

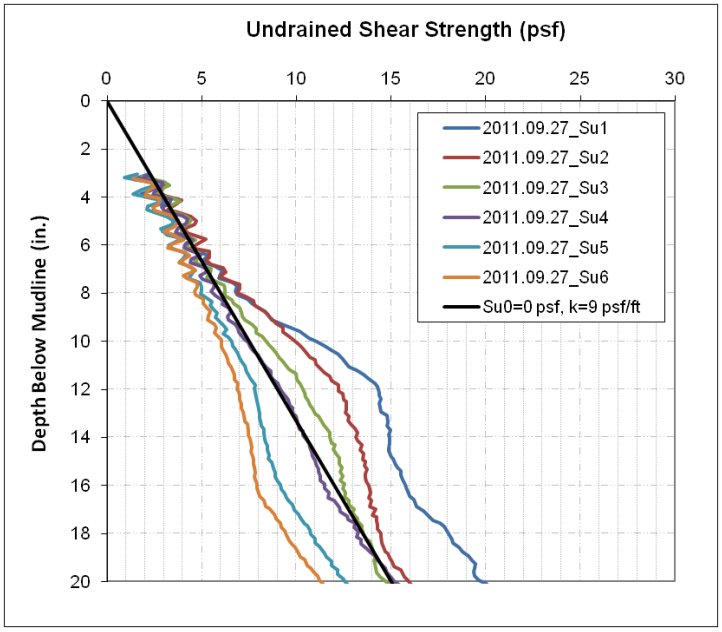

Figure 3.4: Undrained Shear Strength in Normally Consolidated Clay Test Bed (September 27, 2011)

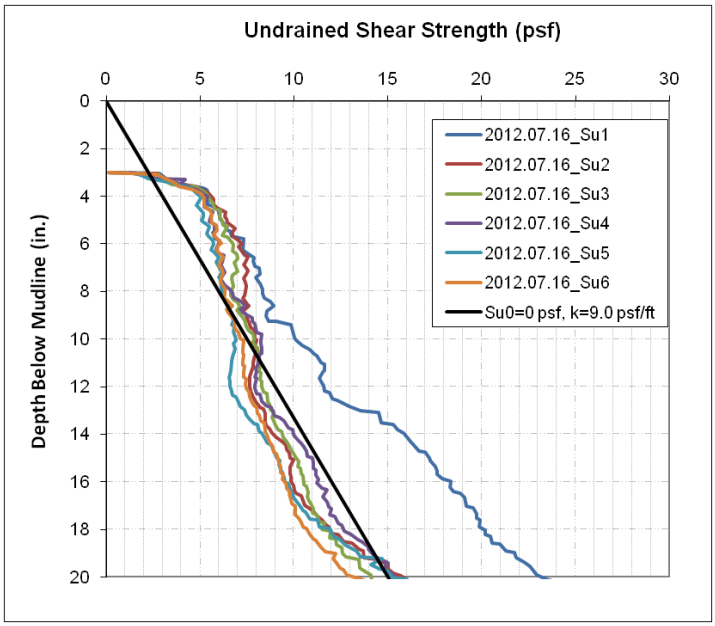

Figure 3.5: Undrained Shear Strength in Normally Consolidated Clay Test Bed (July 16, 2012 – before Installation of the SCF model)

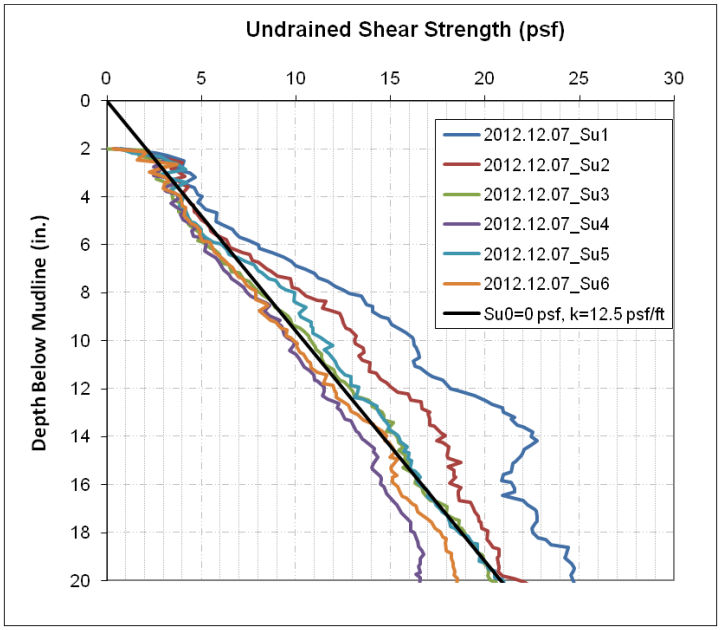

Figure 3.6: Undrained Shear Strength in Normally Consolidated Clay Test Bed (December 7, 2012 – after Pullout of the SCF model)

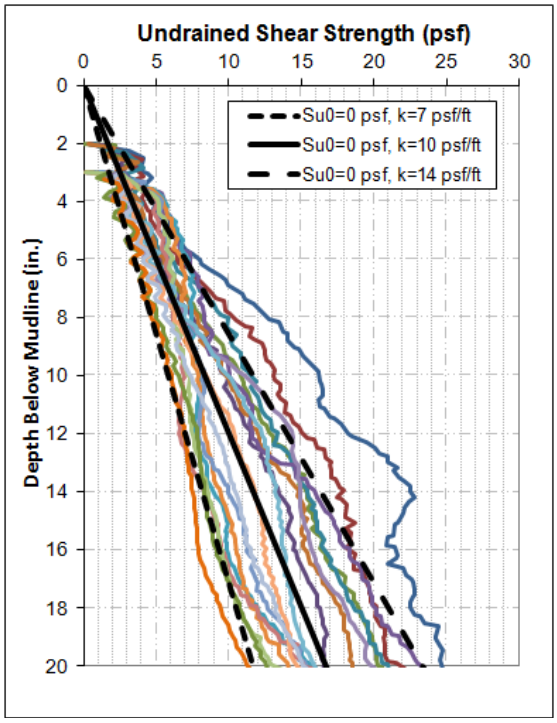

Figure 3.7: Undrained Shear Strength in NC Clay Test Bed (All T-bar Tests)

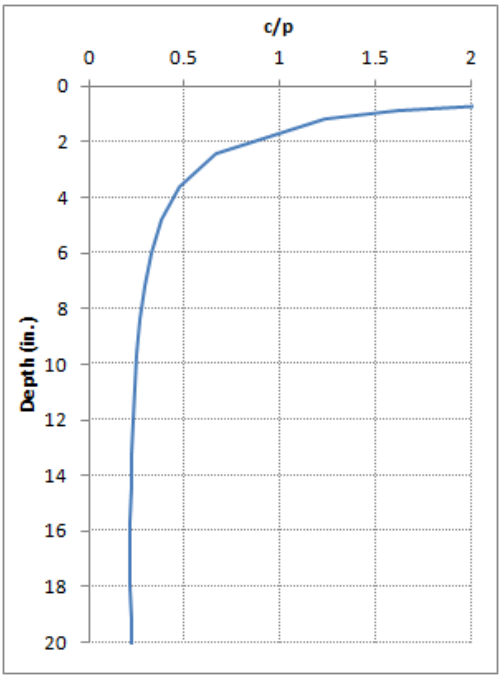

Figure 3.8: Estimated c/p Ratio Profile in Normally Consolidated Clay Test Bed

3.2 Overconsolidated Clay Test Bed

The thermo-plastic tank (see Figure 3.9) which contains the overconsolidated clay is a black, 100-gallon stock tank. The approximate dimensions of the tank are 4 feet in length, 2 feet in width and 2 feet in height. This smaller soil test bed gives us a better control of the strength of the soil. The kaolinite in the thermo-plastic tank were air-dried to a lower water content in order to create a stiffer (a higher overconsolidation ratio) clay test bed. Then, the lower water content kaolinite was mixed and remolded by hand and a steel paddle attached to a drill (see Figure 3.10) to create a relatively uniform soil profile.

Figure 3.9: Overconsolidated Clay Test Bed

Figure 3.10: Drill with Steel Paddle and Mixing Process (Gilbert et al. 2012)

A target undrained shear strength of 40 psf throughout the test bed was chosen and the corresponding target water content was approximately 60% according to the relationships in Figure 3.2. If we assume a submerged unit weight of 40 pcf and consider the mid-depth point of the 6-inch SCF model (at 3 inches deep), the undrained shear strength to vertical effective stress ratio (c/p) can be calculated with the target undrained

shear strength of 40 psf. This target undrained shear strength represent a c/p ratio of 4.0 at 3 inches deep (see Figure 3.11) comparing to a c/p ratio of approximately 0.25 for normally consolidated clay.

The undrained shear strength profile in the overconsolidated clay test bed was measured by the T-bar. Figure 3.12 and 3.13 show the undrained shear strengths in the Overconsolidated Clay Test Bed measure by T-bar tests. The T-bar tests were conducted before installation and pullout of the 6-inch diameter SCF model in the test bed. On both days, the T-bar was repeatedly inserted and pulled out for six cycles to measure the undisturbed and remolded undrained shear strength. According to the T-bar tests, the sensitivity of the test bed was approximately 2 to 2.6. Figure 3.14 shows all of the above mentioned undrained shear strength profiles measured by T-bar. The undisturbed undrained shear strength is estimated to be 45 psf for the upper 8 inches, which is relevant to the 6-inch diameter SCF model. The measured undrained shear strength for the upper 8 inches decreased to 22 psf after remolding the soil by penetrating and pulling out the T-bar for 6 cycles.

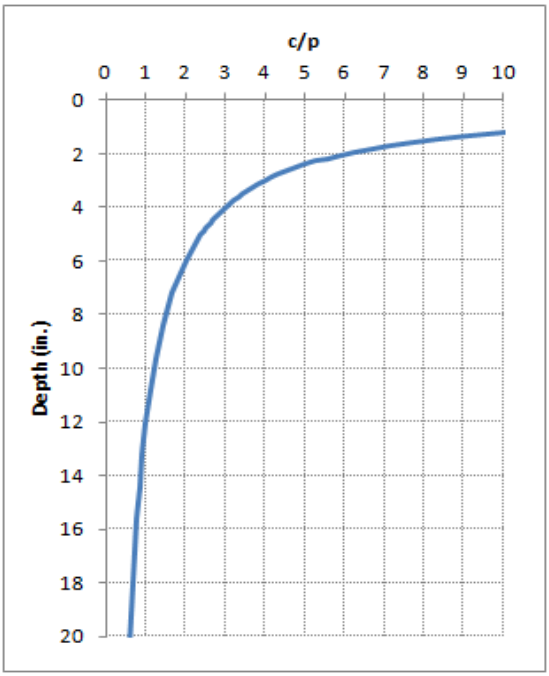

Figure 3.11: Estimated c/p Ratio Profile in Overconsolidated Clay Test Bed

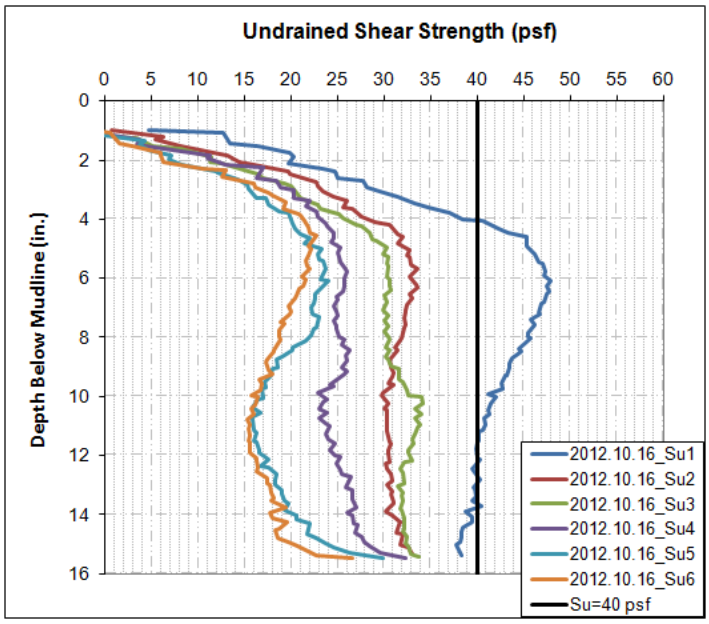

Figure 3.12: Undrained Shear Strength in Overconsolidated Clay Test Bed (October 16, 2012 – before installation of the SCF model)

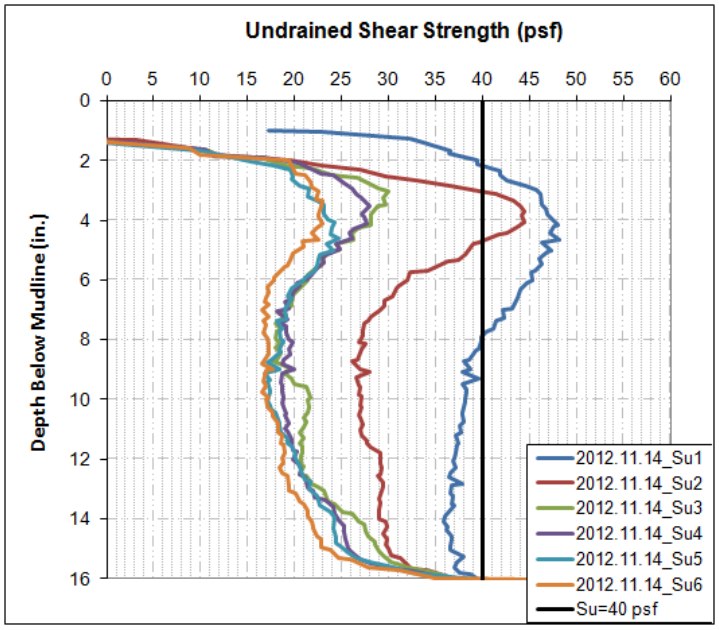

Figure 3.13: Undrained Shear Strength in Overconsolidated Clay Test Bed (November 14, 2012 – after pullout the SCF model)

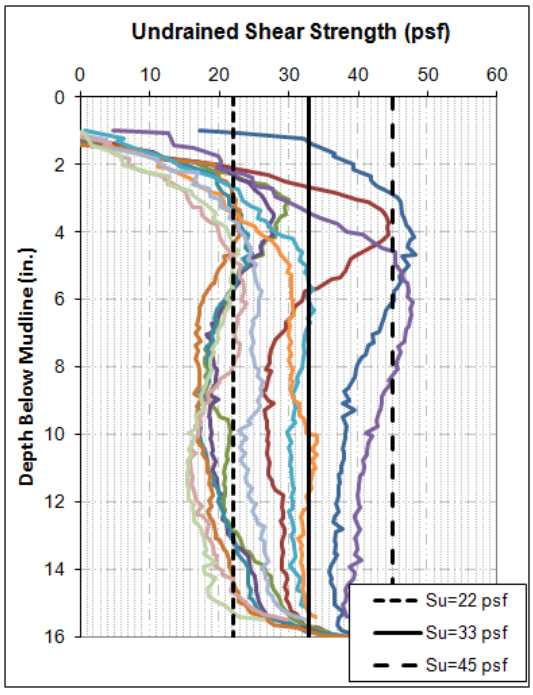

Figure 3.14: Undrained Shear Strength in Overconsolidated Clay Test Bed (All T-bar Tests)

3.3 LOOSE SILICEOUS SAND TEST BED

The loose siliceous sand test bed was prepared in the thermo-plastic tank using the All Purpose Sand (Figure 3.15). The maximum and miminum unit weight of the All Purpose Sand were obtained according to ASTM D 4254 – 00 and ASTM D 4253 – 00. The results are summarized in Table 3.1. The grain size analysis of the sand presented in Table 3.2, Table 3.3, and Figure 3.16 shows that the grain size of the sand is fairly uniform.

The test bed was first prepared by flooding the thermo-plastic tank with water then placing the sand with a scoop from the bottom up. In order to create a loose sand deposit, the falling height of the sand from the scoop through the water to the surface of the sand deposit was controlled to be around 2 inches to minimize the compaction of the sand. The saturated unit weight of the sand in the test bed was approximately 113 pcf; note that this unit weight is less than the minimum from ASTM 4254-00 since the sand was rained through water instead of air.

Figure 3.15: Loose Siliceous Sand Test Bed

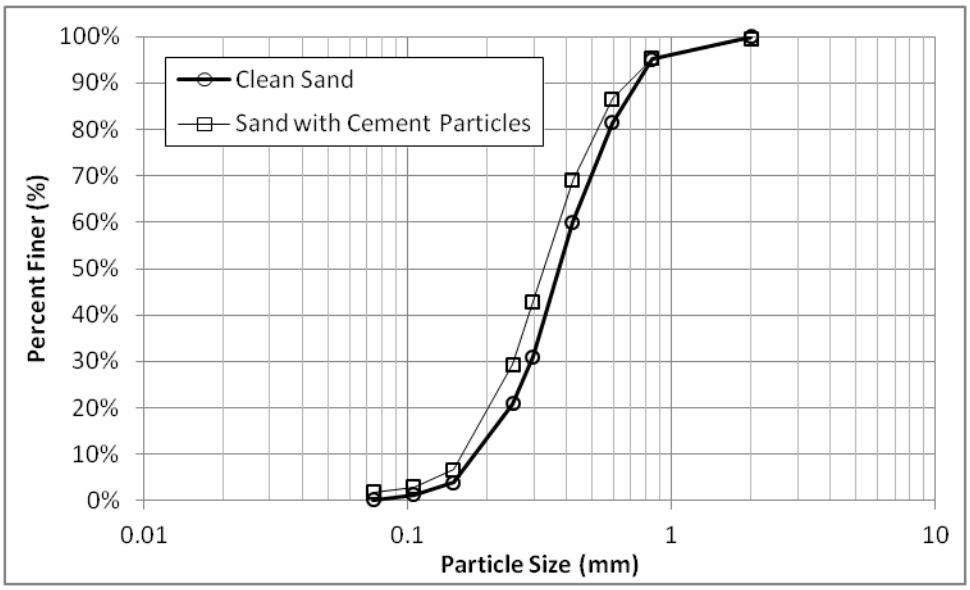

Figure 3.16: Gradation Curves of the All Purpose Sand

	Dry Unit Weight (pcf)		Saturated Unit Weight* (pcf)	
	Clean Sand	Sand with Cemented Particles**	Clean Sand	Sand with Cemented Particles**
Minimum	95	93	122	120
Maximum	111	110	132	131

* Assume the sand is fully saturated and the specific gravity of sand is 2.65
** Contains small amount of cemented sand particles and fine particles of cement. Prepared by breaking the cementation of cemented sand by hand tools.

Table 3.1: Minimum and Maximum Unit Weight of the All Purpose Sand from ASTM

		Clean Sand				Sand with Cemented Particles			
Sieve No.	Opening Size (mm)	Soil Retained (g)	Percent Retained (%)	Cumulative Percent Retained (%)	Percent Finer (%)	Soil Retained (g)	Percent Retained (%)	Cumulative Percent Retained (%)	Percent Finer (%)
10	2	0	0%	0%	100%	4	0%	0%	100%
20	0.841	39.2	5%	5%	95%	34	4%	5%	95%
30	0.595	111.3	14%	19%	81%	71	9%	13%	87%
40	0.42	173.6	21%	40%	60%	142.1	18%	31%	69%
50	0.297	235.9	29%	69%	31%	211.5	26%	57%	43%
60	0.25	81.2	10%	79%	21%	110.9	14%	71%	29%
100	0.149	138.4	17%	96%	4%	183	23%	93%	7%
140	0.105	20.9	3%	99%	1%	30.5	4%	97%	3%
200	0.074	9.5	1%	100%	0%	8.5	1%	98%	2%
Pan		0.9	0%	100%	0%	4.5	1%	99%	1%
	SUM=	810.9				800			

Table 3.2: Sieve Analysis on All Purpose Sand

	Clean Sand	Sand with Cemented Particles
D_{10}	0.185 mm	0.164 mm
D_{30}	0.293 mm	0.252 mm
D_{60}	0.420 mm	0.377 mm
$C_u = \frac{D_{60}}{D_{10}}$	2.3	2.3
$C_c = \frac{{D_{30}}^2}{D_{10}D_{60}}$	1.1	1.0

Table 3.3: Coefficients of Uniformity (C_u) and Curvature (C_c) of the All Purpose Sand

The strength of the loose sand test bed was characterized using a 1.05-inch diameter cone penetrometer (see Figure 3.17). The cone is attached to a 0.5-inch diameter insertion rod and a 200-lb capacity load cell is attached to the top of the rod for resistance measurement. Since the diameter of the insertion rod is only half of the diameter of the

cone, the side shear is negligible comparing to the cone tip resistance during penetration tests. Therefore, the load measured by the load cell can be attributed to the resistance of the cone. The cone tip resistance (q_c) is then calculated by the measured load divided by the cone tip area. The cone penetrometer was pushed into the soil by hand because the force require to penetrate the sand exceeded the capacity of the loading system in our laboratory. During the tests, the penetration depth of the cone was measured by a linear displacement transducer.

Figure 3.18 shows the cone tip resistance of the loose siliceous sand measured by the 1.05-inch diameter cone after pullout of the SCF model. The cone penetration tests were tested at two locations in the test bed that were 12 inches away from the location of SCF model and from the wall of the test bed.

Figure 3.17: 1.05-inch Diameter Cone Penetrometer

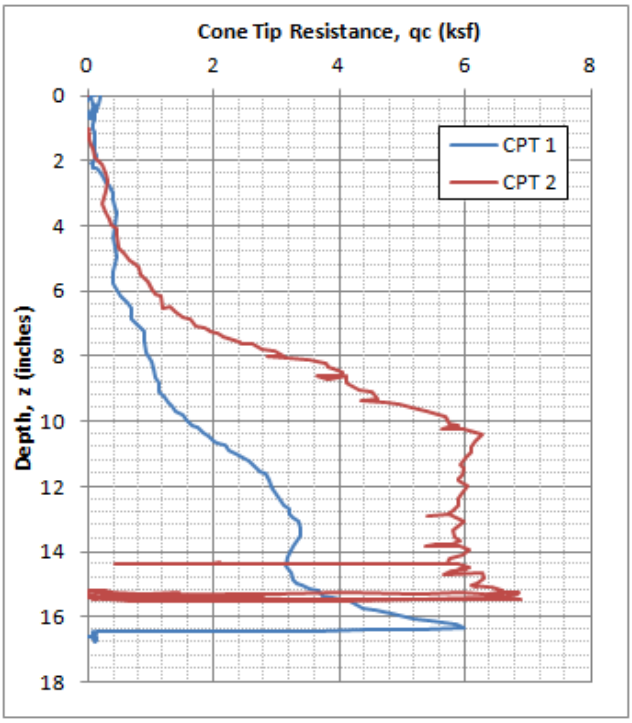

Figure 3.18: Cone Tip Resistance by 1.05-inch Diameter Cone in Loose Siliceous Sand (September 7, 2012 – after pullout of the SCF model)

3.4 CEMENTED SILICEOUS SAND TEST BED

The cemented siliceous sand test bed was prepared in the thermo-plastic tank for the suction can foundation model tests by mixing the siliceous sand with 1% of cement (see Figure 3.19). The siliceous sand we used is the All Purpose Sand and the cement is Alamo Type I Portland Cement.

In order to prepare a uniform cemented sand test bed, the dry sand was first mixed by hand in 5-gallon buckets with 1% of cement comparing to the dry weight of the sand. The cement lumps were crushed by hand to reach a more uniform mixture. Next, water was added to reach a 28% water content and mixed again by hand in the bucket. Then, the cemented sand mixture was placed into the thermo-plastic tank by lifts. A metal plate

tamp was used to compact each lift, and a rubber hammer was used to hit on the outer wall of the tank to densify the mixture. The total unit weight of the cemented siliceous sand was approximately 126 pcf according to the volume of the tank and the weight of sand.

Figure 3.19: Cemented Siliceous Sand Test Bed

The soil strength of the test bed was characterized by unconfined compression test and pushing the 1.05-inch diameter cone into the cemented sand. Figure 3.20 shows the stress-strain curves from the unconfined compression test of the cemented siliceous sand. The two 3-inch high, 1.5-inch diameter specimens were prepared using similar procedure as the Cemented Siliceous Sand Test Bed and were tested according to ASTM D2166 – 06. After a day of curing, the unconfined compression strength of the cemented siliceous sand was 346 psf as shown in Figure 3.20. Figure 3.21 shows the cone penetration test results in the cemented sand test bed using the 1.05-inch diameter cone as presented in the previous section. The cone penetration tests were conducted at three locations in the

test bed. CPT 1 and CPT 2, as shown in Figure 3.21, were tested at two locations in the test bed that were 12 inches away from the location of SCF model and from the wall of the test bed. One additional test, CPT 3, was conducted 6 inches away from CPT 2 and 6 inches way from the wall of the test bed. The three tests reached refusal at depths between 3.5 to 5.5 inches and the cone tip resistance measured at refusal was approximately 28 ksf.

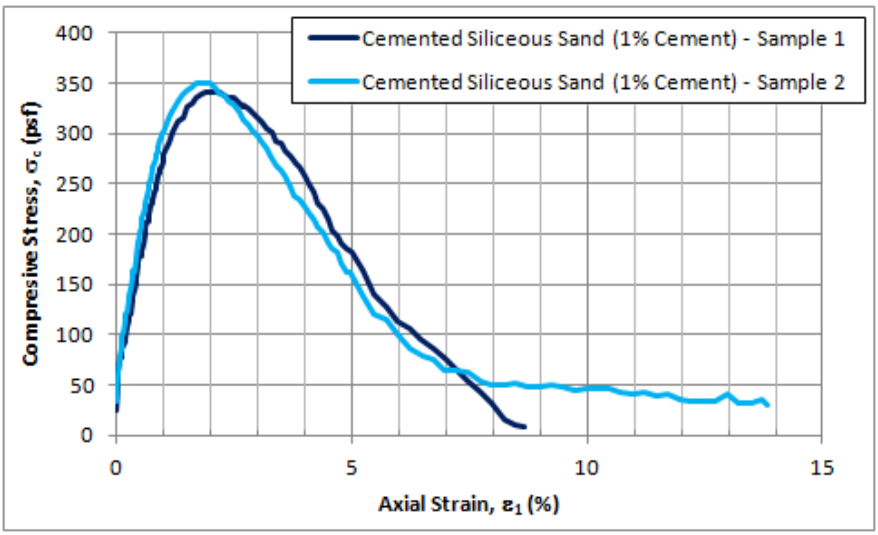

Figure 3.20: Unconfined Compression Tests of Cemented Siliceous Sand

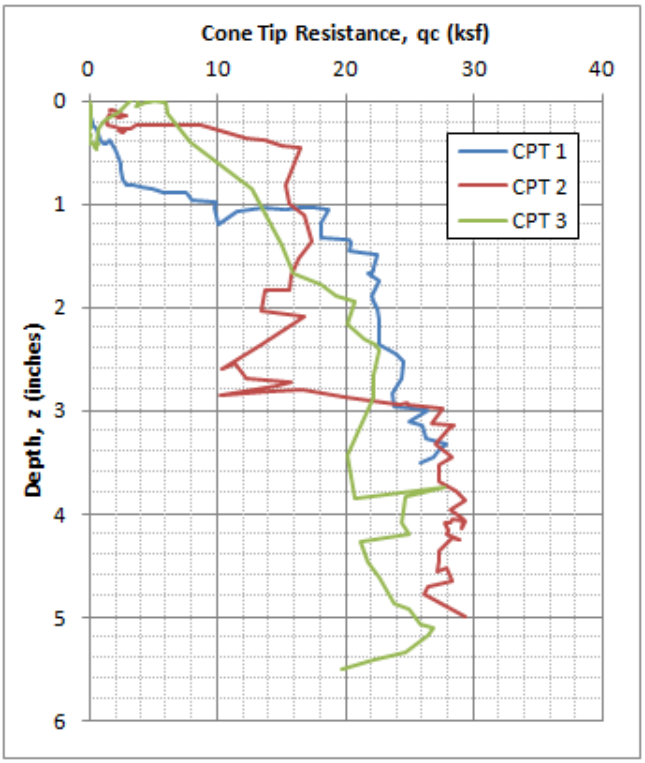

Figure 3.21: Cone Tip Resistance versus Depth in the Cemented Sand Test Bed (Profile Ends at Refusal)

3.5 CEMENTED CALCAREOUS SAND TEST BED

The cemented siliceous sand test bed (see Figure 3.22) was prepared in the thermo-plastic tank by mixing the oyster shell meal with 1% of cement and 40% of water to increase the workability of the mixture. The oyster shell meal (see Figure 3.23) was used to simulate the strength and angular shape of siliceous sands, and the cement used in the mixture was Alamo Type I Portland Cement.

Figure 3.22: Cemented Siliceous Sand Test Bed

Figure 3.23: Oyster Shell Meal

The grain size analysis presented in Table 3.4, Table 3.5, and Figure 3.24 shows that the grain size of the oyster shell meal was not as uniform as the siliceous sand and has a larger proportion of finer particles.

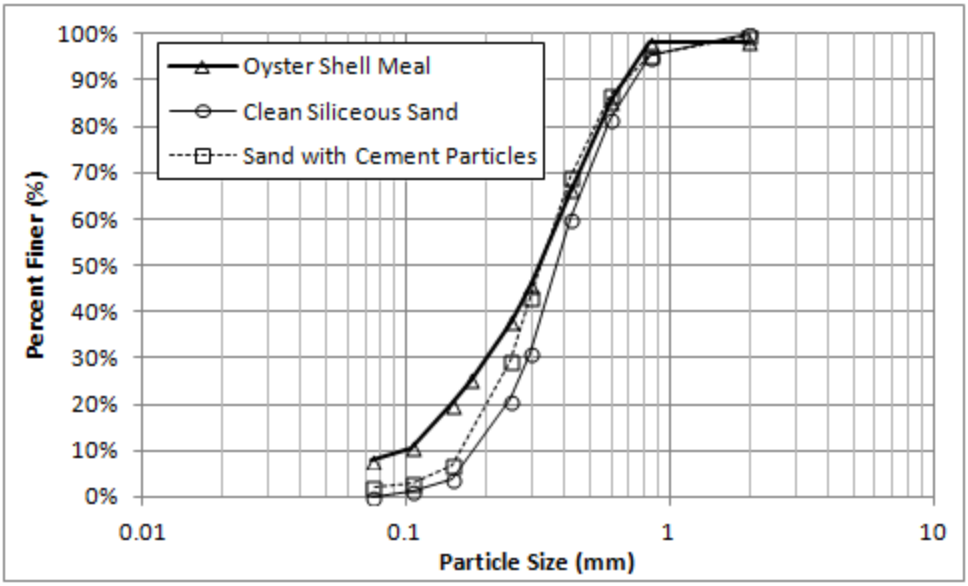

Figure 3.24: Gradation Curves of Oyster Shell Meal

		Oyster Shell Meal			
Sieve No.	Opening Size (mm)	Soil Retained (g)	Percent Retained (%)	Cumulative Percent Retained (%)	Percent Finer (%)
10	2	8.5	2%	2%	98%
20	0.841	1.2	0%	2%	98%
30	0.595	61.9	12%	14%	86%
40	0.42	96.2	19%	34%	66%
50	0.297	102.3	20%	54%	46%
60	0.25	40.09	8%	62%	38%
80	0.177	62.7	13%	75%	25%
100	0.149	26.87	5%	80%	20%
140	0.105	46.7	9%	89%	11%
200	0.074	13.6	3%	92%	8%
Pan		39.7	8%	100%	0%
	SUM=	499.76			

Table 3.4: Sieve Analysis on Oyster Shell Meal

	Oyster Shell Meal
D_{10}	0.091 mm
D_{30}	0.204 mm
D_{60}	0.381 mm
$C_u = \frac{D_{60}}{D_{10}}$	4.18
$C_c = \frac{{D_{30}}^2}{D_{10}D_{60}}$	1.19

Table 3.5: Coefficients of Uniformity (C_u) and Curvature (C_c) of Oyster Shell Meal

In order to prepare a uniform cemented siliceous sand test bed, the dry oyster shell meal was first mixed by hand in 5-gallon buckets with 1% of cement comparing to the dry weight of the oyster shell meal. The cement lumps were crushed by hand to reach a more uniform mixture. Next, water was added to reach a 40% water content and mixed again by hand in the bucket. Then, the mixture was placed into the thermo-plastic tank by lifts. A metal plate tamp was used to compact each lift, and a rubber hammer was used to hit on the outer wall of the tank to densify the mixture. The total unit weight of the cemented calcareous sand was approximately 117 pcf by assuming a specific gravity of 2.56 for oyster shell (Yoon et. al., 2003).

The soil strength of the test bed was characterized by unconfined compression test and pushing the 1.05-inch diameter cone into the cemented calcareous sand. Figure 3.25 and 3.26 show the unconfined compression test results of the cemented calcareous sand with 1, 4, 7, 13, 50 days of curing. The two 3-inch high, 1.5-inch diameter specimens were prepared using similar procedure as the Cemented Calcareous Sand Test Bed and were tested according to ASTM D2166 – 06. The unconfined compression strength of the cemented siliceous sand ranged from around 750 to 1150 psf, which was approximately 2 to 3 times of the strength of the cemented siliceous sand shown in the previous section.

The higher strength could be due to the interlock of angular particles and the chemical reaction between cement and the oyster shell. The peaks occurred at 7% to 10% of axial strain indicating that the cemented calcareous sand is more ductile than the cemented siliceous sand, which has peaks at 2% of axial strain. There seemed to be a slight increase in unconfined compression strength with increasing curing time; however, the trend is not very clear because of the strength variability between specimens.

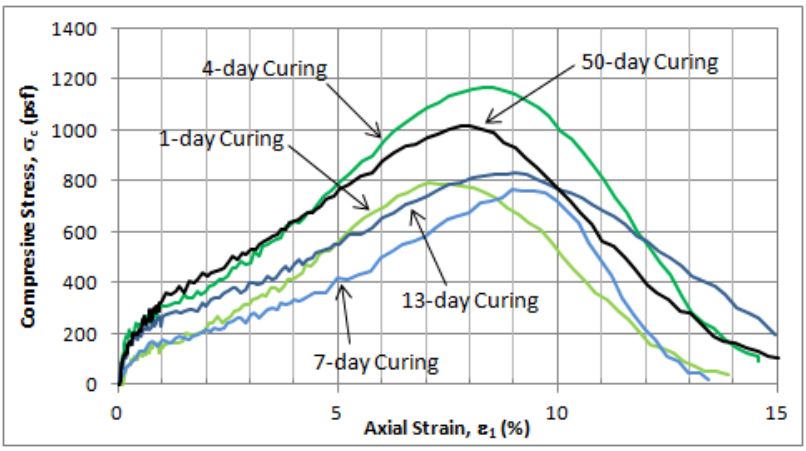

Figure 3.25: Unconfined Compression Tests of Cemented Siliceous Sand (1% Cement Content)

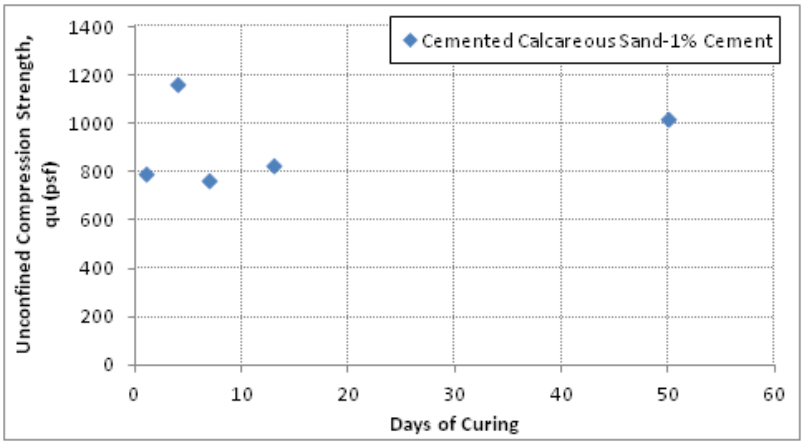

Figure 3.26: Unconfined Compression Strength versus Curing Time for Cemented Siliceous Sand (1% Cement Content)

Figure 3.27 shows the cone penetration test results in the cemented calcareous test bed using the 1.05-inch diameter cone as presented in the previous section. The cone penetration tests were conducted at two locations in the test that were 12 inches away from the location of SCF model and from the wall of the test bed. The three tests reached refusal at depths between 3 to 4 inches and the cone tip resistance measured at refusal ranged from 28 to 34 ksf. The cone penetration tests reached refusal at shallower depths in the cemented calcareous sand than in the cemented siliceous sand, which reached refusal at depths between 3.5 to 5.5 inches.

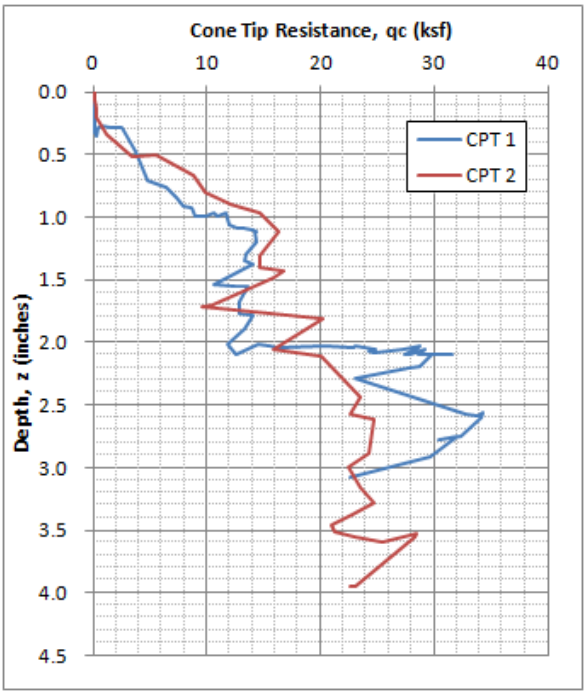

Figure 3.27: Cone Tip Resistance versus Depth in the Cemented Sand Test Bed (Profile Ends at Refusal)

Chapter 4: Suction Can Foundation Scale Models

Two suction can foundation scale models were used in this study: a 1-foot diameter model and a 6-inch diameter model. The dimensions and properties of the two steel models are presented in the following sections.

4.1 One-foot Diameter SCF Model

The 1-foot diameter SCF model (see Figure 4.1) has a 1-foot diameter, 1-foot long suction can and a 3-foot extended arm for applying lateral load. The wall thickness of the suction can is 0.125 inch. A valve installed on the top plate was used to release or increase the pressure inside the suction can. This steel model has a total weight of 38.5 lb.

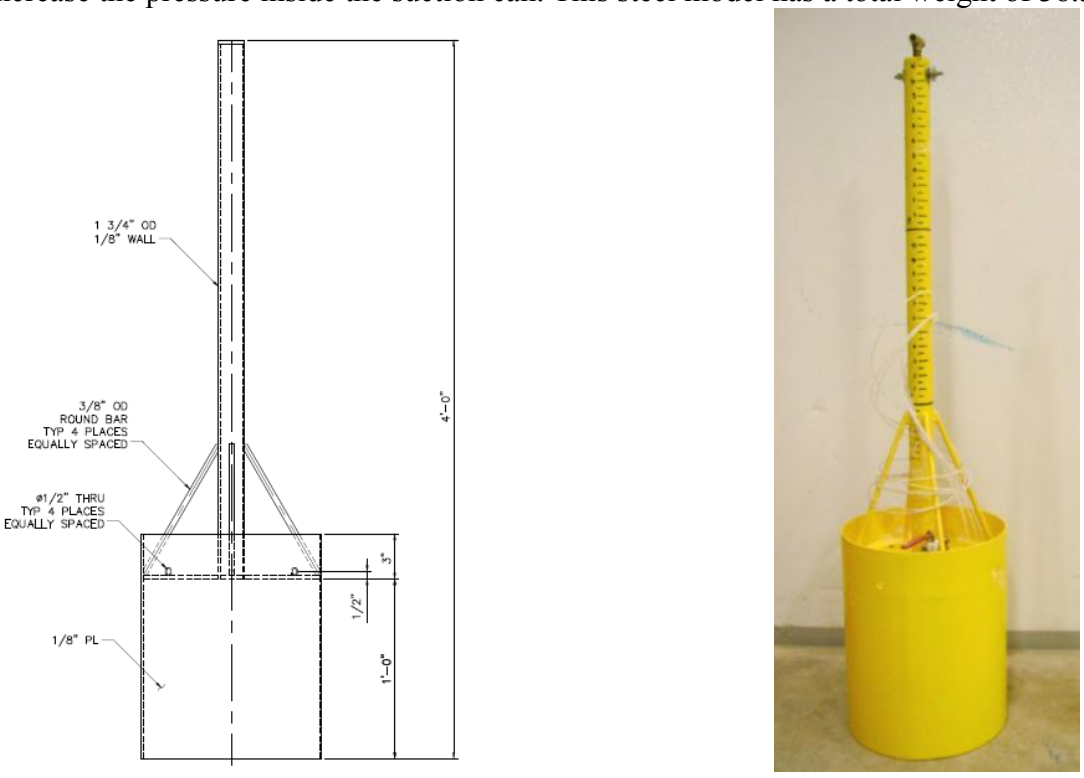

(a) Drawing by Horton Wison Deepwater (b) Photo

Figure 4.1: 1-foot Diameter SCF Model

In order to measure the pore water pressure right below the top plate, one hole on the op plate was drilled and threaded in order to attach a submersible pressure transducer. A layer of nonwoven geotextile was glued blow the top plate to distribute the pore water pressure. For measuring pore water pressures at different depth inside the suction can, three plastic tubes were placed through the top plate with their one ends attached to the inner wall and the other ends connected to pressure transducers. The end of three tubes were located at 1.5, 6.0, and 11.25 inches below the top plate, respectively (designated top, mid, and tip) as shown in Figure 4.2. The ends were covered with nonwoven geotextile patches to prevent soil particles from clogging the tubes while allow water to flow through.

(a) Tubes Though Top Plate (b) Tube Tips with Geotextile on Inner Wall

Figure 4.2: Tubes for Pore Water Pressure Measurement on 1-foot Diameter SCF Model

4.2 SIX-INCH DIAMETER SCF MODEL

The 6-inch diameter SCF model (see Figure 4.3) has a 6-inch diameter, 6-inch long suction can and a 3-foot extended arm for applying lateral load. The wall thickness

of the suction can is 0.125 inch. A valve installed on the top plate was used to release or increase the pressure inside the suction can. This steel model has a total weight of 9.2 lb.

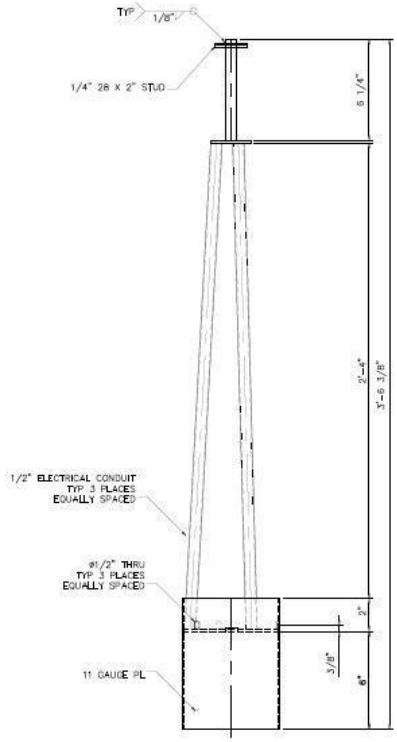

(a) Drawing by Horton Wison Deepwater

(b) Photo

Figure 4.3: 6-inch Diameter SCF Model

Similar to the 1-foot diameter SCF model, one hole on the op plate was drilled and threaded in order to attach a submersible pressure transducer. A layer of nonwoven geotextile patches was also glued blow the top plate to distribute the pore water pressure. However, two plastic tubes instead of three were placed through the top plate with their one ends attached to the inner wall for measuring pore water pressures. The end of two tubes were located at 1.5 and 5 inches below the top plate, respectively (designated top and tip) as shown in Figure 4.2. The ends were covered with nonwoven geotextile

patches to prevent soil particles from clogging the tubes while allow water to flow through.

(a) Tubes Though Top Plate

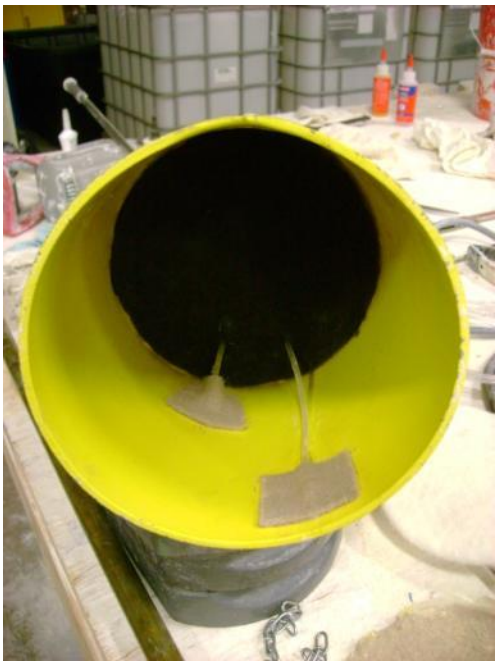

(b) Tube Tips with Geotextile on Inner Wall

Figure 4.4: Tubes for Pore Water Pressure Measurement on 6-inch Diameter SCF Model

Chapter 5: Test Facility and Instrumentation

The load frame, stepper motor, load cell, linear displacement transducer, dial gauge, pressure transducers, tilt meter, data acquisition and control system that were used for this study are presented in the following sections.

5.1 LOAD FRAME

An aluminum load frame was developed to sit on top of the metal tank (Figure 5.1). This load frame was used for the tests conducted in the normally consolidated clay test bed. The loading frame consists of 4 in wide aluminum channels forming a rectangular structure that is 5 ft wide and 4.7 ft tall, and a channel located in the middle of the rectangle. Two 40 in long 3×3×⅜ inch aluminum angles were bolted onto the bottom of the frame. The angles allow the frame to sit on top of a 4 ft wide steel tank and slide along the long dimension. A portion of the rectangular structure was cantilevered off of the angle alignment to allow placement of the motor on the side of the tank.

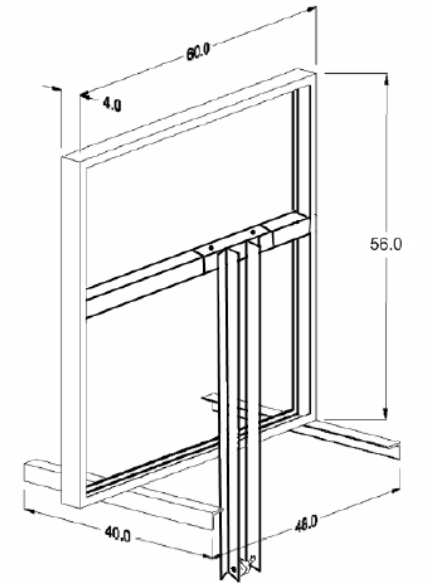

Figure 5.1: Aluminum Load Frame (Kroncke, 2009)

A wooden platform (see Figure 5.2) make out of 2x4 lumbers was built for the model tests in the thermo-plastic tank (overconsolidated clay, loose siliceous sand, cemented siliceous sand, and cemented calcareous sand). An additional 8 ft long, 2x8 wooden member was cantilevered 5 ft off of the aluminum load frame (see Figure 5.3); this cantilevered member was mounted with pulleys for the loading line that connected to the stepper motor.

Figure 5.2: Wooden Load Frame

Figure 5.3: Cantilevered Portion of Load Frame (Gilbert et al. 2012)

5.2 STEPPER MOTOR AND LOADING DEVICE

The loading device consists of primarily of a motor that controls the motion of the loading cables. The device was originally used for tests by El-Gharbawy (1998) and El-Sherbiny (2005). The loading device consists of four main components shown in Figure 5.3: two linear actuators, two stepper motors, two translator drivers, and a computer controller card. Only one actuator and one motor are used in this testing program. The linear actuator was used to transform the rotational motion of the motors into linear translational motion. The motor provides 12.5 inches of vertical motion. The concentric pulley ratio of 3.25 extends the motor displacement to 40.63 in. A data acquisition system, using a National Instruments (NI) motion controller card, is used to control the motor movement (Aubeny et al. 2008).

In order to move the loading device with the load frame, the loading device was mounted on an aluminum plate and suspended from the side of the steel tank, underneath the loading frame (Figure 5.4). An eyebolt was connected to the loading device, where a cable was attached to transfer the motion of the motor to the concentric pulley pair.

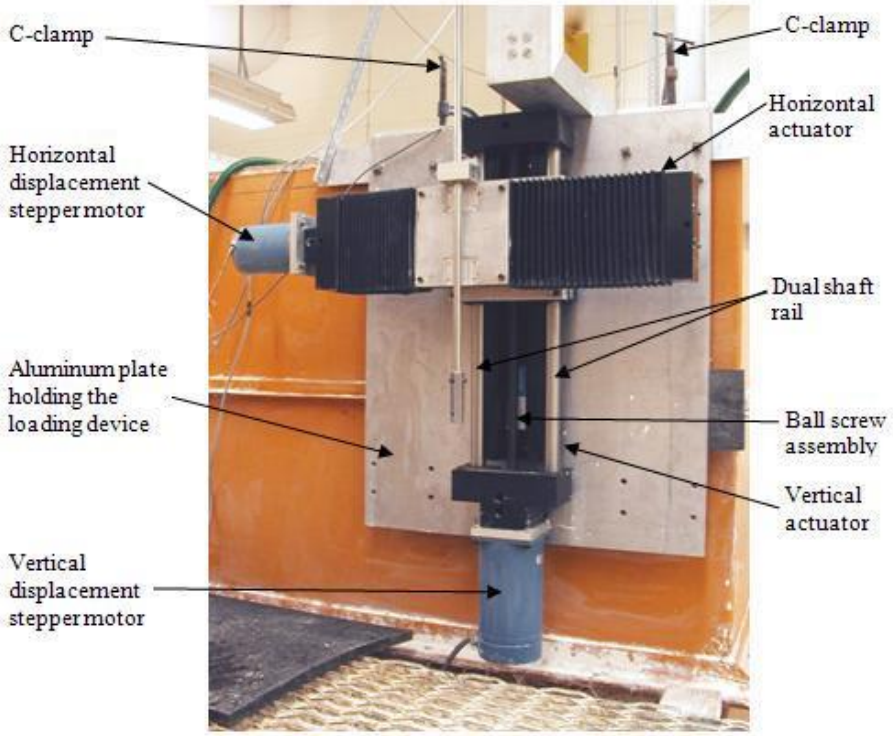

Figure 5.4: Loading Device Components (El-Sherbiny 2005)

5.3 LOAD CELLS

The force is measured with two Lebow load cell for all the testing conducted. One of the Lebow model load cell is rated for 100 lbs and the other is 200 lbs (see Figure 5.5). The 200-lb rated load cell was used for cone penetration tests and pullout tests of the SCF model, while the 100-lb rated load cell was used for the rest of the SCF scale model test including T-bar tests.

Figure 5.5: Lebow Load Cell

5.4 LINEAR DISPLACEMENT TRANSDUCER

Displacement measurements were recorded using an MTS® Temposonics® 2-meter travel position sensor (see Figure 5.6). The sensor was used for measuring vertical or lateral displacement of the SCF model during installation, lateral load tests, pullout tests, and also for cone penetration tests. For displacement measurements using the sensor, one end of a fishing line is attached to the magnet movable long the track of the sensor with the other end connecting to the object that is being measured. The sensor head at the end of the track detects the position of the magnet by the magnetic field and therefore can register the displacement of the object that connected to the magnet. For visual verification of displacement, a steel measuring tape was secured next to the sensor (see Figure 5.7).

Figure 5.6: Linear Displacement Transducer (MTS Systems Corporation)

Figure 5.7: Linear Displacement Transducer (Miller 2009)

5.5 DIAL GAUGE

A mechanical dial gauge by Chicago Dial Indicator (see Figure 5.8) was used for measuring the settlement or vertical movement of the SCF model. This dial gauge has a graduation of 0.001 inch and a total range of travel of 1 inch. An adjustable wooden holder was built to mount the dial gauge on the load frame and accommodate the dial gauge to measure the displacement near the top of the extended arm of the SCF model.

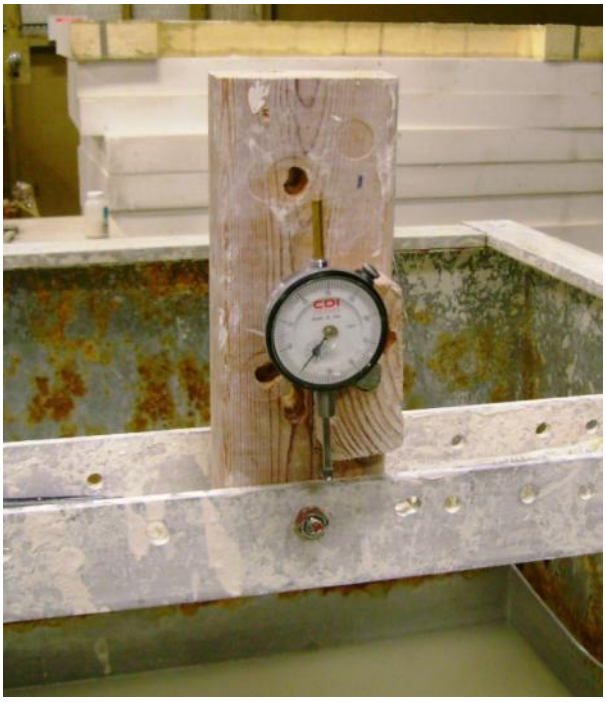

Figure 5.8: CDI Dial Gauge

5.6 PRESSURE TRANSDUCERS

Submersible Druck pressure transducers (see Figure 5.9), Model PDCR 1830, were used to measure excess pore water pressures inside the suction can for this study. The pressure transducers were previously used in the research on the suction caissons (El-Sherbiny 2005). The pressure transducers had an operational pressure range of ±10 psi; however, the transducers were calibrated for use in the pressure range of ±2 psi. The pressure transducers were chosen to have the full range of ±10 psi to ensure that the safe range would not be exceeded during tests. A brass-adapter was used to transform from the threading at the sensing end of the transducer to a quick connect fitting for direct connection to the ⅛-inch tubing connecting to the sensing tip (geotextile patch) on the wall of SCF models.

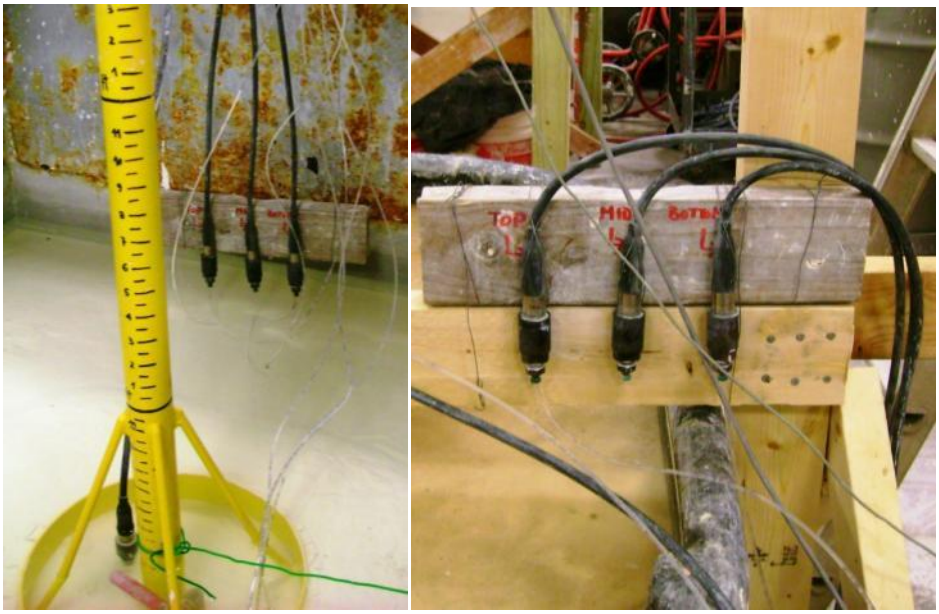

Figure 5.9: Druck PDRC 1830 Pressure Transducers

5.7 TILT METER

A Crossbow CXTA02 tilt meter was used to measure the tilt of the caisson in two orthogonal directions and had a full range of ± 70^{o} with a linear range of ± 20^{o}. The angle of tilt measured using the tilt meter is theoretically proportional to the sine of the ratio of the change in output voltage to the sensitivity. However, for small angles within the linear range, the angle of tilt can be assumed proportional to the change in output voltage with a nonlinearity of 2% full-scale as reported by the manufacturer.

Figure 5.10: Crossbow CXTA02 Tilt Meter (Crossbow Technology, Inc.)

Chapter 6: Tests in Normally Consolidated Clay Test Bed

The 1-foot diameter SCF model was used in the normally consolidated clay (NC clay) test bed. The properties of the normally consolidated clay test bed can be found in Section 2.1. The scale model tests conducted in this test bed includes: installation, lateral load tests, pore water pressure dissipation between tests, hydraulic lifting process, axial load tests, ultimate axial capacity tests, and pullout. The test procedure and the summary of test results are presented in the following sections.

6.1 INSTALLATION

The 1-foot diameter SCF model was installed in the normally consolidated clay by its own weight. The total weight of the model plus the pressure transducer on the model was 39.13 lbs. The valve on the top plate was opened to allow water flowing out of the suction can during installation, and was subsequently closed once the model was fully installed without further downward movement. The valve was kept closed for all the tests expect the jack up process as presented in Section 6.3. During installation, the penetration rate was controlled at 1.5 in./min using a steel wire hanging the model from the load frame and connected to the stepper motor (see Figure 6.1). A load cell was used to measure the tension in the steel wire, and the linear displacement transducer was also connected to the model to monitor the vertical displacement.

Figure 6.2 shows the vertical load (or tension in the loading line) versus the foundation tip depth below mudline during installation. The tension in the loading line decreases from around 40 lb (total weight of the model) when the model is hanging in the air (where tip was 2.3 inches above mudline) to 0 lb when the model is installed completely and all the weight is taken by the soil.

The force required for the SCF model to penetrate for 1 foot for installation can be calculated by the inner and outer wall side shear resistance plus the bearing resistance from the tip area of the cylindrical wall. The calculated total resistance for installation according to API (see Equation 2.1) is approximately 26 lb, which is less than the (net) weight of the suction can. This confirms that the 1-foot diameter SCF model can be installed in the normally consolidated clay test bed by its own weight. Note that for the calculation of the installation resistance, an undrianed shear gradient of 14 psf/ft with zero undrained shear strength at mudline was used for the normally consolidated clay according to Section 2.1. The adhesion factor between the soil and the foundation (α) is assumed to be 0.5 (based on α=1/sensitivity and sensitivity of soil = 2) for both inner and outer wall. The bearing capacity factor for tip resistance of the wall (N_c) is assumed to be 7.5, which is an analog to a buried strip footing (API RP 2SK A2008).

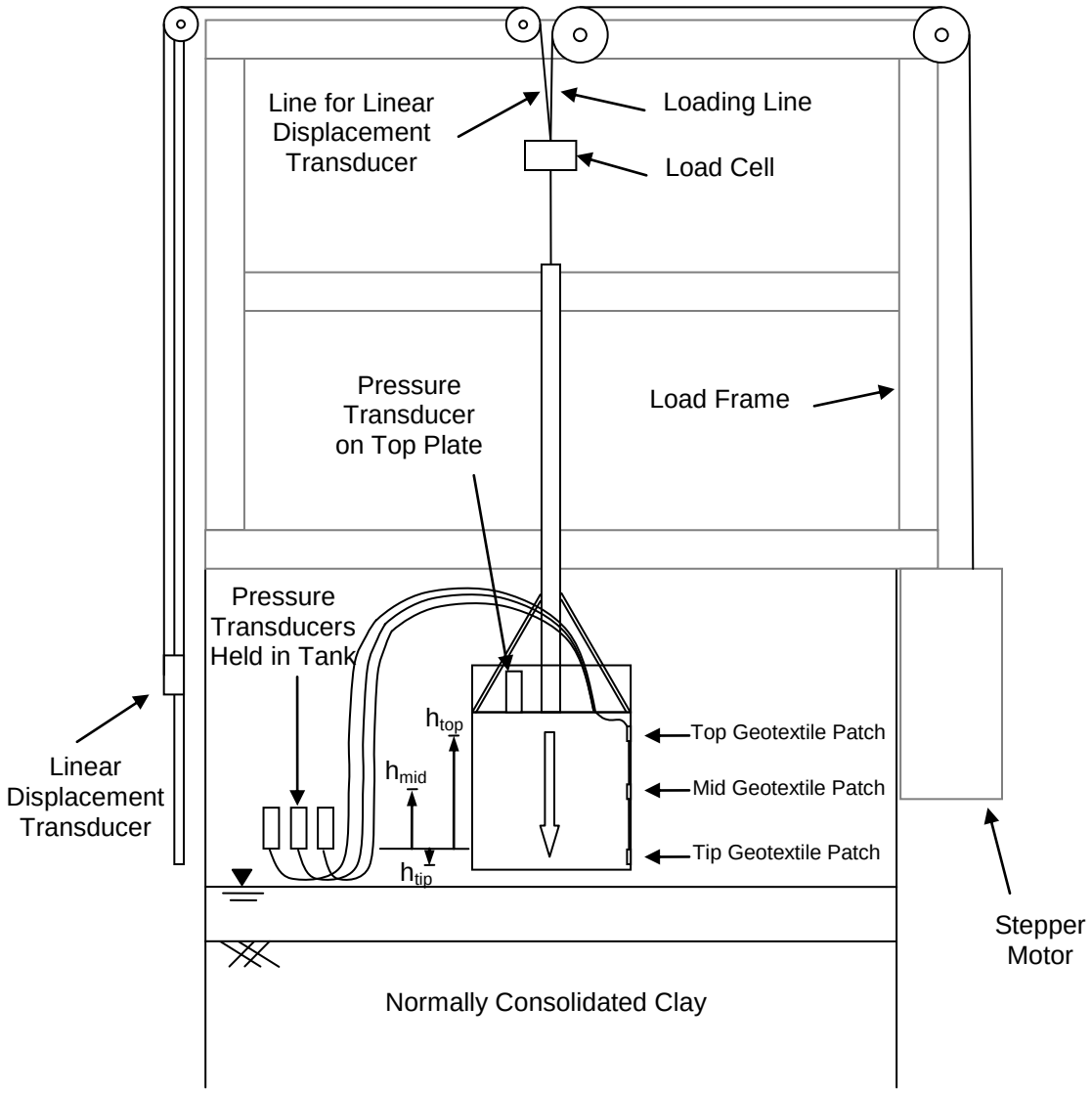

Figure 6.1: Schematic for Installation of 1-foot Diameter SCF Model in Normally Consolidated Clay

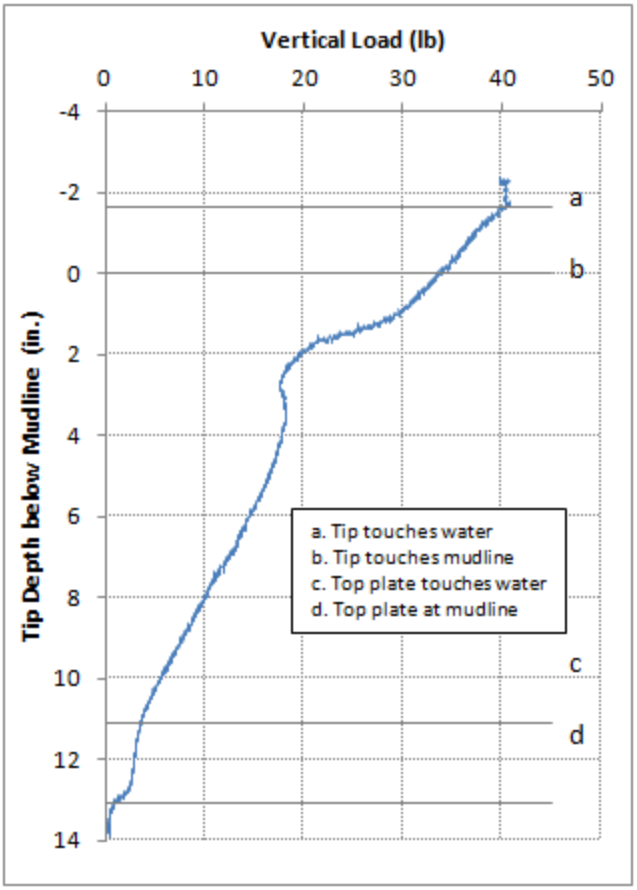

Figure 6.2: Vertical Load versus Tip Depth below Mudline during Installation of 1-foot Diameter Model in Normally Consolidated Clay

Figure 6.3 shows the measured pore water pressures versus vertical displacement. Since the elevation of the end the pore water pressure tube changes when the model is moving downward, elevation head correction for Top, Mid, and Tip pore water pressures are required. As shown in Figure 6.1, in order to obtain the pore water pressure at Top, Mid, and Tip locations, the water head (h_{top}, h_{mid}, and h_{tip}) need to be subtracted from the measured pressures. Therefore, the additional pressures due to the weight of the water in the tubes are not included in the pore water pressures as shown in Equation 6.1. The corrected pore water pressures versus vertical displacement are shown in Figure 6.4.

$$p_{pore,i} = p_{measured,i} - h_i\gamma_w \qquad \text{(Equation 6.1)}$$

$p_{pore,i}$ = pore water pressure at Top, Mid, or Tip corrected for elevation change (psf)

$p_{measured,i}$ = measured pore water pressure for Top, Mid, or Tip (psf)

h_i = elevation difference between pressure transducers and water tube ends at Top, Mid, or Tip (ft)

γ_w = unit weight of water = 62.4 pcf

Note that the values of h_i are variables which changes with the vertical displacement. Elevation correction is not required for the transducer attached on the top plate because it moves with the model during installation.

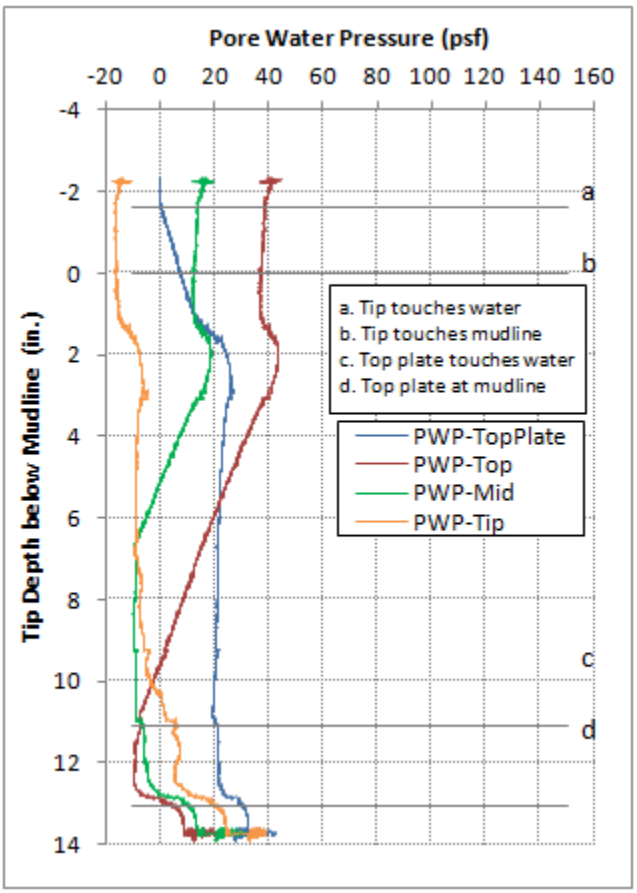

Figure 6.3: Measured Pore Water Pressure versus Tip Depth during Installation of 1-foot Diameter Model in Normally Consolidated Clay

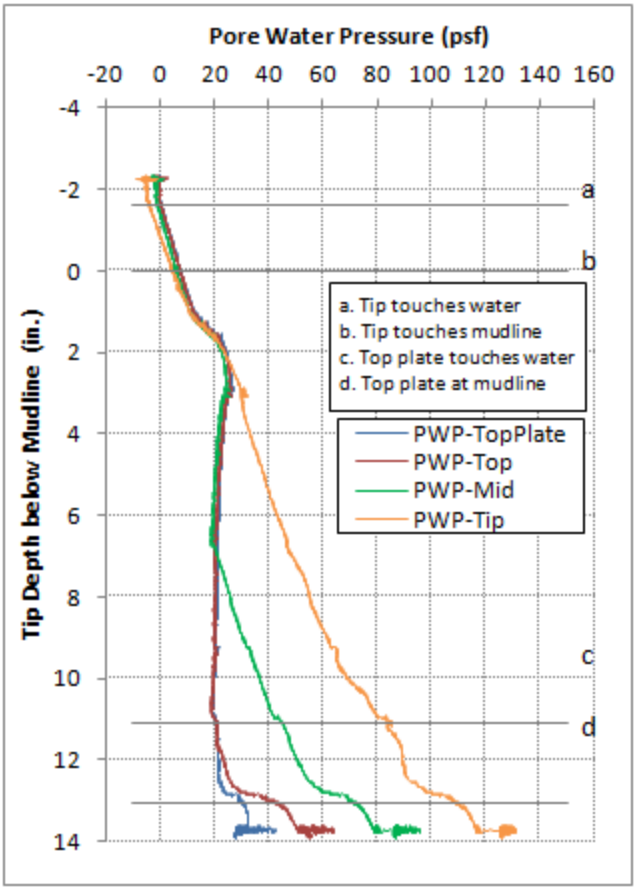

Figure 6.4: Pore Water Pressure (Corrected for Elevation Change) versus Tip Depth during Installation of 1-foot Diameter Model in Normally Consolidated Clay

Figure 6.4 shows that the pore water pressures stay around 0 psf before the tip of the SCF model touches the water and the whole model is in the air. Soon after the tip of the model touches the water, the Tip geotextile patch is also submerge in the water. Therefore, the Tip pore water pressure increases almost linearly because the model is moving downward at a constant rate and so does the water pressure. In addition, Excess pore water pressure generated during the penetration also attribute to the increase of pressure. The other pressures (Top Plate, Top, and Mid) also increase linearly at the same time because the air is being compressed inside the suction can and the air has not yet

"broken through" the saturated geotextile right below the top plate and the valve. When the foundation penetrates to 2 inches, the air trapped inside the suction can starts to release through the valve. Therefore, the pressure inside stops increasing and remains constant around 20 psf as shown by the Top Plate, Top, and Mid pressures. When the foundation penetrates 7 inches, the Mid geotextile patch is submerged in the water and the pressure starts to increase linearly. The Top and Top Plate geotextile are submerged at penetrations of 11 and 13 inches, respectively.

Figure 6.5 compares the calculated hydrostatic pressures with the pore water pressures at Top, Mid, and Tip. The pore water pressures match the hydrostatic pressures very well until each of the geotextile patch are embedded deep enough in the clay to generate excess pore water pressure (pore water pressure minus hydrostatic pressure).

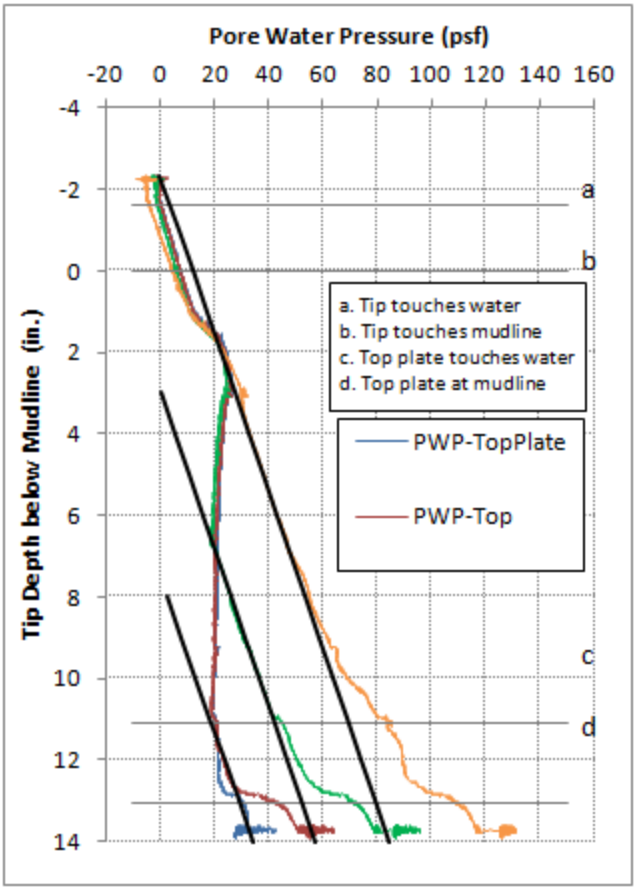

Figure 6.5: Comparing Pore Water Pressure (Corrected for Elevation Change) with Hydrostatic Pressure during Installation in Normally Consolidated Clay

6.2 Lateral Load Tests

Two-way, displacement controlled, cyclic lateral load tests were conducted in order to simulate the behavior of the suction can foundation and buoyant tower system in storm waves. The lateral resistance, the walking displacement (translational permanent displacement), and the settlement were measured for 1000 cycles of lateral load with the 1-foot diameter SCF model in the normally consolidated clay.

As shown in Figure 6.6, 6.7, and 6.8, cyclic lateral displacement was applied on the extended arm of the model at 3 ft above the mudline such that the model rotates

cyclically with a cyclic total rotation of 1, 2, or 5 degrees (±0.5, ±1.0, or ±2.5 degrees from vertical). The model was tested with periods of 3, 5, and 10 seconds for each rotation angles. The lateral displacements were applied though the loading line by the pulley and stepper motor system (see Figure 6.7 and 6.8). Dummy Weights were hanged from the opposite side from the motor to counter act the lateral movement since the motor system can only pull the model to the right (the motor side).

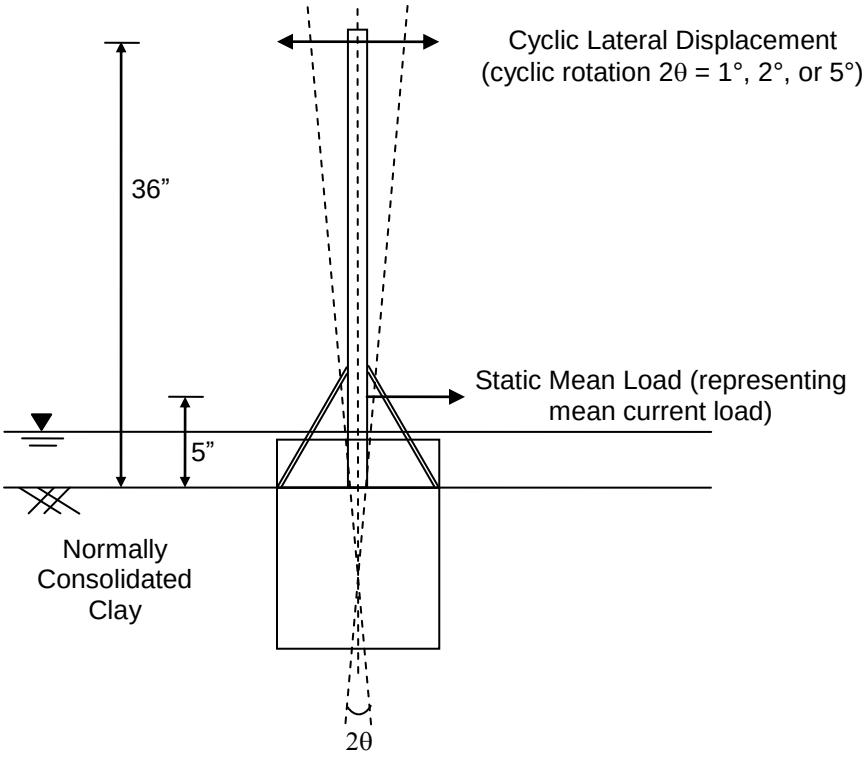

Figure 6.6: Schematic for Lateral Loads Applied on 1-foot Diameter SCF Model

A static mean load was applied at 5 inches above mudline to simulate the current load (see Figure 6.6). The mean load was applied by a dead weight and the loading line-pulley system as shown in Figure 6.7 and 6.8. The applied mean loads, which were

proportional to the model rotation, were 1.8, 3.6, and 9.0 lb for rotation angles of 1, 2, and 5 degrees respectively.

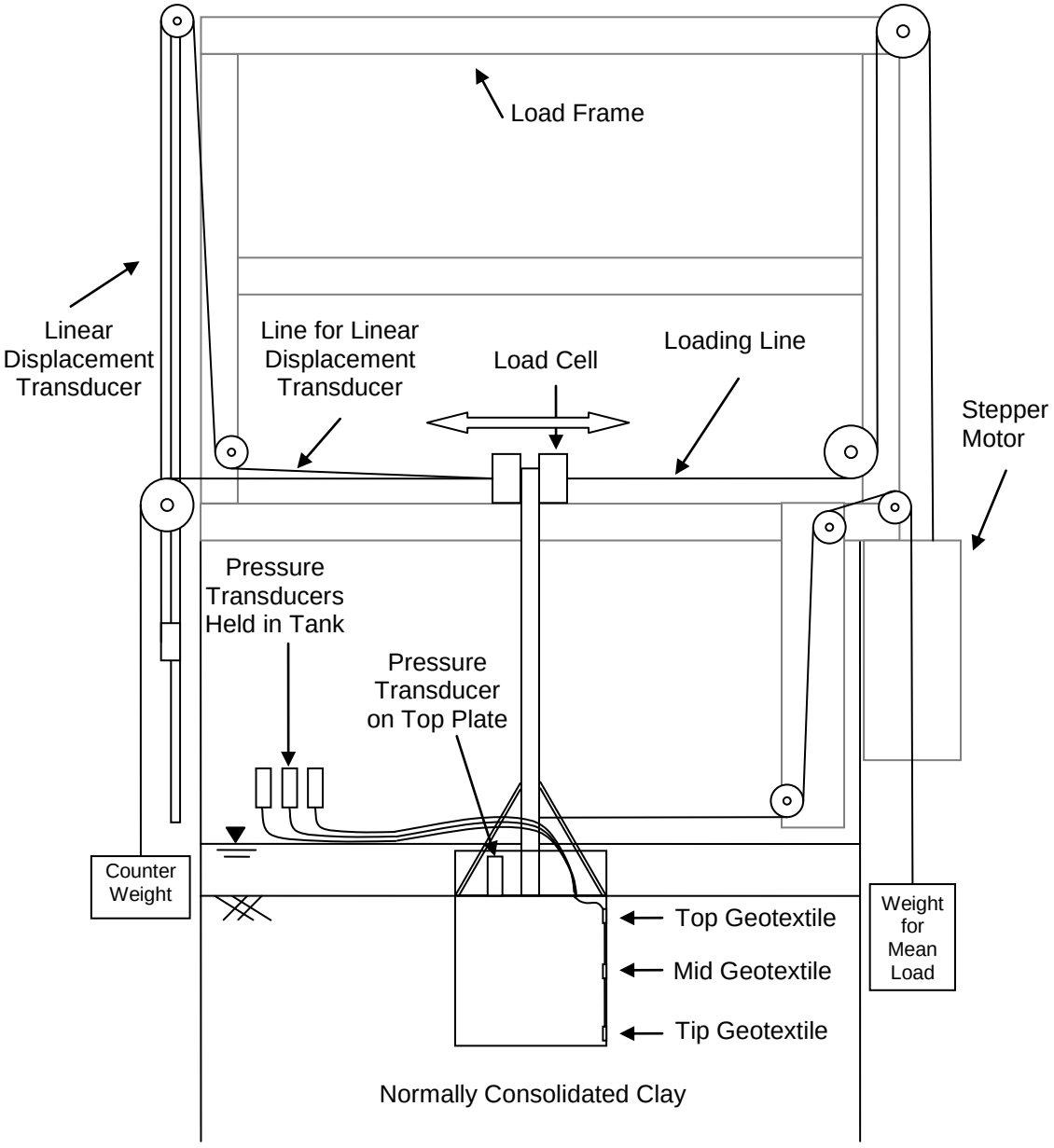

Figure 6.7: Schematic for Lateral Load Tests of 1-foot Diameter SCF Model in Normally Consolidated Clay

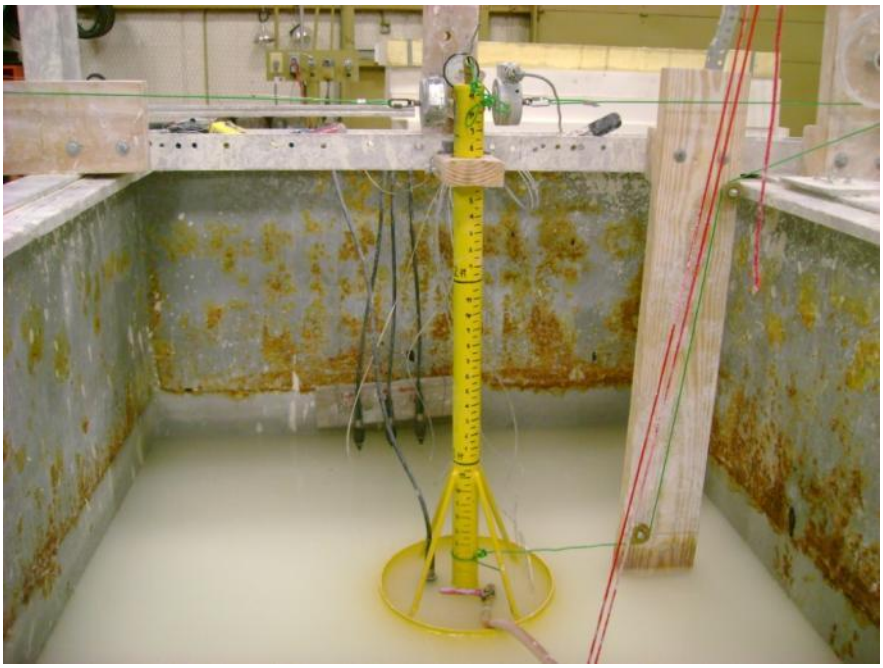

Figure 6.8: Lateral Load Tests of 1-foot Diameter SCF Model in Normally Consolidated Clay

The lateral load required to rotate the model was measured by a load cell attached to the extended arm on the right side. The lateral displacement was measured by the linear displacement transducer with a fishing line connecting to the extended arm (see Figure 6.7). The tilt meter was placed near the top of the extended arm of the model to measure the tilt angle (see Figure 6.9). A dial gauge installed near the top of the extended arm (see Figure 6.9) was used to measure the settlement of the model by comparing the reading before and after 1000 cycles of load. The walking displacement (translational permanent displacement due to the mean load) of the model was obtained by comparing the linear displacement transducer reading before and after 1000 cycles of load. The model was ensured to be leveled and the extended arm to be vertical according to the tilt meter readings and occasionally checked using a level. Pore water pressures inside the

suction can were monitored by one pressure transducer directly attached to the top plate of the model and three others connected to Top, Mid, and Tip location on the inner wall with water tubes (see Figure 6.7 and 6.8).

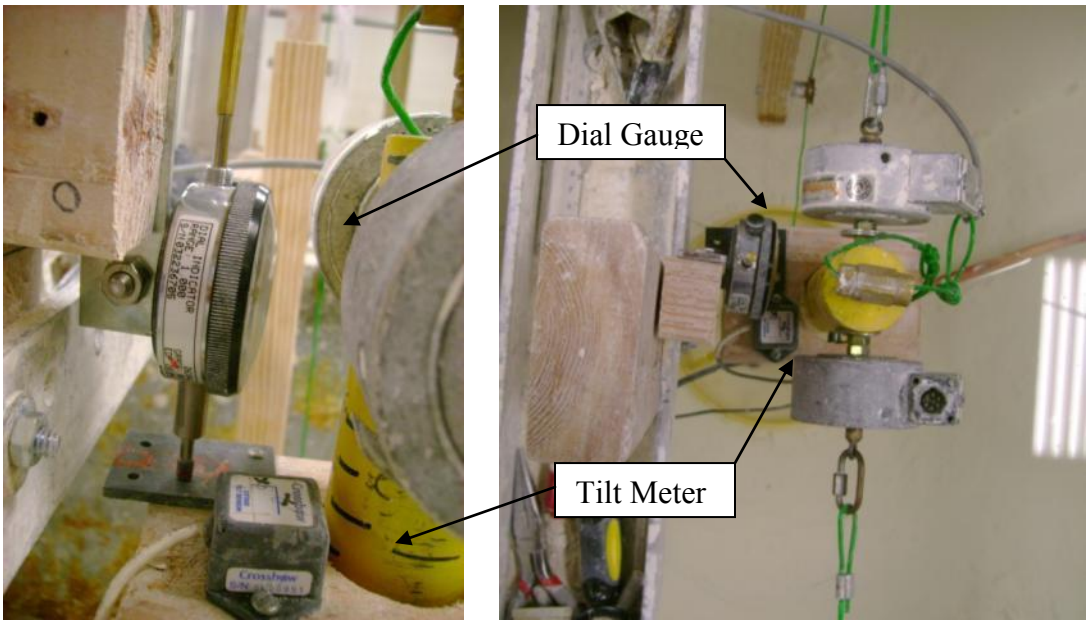

(a) Side View (b) Top View

Figure 6.9: Tilt Meter and Dial Gauge on 1-foot Diameter SCF Model

6.2.1 Walking and Settlement

Table 6.1 shows the walking displacement and the settlements of the 1-foot diameter SCF model after 1000 cycles of lateral load for each rotation and period combination in the normally consolidated clay test bed. Two tests were repeated because of using an incorrect mean load and unintentionally leaving the top plate valve open during the tests. The walking displacement and settlement of the model are illustrated in Figure 6.10 and 6.11 respectively except the two tests that did not meet the original test requirements.

Figure 6.10 shows the walking displacement versus different ration angles and load periods for the lateral load tests in normally consolidated clay. The walking of the model is negligible with 1 degree of rotation. However, the walking displacement increases with increasing rotation of the model. For 2-degree rotation, the walking displacement increases to 0.37 inch (3% of the foundation diameter or D) with a loading period of 3 seconds. For 5-degree rotation, the model walks significantly due to the 9 lbs of mean load pulling the model to the right (the motor side); the walking distance ranges from 1.25 to 1.98 inches (0.1 to 0.17 D) with periods from 10 to 3 seconds. Walking of the model is more prominent with larger rotations and shorter periods.

Soil Type	SCF Model	Rotation (degrees)	Period (seconds)	Mean Load (lbs)	Walking Displ. (inches)	Settlement (inches)	Test Date
Normally Consolidated Clay	1-foot Diameter Model	1	3*	0.9*	0.00	0.129	7/23/2012
			3	1.8	0.00	0.111	7/23/2012
			5	1.8	-0.05	0.121	7/23/2012
			10	1.8	0.00	0.080	7/23/2012
		2	3**	3.6	0.30	0.432	7/16/2012
			3	3.6	0.37	1.110	7/16/2012
			5	3.6	0.25	1.290	7/17/2012
			10	3.6	0.05	0.469	7/17/2012
		5	3	9.0	1.98	2.183	7/24/2012
			5	9.0	1.47	2.738	7/24/2012
			10	9.0	1.25	2.915	7/25/2012

* Tested with half (0.9 lb) of the target mean load (1.8 lb). This was later repeated with 1.8 lb of mean load.

** Tested with top plate valve open for 246 cycles. This test was later repeated with the valve shut.

Table 6.1: Walking and Settlement of 1-foot Diameter SCF Model after 1000 cycles of lateral load in Normally Consolidated Clay

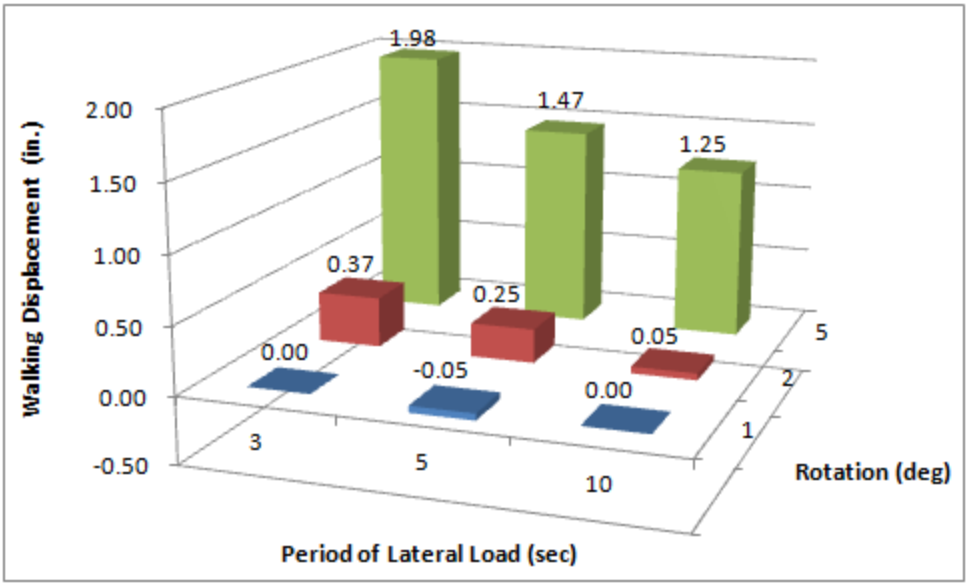

Figure 6.10: Walking of 1-foot Diameter SCF Model in Normally Consolidated Clay

Figure 6.11 shows the settlement versus different ration angles and load periods for the lateral load tests in normally consolidated clay. According to this figure, the settlement increases with increasing rotation of the model. Settlements of the model are not significant (approximately 0.01 D) with 1 degree of rotation. For 2-degree rotation, settlements increase to between 0.469 and 1.110 inches (0.04 to 0.11 D). For 5-degree rotation, the model has a significant settlement ranging from 2.183 to 2.915 inches (0.18 to 0.24 D).

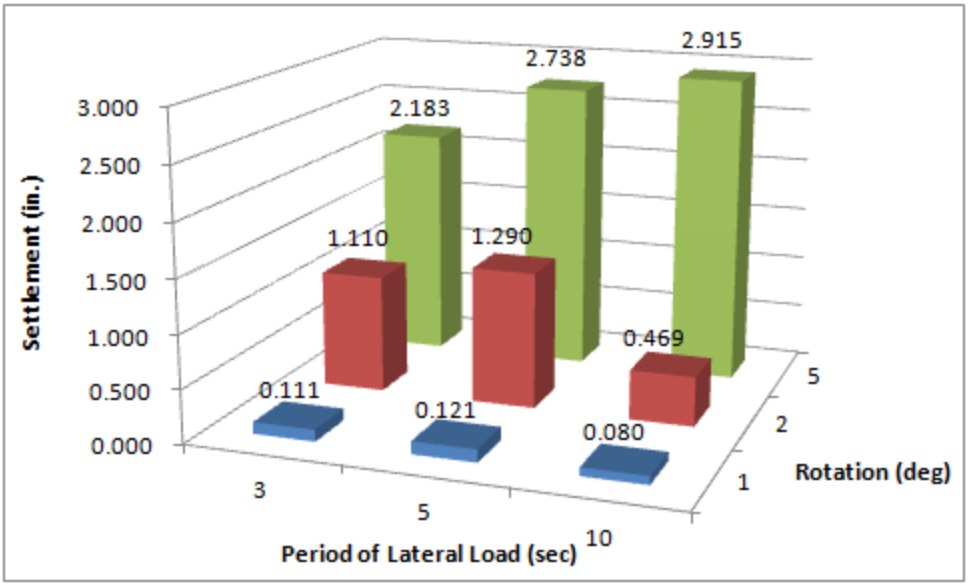

Figure 6.11: Settlement of 1-foot Diameter SCF Model in Normally Consolidated Clay

Pictures of the 1-foot SCF model after lateral load tests in the normally consolidated clay are shown in Figure 6.12 and Figure 6.13. The circular zone of disturbed soil extended to approximately 0.8 diameter out from the model. No significant gap formed between the model and the soil during the lateral tests except a small gap opened up during 5-degree rotation tests. Figure 6.13 shows that the model was covered with clay and was pull closer to the right at the end of the test because of the significant settlement and walking.

Figure 6.12: SCF Model after 1 and 2-degree Lateral Load Tests in NC Clay

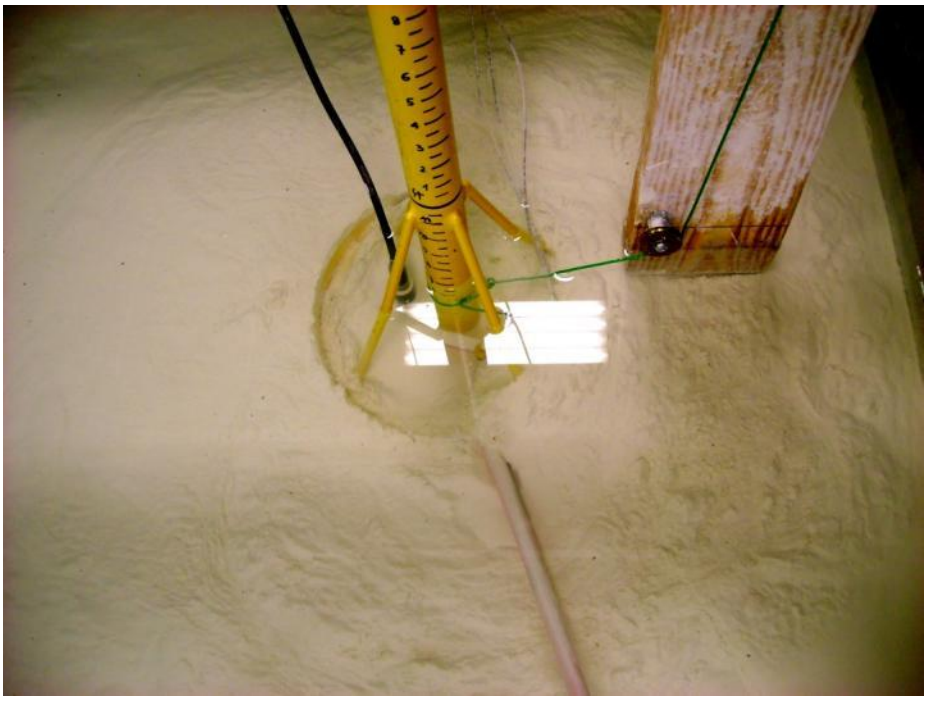

Figure 6.13: SCF Model after 5-degree Lateral Load Tests in NC Clay

6.2.2 Lateral Load, Displacement, Pore Water Pressure, and Tilt Angle

In terms of the lateral load, lateral displacement, pore water pressure, and tilt angle measurements, the 2-degree rotation and 5-second period test is taken as an example for the lateral tests in normally consolidated clay.

The time history of the 1000-cycle lateral load and lateral displacement are presented in Figure 6.14 and 6.15. The lateral load and displacement are both measured at 3 ft above the top plate of the model (or 3 ft above the mudline) as shown in Figure 6.6. The hysteresis loops of later load versus lateral displacement are shown in Figure 6.16.

In Figure 6.14, positive lateral displacement indicates that the model tilts to the right while negative displacement indicates left tilting movement. The lateral displacement shifts to the right side (to the positive side) slightly as the load cycle increases because the model walks to the right for 0.25 inch at the end of the test. The load shown in Figure 6.15 and 6.16 are obtained by subtracting the weight of counter weights (see Figure 6.7) from the lateral load measured by the load cell. The original measured lateral load in Figure 6.15 fluctuated periodically with a mean around 10 lb. After subtracting the 10.53 lb load from the counter weight, the mean shifted closer to 0 lb while showing positive loads when the model tilts to the right and negative loads when it tilts to the left. However, the mean is approximately -1.3 lb instead of 0 lb because of the presence of mean load (3.6 lb in this case) as shown in Figure 6.6 and 6.7. The shift of measured lateral load due to the 3.6-lb mean load can be estimated using force and moment equilibrium as shown in Figure 6.17 by assuming the soil reaction acting at the 2/3 of the length of the suction can.

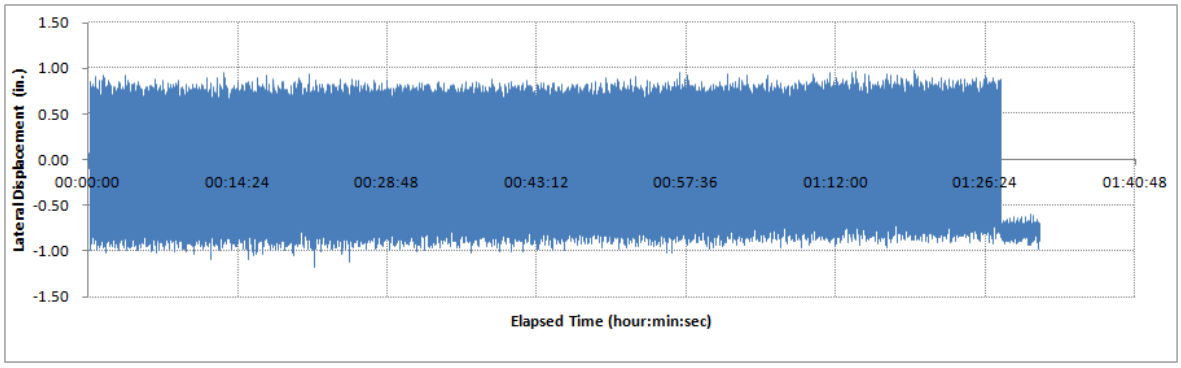

Figure 6.14: Lateral Displacement of 1-foot Model in NC Clay (2° rotation, 5-sec period)

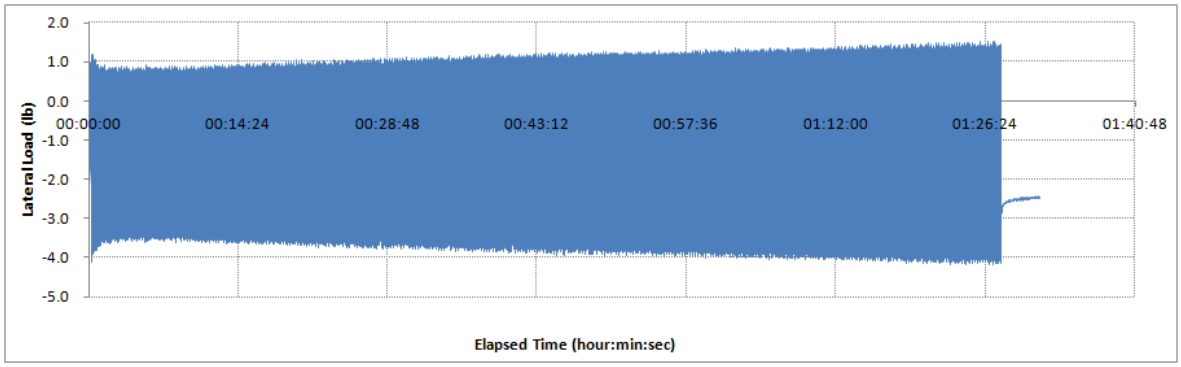

Figure 6.15: Lateral Load of 1-foot Model in NC Clay (2° rotation, 5-sec period)

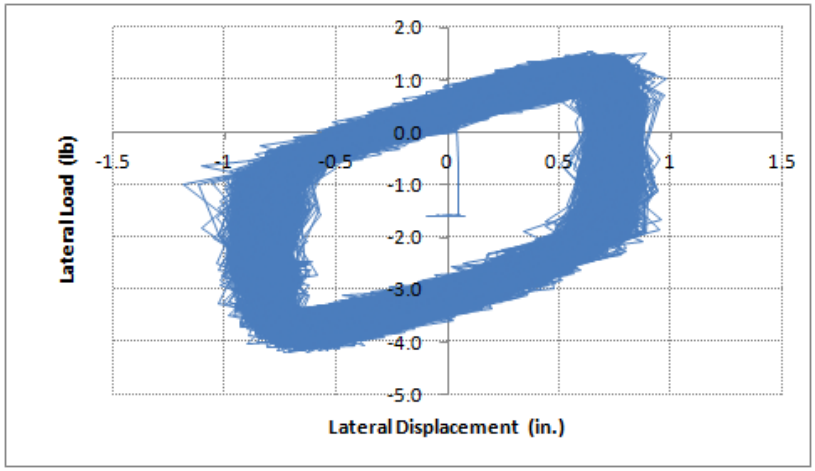

Figure 6.16: Lateral Load versus Lateral Displacement of 1-foot Model in NC Clay (2° rotation, 5-sec period)

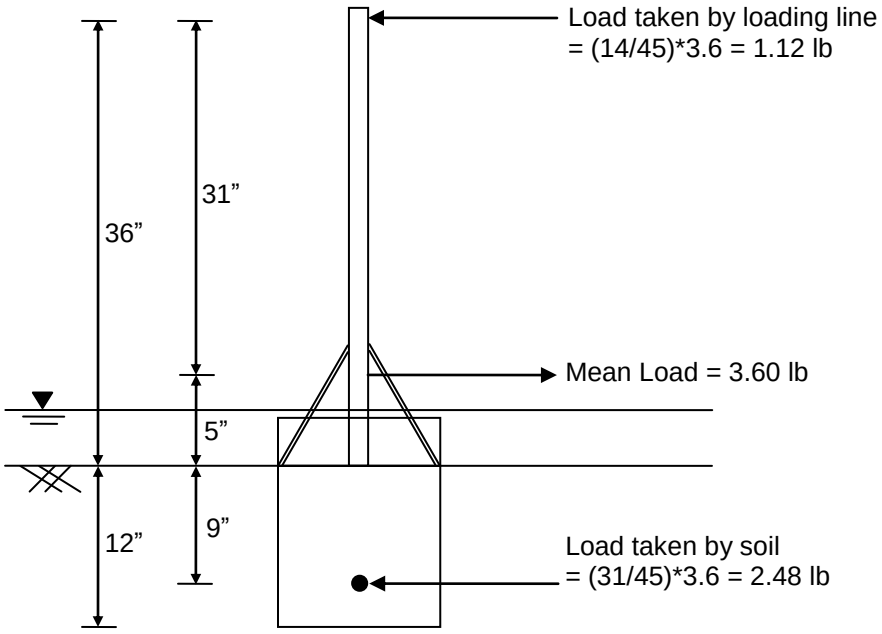

Figure 6.17: Change of Tension in Lading Line due to Mean Load of 1-foot Model in NC Clay (2° rotation, 5-sec period)

In Figure 6.15, the measured lateral load (or lateral resistance) is higher in the first cycle because of the effect of setup and, subsequently, the lateral load decreases in couple cycles due to the soil disturbance. Then, the lateral load starts to increase again throughout the rest of the tests; the range of load was 0.8 to -3.5 lb before it increases to 1.5 to -4.1 lb. The range of load increases by 30% (increases from 4.3 lb to 5.6 lb). This “stiffening” behavior may be attributed to the settlement of the model because the model penetrates deeper into the soil. The settlement of the model for 2-degree rotation and 5-second period is 1.29 inches as shown in Table 6.1.

In order to demonstrate the “stiffening” effect due to settlement, the program FALL16 is used to calculate the lateral capacity of the model before and after the 1.29-inch settlement occurs. Table 6.2 summarized the input parameters and Table 6.3 shows

the calculated lateral capacity using FALL16 with and without the 1.29-inch settlement. The lateral capacity increases by 25% if a settlement of 1.29 inches occurs. This 25% increase in lateral capacity due to settlement explains most part of the 30% increase in the measured lateral load in the test. Soil stiffening due to the cyclic load can also contribute to part of the increase. Figure 6.18 shows that the "stiffening" is not significant for 1-degree lateral load tests because the settlement is approximately 1/10 of the 2-degree tests. Other factors such as soil stiffening due to cyclic loadings can also contribute to the "stiffening" behavior.

In general, the lateral resistance of the foundation increases with increasing rotation angle of the model in normally consolidated clay. The difference is more prominent when the rotation increases from 2 degrees to 5 degrees. However, the difference of the lateral load for different loading period is not significant.

Caisson Diameter	Load Inclination	Soil Strength at mudline	Soil Strength Gradient	Soil Unit Weight	Interface Friction Coeff. α
1 ft	0 deg	0 psf	7 psf/ft	40 pcf	1.0

- Undrained shear strength gradient of 7 psf/ft represents a remolded strength in the normally consolidated clay test bed (see Section 2.1).

Table 6.2: Input Parameters for Calculating Lateral Capacity using FALL16

Settlement	Caisson Length	Depth of Load Application	Depth to Center of Rotation	Lateral Capacity	Increase in Lateral Capacity due to Settlement
0.00 in.	1.00 ft	-3.00 ft	0.70 ft	3.10 lb	-
1.29 in.	1.12 ft	-2.88 ft	0.80 ft	3.88 lb	25%

Table 6.3: Calculated Lateral Capacity with and without Settlement by FALL16

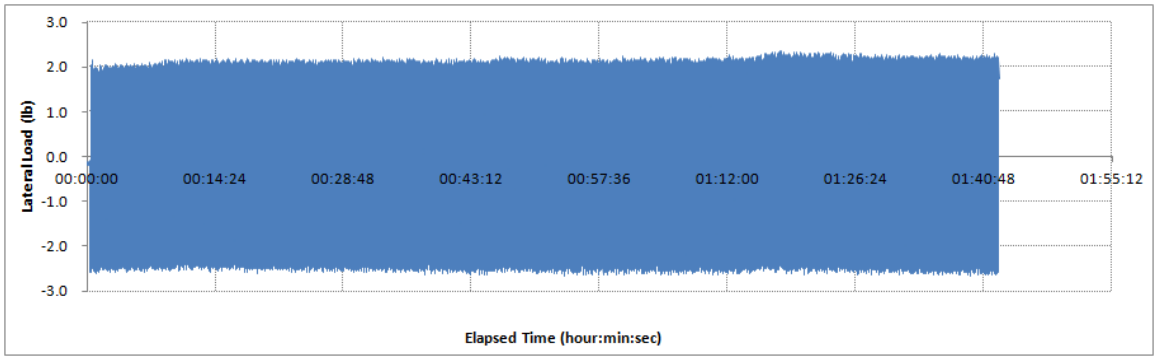

Figure 6.18: Lateral Load of 1-foot Model in NC Clay (1° rotation, 5-sec period)

The excess pore water pressures for the 2-degree rotation and 5-second period lateral load test are shown in Figure 6.19 and 6.20. The excess pore water pressures are calculated by subtracting the hydrostatic pressures from the corresponding measured pore water pressures. The figures indicate that the excess pore water pressure has larger fluctuations near the tip of the model (closer to the failure plane under the suction can) under cyclic lateral loads. The mean excess pore water pressure is between 40 to 70 psf because the excess pore water pressure built up due to the weight of the model has not dissipated. The total stress under the 1-foot diameter model with 35 lb net weight is approximately 45 psf, which is consistent with the measured mean excess pore water pressure. Since the tubes and the geotextile patches for pressure measurements are on the right side of the inner wall of the model, the excess pore water pressures increase when the model tilts to the right and decrease when it tilts to the left because of the suction generated.

The tilt angles for the 2-degree rotation and 5-second period lateral load test are shown in Figure 6.21 and 6.22. The tilts angles are measured in both the loading direction (left-right direction in Figure 6.7) and the direction perpendicular to loading (in-and-out of paper direction in Figure 6.7). The tilt angle in the direction perpendicular to loading is

close to zero degree as expected. The tilt angle in the loading direction fluctuates between -1.5 and 1.7 degrees, where the positive angle indicates that model tilts to the left and negative angle indicates right-tilting movement. The measured tilt angle is larger than the target tilt of -1.0 to 1.0 degree because the tilt meter is not accurate under fast acceleration and de-acceleration. Therefore, the tilt angle is more accurate for 10-second period tests but less accurate for tests with shorter loading period.

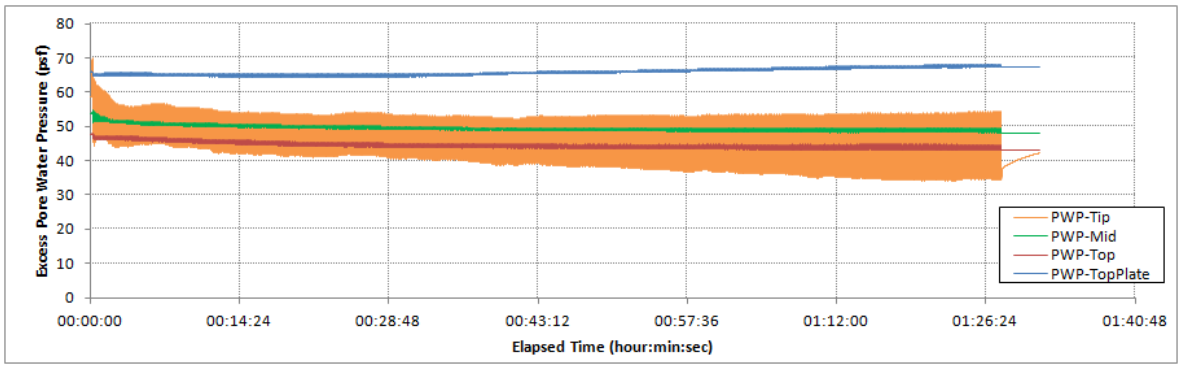

Figure 6.19: Excess Pore Water Pressure of 1-foot Model in NC Clay (2° rotation, 5-sec period)

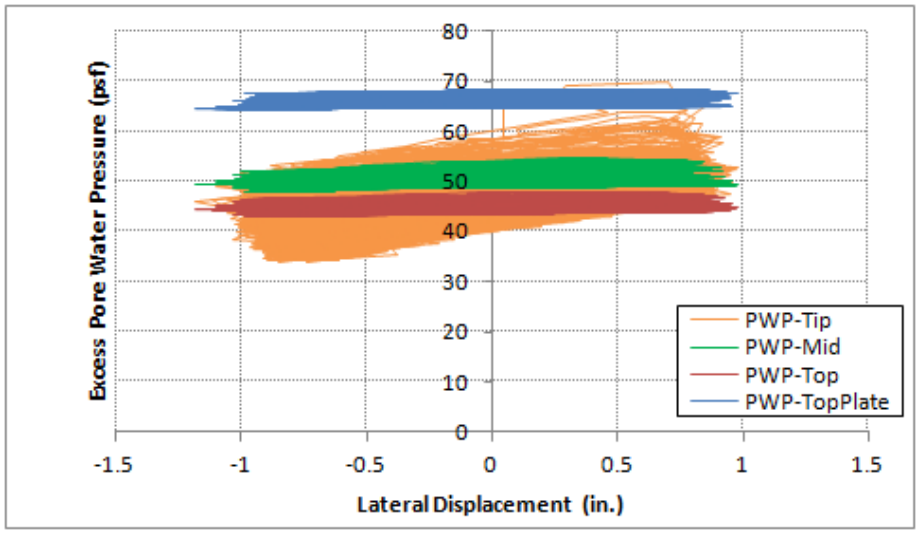

Figure 6.20: Excess Pore Water Pressure versus Lateral Displacement of 1-foot Model in NC Clay (2° rotation, 5-sec period)

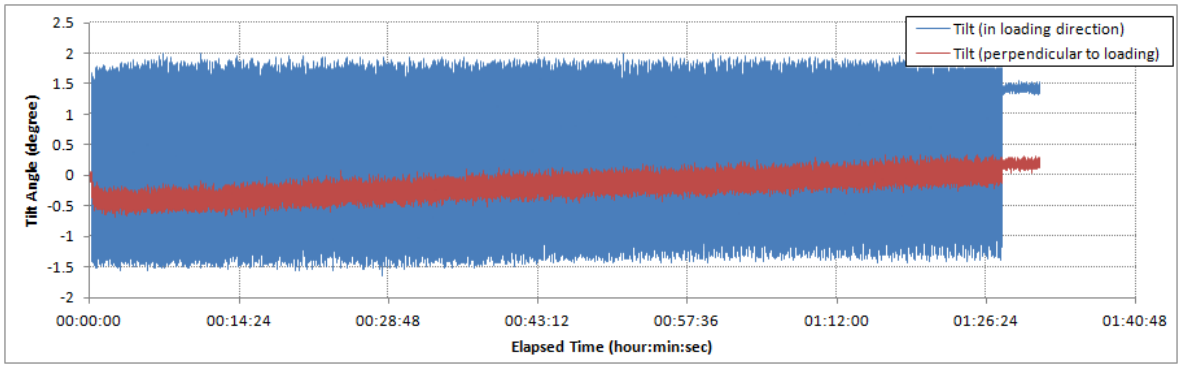

Figure 6.21: Tilt Angles of 1-foot Model in NC Clay (2° rotation, 5-sec period)

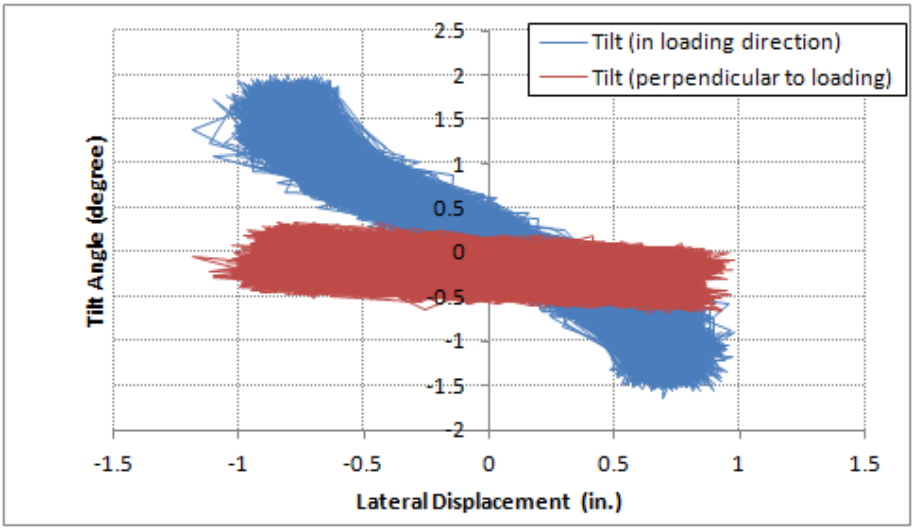

Figure 6.22: Excess Pore Water Pressure versus Lateral Displacement of 1-foot Model in NC Clay (2° rotation, 5-sec period)

6.3 HYDRAULIC LIFTING

In order to raise the model back to its original elevation to overcome accumulated settlement after several lateral load tests, the model was hydraulically lifted by increasing the pressure inside the suction can. The model start to move upward when the increase water pressure is large enough to overcome the weight of the model and the friction

between the soil and the wall of the suction can. When the model was raised up, the soil plug inside the suction can was push out by the injected water through the valve. Static hydraulic head was applied through a water hose with one end connected to the valve on the top plate of the model while the water hose was hold vertically at the other end. The water hose was used as a standing pipe and the water head was kept at around 15 inches above the water level in the tank by pouring water consistently into hose through a funnel (see Figure 6.23). The valve was closed when the model was raised back to its original elevation.

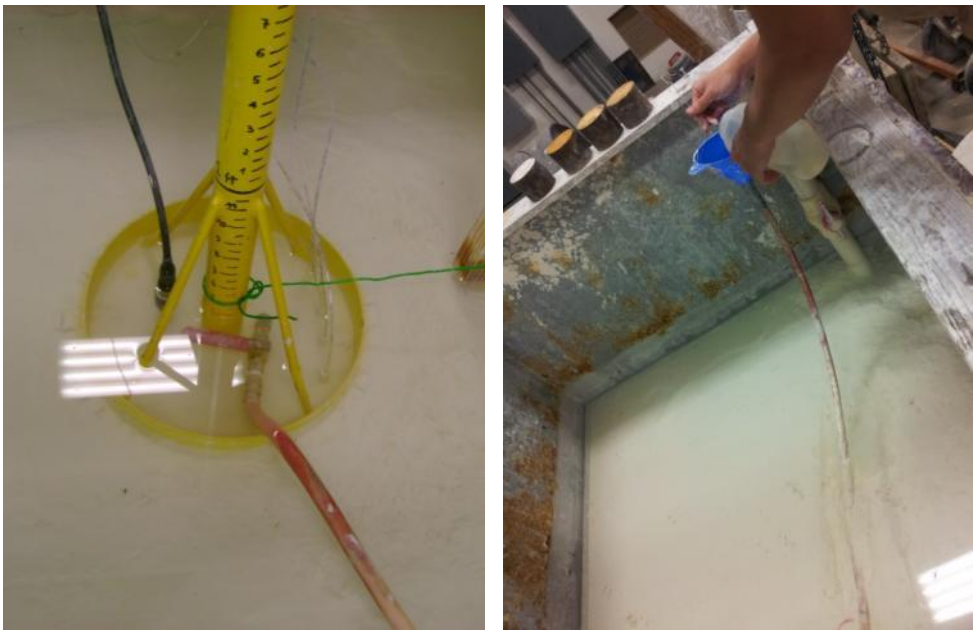

(a) Valve and Water Hose (b) Standing Pipe and Funnel

Figure 6.23: Hydraulic Lifting Process for 1-foot Diameter SCF Model in NC Clay

The excess pore water pressures measured during the jack up process are shown in Figure 6.24 to 6.27. In general, once the valve on the model is opened, positive excess pore water pressures of around 20 psf are measured at Top Plate, Top, and Mid location;

however, negative excess pressures are measured at Tip when the model is moving upward. Note that through the four hydraulic lifting processes, the model was raised up for around 10 inches in total which means the soil plug was also push out for 10 inches. Since the length of the suction can is 12 inches, there was only a 2-inch thick soil plug in the suction can at the end of the tests. Therefore, some slurry water leaked out from between soil and wall during the last hydraulic lifting process.

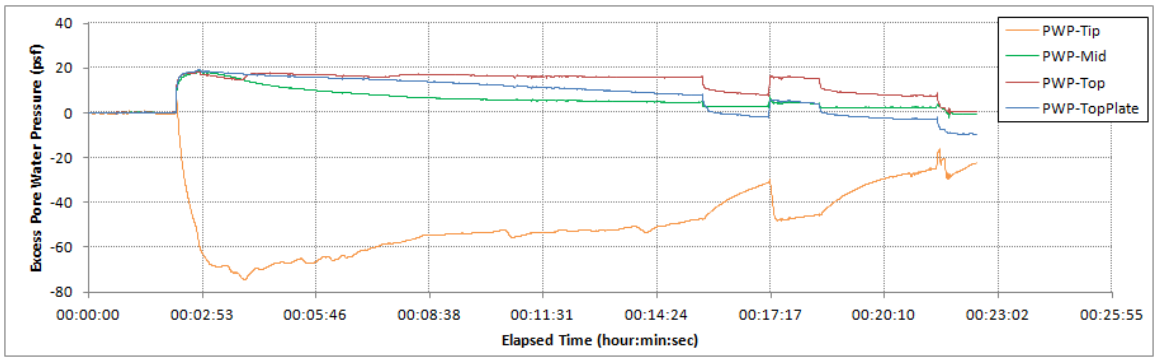

Figure 6.24: Jack up 1-foot Model in NC Clay for 2.5 inches (7/17/2012)

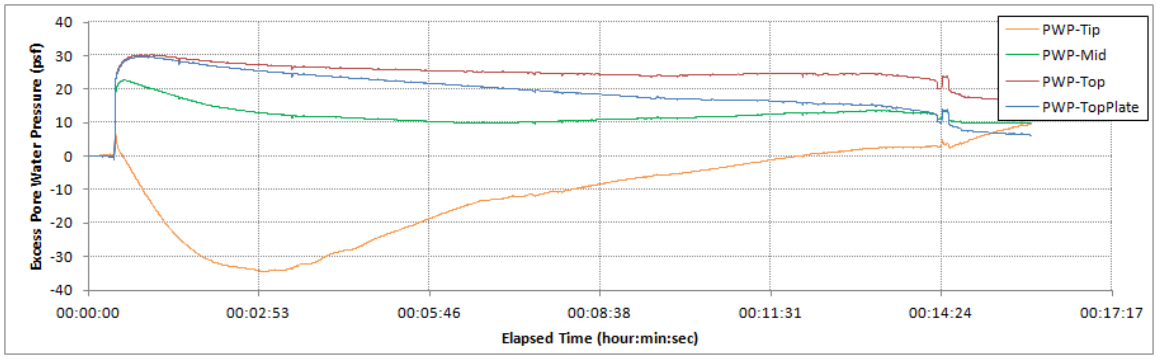

Figure 6.25: Jack up 1-foot Model in NC Clay for 2.25 inches (7/23/2012)

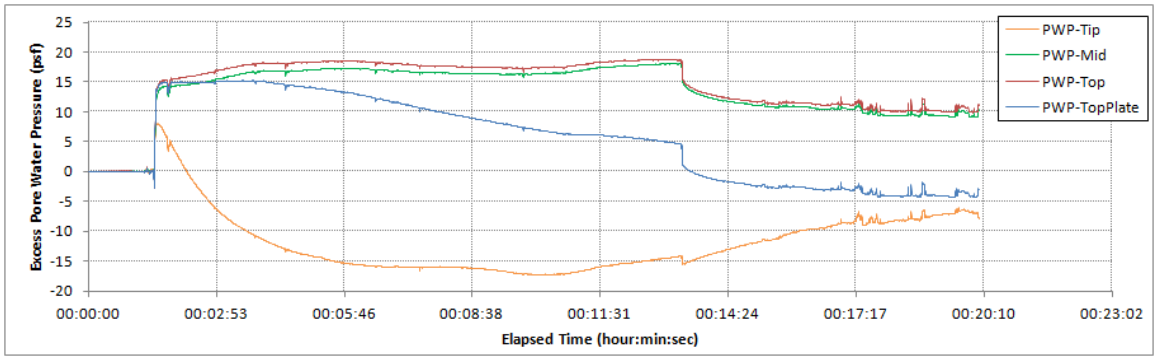

Figure 6.26: Jack up 1-foot Model in NC Clay for 2.7 inches (7/24/2012)

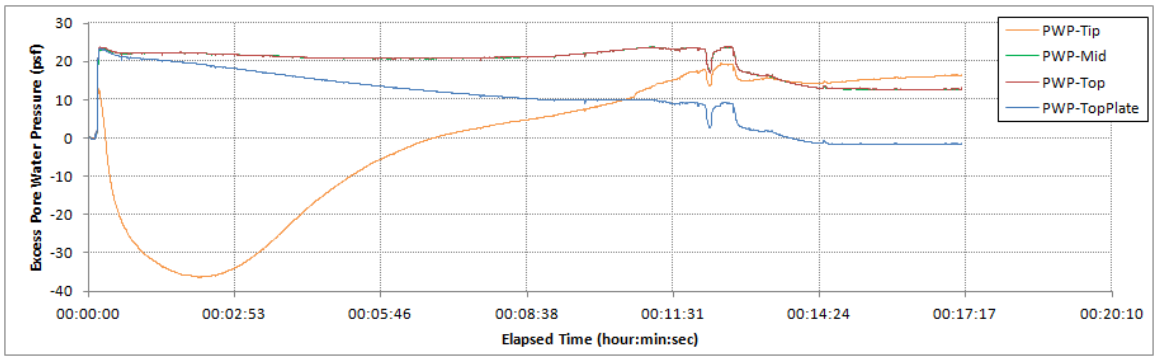

Figure 6.27: Jack up 1-foot Model in NC Clay for 2.7 inches (7/25/2012)

6.4 Pore Water Pressure Dissipation

Pore water pressures were monitored between some of the lateral load tests that were conducted at least 15 hours apart without disturbance during these time periods. Figure 6.28 to 6.30 show the measured pore water pressure inside the suction can during three of these time period. The Top Plate pore water pressure is higher than those at other locations For the other three pore water pressure measurements, the pressure closer to the tip are usually higher at the beginning because of its location is closer to the failure plane under the model, and therefore, higher excess pore water pressured is generated during the lateral tests. However, the excess pore water pressure dissipates faster at Tip because

of a shorter drainage path (closer to the outside of the suction can). As a result, the Tip pressure ends up with the lowest pressure after couple hours of dissipation.

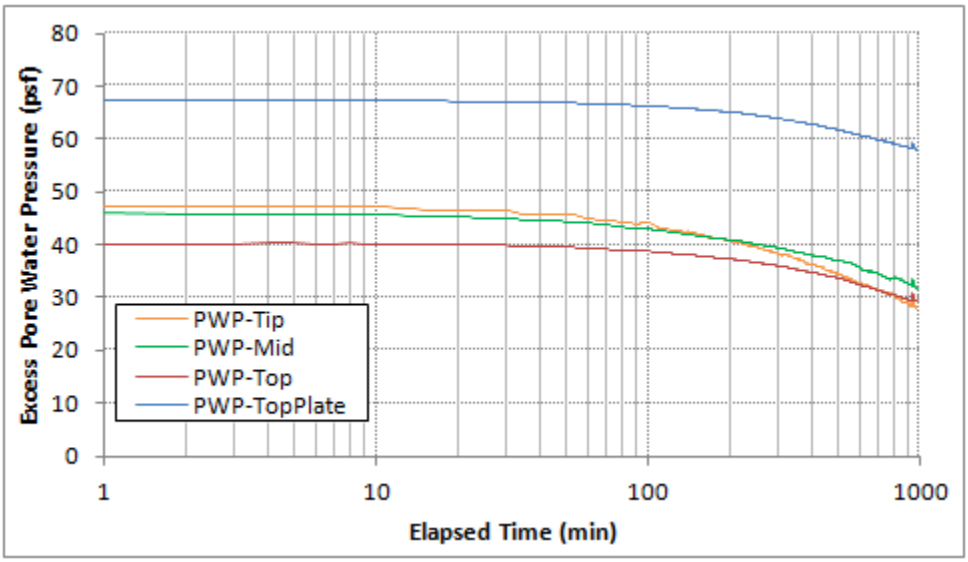

Figure 6.28: Pore Water Pressure Dissipation for 16 hours for 1-foot Model in NC Clay

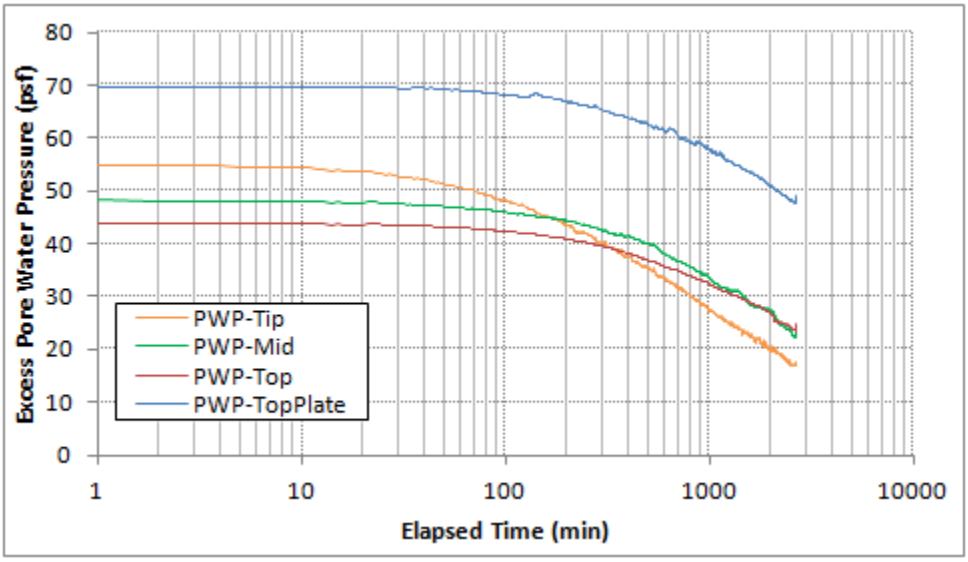

Figure 6.29: Pore Water Pressure Dissipation for 44 hours for 1-foot Model in NC Clay

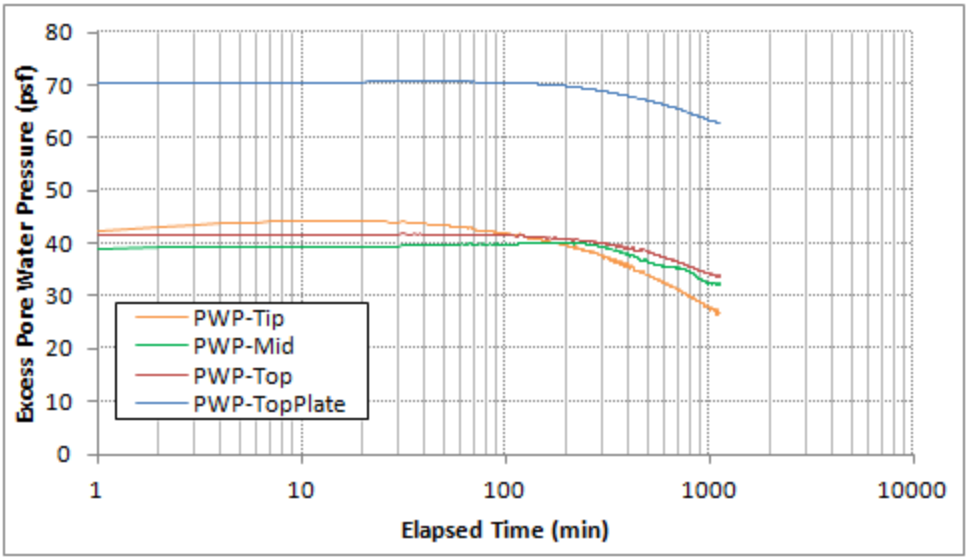

Figure 6.30: Pore Water Pressure Dissipation for 19 hours for 1-foot Model in NC Clay

6.5 Axial Load Tests

In order to evaluate the axial stiffness of the SCF model, axial load tests on the 1-foot diameter model were conducted by placing several 5-lb weights on the model in steps. Two 5-lb weights were placed on the model at a time to apply approximately 10, 20, and 30 lb of load with around 30 seconds for each step. The vertical displacement of the model was monitored using a dial gauge. Figure 6.31 shows the load-displacement curves of three loading-unloading cycles. The loads shown in the figure are corrected for the buoyancy of the steel weights since some of the weights or parts of the weights were submerged in the water during the tests.

The excess pore water pressures of the three cycles of axial load tests are shown in Figure 6.32 to 6.34. The theoretical excess pore water pressures shown in the figure were calculated by taking the submerged weight of weights placed on the model divided by the circular cross-section area of the model. The calculated excess pore water pressures are higher than the measured ones because it's not a simple one dimensional

loading case. The total stress does not confined in the soil under or in the suction can but part of it spreads out in a 3 dimensional space.

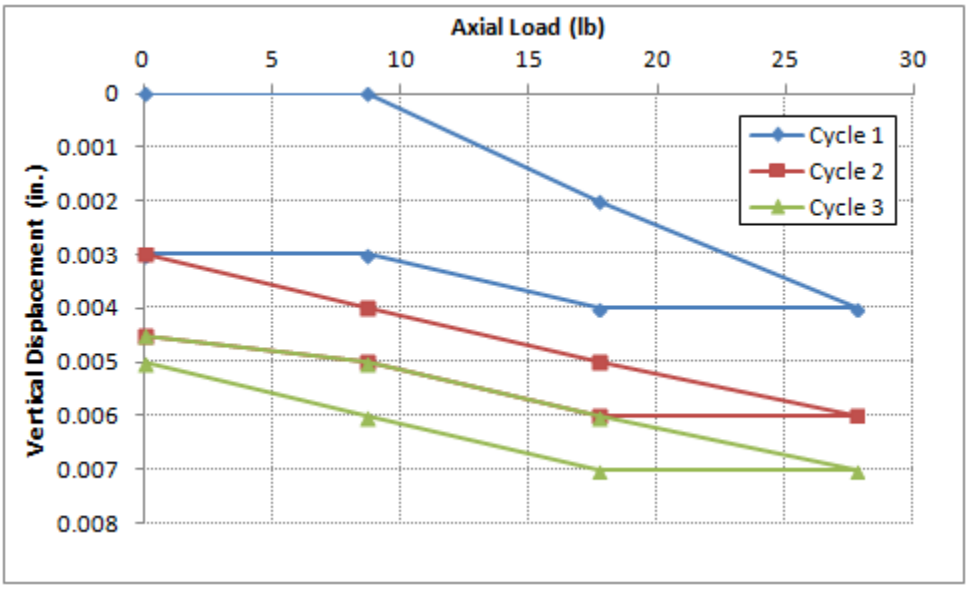

Figure 6.31: Load-Displacement Curve from Axial Load Tests

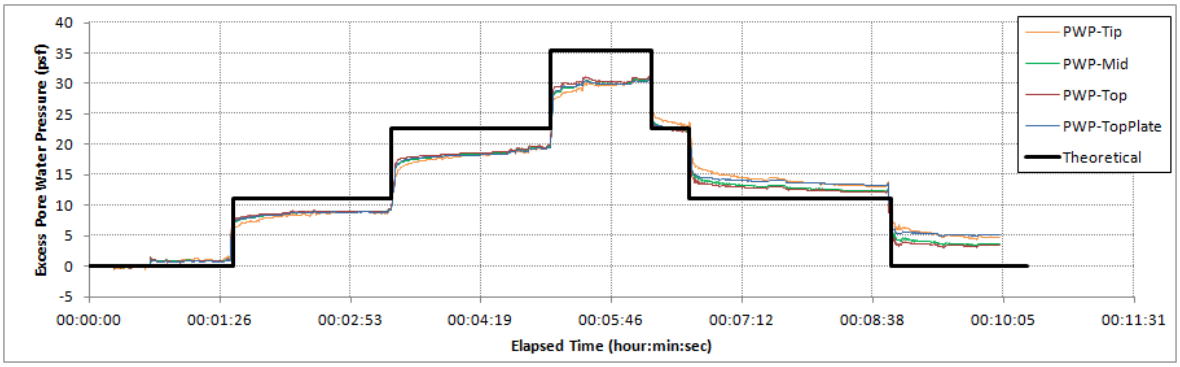

Figure 6.32: Excess Pore Water Pressure from Axial Load Test (Cycle 1)

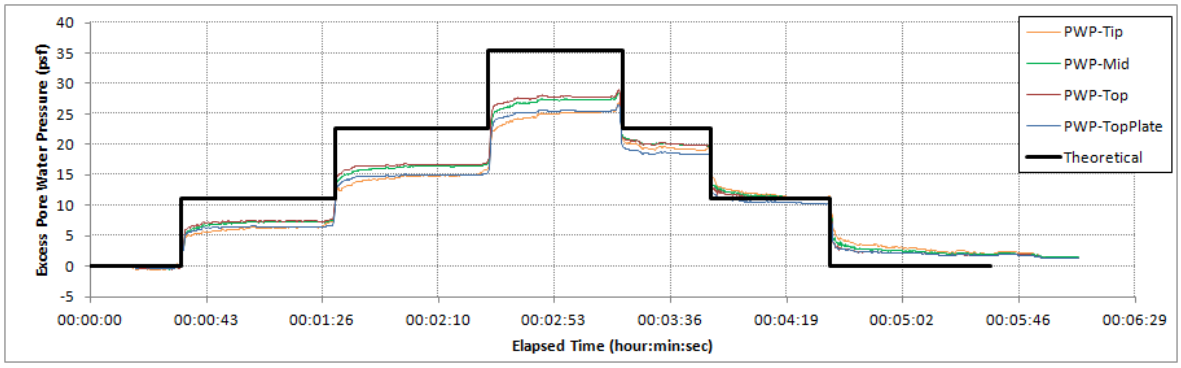

Figure 6.33: Excess Pore Water Pressure from Axial Load Test (Cycle 2)

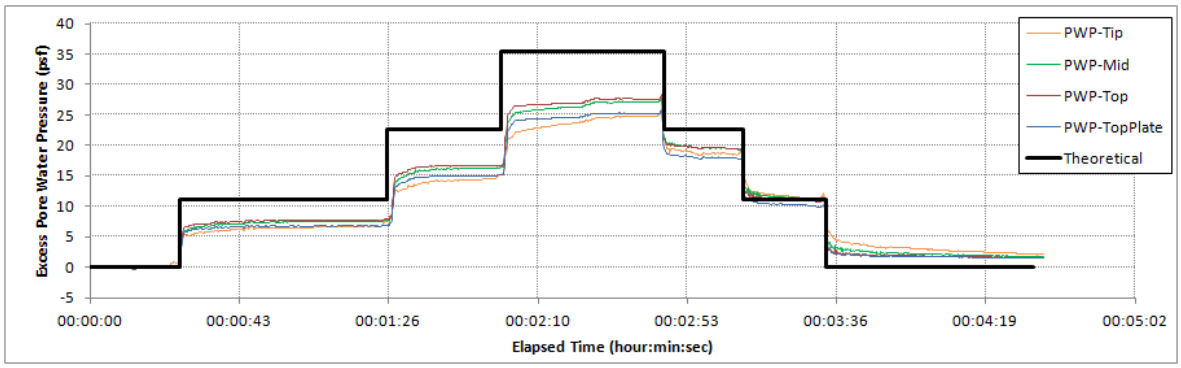

Figure 6.34: Excess Pore Water Pressure from Axial Load Test (Cycle 3)

6.6 Ultimate Axial Capacity Tests

Ultimate axial capacity tests were conducted after all the axial and lateral load tests were completed. The axial load was applied by stacking weights on the model in steps, and the vertical displacement of the model was measured by a dial gauge (see Figure 6.35).

Figure 6.35: Ultimate Axial Capacity Test for 1-foot Diameter SCF Model in NC Clay

Two ultimate axial capacity tests were performed and the load-displacement curves are shown in Figure 6.36. The loads shown in the figure are corrected for the buoyancy of the steel weights since some of the weights or parts of the weights were submerged in the water during the tests. Note that the weight of the model was not included in the axial load shown in Figure 6.36. Test 1 was conducted with a constant 20-lb load increment throughout the test while Test 2 was conducted with smaller load increments close to failure. At last load increment of Test 2, the model kept moving downward and the accumulated displacement staring from Test 1 exceeded the stroke of the dial gauge; therefore, the test was terminated when the displacement reached 0.5 inch.

According to the tests, the ultimate axial capacity in compression for the 1-foot diameter SCF model is approximately 70 lb in normally consolidated clay.

The capacity of the 1-foot diameter SCF model can be calculated by the outer wall side shear resistance plus the bearing from plugged circular tip area of the suction can. The calculated axial capacity due to soil resistance using the API method (see Equation 2.4) is approximately 97 lb, which matches well with than the (net) weight of the model plus the extra 70 lb weights placed on the model (approximately 105 lb in total). Note that for the calculation of the axial capacity, an undrianed shear gradient of 14 psf/ft with zero undrained shear strength at mudline was used according to the T-bar tests. The adhesion factor between the soil and the model (α) is assumed to be 0.8 for both inner and outer wall according to previous studies on suction caissons (El-Sherbiny 2005). The bearing capacity factor for the plugged tip resistance (N_c) is assumed to be 7.2 by using depth correction suggested by Skempton (1951) for square footing ($D_f/B = 1$ and therefore $d_c = 1.2$).

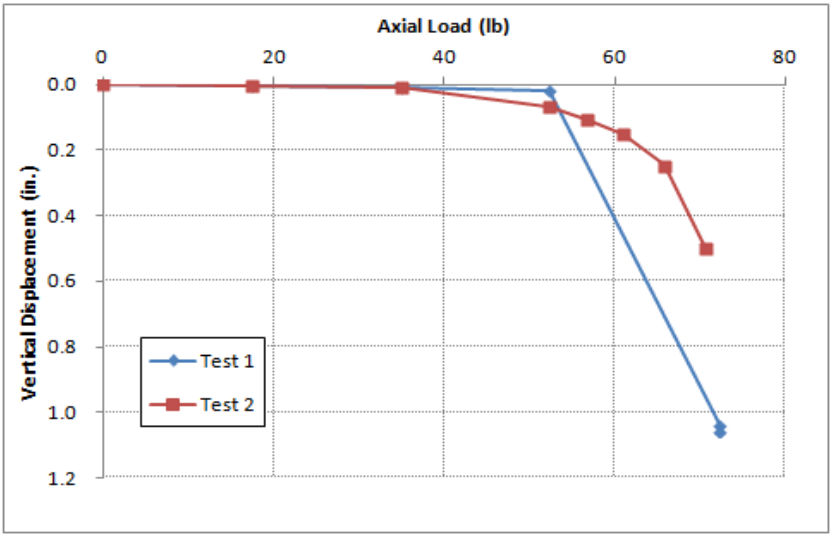

Figure 6.36: Load-Displacement Curves from Ultimate Axial Capacity Tests

The excess pore water pressures of ultimate axial capacity tests are shown in Figure 6.37 and 6.38. The theoretical excess pore water pressures shown in the figure were calculated by taking the submerged weight of weights placed on the model divided by the circular cross-section area of the model. The calculated excess pore water pressures are higher than the measured ones in general. The measured excess pore water pressures in Test 1 are closer to the calculated pressure.

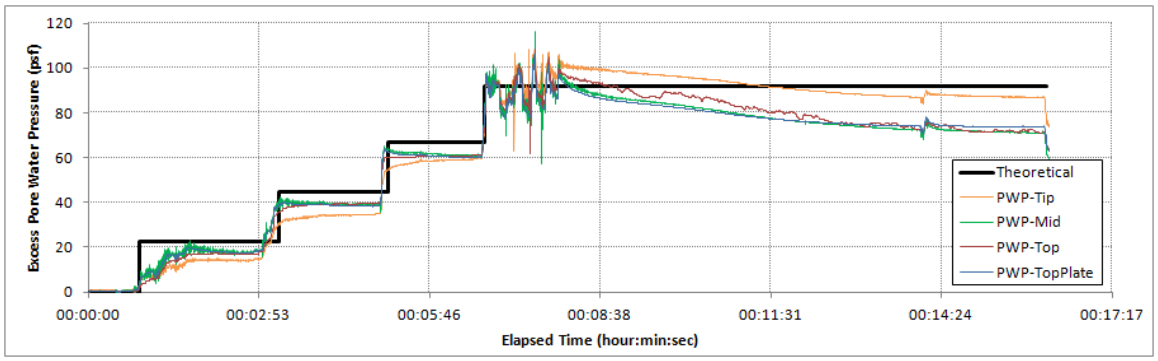

Figure 6.37: Excess Pore Water Pressure from Ultimate Axial Capacity Test 1

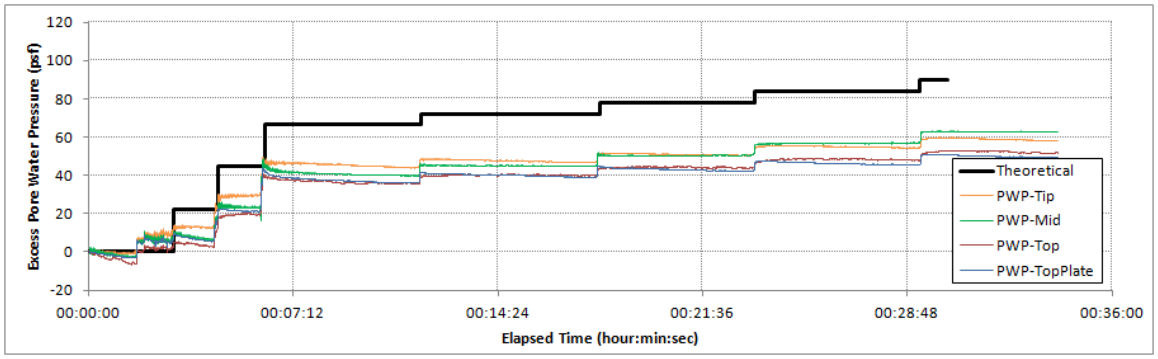

Figure 6.38: Excess Pore Water Pressure from Ultimate Axial Capacity Test 2

6.7 PULLOUT

The 1-foot diameter SCF model was pulled out of the normally consolidated clay after all the tests were completed. Since the capacity of the SCF model in normally consolidated clay exceeds the capacity of our loading system, the model was pulled out manually. The load cell and the linear displacement transducer were attached to the model to measure the load and vertical displacement, respectively. A layer of clay (less than 1/4 inch thick) sticks on the wall of the model indicating an undrained loading condition during pullout. The suction can was plugged when it was pulled out, but the soil plug fell off within one minute. The pullout results are shown in Figure 6.39 to 6.43.

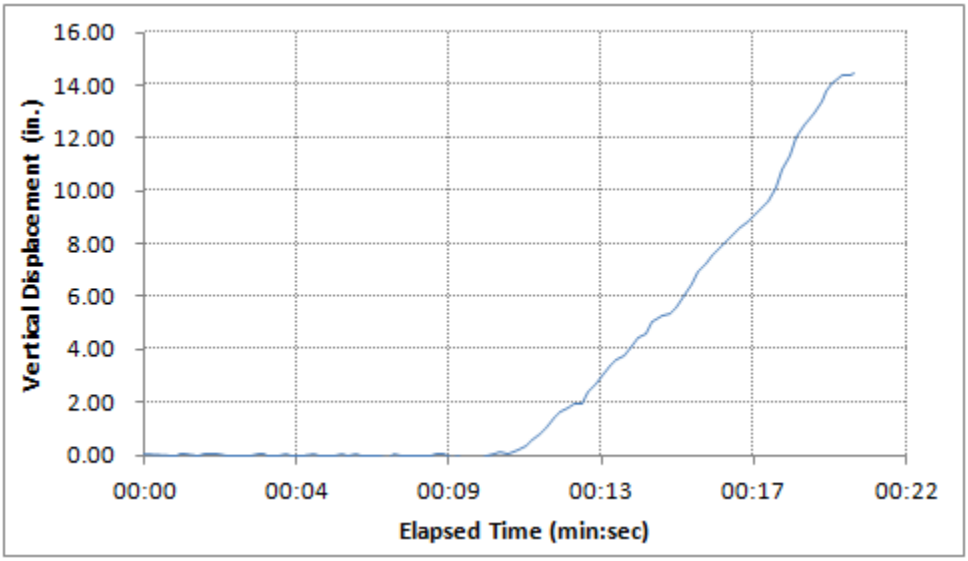

Figure 6.39: Vertical Displacement of 1-foot SCF Model Pullout Test in NC Clay

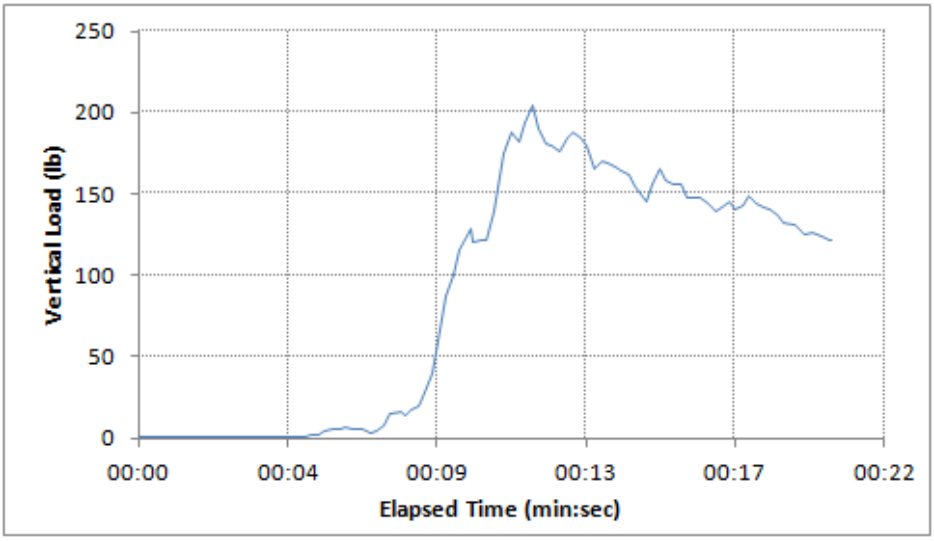

Figure 6.40: Vertical Load of 1-foot SCF Model Pullout Test in NC Clay

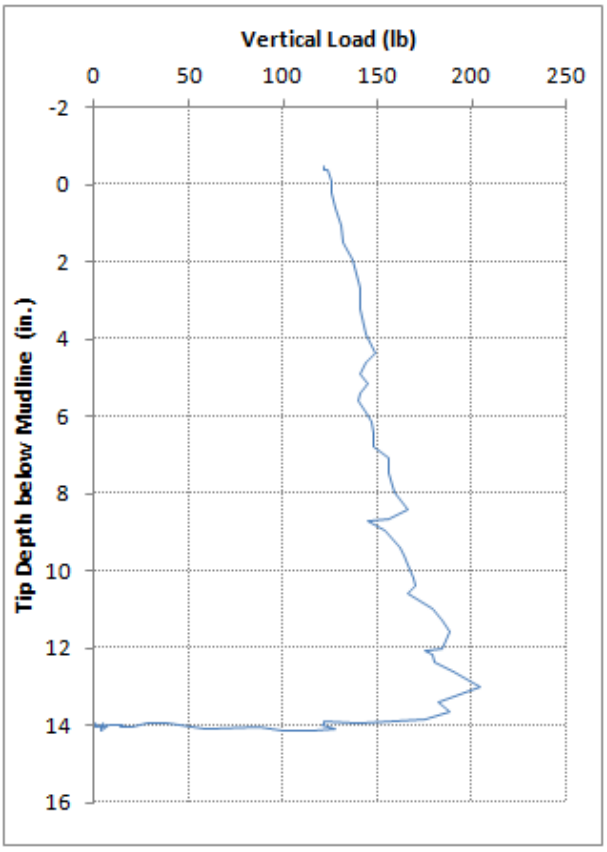

Figure 6.41: Load-Displacement Curve of 1-foot SCF Model Pullout Test in NC Clay

Figure 6.39 to 6.41 show the measured vertical load and displacement during the pullout process. Note that the foundation settled 2 inches before pullout. Therefore, in Figure 6.41, the tip depth starts at 14 inches below the mudline. The peak load of 204 lb occurs at 1 inch of vertical displacement. The measured pore water pressures during pullout are presented in Figure 6.42 and 6.43. Negative pore water pressures in the figures indicate suction was developed inside the suction can to provide resistance to pullout.

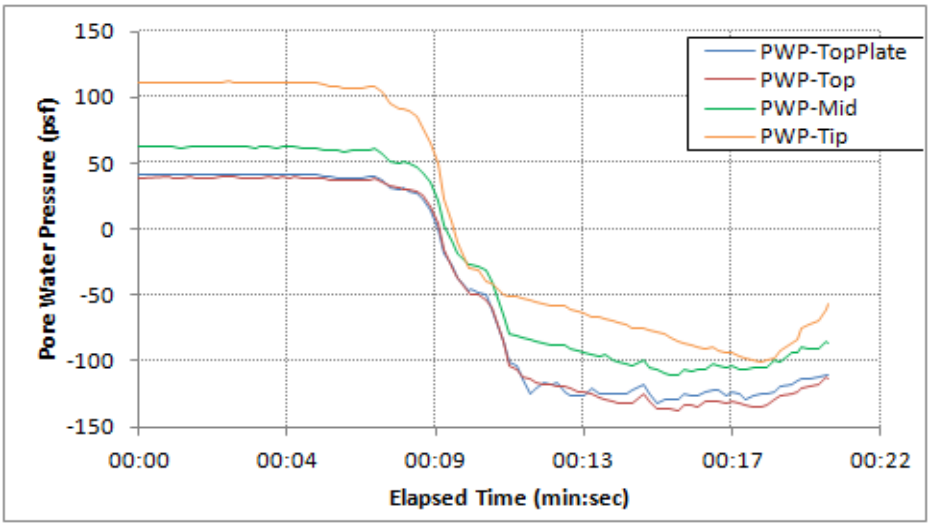

Figure 6.42: Pore Water Pressures of 1-foot SCF Model Pullout Test in NC Clay

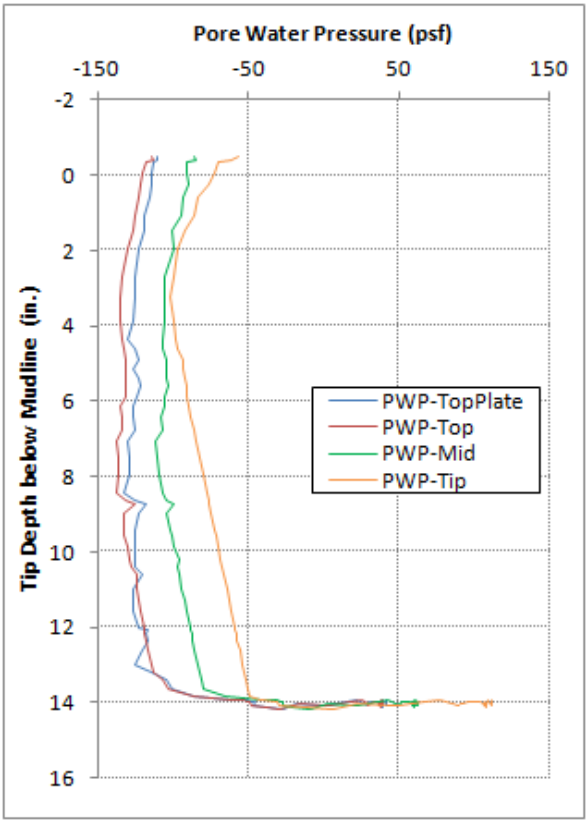

Figure 6.43: Pore Water Pressures versus Tip Depth of 1-foot SCF Model Pullout Test in NC Clay

6.8 Summary for Tests in Normally consolidated Clay

The undrained shear strength increased linearly with depth in normally consolidated kaolinite test bed. The undrained shear strength at mudline was approximately 0 psf with a gradient of 14 psf/ft measured by a T-bar penetrometer. The measured undrained shear strength gradient decreased to 7 psf/ft after remolding the soil by penetrating and pulling out the T-bar for 6 cycles.

The 1-foot diameter SCF model was installed in the normally consolidated clay by penetrating under its own weight. The weight of the suction can was greater than the penetration resistance calculated by the limit analysis method recommend by API RP

2SK (A 2008) with α equal to the inverse of sensitivity and $N_c = 7.5$ for the tip area of the wall. This calculation confirmed that the caisson can be installed by self weight.

For the 1000-cycle lateral load tests, walking and settlements of the suction can are not significant (less than 0.01 diameter of the suction can or 0.01 D) with 1-dregree (±0.5 degree) rotation. More significant settlements (up to 0.11 D) may occur with 2-degree (±1 degree) rotation under the weight of the steel model. With 5-degree (±2.5 degrees) rotation, the walking displacement and settlement may go up to 0.17 D and 0.24 D, respectively. After the cyclic lateral tests, a circular zone of disturbed soil on the surface extended to approximately 0.8 diameter out from the suction can. No significant gap formed between the foundation and the soil during the lateral tests except a small gap opened up during 5-degree rotation tests.

The measured lateral load (or lateral resistance) is higher in the first couple cycles because of the effect of setup and, subsequently, the measured lateral load decreases in a couple of cycles due to the soil disturbance. In the tests with larger rotations (2- and 5-degree tests), the lateral resistance increases with the number of loading cycle; this "stiffening" behavior may be attributed to the settlement of the foundation because it penetrates deeper into the soil. The overconsolidation of soil around the wall of the foundation due to cyclic loading may also contribute to this stiffening effect. The difference in the measured lateral load for cyclic loading period of 3, 5, and 10 seconds is not significant which indicates that there is little stain rate effect in this range of loading periods.

During cyclic lateral load tests in normally consolidated clay, the excess pore water pressure in the soil plug has larger cyclic fluctuations near the tip of the suction can comparing to that under the top plate because it is closer to the failure plane under the suction can. The excess pore water pressure built up due to the weight of suction can after

installation never fully dissipated during the period of tests (10 days) in normally consolidated clay.

The ultimate axial capacity in compression for the 1-foot diameter SCF model in the normally consolidated clay test bed is close to the axial capacity calculated by the limit analysis recommended by API with Nc = 7.2 for bearing (corrected for embedment by the method suggested by Skempton, 1951) and $\alpha = 0.8$ for side shear. During the pullout test, a peak load was measured at 0.08 diameter of vertical displacement. Negative pore water pressure (suction) was developed inside the suction can which provides a large proportion of pullout resistance in terms of reversed end bearing. A layer of clay (less than 1/4 inch thick) sticks on the wall of the suction can indicate that it was under undrained loading condition during pullout. The suction can was plugged when it was pulled out, but the soil plug fell off within one minute.

Chapter 7: Tests in Overconsolidated Clay Test Bed

The 6-inch diameter SCF model was used in the overconsolidated clay (OC clay) test bed. The properties of the normally consolidated clay test bed can be found in Section 2.2. The scale model tests conducted in this test bed includes: installation, lateral load tests, axial load tests, ultimate axial capacity test, and pullout. The test procedure and the summary of test results are presented in the following sections.

7.1 INSTALLATION

The 6-inch diameter SCF model was installed in the overconsolidated clay first by its own weight and later by placing extra weights on the model to facilitate the penetration process. The total weight of the model plus the pressure transducer on the model was 9.83 lbs. The valve on the top plate was opened to allow water flowing out of the suction can during installation, and was subsequently closed once the model was fully installed without further downward movement. The valve was kept closed throughout the rest of the tests in OC clay.

At the beginning of installation, the model penetrated into the soil by its own weight to a depth around 0.5 inches. Ten-lb weights were placed on the model in steps up to 30 lbs to fully penetrate the model into the overconsolidated clay with the top plate of the model at mudline (see Figure 7.1). The linear displacement transducer was connected to the model to monitor the vertical displacement. Figure 7.2 shows the vertical displacement of the model during installation. At the end of the installation, the model was twisted 90 deg by hand to align the load cell on the model with the loading line for lateral load tests.

Figure 7.1: Installation of the 6-inch Diameter SCF Model in OC Clay

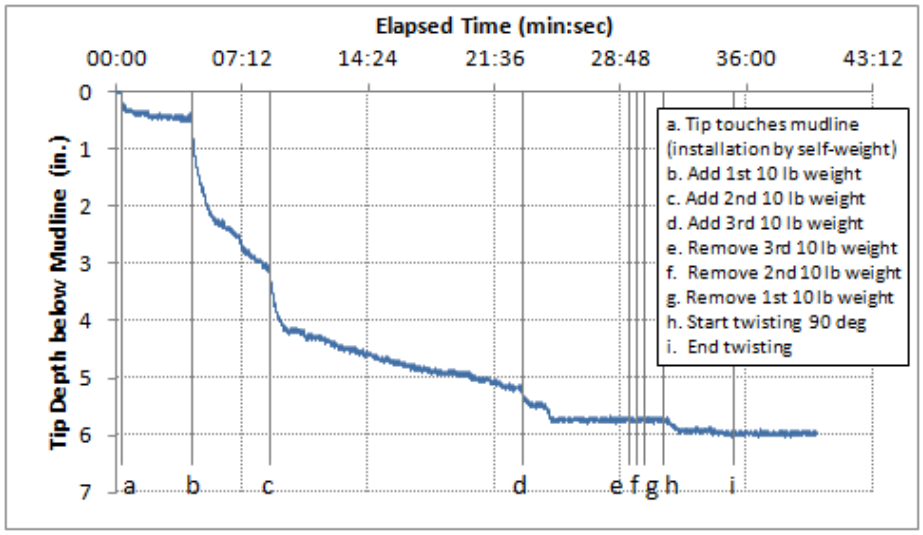

Figure 7.2: Vertical Displacement of 6-inch Diameter Model during Installation in Overconsolidated Clay

The force required for the SCF model to penetrate for 6 inches for installation can be calculated by the inner and outer wall side shear resistance plus the bearing resistance from the tip area of the cylindrical wall. The calculated penetration resistance according

to API (see Equation 2.1) is around 43 lb, which is close to the (net) weight of the model plus the extra 30 lb weights. This confirms that the 6-inch diameter SCF model can be installed in the overconsolidated clay test bed by its own weight plus the 30 lb weights. Note that for the calculation of the installation resistance, a constant undrianed shear strength of 45 psf was used for overconsolidated clay according to Section 3.2. The adhesion factor between the soil and the foundation (α) is assumed to be 0.5 (based on α=1/sensitivity and sensitivity of soil = 2) for both inner and outer wall. The bearing capacity factor for tip resistance of the wall (N_c) is assumed to be 7.5, which is an analog to a buried strip footing (API RP 2SK A2008).

Figures 7.3 and 7.4 show the measured pore water pressures during installation. The pore water pressures at Top and Tip were corrected for elevation head as described in Section 7.1. The pressure transducers for Top and Tip were fixed 9 inches above the mudline on the load frame. The Top Plate pore water pressure was attached directly to top plate of the model and therefore no elevation head correction is required.

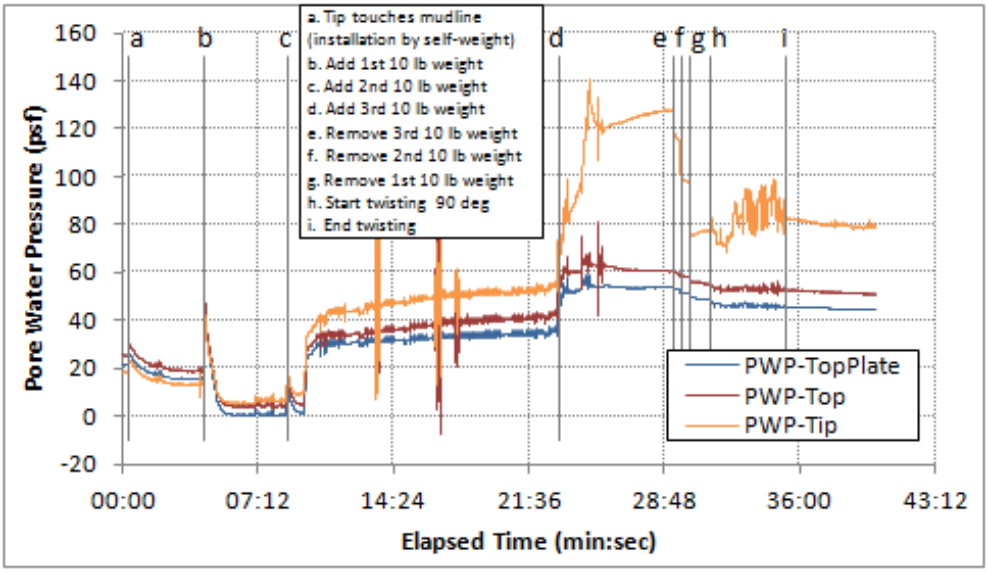

Figure 7.3: Pore Water Pressures of 6-inch Diameter Model during Installation in Overconsolidated Clay

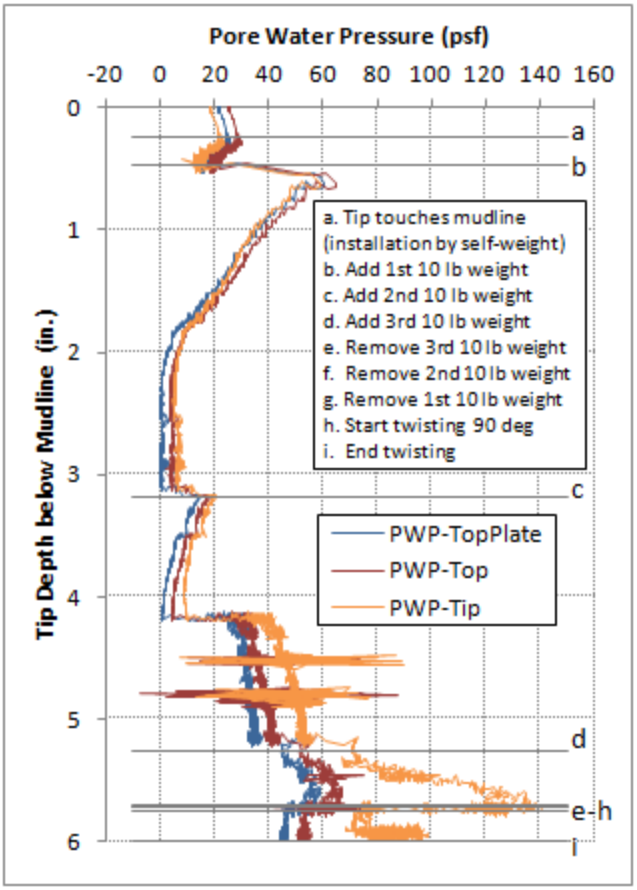

Figure 7.4: Pore Water Pressures of 6-inch Diameter Model during Installation in Overconsolidated Clay

7.2 Lateral Load Tests

Two-way, displacement controlled, cyclic lateral load tests for 6-inch diameter SCF model were conducted in overconsolidated clay test bed. The lateral tests are similar to those presented in Section 7.2 for 1-foot diameter SCF model in normally consolidated clay. The lateral resistance, the walking displacement (translational permanent displacement), and the settlement were measured under 1000 cycles of lateral load in these tests.

As shown in Figure 7.5 and 7.6, cyclic lateral displacement was applied on the extended arm of the model at 3 ft above the mudline such that the model rotates cyclically with a cyclic total rotation of 1, 2, or 5 degrees (±0.5, ±1.0, or ±2.5 degrees from vertical). The model was tested with periods of 3, 5, and 10 seconds for each rotation angles. The static mean load to simulate current load was applied at 5 inches above mudline to simulate the current load (see Figure 7.5). The applied mean loads were 0.25, 0.5, and 1.25 lb for rotation angles of 1, 2, and 5 degrees respectively.

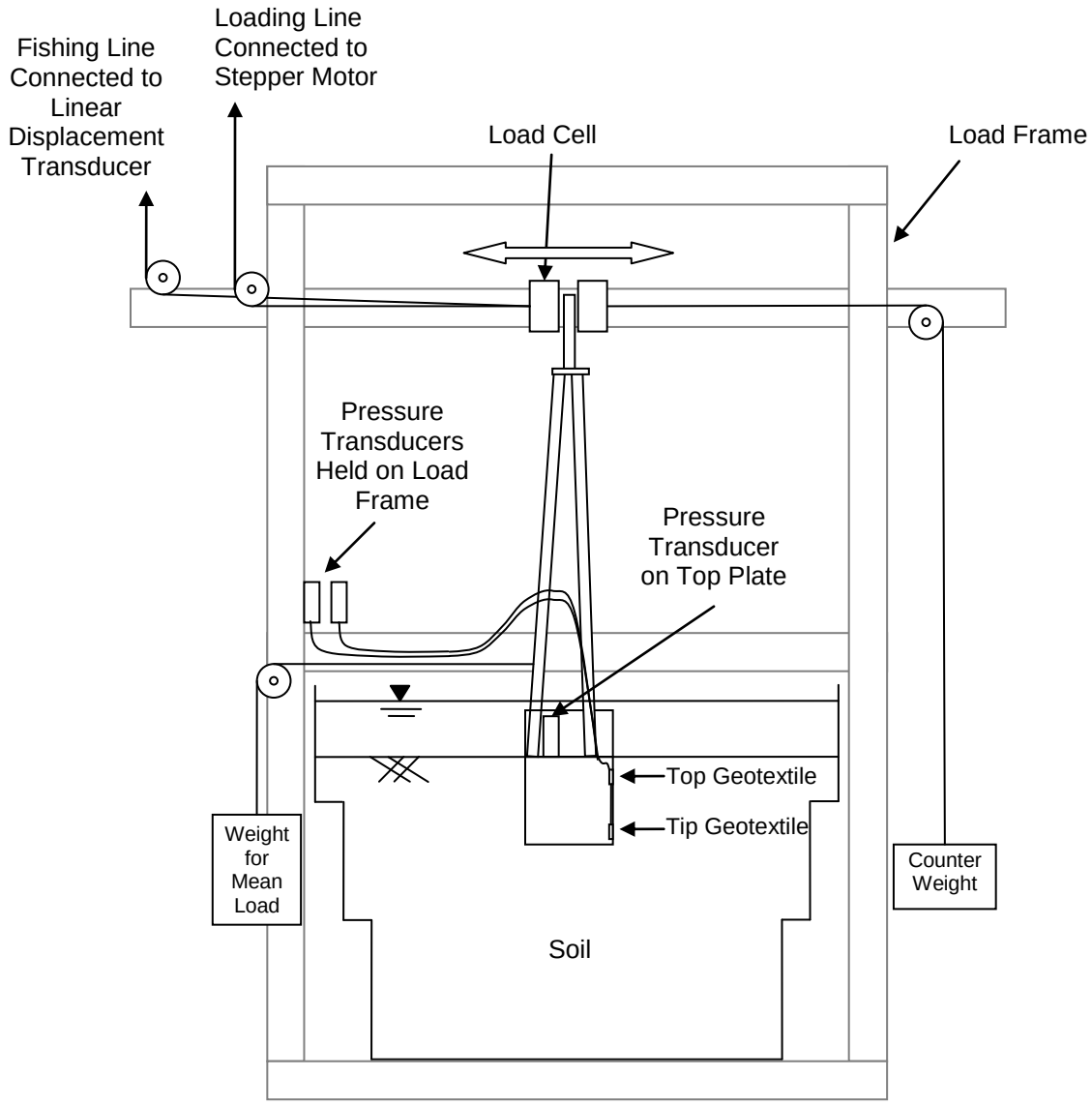

Figure 7.5: Schematic for Lateral Load Tests of 6-inch Diameter SCF Model in Overconsolidated Clay

Figure 7.6: Lateral Load Tests of 6-inch Diameter SCF Model in Overconsolidated Clay

The lateral load required to rotate the model was measured by a load cell attached to the extended arm on the right side. The lateral displacement was measured by the linear displacement transducer with a fishing line connecting to the extended arm (see Figure 7.5). The tilt meter was placed near the top of the extended arm of the model to measure the tilt angle. A dial gauge installed near the top of the extended arm (see Figure 7.7) was used to measure the settlement of the model. The walking displacement of the model was obtained by comparing the linear displacement transducer reading before and after 1000 cycles of load. The model was ensured to be leveled and the extended arm to be vertical according to the tilt meter readings and occasionally checked using a level. Pore water pressures inside the suction can were monitored by one pressure transducer

directly attached to the top plate of the model and two others connected to Top and Tip location on the inner wall with water tubes (see Figure 7.5).

(a) Dial Gauge (b) Tilt Meter

Figure 7.7: Dial Gauge and Tilt Meter on 6-inch Diameter SCF Model

7.2.1 WALKING AND SETTLEMENT

Table 7.1 shows the walking displacement and the settlements of the 6-inch diameter SCF model after 1000 cycles of lateral load for each rotation and period combination in the overconsolidated clay test bed. The 5-degree rotation tests were repeated because a gap between the model wall and soil (see Figure 7.12) was formed due to excessive movement of the motor. The gap was subsequently closed by pushing downward on the soil surface (see Figure 7.14). Then, the 5-degree rotation tests were conducted again after 3 days of setup for the model foundation. Walking and settlement both tend to decrease after the gap was closed. The walking displacement and settlement of the model

for all the lateral load tests are illustrated in Figure 7.8 and 7.9 respectively except the 5-degree tests with a gap. Note that the negative values of walking displacement indicate that the model walks in the opposite direction of the mean load.

Soil Type	SCF Model	Rotation (degrees)	Period (seconds)	Mean Load (lbs)	Walking Displ. (inches)	Settlement (inches)	Test Date
Over-consolidated Clay	6-inch Diameter Model	1	3	0.25	-0.11	0.034	10/18/2012
			5	0.25	0.07	0.016	10/19/2012
			10	0.25	-0.12	0.000	10/19/2012
		2	3	0.50	0.00	0.032	10/30/2012
			5	0.50	0.08	0.014	10/30/2012
			10	0.50	0.00	0.013	10/30/2012
		5*	3	1.25	0.22	0.315	10/31/2012
			5	1.25	-0.19	0.112	10/31/2012
			10	1.25	-0.04	0.127	10/31/2012
		5**	3	1.25	-0.07	0.135	11/5/2012
			5	1.25	0.17	0.092	11/5/2012
			10	1.25	-0.03	0.066	11/5/2012

* A gap between the model wall and soil was formed due to excessive movement of the motor. The gap was on the mean load side and had a width of approximately 3/4 inch at mudline.

** Closed the gap by pushing downward on the soil surface. The model was allowed to setup for 3 days after closing the gap.

- Additional note: negative values of walking displacement indicate that the model walks in the opposite direction of the mean load.

Table 7.1: Walking and Settlement of 6-inch Diameter SCF Model after 1000 Cycles of Lateral Load in Overconsolidated Clay

Figure 7.8 shows that walking of the model in overconsolidated clay is not significant for all the ration angles and loading periods. The walking displacements are all within 0.03 diameter of the model (less than 0.03 D). Figure 7.9 shows that the settlement of the model increases with increasing rotation of the model or decreasing

loading period. Although the settlements increase significantly when the rotation angle increases from 2 degrees to 5 degrees, the settlements are still within 0.02 diameter of the model (less than 0.02 D).

Pictures of the 6-inch SCF model after lateral load tests in the overconsolidated clay are shown in Figure 7.10 to 7.15. Fissures and cracks formed in the clay around the model after cyclic lateral loadings. The circular zone of disturbed soil extended to approximately 0.6 diameters out from the model. A narrow gap (less than 1/4 inch wide) was opened up around the model under cyclic lateral loading and was filled with slurry quickly after few hundred cycles of loading (see Figure 7.10 and 7.11).

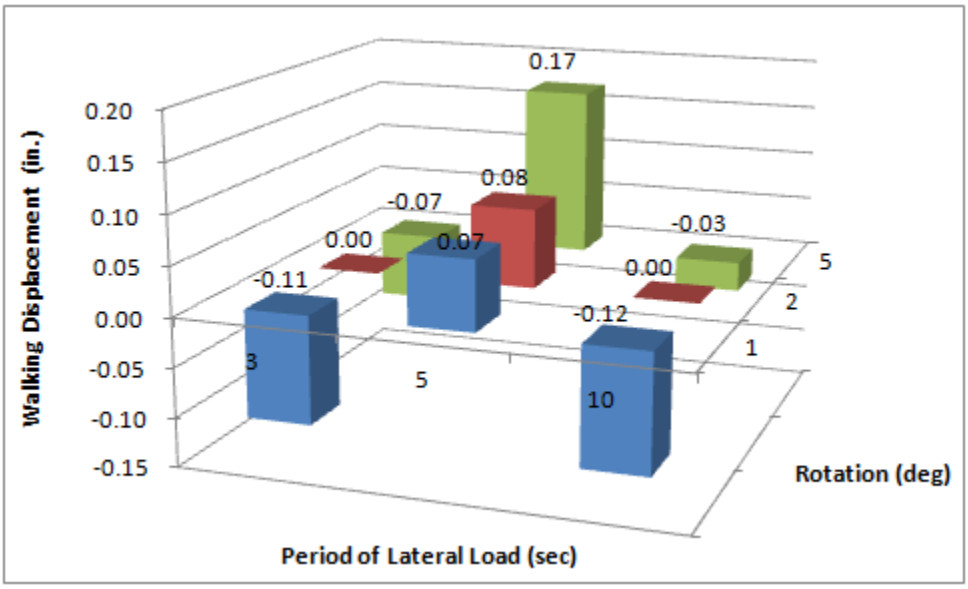

Figure 7.8: Walking of 6-inch Diameter SCF Model in Overconsolidated Clay

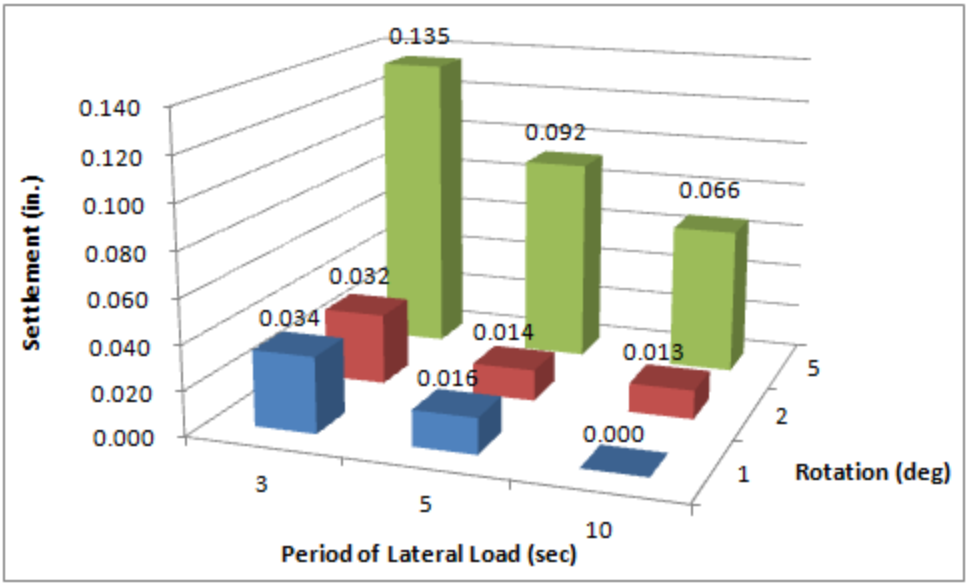

Figure 7.9: Settlement of 6-inch Diameter SCF Model in Overconsolidated Clay

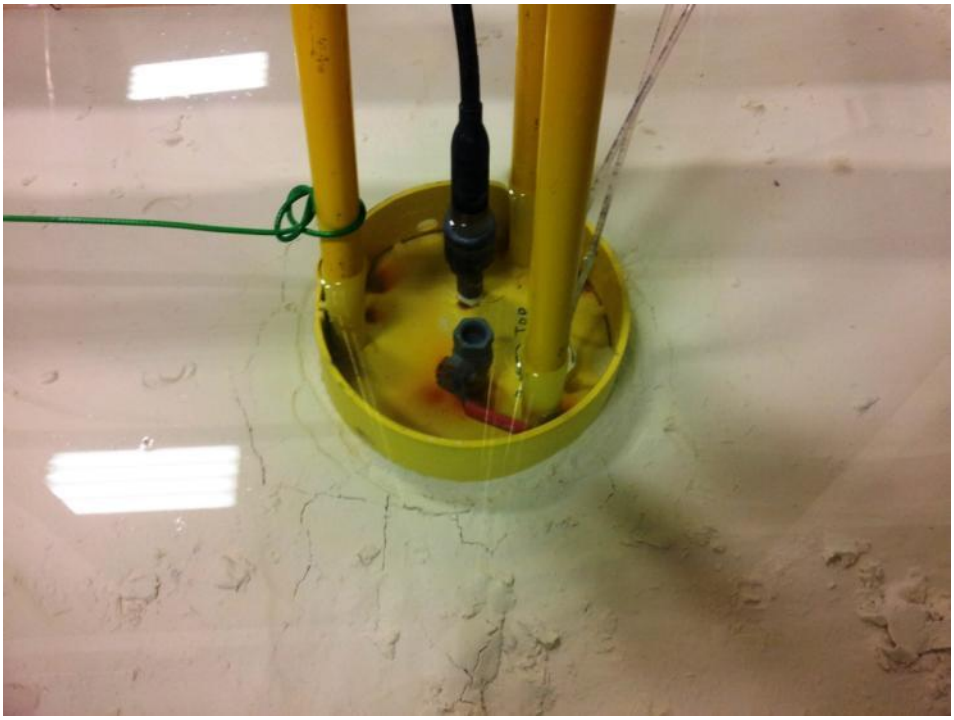

Figure 7.10: SCF Model after 1-degree Lateral Load Tests in OC Clay

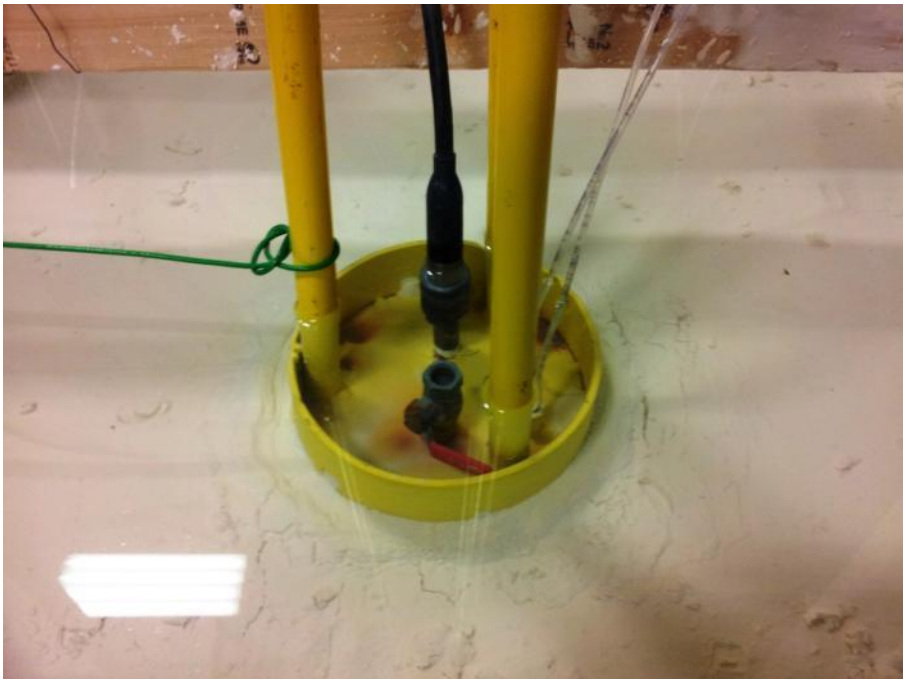

Figure 7.11: SCF Model after 2-degree Lateral Load Tests in OC Clay

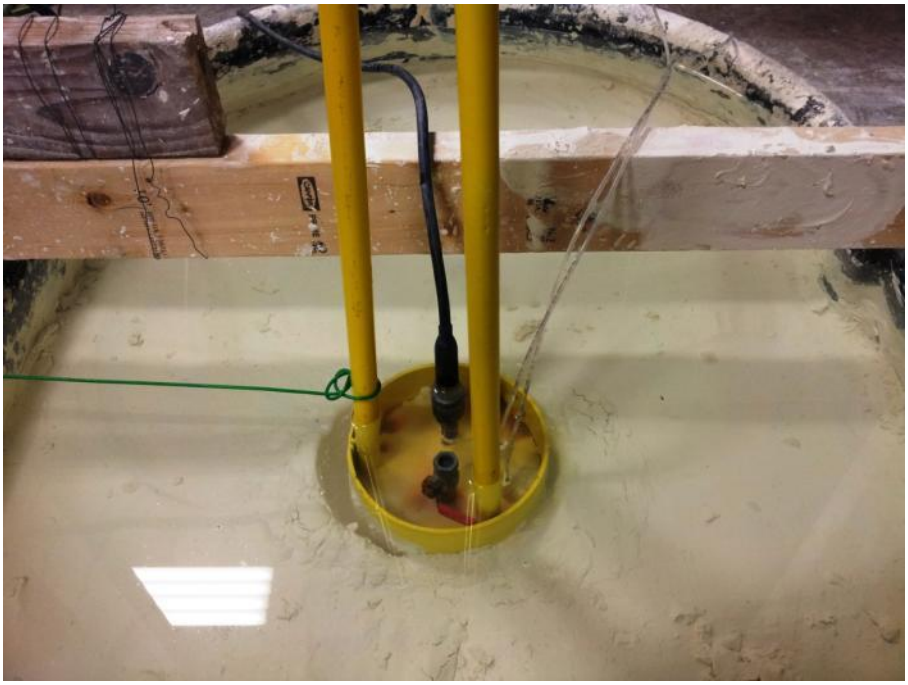

Figure 7.12: Gap Created before 5-degree Lateral Load Tests in OC Clay (with the Gap)

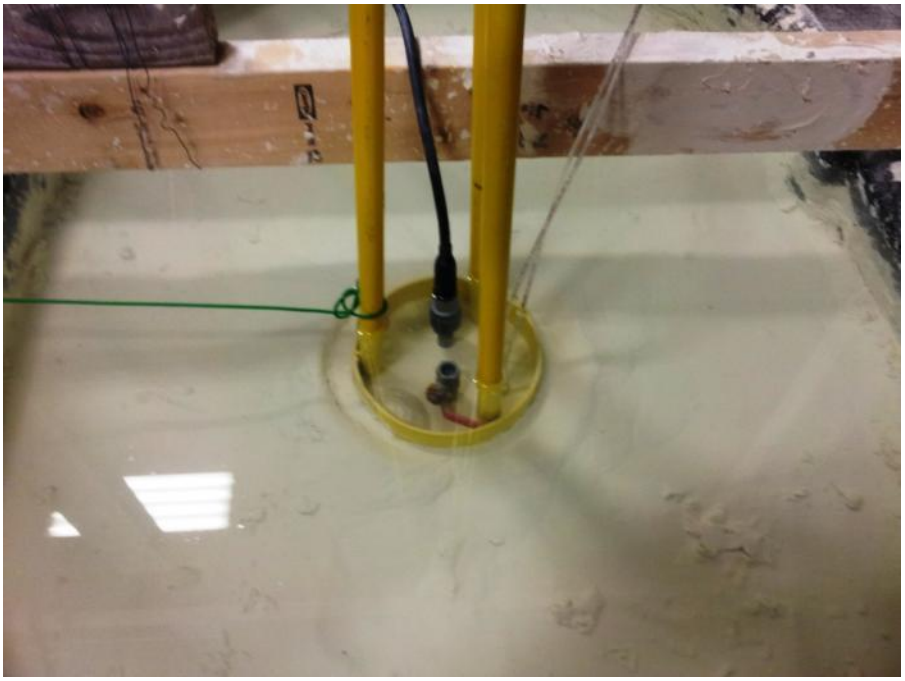

Figure 7.13: SCF Model after 5-degree Lateral Load Tests in OC Clay

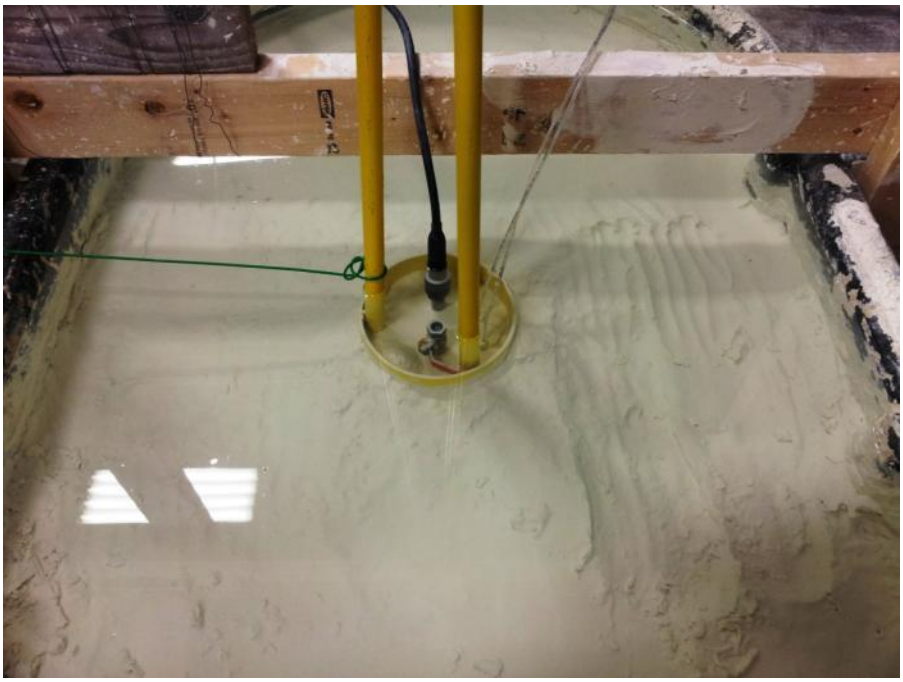

Figure 7.14: SCF Model after Closing the Gap Manually

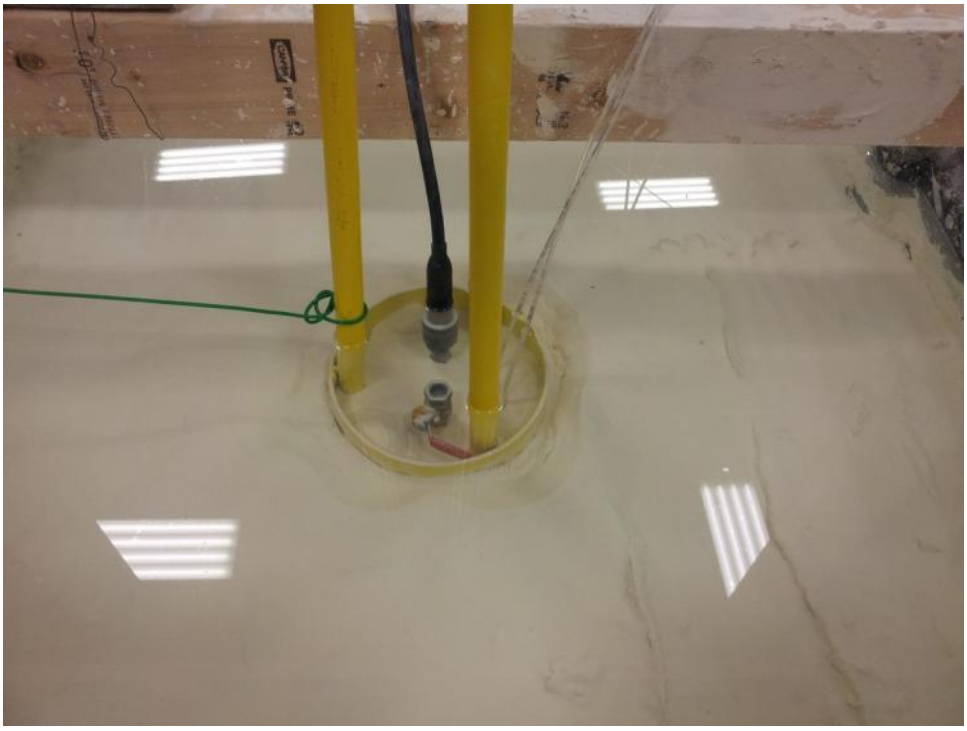

Figure 7.15: SCF Model after Repeated 5-degree Lateral Load Tests in OC Clay

7.2.2 Lateral Load, Displacement, Pore Water Pressure, and Tilt Angle

In terms of the lateral load, lateral displacement, pore water pressure, and tilt angle measurements, the 2-degree rotation and 5-second period test is taken as an example for the lateral tests in overconsolidated clay.

The time history of the 1000-cycle lateral load and lateral displacement are presented in Figure 7.16 and 7.17. The lateral load and displacement are both measured at 3 ft above the top plate of the model (or 3 ft above the mudline) as shown in Figure 7.5. The hysteresis loops of later load versus lateral displacement are shown in Figure 7.18.

In Figure 7.16, positive lateral displacement indicates that the model tilts to the right while negative displacement indicates left tilting movement. The lateral

displacement fluctuates within a stable range and shows no sign of shifting which indicates that the model has no significant walk. The load shown in Figure 7.17 and 7.18 are obtained by subtracting the weight of counter weights (see Figure 7.5) from the lateral load measured by the load cell. The load cell registers positive loads when the model tilts to the left and negative loads when it moves to the right. The lateral load shifted slightly to the negative side because of the presence of the mean load as discussed in Section 6.2.2 for lateral load tests in normally consolidated clay.

In Figure 7.17, the measured lateral load (or lateral resistance) fluctuates in a relatively stable range. This test was conducted immediately after the 2-degree, 3-second period test, and therefore, no setup effects were shown in terms of the measured lateral load. No "stiffening" effects (as discussed in Section 6.2.2 for the tests in normally consolidated clay) were observed in the later part of the test because the model has no significant settlement during this test.

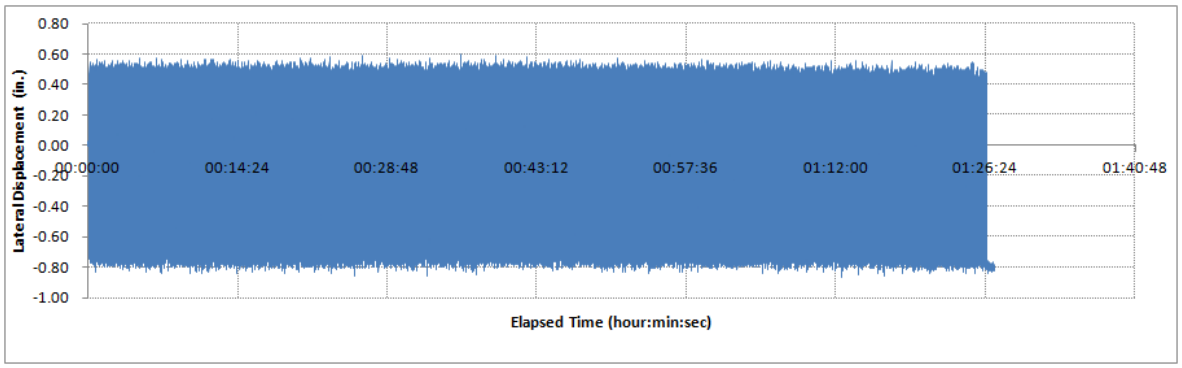

Figure 7.16: Lateral Displacement of 6-inch Model in OC Clay (2° rotation, 5-sec period)

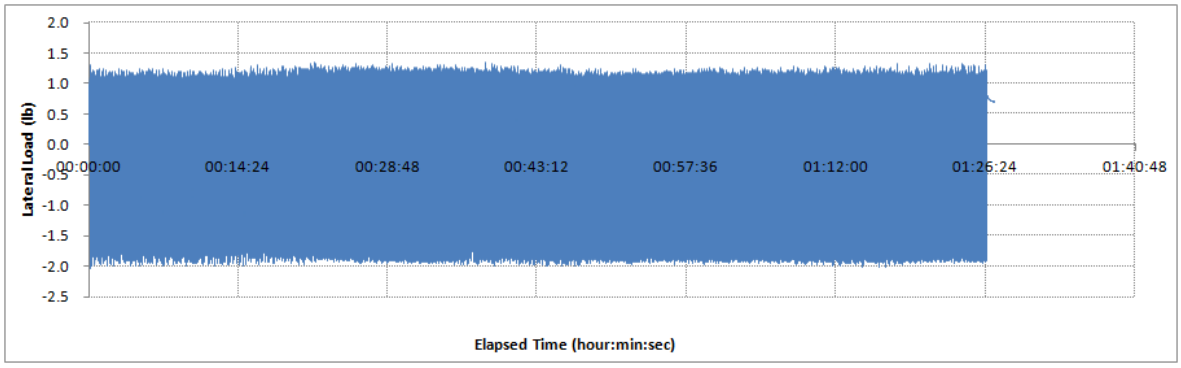

Figure 7.17: Lateral Load of 6-inch Model in OC Clay (2° rotation, 5-sec period)

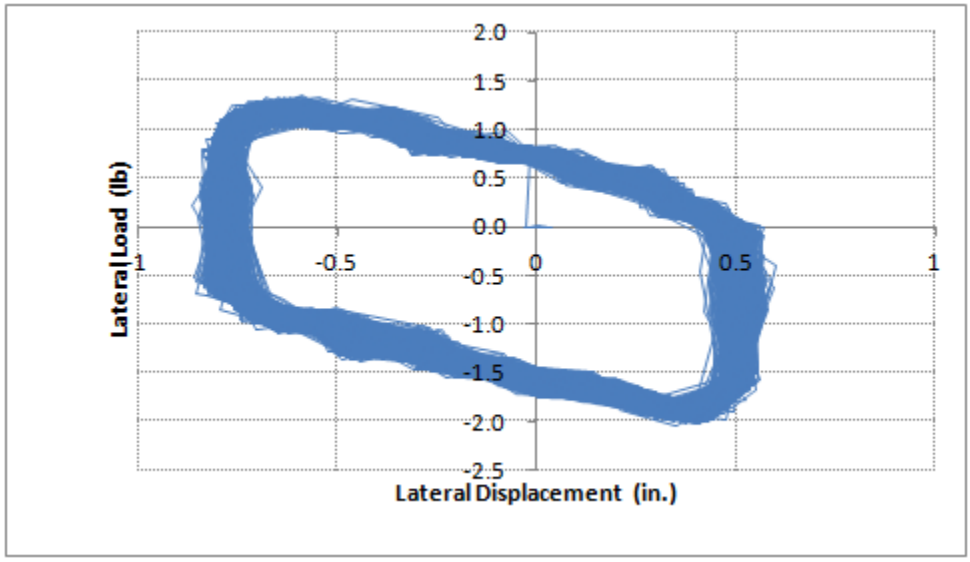

Figure 7.18: Lateral Load versus Lateral Displacement of 6-inch Model in OC Clay (2° rotation, 5-sec period)

Measured lateral loads were relatively stable without significant stiffening or softening effects in most of the tests in coverconsolidated clay. However, softening behavior was usually observed (see Figure 7.19 for example) within the first 100 cycles in the first tests (usually 3-second period tests) at the same rotation angle, because the overconsolidated clay was being remolded. An exception is the first 5-degree rotation, 3-

second period test with a gap accidentally formed before this test. No softening behavior presented at the beginning of this test (see Figure 7.20) due to the gap between the model and the clay. After closing the gap, the test was re-conducted and the softening effect occurred at the beginning of the test again (see Figure 7.21) similar to other 3-second period tests. Figure 7.21 shows that although the measured lateral load (or lateral resistance) was higher in the test without the gap than the test with the gap (see Figure 7.20), the lateral load eventually dropped to approximately the same as the test with the gap.

In general, lateral resistance of the foundation increases with increasing rotation angle of the model in overconsolidated clay. However, the difference of the lateral load for different loading period is not significant. This observation is similar to that from the tests in normally consolidated clay.

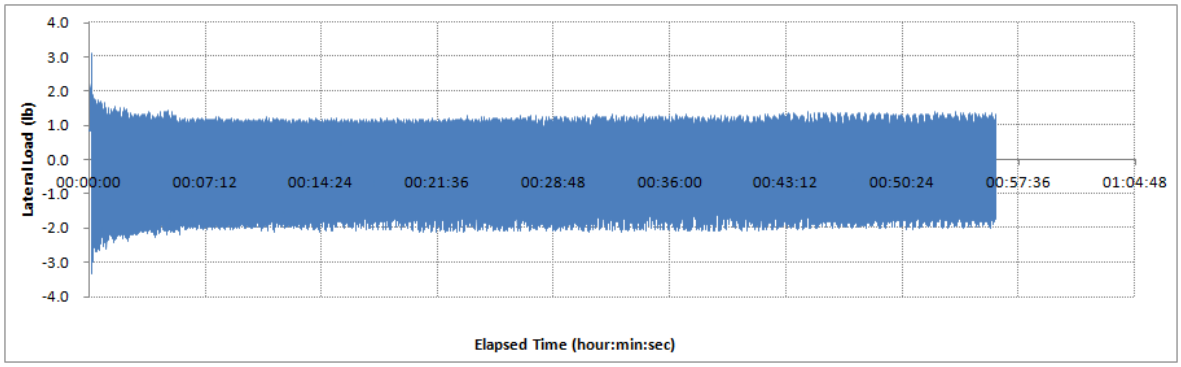

Figure 7.19: Lateral Load of 6-inch Model in OC Clay (2° rotation, 3-sec period)

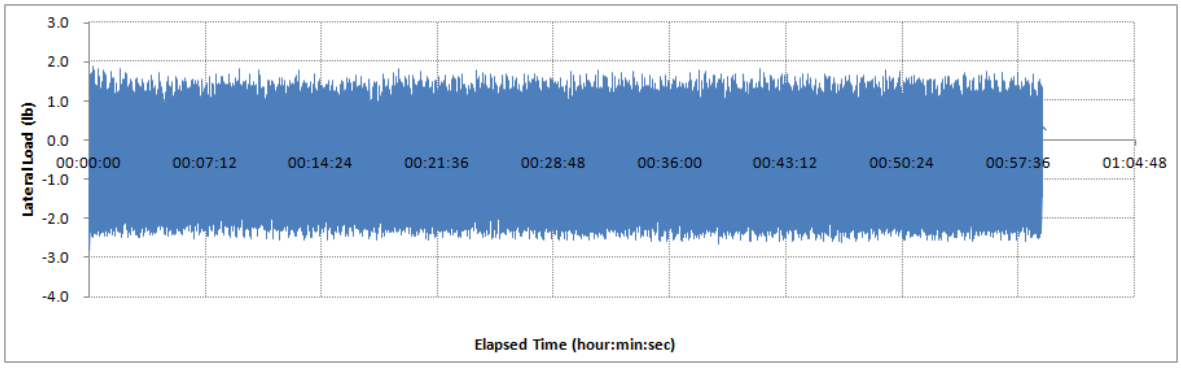

Figure 7.20: Lateral Load of 6-inch Model in OC Clay (5° rotation, 3-sec period with gap)

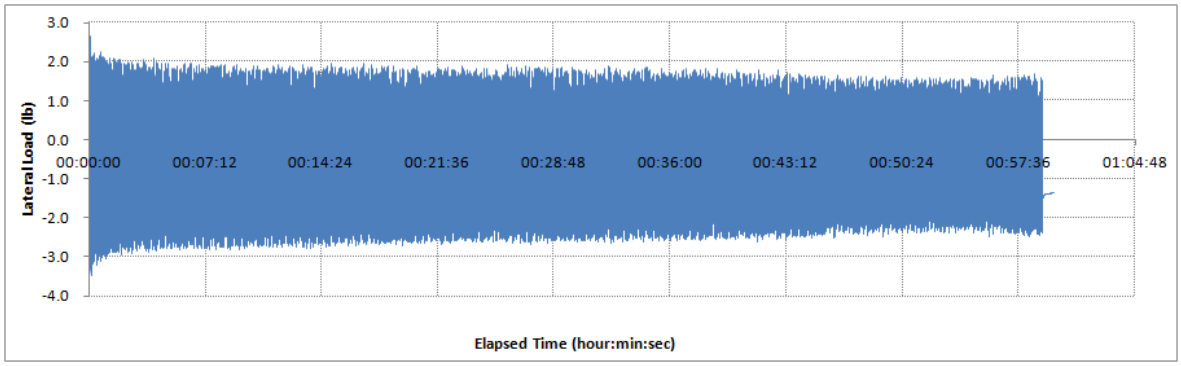

Figure 7.21: Lateral Load of 6-inch Model in OC Clay (repeated 5° rotation, 5-sec period test with gap closed)

The excess pore water pressures for the 2-degree rotation and 5-second period lateral load test are shown in Figure 7.22 and 7.23. The excess pore water pressures are calculated by subtracting the hydrostatic pressures from the corresponding measured pore water pressures. Similar to the tests in the normally consolidated clay, the excess pore water pressure has larger fluctuations near the tip of the model (closer to the failure plane under the suction can) under cyclic lateral loads.

Since the tubes and the geotextile patches for pressure measurements are on the right side of the inner wall of the model, the excess pore water pressures increase when

the model tilts to the right and decrease when it tilts to the left because of the suction generated. The excess pore water pressures are less than those from the 1-foot diameter model in the normally consolidated clay because the 6-inch model has a lighter weight and thus less total stress. However, the ranges of the excess pore water pressure fluctuation are similar for the 1-foot diameter model in normally consolidated clay.

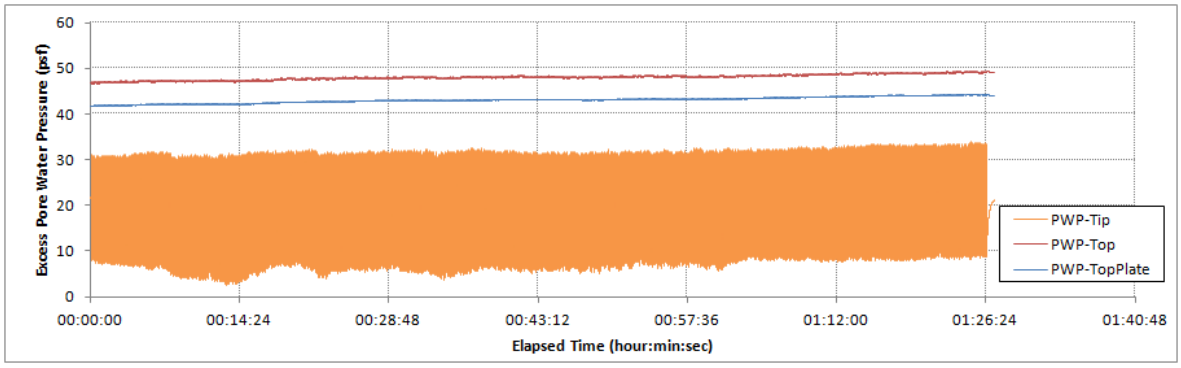

Figure 7.22: Excess Pore Water Pressure of 6-inch Model in OC Clay (2° rotation, 5-sec period)

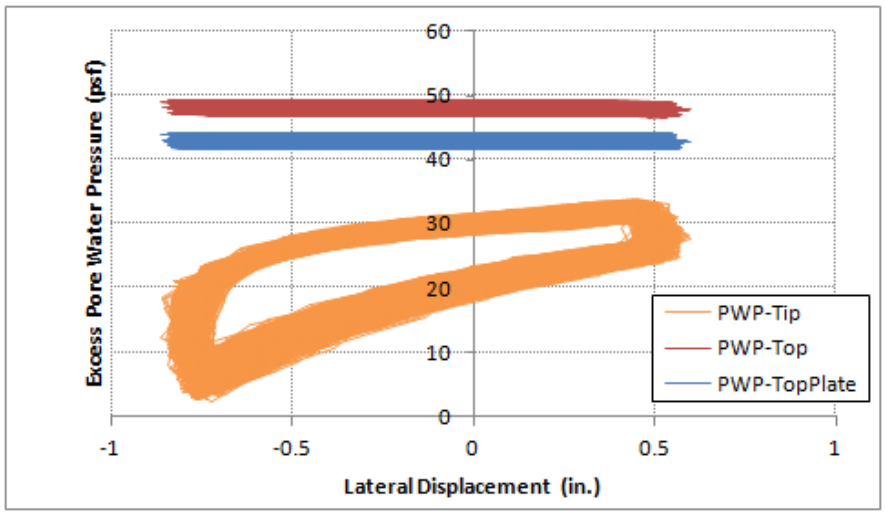

Figure 7.23: Excess Pore Water Pressure versus Lateral Displacement of 6-inch Model in OC Clay (2° rotation, 5-sec period)

The tilt angles for the 2-degree rotation and 5-second period lateral load test are shown in Figure 7.24 and 7.25. The tilt angle in the direction perpendicular to loading is close to zero degree as expected. The tilt angle in the loading direction fluctuates between -1.3 and 1.4 degrees, where the positive angle indicates that model tilts to the left and negative angle indicates right-tilting movement. The measured tilt angle is larger than the target tilt of -1.0 to 1.0 degree because the tilt meter is not accurate under fast acceleration and de-acceleration. Therefore, the tilt angle is more accurate for 10-second period tests but less accurate for tests with shorter loading period.

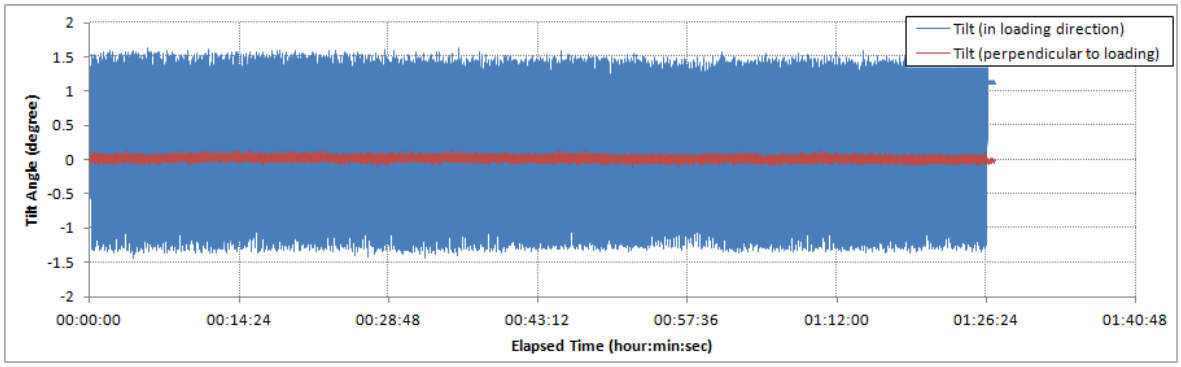

Figure 7.24: Tilt Angles of 1-foot Model in OC Clay (2° rotation, 5-sec period)

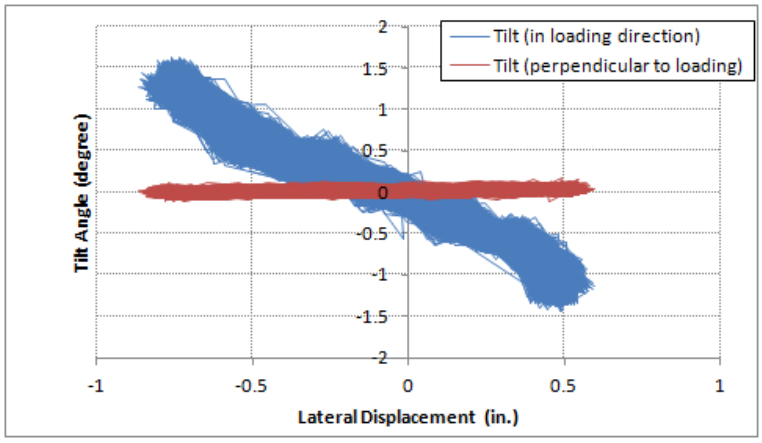

Figure 7.25: Excess Pore Water Pressure versus Lateral Displacement of 1-foot Model in OC Clay (2° rotation, 5-sec period)

7.3 AXIAL LOAD TESTS

Axial load tests on the 6-inch diameter model in overconsolidated clay were conducted by placing several 5-lb weights on the model in steps. The weights were placed on the model in steps to apply approximately 10, 20, and 30 lb of load with around 30 seconds for each step. The vertical displacement of the model was monitored using a dial gauge. Figure 7.26 shows the load-displacement curves of three loading-unloading cycles.

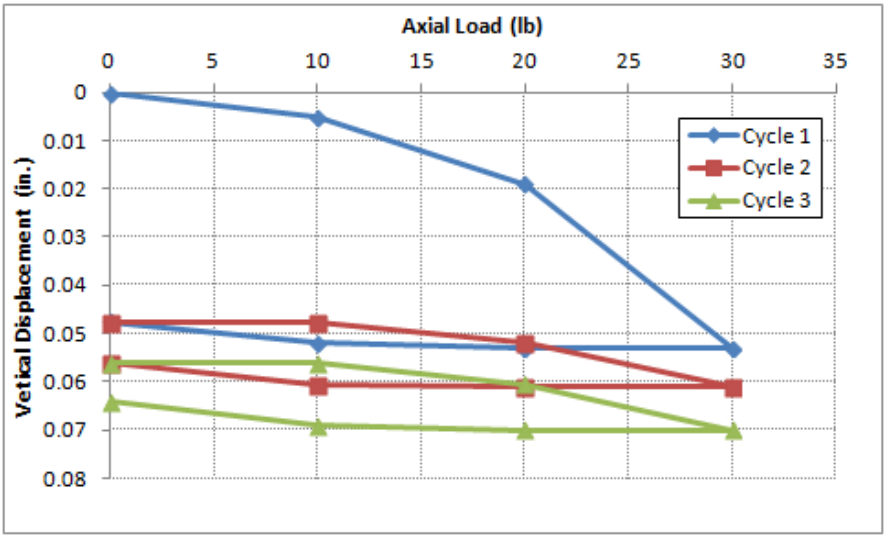

Figure 7.26: Load-Displacement Curve from Axial Load Tests

The excess pore water pressures of the three cycles of axial load tests are shown in Figure 7.27 to 7.29. The theoretical excess pore water pressures shown in the figure were calculated by taking the submerged weight of weights placed on the model divided by the circular cross-section area of the model. The calculated excess pore water pressures are higher than the measured ones because it's not a simple one dimensional loading case. The total stress does not confined in the soil under or in the suction can but part of it spreads out in a 3 dimensional space.

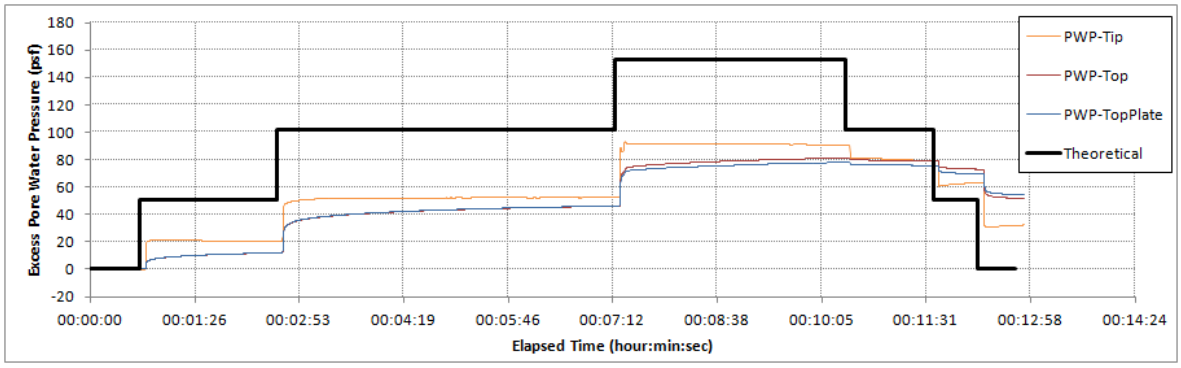

Figure 7.27: Excess Pore Water Pressure from Axial Load Test (Cycle 1)

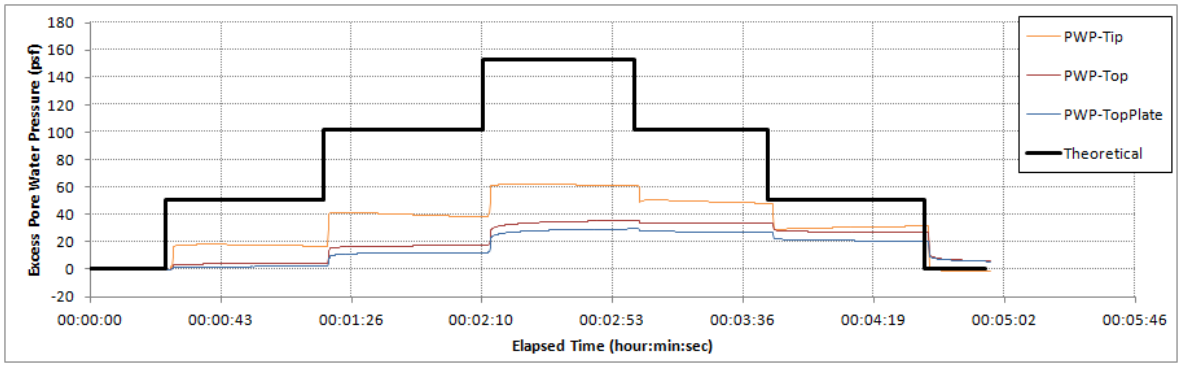

Figure 7.28: Excess Pore Water Pressure from Axial Load Test (Cycle 2)

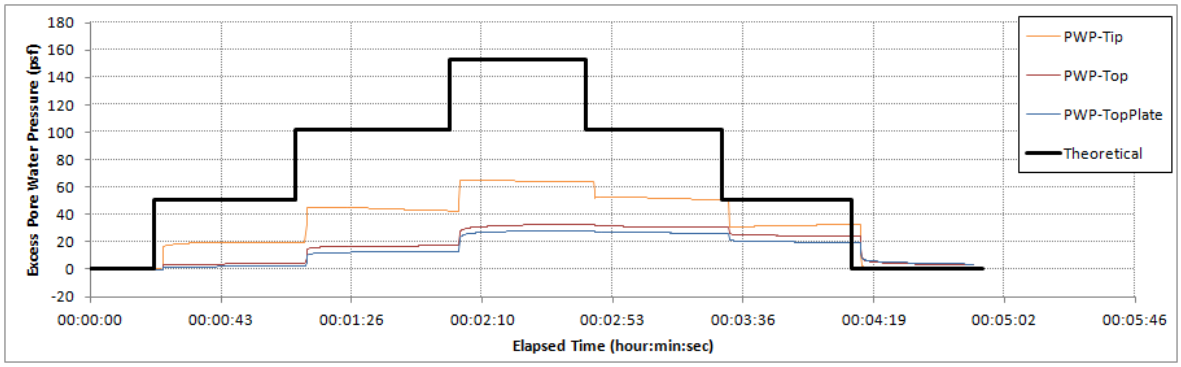

Figure 7.29: Excess Pore Water Pressure from Axial Load Test (Cycle 3)

7.4 ULTIMATE AXIAL CAPACITY TEST

Ultimate axial capacity tests were conducted after all the axial and lateral load tests were completed. The axial load was applied by stacking weights on the model in steps, and the vertical displacement of the model was measured by a dial gauge.

The load-displacement curve from the ultimate axial capacity test is shown in Figure 7.30. Note that the weight of the model was not included in the axial load shown in Figure 7.30. If failure is defined by reaching a displacement of 0.1 diameter of the model (0.6 inch), the ultimate axial capacity in compression for the 6-inch diameter SCF model is approximately 50 lb in overconsolidated clay.

The capacity of the 6-inch diameter SCF model can be calculated by the outer wall side shear resistance plus the bearing from plugged circular tip area of the suction can. The calculated axial capacity is approximately 83 lb by using the API method (see Equation 2.4) and assuming no gap between the foundation and the soil. Note that for the calculation of the installation resistance, a constant undrained shear strength of 45 psf/ft is assumed according to the T-bar tests conducted on the same day. The adhesion factor between the soil and the model (α) is calculated to be 0.36 according to Equation 7.1 (API RP 2GEO 2011). Since α varies with depth, a depth averaged α is calculated by integrating α along the length of the foundation and then divided by the foundation length. The bearing capacity factor for the plugged tip resistance (N_c) is assumed to be 7.2 by using depth correction suggested by Skempton (1951) for square footing ($D_f/B = 1$ and therefore $d_c = 1.2$). If we assume a gap exists, which was observed in the lateral load tests, the side shear on the foundation can be close to zero. In this case, the calculated axial capacity is approximately 70 lb, which is closer to the weight of the model plus the 52 lb external load required to fail foundation (approximately 61 in total).

$$\alpha = 0.5\Psi^{-0.5} \quad \text{for } \Psi \leq 1.0 \qquad \text{(Equation 7.1)}$$

$$\alpha = 0.5\Psi^{-0.25} \quad \text{for } \Psi > 1.0$$

with the constraint that $\alpha \leq 1.0$

where

$$\Psi = \frac{s_u}{p'_0(z)}$$

$p'_0(z) =$ effective vertical stress at depth z

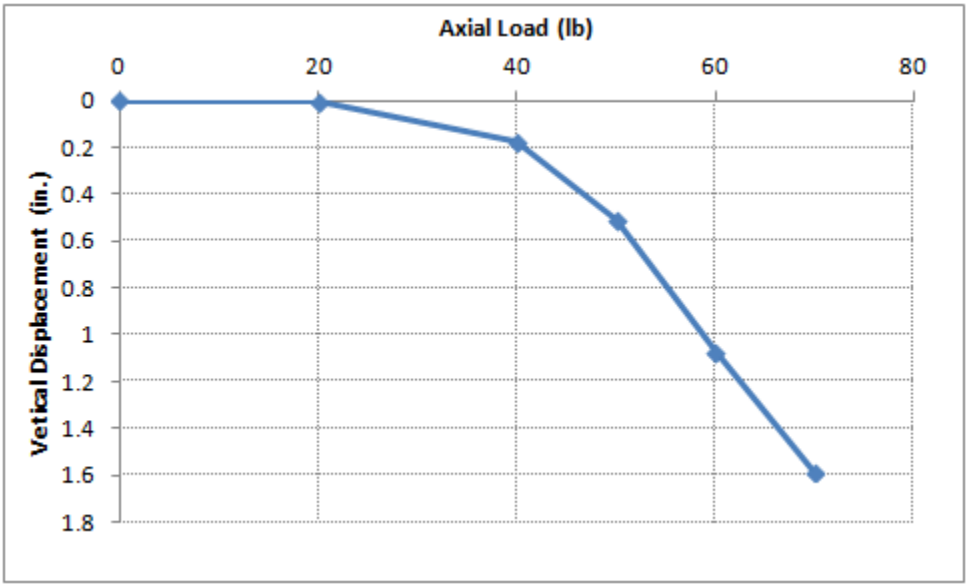

Figure 7.30: Load-Displacement Curve from Ultimate Axial Capacity Test

The excess pore water pressures of ultimate axial capacity tests are shown in Figure 7.31. The theoretical excess pore water pressures shown in the figure were calculated by taking the submerged weight of weights placed on the model divided by the circular cross-section area of the model. The calculated excess pore water pressures are higher than the measured ones in general. All the pressure transducers reached their capacity when 40 lbs of weight were placed on the model (when the calculated pressure

reached 200 psf in Figure 7.31); therefore, the excess pore water pressures were cutoff in the rest of the test.

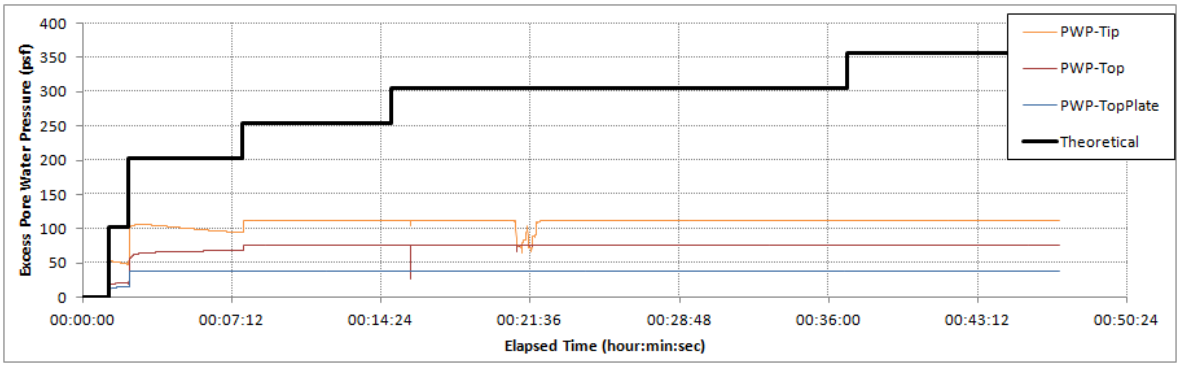

Figure 7.31: Excess Pore Water Pressure from Ultimate Axial Capacity Test

7.5 PULLOUT

The 6-inch diameter SCF model was pulled out of the overconsolidated clay after all the tests were completed. Since the capacity of the SCF model in overconsolidated clay exceeds the capacity of our loading system, the model was pulled out manually. The load cell and the linear displacement transducer were attached to the model to measure the load and vertical displacement, respectively. Figure 7.32 shows picture of the model after pullout test. A layer of clay (less than 1/4 inch thick) sticks on the wall of the model indicating an undrained loading condition during pullout. The suction can was plugged when it was pulled out, but the soil plug fell off within one minute (see Figure 7.32). The behavior is similar to the pullout test in normally consolidated clay. The pullout test results in overconsolidated clay are shown in Figure 7.33 to 7.37.

Figure 7.32: The 6-inch Diameter SCF Model after Pullout from OC Clay

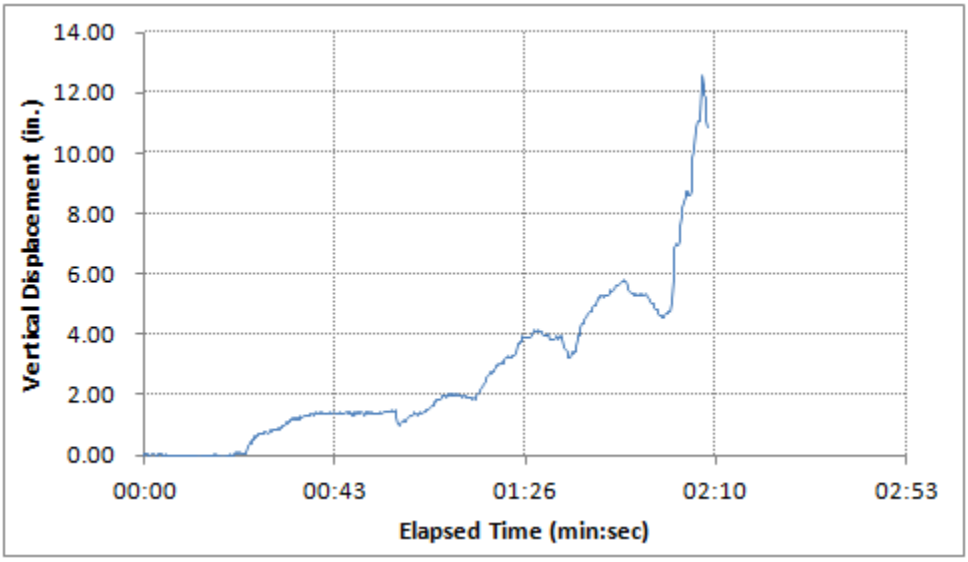

Figure 7.33: Vertical Displacement of 6-inch SCF Model Pullout Test in OC Clay

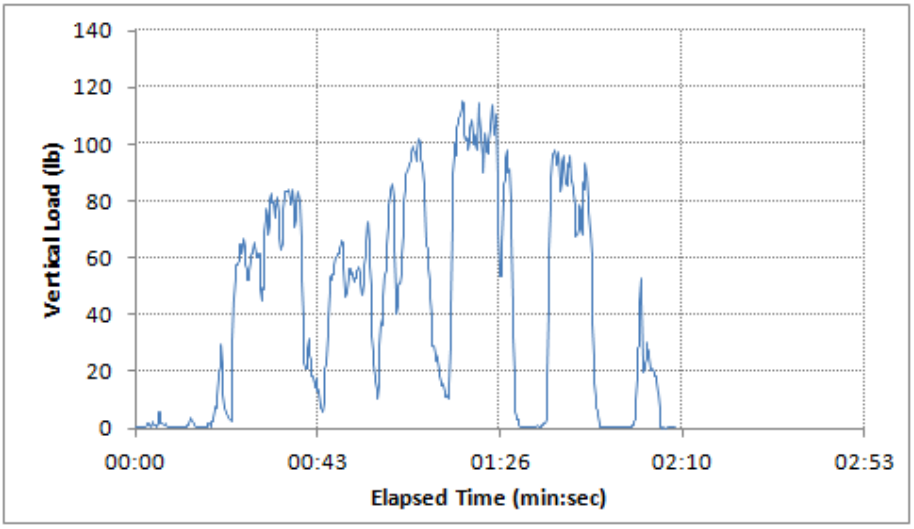

Figure 7.34: Vertical Load of 6-inch SCF Model Pullout Test in OC Clay

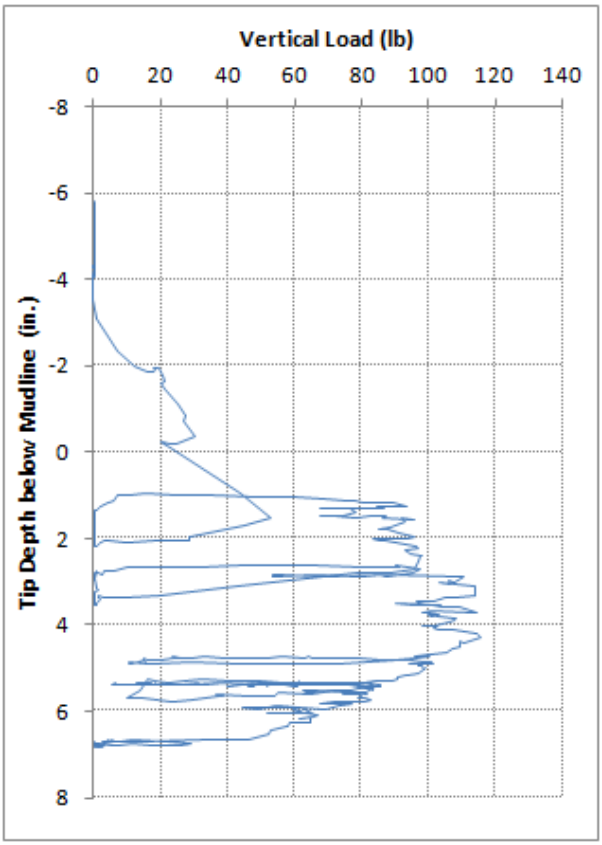

Figure 7.35: Load-Displacement Curve of 6-inch SCF Model Pullout Test in OC Clay

Figure 7.33 to 7.35 show the measured vertical load and displacement during the pullout process. A peak load of 115 lb was measured at 2.46 inches of vertical displacement. The measured pore water pressures during pullout are presented in Figure 7.36 and 7.37. Negative pore water pressures in the figures indicate suction was developed inside the suction can to provide resistance to pullout. Note that all the pressure transducers reached their capacity after the model was pulled upward for 1 inch; therefore, the pore water pressures were cut off in the rest of the test. The pressure increase at Top and Tip after 1 inch is an artificial effect of elevation head correction as presented in Section 5.1.

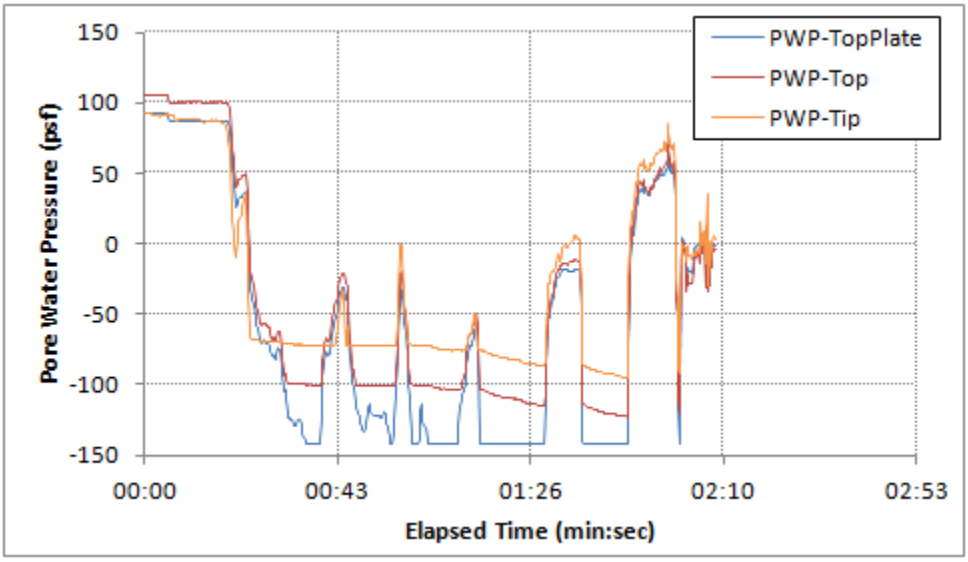

Figure 7.36: Pore Water Pressures of 6-inch SCF Model Pullout Test in OC Clay

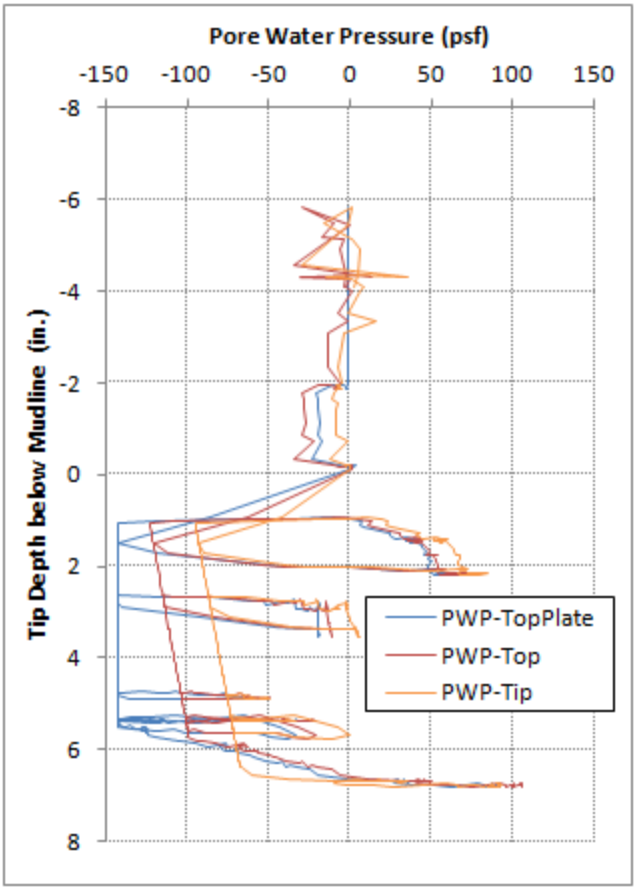

Figure 7.37: Pore Water Pressures versus Displacement of 6-inch SCF Model Pullout Test in OC Clay

7.6 Summary for Tests in Overconsolidated Clay

The overconsolidated kaolinite test bed had a nearly constant undrained shear strength profile. The undrained shear strength was approximately 45 psf measured by a T-bar penetrometer. This undrained shear strength corresponds to a c/p ratio of approximately 4.0 at the mid-depth of the 6-inch suction can. The measured undrained shear strength decreased to 22 psf after remolding the soil by penetrating and pulling out the T-bar for 6 cycles.

The 6-inch diameter SCF model was installed in the overconsolidated clay by pushing in with dead weights. The penetration resistance was consistent with the calculation recommend by API RP 2SK (A 2008) with α equal to the inverse of sensitivity and $N_c = 7.5$ for the tip area of the wall.

For the 1000-cycle lateral load tests, walking of the suction can in overconsolidated clay is not significant (less than 0.03 diameter of the suction can or 0.03 D) for all the 1-, 2-, and 5-degree rations (±0.5, ±1, and ±2.5 degrees) and all the 2-, 5-, and 10-second loading periods. The settlements of the suction can are not significant (less than 0.02 D). Settlement increases with increasing rotation of the foundation and seems to increase with decreasing loading period. The increase in settlement is more prominent when the rotation increases from 2 degrees to 5 degrees. Fissures and cracks formed in the clay around the suction can after cyclic lateral loadings. The circular zone of disturbed soil on the surface extended to approximately 0.6 diameters out from the foundation. A gap (less than 1/4 inch wide) was opened up around the foundation under cyclic lateral loading and was filled with slurry quickly after few hundred cycles of loading.

Measured lateral loads (or lateral resistance) are relatively stable without significant stiffening or softening effects in most of the tests in coverconsolidated clay. However, softening behavior usually occurs within the first 100 cycles in the first tests at the same rotation angle, because the overconsolidated clay is being remolded. If the suction can is loaded laterally with a pre-existing gap between the wall and soil, the measured lateral resistance is stable from the first cycle throughout the test. If the foundation is loaded without the presence of a gap, the lateral resistance tends to be higher in the first couple of the loading cycles and then drop to approximately the same magnitude as the test conducted with a pre-existing gap. The difference in the measured

lateral load for different loading period (3, 5, and 10 seconds) is not significant which indicates that there is little stain rate effect in this range of loading periods. This observation is consistent with the tests in normally consolidated clay.

During cyclic lateral load tests, the excess pore water pressure in the soil plug has larger cyclic fluctuations near the tip comparing to that under the top plate because it is closer to the failure plane under the suction can. This result is also similar to the tests in normally consolidated clay. After installation, the excess pore water pressure built up due to the weight of the suction can never fully dissipated during the period of tests (25 days) in overconsolidated clay.

In overconsolidated clay, there was no clear failure based on the load-displacement curve when the suction can is loaded in compression. Therefore, failure is defined by reaching a displacement of 0.1 diameter of the suction can (0.6 inch). The ultimate axial capacity in compression for the 6-inch diameter SCF model is close to the calculated axial capacity using the method recommended by API with $N_c = 7.2$ (corrected for embedment using the method suggested by Skepmton, 1951) and assuming the presence of a gap ($\alpha = 0$). During the pullout test, a peak load was measured at 0.41 diameter of vertical displacement. Negative pore water pressure (suction) was developed inside the suction can which provides a large proportion of pullout resistance in terms of reverse end bearing. A layer of clay (less than 1/4 inch thick) sticks on the wall of the suction can indicates that it was under undrained loading condition during pullout. The suction can was plugged when it was pulled out, but the soil plug fell off within one minute.

Chapter 8: Tests in Loose Siliceous Sand Test Bed

The 6-inch diameter SCF model was used for the scale model tests in the loose siliceous sand test bed. The properties of the loose siliceous sand test bed can be found in Section 2.3. The scale model tests conducted in this test bed includes: lateral load tests, axial load tests, proof load test, and pullout. The test procedure and the summary of test results are presented in the following sections.

8.1 INSTALLATION

The 6-inch diameter SCF model was placed in the test bed while preparing the loose sand deposit that represents a "wish in place" condition. As presented in Section 2.3, the test bed was prepared by first flooding the tank and then the sand was rained into the water carefully to create a loose sand deposit. Subsequently, the model was carefully twisted into the deposit to minimize the compaction of sand. Figure 8.1 shows the 6-inch model installed in the loose siliceous sand test bed.

Figure 8.1: 6-inch Diameter SCF Model in Loose Siliceous Sand

8.2 LATERAL LOAD TESTS

Two-way, displacement controlled, cyclic lateral load tests for 6-inch diameter SCF model were conducted in the loose siliceous sand test bed. The lateral tests are similar to those presented in Section 8.2 for 6-inch diameter SCF model in overconsolidated clay. The lateral resistance, the walking displacement (translational permanent displacement), and the settlement were measured under 1000 cycles of lateral load in these tests.

8.2.1 Walking and Settlement

Table 8.1 shows the walking displacement and the settlements of the 6-inch diameter SCF model after 1000 cycles of lateral load for each rotation and period combination in the loose siliceous sand test bed. The walking displacement and settlement of the model for all the lateral load tests are illustrated in Figure 8.2 and 8.3, respectively. Note that the negative values of walking displacement indicate that the model walks in the opposite direction of the mean load; negative values of settlement indicate that the model moves upward.

Soil Type	SCF Model	Rotation (degrees)	Period (seconds)	Mean Load (lbs)	Walking Displ. (inches)	Settlement (inches)	Test Date
Loose Siliceous Sand	6-inch Diameter Model	1	3	0.25	0.17	0.045	8/16/2012
			5	0.25	0.00	-0.003	8/16/2012
			10	0.25	0.03	-0.007	8/16/2012
		2	3	0.50	0.07	-0.069	8/17/2012
			5	0.50	0.07	0.138	8/17/2012
			10	0.50	-0.07	0.091	8/17/2012
		5	3	1.25	0.20	0.058	8/28/2012
			5	1.25	0.12	-0.315	8/28/2012
			10	1.25	-0.10	-1.073	8/28/2012

* Note: negative values of walking displacement indicate that the model walks in the opposite direction of the mean load; negative values of settlement indicate that the model moves upward.

Table 8.1: Walking and Settlement of 6-inch Diameter SCF Model after 1000 Cycles of Lateral Load in Loose Siliceous Sand

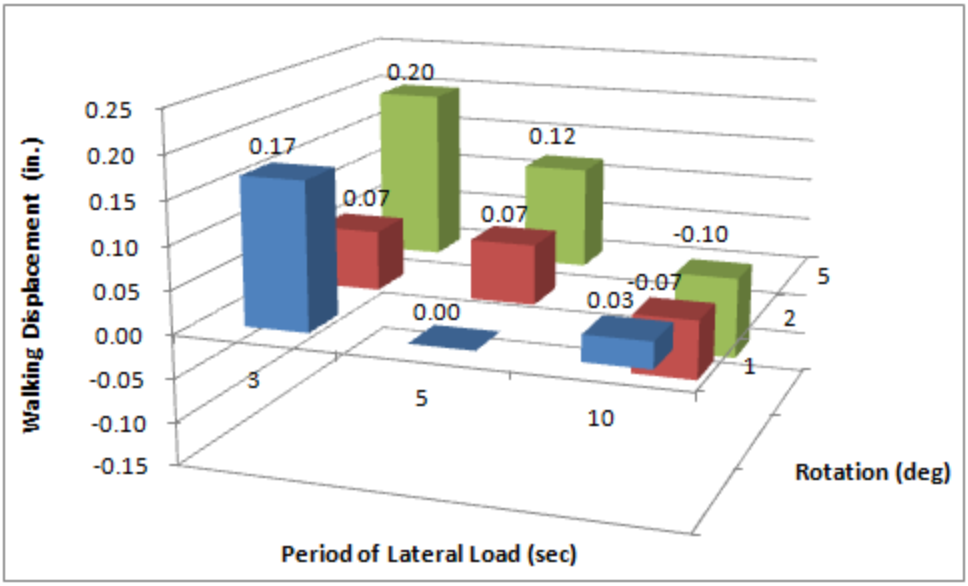

Figure 8.2: Walking of 6-inch Diameter SCF Model in Loose Siliceous Sand

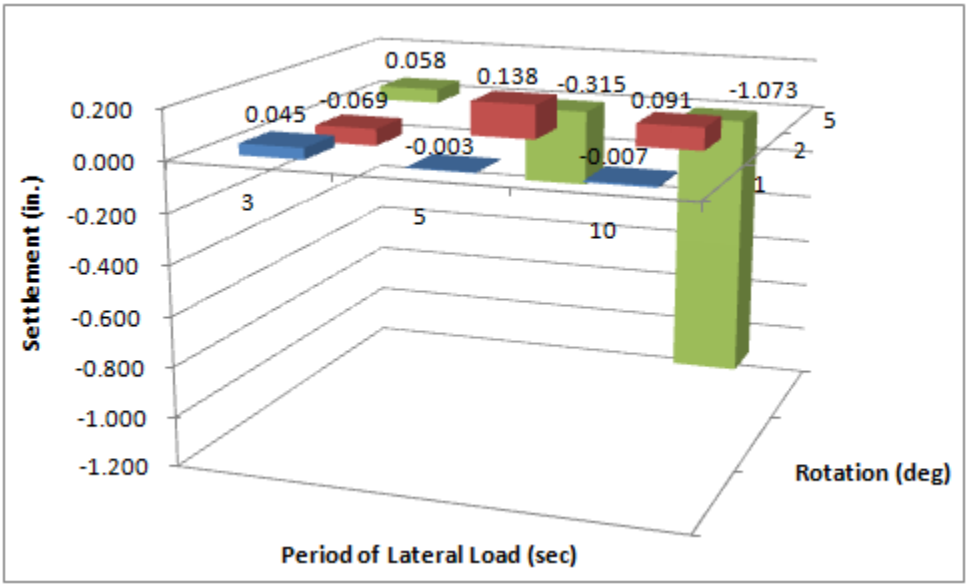

Figure 8.3: Settlement of 6-inch Diameter SCF Model in Loose Siliceous Sand

Figure 8.2 shows that walking of the model in loose siliceous sand is not significant for all the ration angles and loading periods. The walking displacements are

all within 0.03 diameter of the model (less than 0.03 D). Figure 8.3 shows no significant settlement of the model with 1 and 2-degree rotations (less than 0.02 D). However, the model may have more significant settlements or upward movements with 5-degree rotation. In the 5-degree, 10-second period test, the model moves upward for 1.07 inches (0.18 D) after 1000 cycles of lateral load.

Pictures of the 6-inch SCF model after lateral load tests in loose siliceous sand are shown in Figure 8.4 to 8.6. Localized liquefaction of the loose sand around the model was observed when the model was rotating cyclically because of the increase in pore water pressure. The sand flowed around the model during the lateral load test. After cycles of lateral loading, a cone-shape depression formed around the model on the surface of the sand deposit. The cone-shape depression extended to approximately 0.5 diameters out from the model (see Figure 8.4 to 8.6).

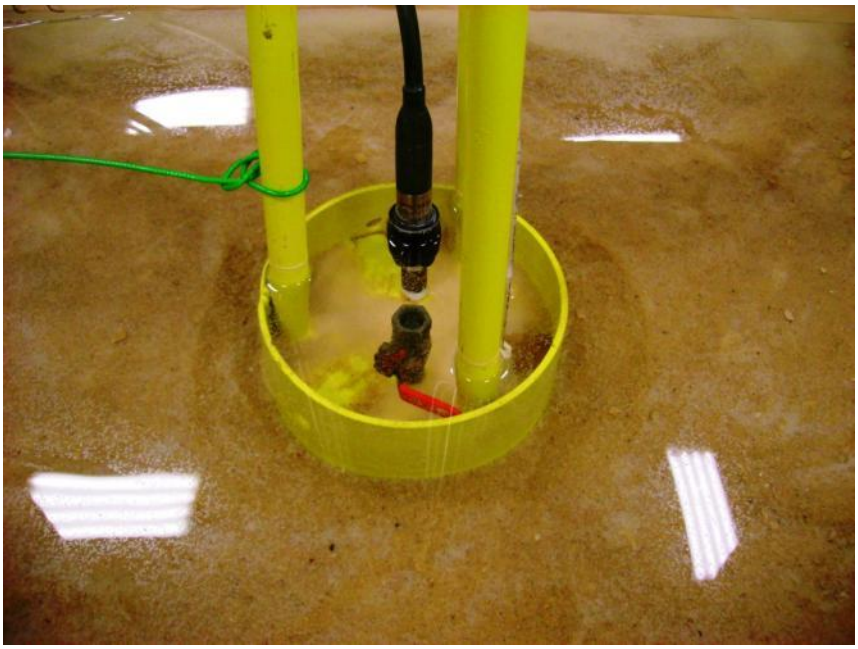

Figure 8.4: SCF Model after 1-degree Lateral Load Tests in Loose Siliceous Sand

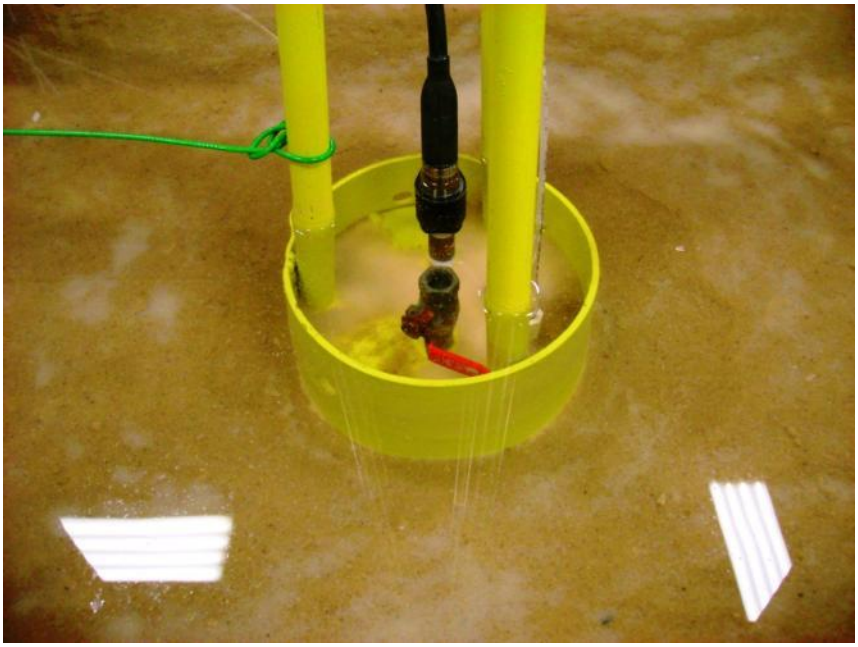

Figure 8.5: SCF Model after 2-degree Lateral Load Tests in Loose Siliceous Sand

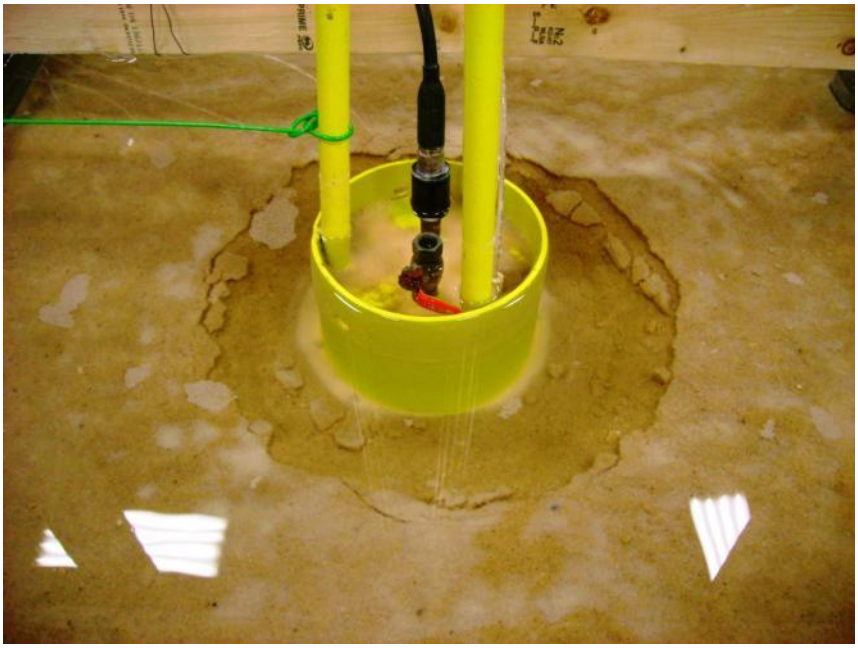

Figure 8.6: SCF Model after 5-degree Lateral Load Tests in Loose Siliceous Sand

8.2.2 Lateral Load, Displacement, Pore Water Pressure, and Tilt Angle

In terms of the lateral load, lateral displacement, pore water pressure, and tilt angle measurements, the 2-degree rotation and 5-second period test is taken as an example for the lateral tests in loose siliceous sand.

The time history of the 1000-cycle lateral load and lateral displacement are presented in Figure 8.7 and 8.8. The lateral load and displacement are both measured at 3 ft above the top plate of the model (or 3 ft above the mudline) as shown in Figure 6.4. The hysteresis loops of later load versus lateral displacement are shown in Figure 8.9.

In Figure 8.7, positive lateral displacement indicates that the model tilts to the right while negative displacement indicates left tilting movement. The lateral displacement fluctuates within a stable range and shows no sign of shifting which indicates that the model has no significant walk. The load shown in Figure 8.8 and 8.9 are obtained by subtracting the weight of counter weights (see Figure 6.4) from the lateral load measured by the load cell. The load cell registers positive loads when the model tilts to the left and negative loads when it moves to the right. The lateral load shifted slightly to the negative side because of the presence of the mean load as discussed in Section 6.2.2.

In Figure 8.8, the measured lateral load (or lateral resistance) fluctuates in a relatively stable range. No significant stiffening or softening effects were observed in the 2-degree rotation, 5-second period test. Similar trend was observed in most of the lateral load tests except the first lateral load test (1-degree, 3-second test) and the two of the 5-degree rotation tests (5 and 10-second period tests). The lateral loads measured in these tests are shown in Figure 8.10 to 8.12. For the 1-degree rotation, 3-second period test, stiffening behavior was observed (see Figure 8.10) because this is the first test in the loose siliceous sand deposit and the sand was densified slightly under the cyclic loading.

For 5 and 10-second period tests with 5-degree rotation, "softening" behavior was observed (see Figure 8.11 and 8.12) because the model moved upward for 0.3 and 1.1 inches in these two tests, respectively.

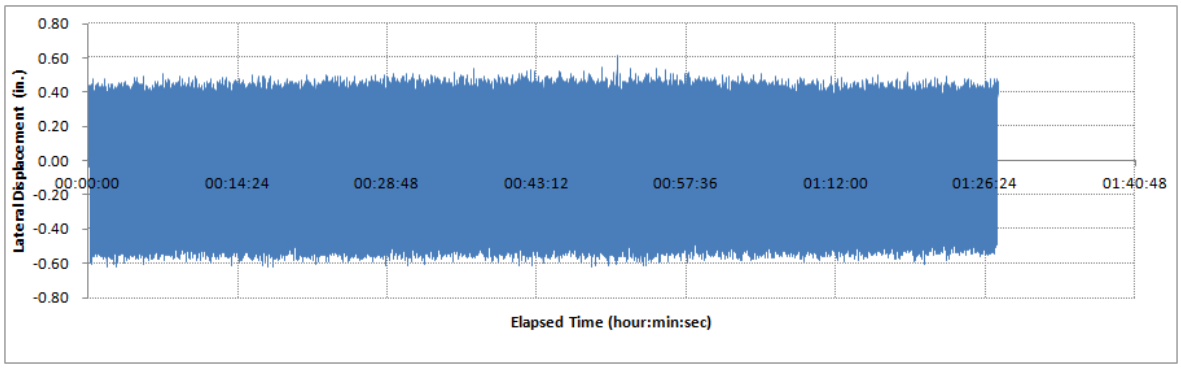

Figure 8.7: Lateral Displacement of 6-inch Model in Loose Siliceous Sand (2°, 5 sec)

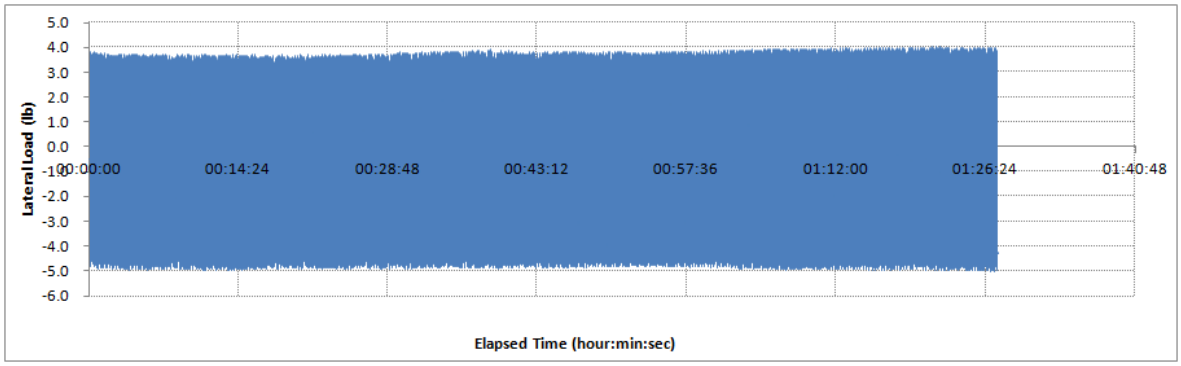

Figure 8.8: Lateral Load of 6-inch Model in Loose Siliceous Sand (2°, 5 sec)

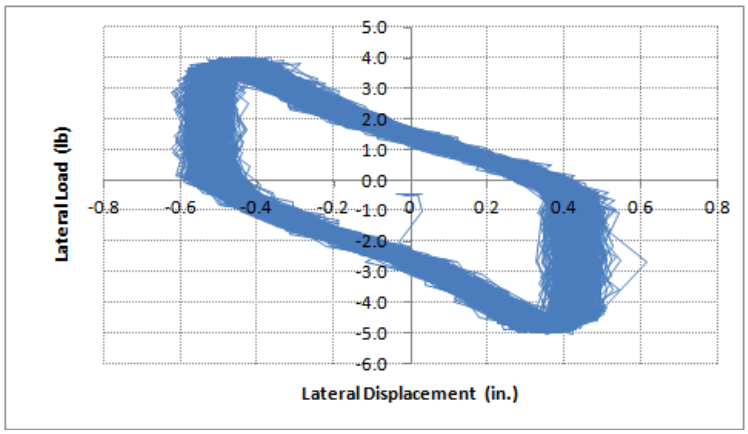

Figure 8.9: Lateral Load versus Lateral Displacement of 6-inch Model in Loose Siliceous Sand (2°, 5 sec)

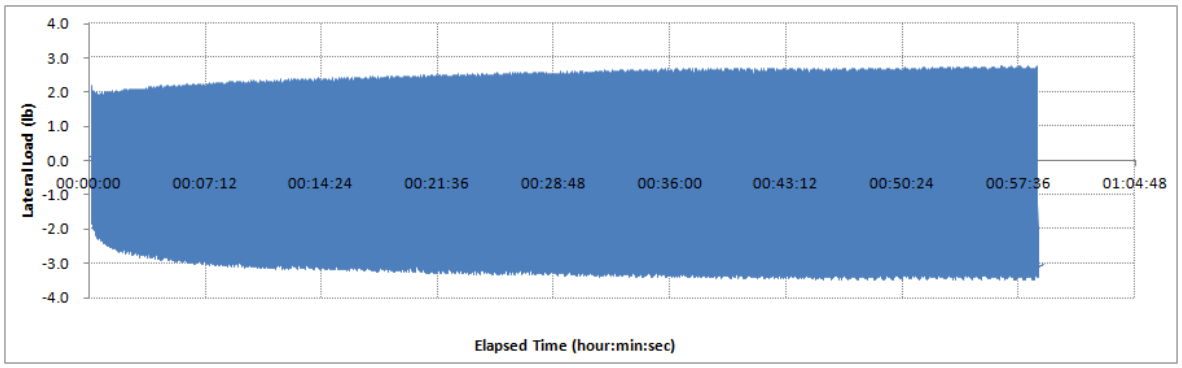

Figure 8.10: Lateral Load of 6-inch Model from First Lateral Load Test in Loose Siliceous Sand (1°, 3 sec)

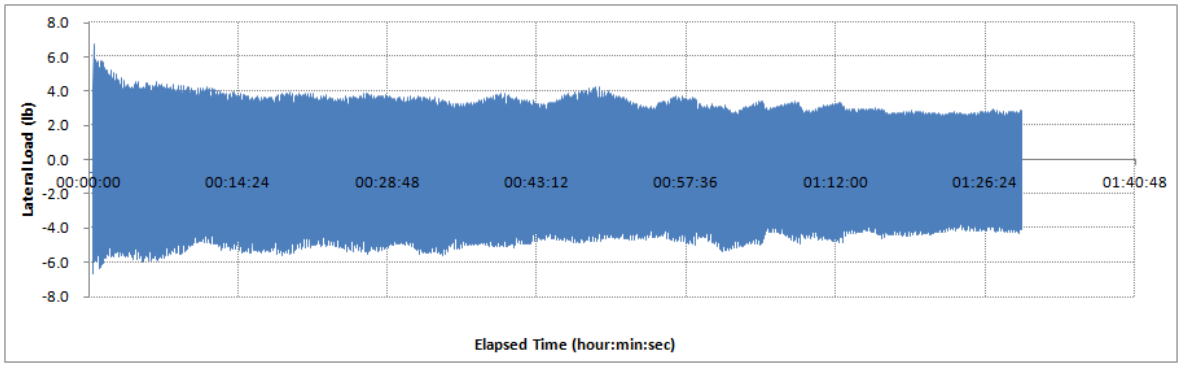

Figure 8.11: Lateral Load of 6-inch Model in Loose Siliceous Sand (5°, 5 sec)

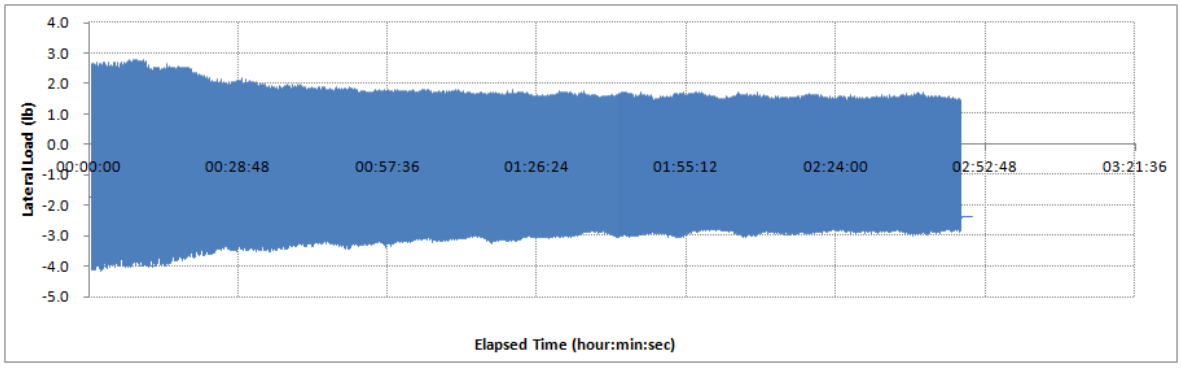

Figure 8.12. Lateral Load of 6-inch Model in Loose Siliceous Sand (5°, 10 sec)

In general, the lateral resistance of the foundation increases with increasing rotation angle of the model in loose siliceous sand. However, the difference of the lateral load for different loading period is not significant. This observation is similar to those from the tests in clay.

The excess pore water pressures for the 2-degree rotation and 5-second period lateral load test are shown in Figure 8.13 and 8.14. The excess pore water pressures are calculated by subtracting the hydrostatic pressures from the corresponding measured pore water pressures. The pressure at Tip still has a larger range of fluctuation; however, the excess pore water pressures are more uniform inside the suction can in the loose siliceous sand comparing to the tests in clay. The excess pore water pressure redistribute much more quickly inside the suction can in sand because of its higher permeability. Previous tests in clay show that the pore water pressures increase when the model tilt to the right and decrease when the model tilt to the other side because of the generated suction. However, in sand, pore water pressures increase whether the model tilts to either direction and subsequently decreases when the model is changing its tilting direction due to the cyclic loads. This can also be attributed to the high permeability of sand.

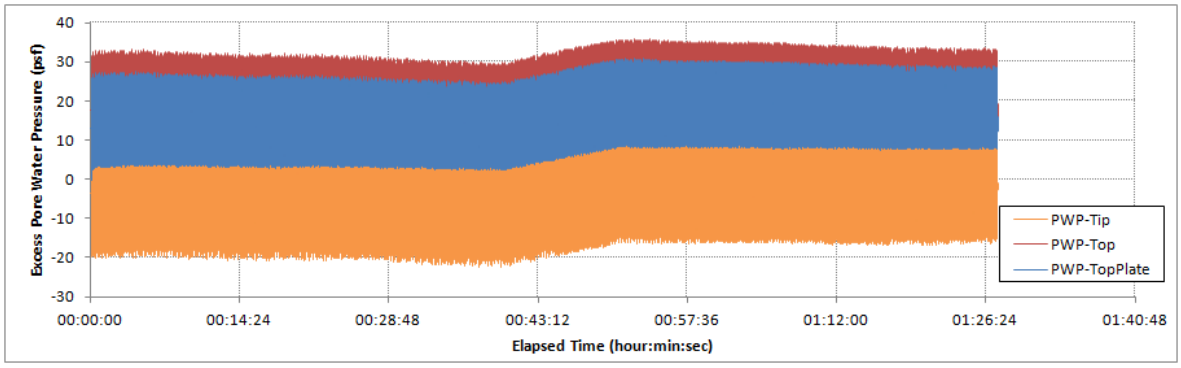

Figure 8.13: Excess Pore Water Pressure of 6-inch Model in Loose Siliceous Sand (2° rotation, 5-sec period)

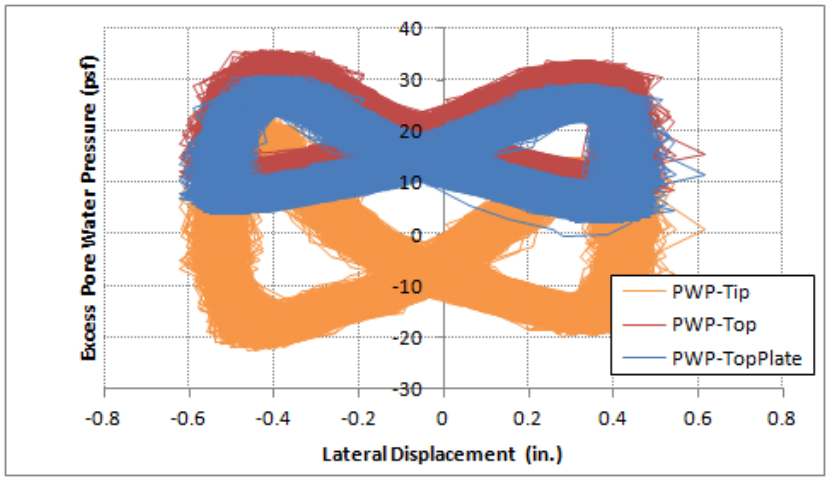

Figure 8.14: Excess Pore Water Pressure versus Lateral Displacement of 6-inch Model in Loose Siliceous Sand (2° rotation, 5-sec period)

The tilt angles for the 2-degree rotation and 5-second period lateral load test are shown in Figure 8.15 and 8.16. The tilt angle in the direction perpendicular to loading is close to zero degree as expected. The tilt angle in the loading direction goes between +/- 1.0 degree, where the positive angle indicates that model tilts to the left and negative angle indicates right-tilting movement.

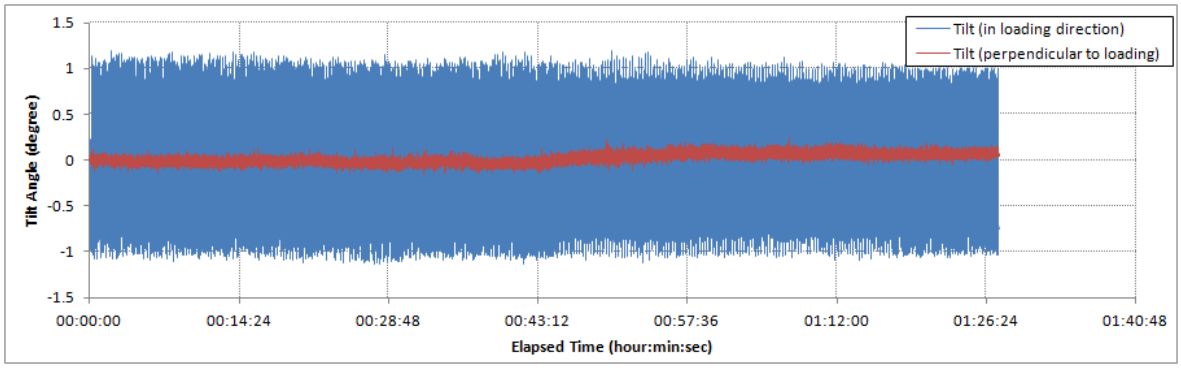

Figure 8.15: Tilt Angles of 1-foot Model in Loose Siliceous Sand (2° rotation, 5-sec period)

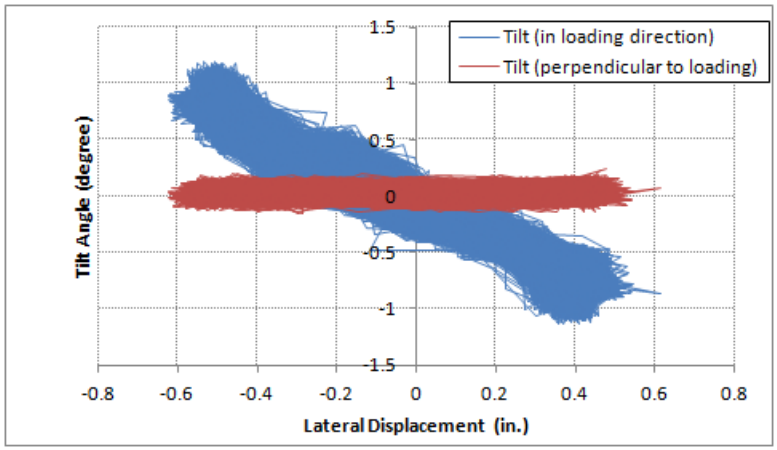

Figure 8.16: Excess Pore Water Pressure versus Lateral Displacement of 1-foot Model in Loose Siliceous Sand (2° rotation, 5-sec period)

8.3 Axial Load Tests

Axial load tests on the 6-inch diameter model in loose siliceous sand were conducted by placing several 5-lb weights on the model in steps. A piece of plywood was place on the model to for stacking the weights (see Figure 8.17). The weights were placed on the model in steps to apply approximately 10, 20, and 30 lb of load with around 30 seconds for each step. The vertical displacement of the model was monitored using a dial

gauge. Figure 8.18 shows the load-displacement curves of three loading-unloading cycles.

The excess pore water pressures of the three cycles of axial load tests are shown in Figure 8.19 to 8.21. The theoretical excess pore water pressure is assumed to be zero because the high permeability of the sand and the loading is under a drained condition. The measured excess pore water pressures are essentially zero, which match well with the assumed drained condition. The pore water pressure at Top Plate varies slightly with the increase or decrease of weights on the model; however, the variation is very small (within 2 psf).

Figure 8.17: Axial Load Test in Loose Siliceous Sand

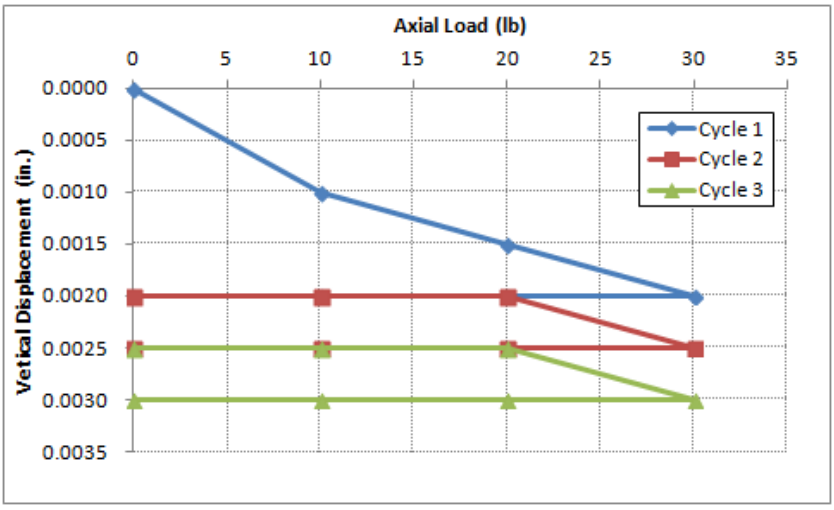

Figure 8.18: Load-Displacement Curve from Axial Load Tests

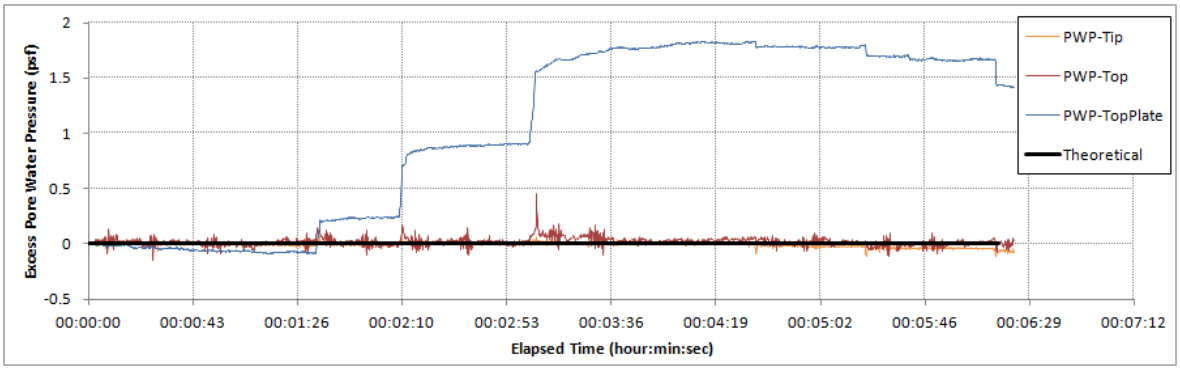

Figure 8.19: Excess Pore Water Pressure from Axial Load Test (Cycle 1)

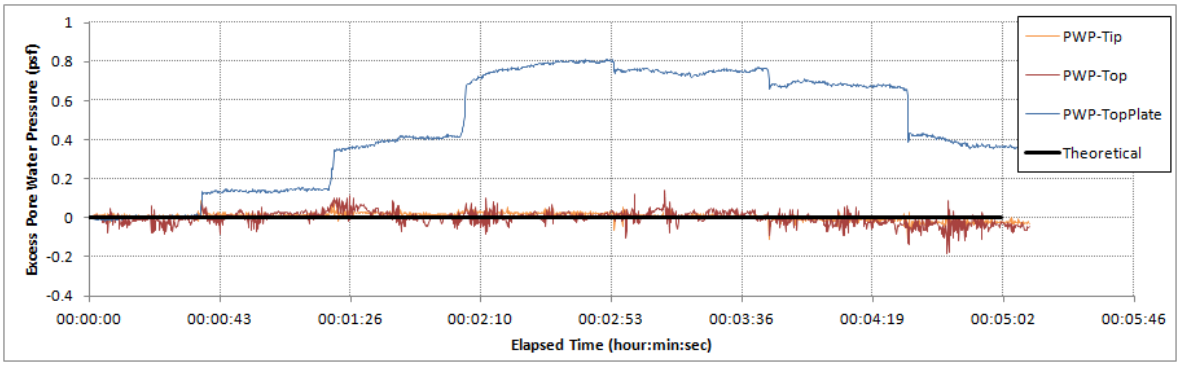

Figure 8.20: Excess Pore Water Pressure from Axial Load Test (Cycle 2)

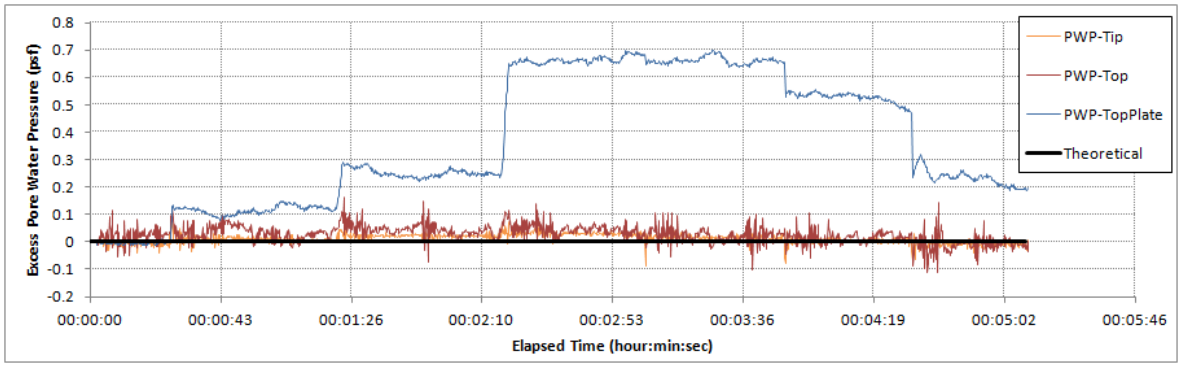

Figure 8.21: Excess Pore Water Pressure from Axial Load Test (Cycle 3)

8.4 PROOF LOAD TESTS

Proof load tests were conducted instead of ultimate axial capacity test because the load required to failure the model foundation in sand exceeds the capacity our loading system. The proof load tests were conducted after all the axial and lateral load tests were completed. The axial proof load was applied by stacking weights on the model in steps, and the vertical displacement of the model was measured by a dial gauge. The model was loaded up to 292 lb and then uploaded for two cycles. The load-displacement curves from the two proof tests are shown in Figure 8.22. The maximum vertical displacement of around 0.06 diameter of the model (0.06 D) was measured under the 292 lb proof load in the first cycle. Note that the axial load does not include the weight of the model.

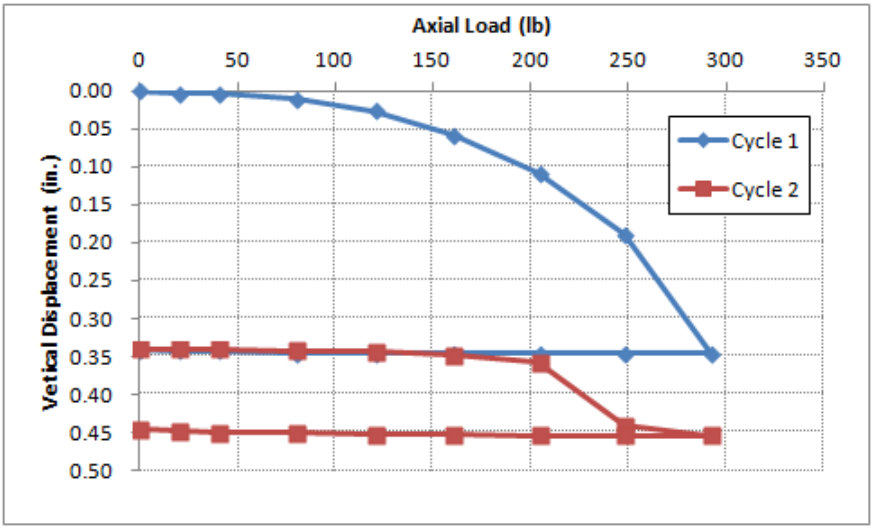

Figure 8.22: Load-Displacement Curve from Proof Load Tests

The excess pore water pressures from the proof load tests are shown in Figure 8.23 and 8.24. The theoretical excess pore water pressure is assumed to be zero because the high permeability of the sand and the loading is under a drained condition. For Cycle 2 of the proof load tests, the excess pore water pressures (see Figure 8.24) are essentially zero before the model is loaded to 248 lb, where the model start to settle more significantly (see Figure 8.22). However, since the model deformed more in Cycle 1, the higher excess pore water pressures (see Figure 8.23) are generated much earlier in the test.

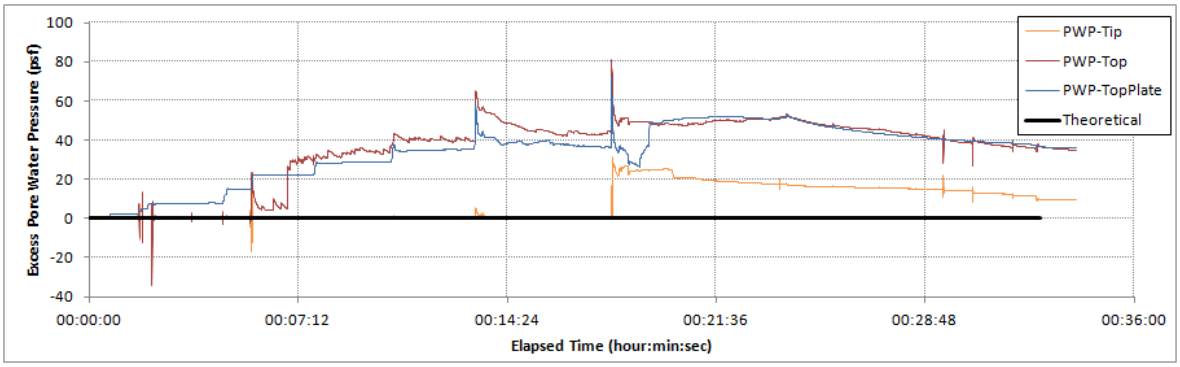

Figure 8.23: Excess Pore Water Pressure from Proof Load Test (Cycle 1)

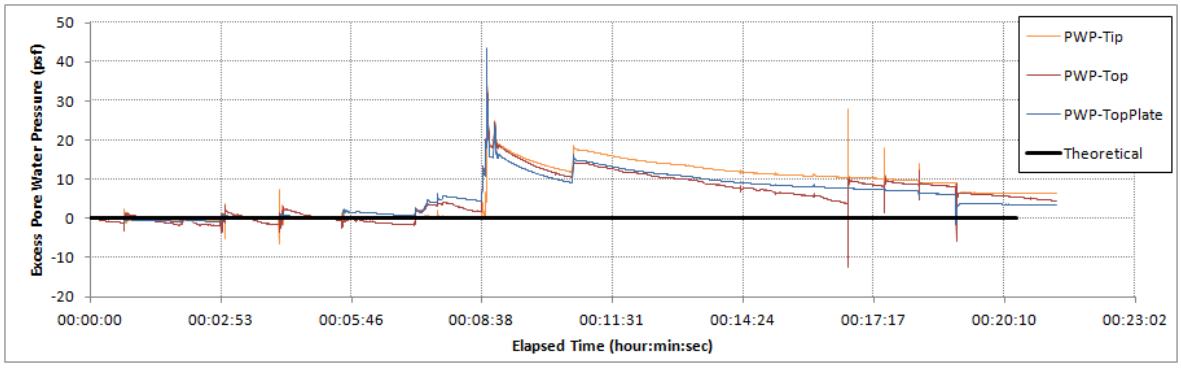

Figure 8.24: Excess Pore Water Pressure from Proof Load Test (Cycle 2)

8.5 PULLOUT

The 6-inch diameter SCF model was pulled out of the loose siliceous sand manually after all the tests were completed. The load cell and the linear displacement transducer were attached to the model to measure the load and vertical displacement, respectively. The suction can was plugged when it was pulled out, but the soil plug fell off within seconds. The pullout test results in loose siliceous sand are shown in Figure 8.25 to 8.29.

Figure 8.25 to 8.27 show the measured vertical load and displacement during the pullout process. A peak load of 46 lb was measured at 0.43 inch of vertical displacement. The model was completely pulled out of soil only after 3.5 inches of displacement (instead of 6 inches) because part of the suction can was above mudline due to the upward movement for the last couple lateral load tests. The measured pore water pressures during pullout are presented in Figure 8.28 and 8.29. Negative pore water pressures in the figures indicate suction was developed inside the suction can to provide resistance to pullout. When suction in the suction can decreases, the measured vertical

load also drops significantly and the soil plug starts to fall out which further decreases the vertical load.

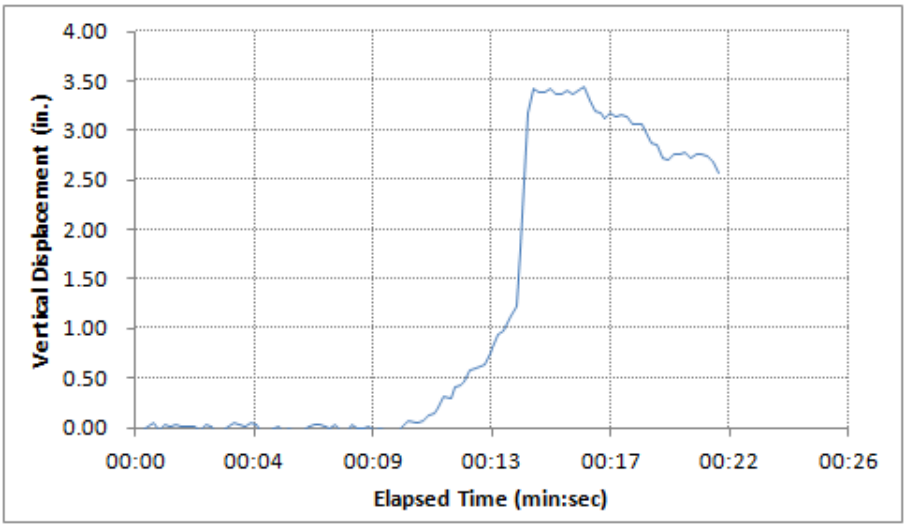

Figure 8.25: Vertical Displacement of 6-inch SCF Model Pullout Test in Loose Siliceous Sand

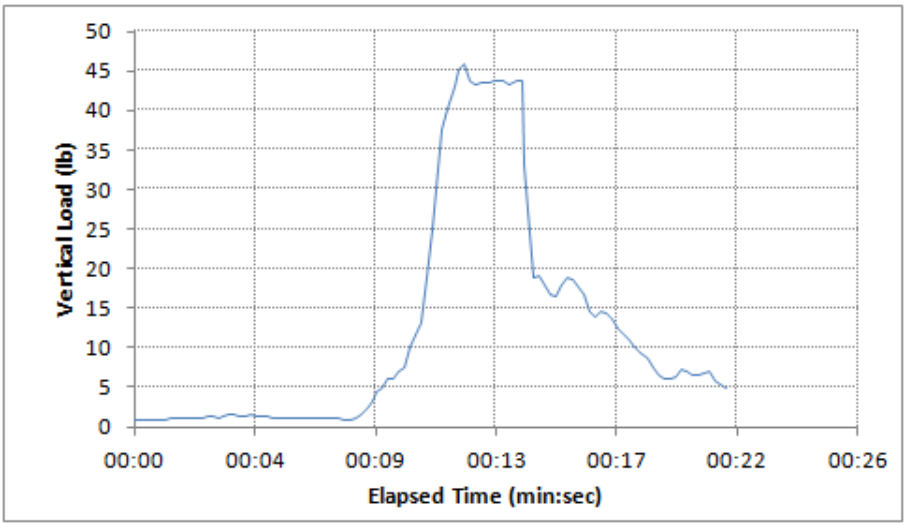

Figure 8.26: Vertical Load of 6-inch SCF Model Pullout Test in Loose Siliceous Sand

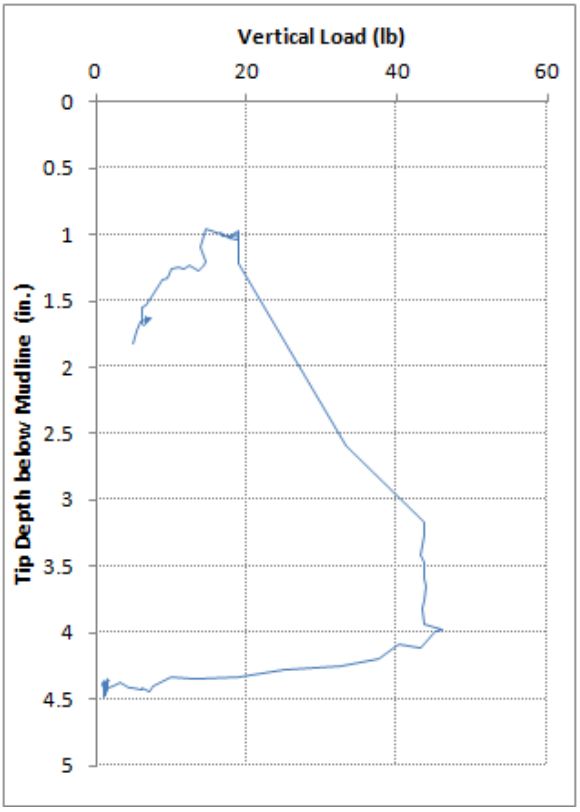

Figure 8.27: Load-Displacement Curve of 6-inch SCF Model Pullout Test in Loose Siliceous Sand

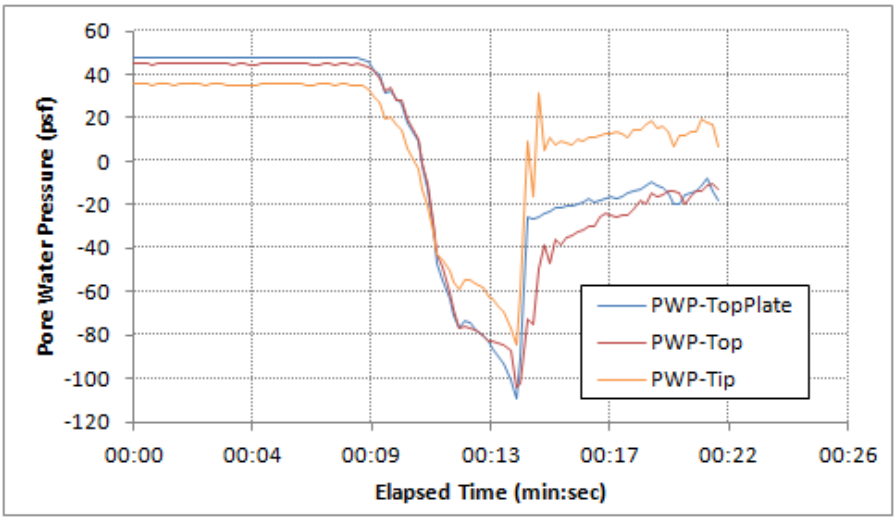

Figure 8.28: Pore Water Pressures of 6-inch Model Pullout Test in Loose Siliceous Sand

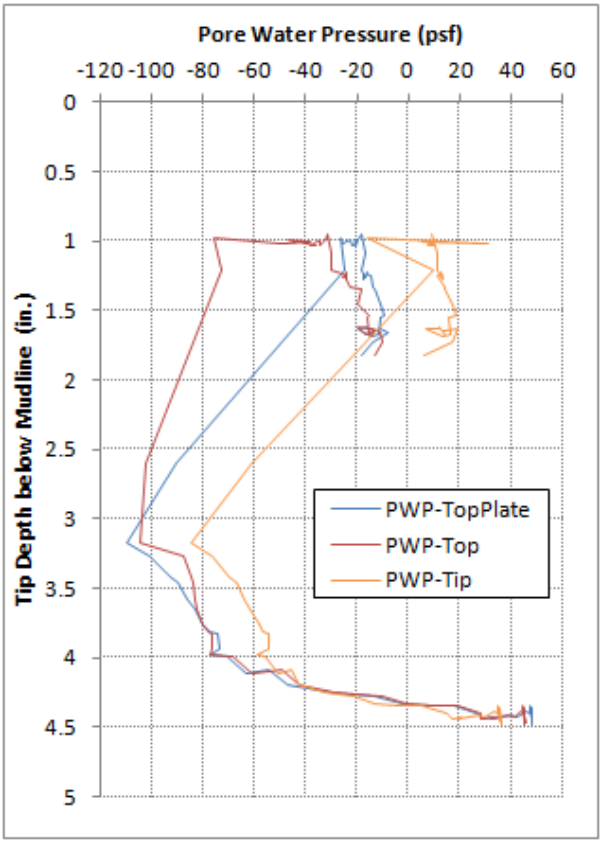

Figure 8.29: Pore Water Pressures versus Displacement of 6-inch SCF Model Pullout Test in Loose Siliceous Sand

8.6 Summary for Tests in Loose Siliceous Sand

The poorly graded siliceous sand in the loose siliceous sand test bed had a mean grain size of 0.4 mm with an estimated saturated unit weight of 113 pcf. The cone tip resistance at 6 inches deep was between 400 to 1200 psf according to cone penetrometer tests. The 6-inch diameter SCF model was installed in the loose siliceous sand by carefully placing the suction can in the test bed while preparing the loose sand deposit to represent a “wish in place” condition.

For the 1000-cycle lateral load tests, walking of the suction can in loose siliceous sand was not significant (less than 0.03 D) for all the applied 1-, 2-, and 5-degree (±0.5, ±1, and ±2.5) rations and 3-, 5-, and 10-second loading periods. No significant settlement (less than 0.02 D) of the suction can occurs with 1- and 2-degree rotations. However, the foundation may have more significant settlements or upward movements (up to 0.18 D) with 5-degree rotation. During the lateral tests, it was observed that the sand flowed around the cyclically loaded foundation. This localized liquefaction of the loose sand around the suction can was caused by the increase in pore water pressure during cyclic loading. After cycles of lateral loading, a cone-shape depression formed around the suction can on the surface of the sand deposit. The cone-shape depression extended to approximately 0.5 diameters out from the suction can.

Measured lateral loads (or lateral resistance) were relatively stable without significant stiffening or softening effects in most of the tests in loose siliceous sand. However, stiffening behavior was observed in the first lateral load test in this test bed because the loose siliceous sand deposit was densified slightly under the cyclic loading. Two of the 5-degree lateral load tests showed "softening" behavior because of upward movements of the suction can that reduced the side resistance of the suction can. The difference in the measured lateral load for different loading period (3, 5, and 10 seconds) is not significant which indicates that there is little stain rate effect in this range of loading periods. This observation is consistent with the tests in clay.

During cyclic lateral load tests, the pressure in the soil plug near the tip of the suction can has a larger range of cyclic fluctuation comparing to that under the top plate; however, the excess pore water pressures are more uniform inside the suction can in the loose siliceous sand comparing to the tests in clay. The excess pore water pressures

redistribute much more quickly inside the suction can in sand because of its higher permeability.

Proof load tests were conducted instead of ultimate axial capacity test because the load required to fail the model foundation in sand exceeds the capacity our loading system. The suction can was loaded up to approximately 85% of its estimated ultimate capacity and then uploaded for two cycles. A maximum vertical displacement of around 0.06 D was measured under the maximum proof load in the first cycle. No significant excess pore water pressure builds up during the test until the foundation starts to move more significantly when the axial load was close to the maximum proof load. During the pullout test, a peak load of approximately 15% of the axial capacity in compression was measured at 0.08 diameter of vertical displacement. Negative pore water pressure (suction) was developed inside the suction can while the suction was loaded in tension. The suction can was plugged when it was pulled out, but the soil plug fell off within seconds.

Chapter 9: Tests in Cemented Siliceous Sand Test Bed

The 6-inch diameter SCF model was used for the scale model tests in the cemented siliceous sand test bed. The properties of the cemented siliceous sand test bed can be found in Section 2.4. The scale model tests conducted in this test bed includes: lateral load tests, axial load tests, proof load test, and pullout. The test procedure and the summary of test results are presented in the following sections.

9.1 INSTALLATION

The 6-inch diameter SCF model was placed in the test bed while preparing the cemented sand deposit that represents a "wish in place" condition. The model was carefully twisted into the sand-cement mixture before the initial set of cement. The test bed was allowed to cure for 40 hours before any test was conducted. Figure 9.1 shows the 6-inch model installed in the cemented siliceous sand test bed.

Figure 9.1: 6-inch Diameter SCF Model in Cemented Siliceous Sand

9.2 LATERAL LOAD TESTS

Two-way, displacement controlled, cyclic lateral load tests for 6-inch diameter SCF model were conducted in the cemented siliceous sand test bed. The lateral tests are similar to those presented in Section 6.2 for 6-inch diameter SCF model in overconsolidated clay. The lateral resistance, the walking displacement (translational permanent displacement), and the settlement were measured under 1000 cycles of lateral load in these tests.

9.2.1 Walking and Settlement

Table 9.1 shows the walking displacement and the settlements of the 6-inch diameter SCF model after 1000 cycles of lateral load in the cemented siliceous sand test bed. The first 1-degree rotation, 3-second period test was conducted with the load frame

rocking on the tank because of the higher resistance in the cemented sand. This test was later repeated with the load frame camped on the tank to create a more rigid loading system. The walking displacement and settlement of the model for all the lateral load tests are illustrated in Figure 9.2 and 9.3, respectively except the test with unstable load frame.

Soil Type	SCF Model	Rotation (degrees)	Period (seconds)	Mean Load (lbs)	Walking Displ. (inches)	Settlement (inches)	Test Date
Cemented Siliceous Sand	6-inch Diameter Model	1	3*	0.25	-0.40	0.000	8/3/2012
			3	0.25	-0.12	0.027	8/10/2012
			5	0.25	-0.01	0.015	8/10/2012
			10	0.25	-0.02	-0.044	8/10/2012
		2	3	0.50	-0.05	-0.030	8/13/2012
			5	0.50	0.08	0.008	8/13/2012
			10	0.50	0.05	-0.031	8/13/2012
		5	3	1.25	-0.09	0.550	8/14/2012
			5	1.25	0.22	-0.001	8/14/2012
			10	1.25	0.00	-0.599	8/14/2012

* Tested with unstable load frame.

- Note: negative values of walking displacement indicate that the model walks in the opposite direction of the mean load; negative values of settlement indicate that the model moves upward.

Table 9.1: Walking and Settlement of 6-inch Diameter SCF Model after 1000 Cycles of Lateral Load in Cemented Siliceous Sand

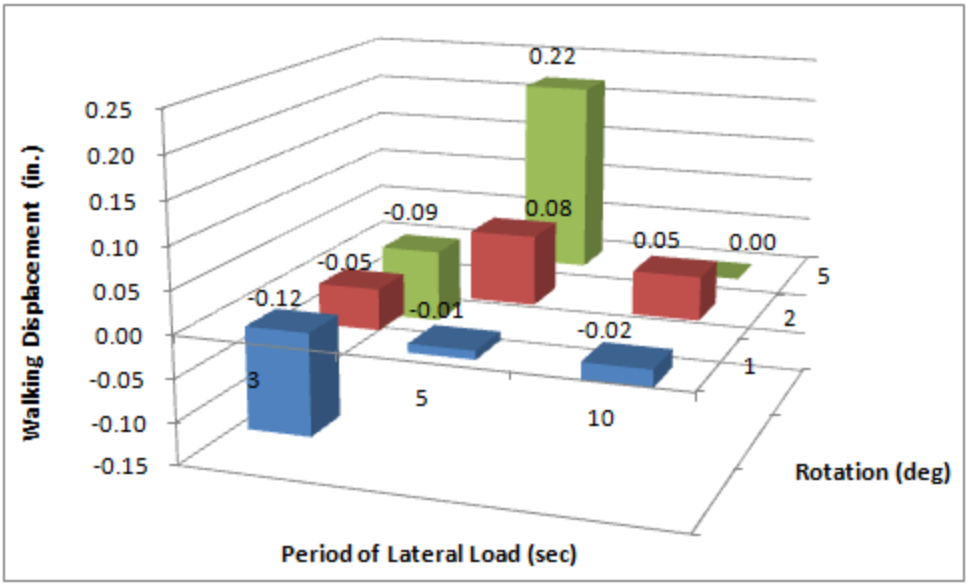

Figure 9.2: Walking of 6-inch Diameter SCF Model in Cemented Siliceous Sand

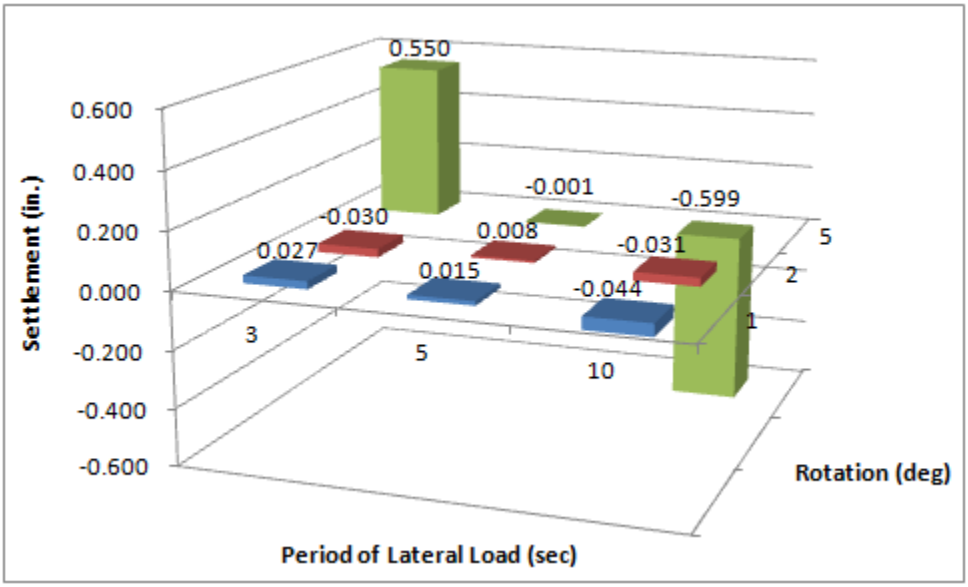

Figure 9.3: Settlement of 6-inch Diameter SCF Model in Cemented Siliceous Sand

Figure 9.2 shows that walking of the model in cemented siliceous sand is not significant for all the ration angles and loading periods. The walking displacements are

all within 0.04 diameter of the model (less than 0.04 D). Figure 9.3 shows no significant settlement of the model with 1 and 2-degree rotations (less than 0.01 D). However, the model may have more significant settlements or upward movements with 5-degree rotation. The settlement or upward movement can be around 0.1 D after 1000 cycles of lateral load.

Pictures of the 6-inch SCF model after lateral load tests in cemented siliceous sand are shown in Figure 9.4 to 9.6. Fissures and cracks in the cemented siliceous sand around the model formed right after the tests were started. The cementation near the model was broken after cycles of load and turned the cemented sand into loosed sand. Localized liquefaction of the loosed sand around the model was observed when the model was rotating cyclically because of the increase in pore water pressure. The sand flowed around the model during the lateral load test. After cycles of lateral loading, a cone-shape depression formed around the model on the surface of the sand deposit. The cone-shape depression and fissured zone extended to approximately one diameter out from the model (see Figure 9.4 to 9.6).

Figure 9.4: SCF Model after 1-degree Lateral Load Tests in Cemented Siliceous Sand

Figure 9.5: SCF Model after 2-degree Lateral Load Tests in Cemented Siliceous Sand

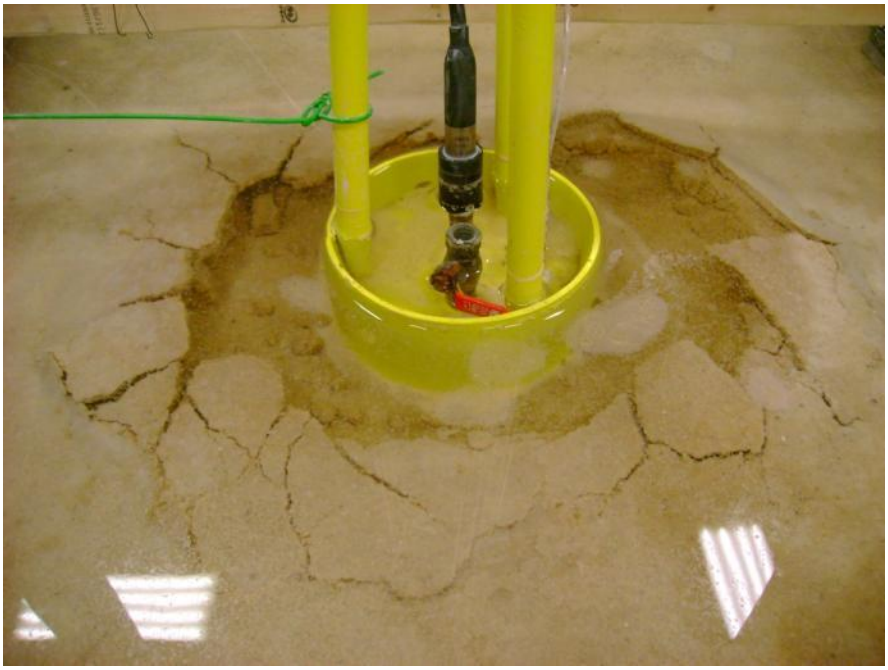

Figure 9.6: SCF Model after 5-degree Lateral Load Tests in Cemented Siliceous Sand

9.2.2 Lateral Load, Displacement, Pore Water Pressure, and Tilt Angle

In terms of the lateral load, lateral displacement, pore water pressure, and tilt angle measurements, the 2-degree rotation and 5-second period test is taken as an example for the lateral tests in cemented siliceous sand.

The time history of the 1000-cycle lateral load and lateral displacement are presented in Figure 9.7 and 9.8. The lateral load and displacement are both measured at 3 ft above the top plate of the model (or 3 ft above the mudline) as shown in Figure 6.4. The hysteresis loops of later load versus lateral displacement are shown in Figure 9.9.

In Figure 9.7, positive lateral displacement indicates that the model tilts to the right while negative displacement indicates left tilting movement. The lateral displacement fluctuates within a stable range and shows no sign of shifting which indicates that the model has no significant walk. The load shown in Figure 9.8 and 9.9 are

obtained by subtracting the weight of counter weights (see Figure 6.4) from the lateral load measured by the load cell. The load cell registers positive loads when the model tilts to the left and negative loads when it moves to the right. The lateral load shifted slightly to the negative side because of the presence of the mean load as discussed in Section 6.2.2.

In Figure 9.8, the measured lateral load (or lateral resistance) goes within a relatively stable range with no significant stiffening or softening effects. Similar trend was observed in most of the lateral load tests except the four tests shown in Figure 9.10 to 9.13. For the repeated 1-degree rotation, 3-second period test, stiffening behavior was observed (see Figure 9.10). In contrast, softening behavior was observed at the beginning of the 2-degree, 3-second test (see Figure 9.11) because it was the first 2-degree rotation test and the cementation was being broken in the first couple cycles. For the 5-degree, 3-second test (see Figure 9.12), softening behavior occurred at the beginning because of the cementation was being broken, while stiffening behavior occurred in the rest of the test because the model settled more than 0.5 inch. For the 5-degree, 10-second test (Figure 9.13), softening behavior was observed because the model moved upward.

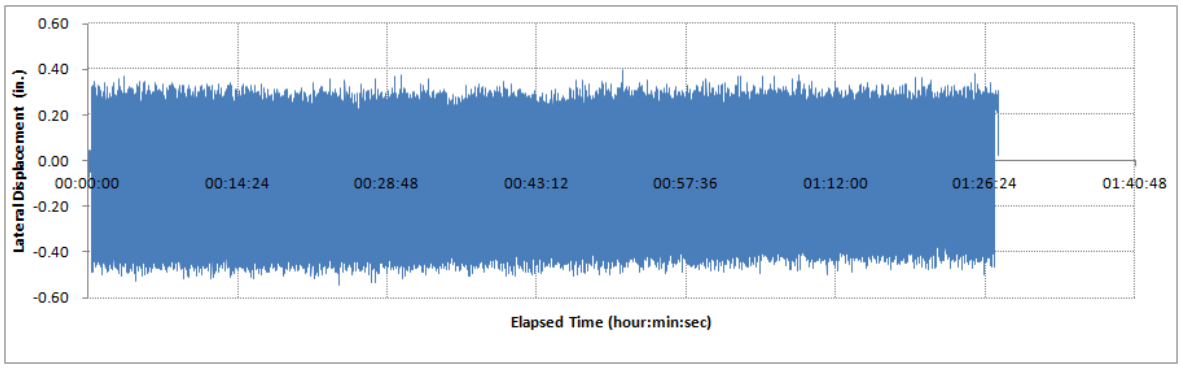

Figure 9.7: Lateral Displacement of 6-inch Model in Cemented Siliceous Sand (2°, 5 sec)

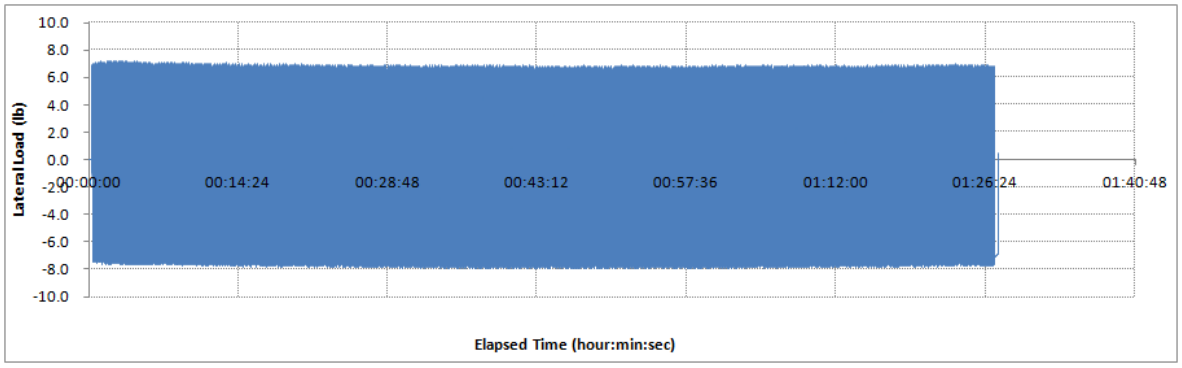

Figure 9.8: Lateral Load of 6-inch Model in Cemented Siliceous Sand (2°, 5 sec)

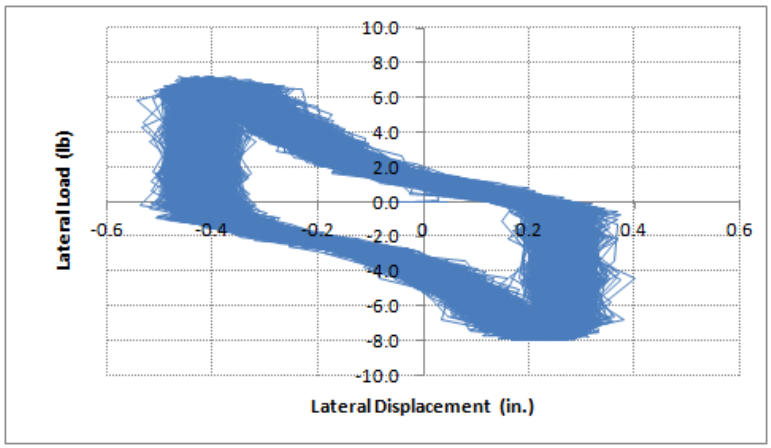

Figure 9.9: Lateral Load versus Lateral Displacement of 6-inch Model in Cemented Siliceous Sand (2°, 5 sec)

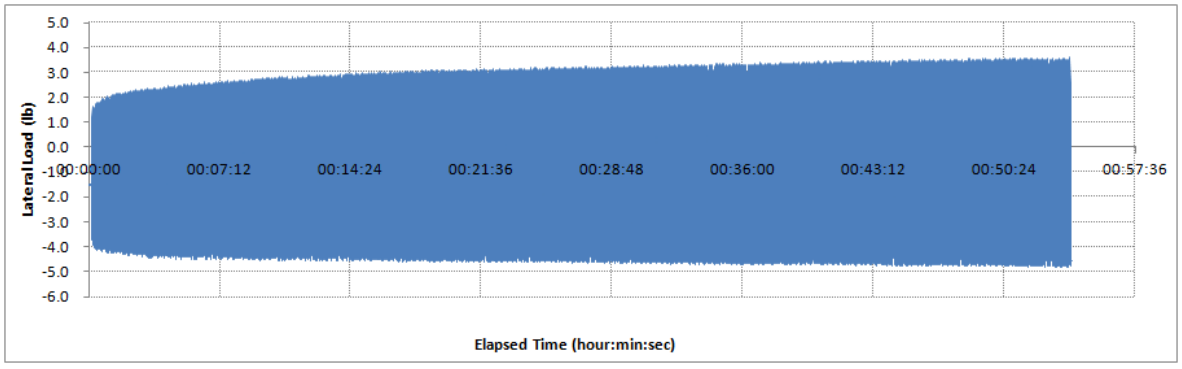

Figure 9.10: Lateral Load of 6-inch Model in Cemented Siliceous Sand (1°, 3 sec)

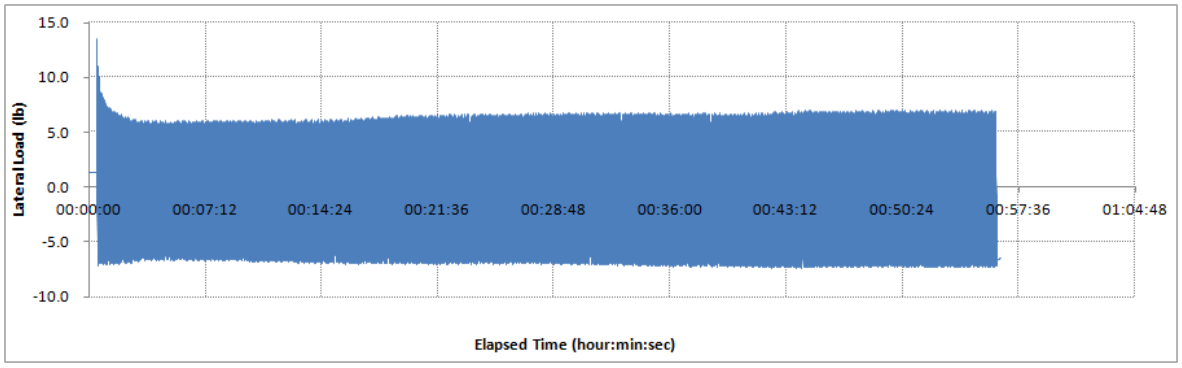

Figure 9.11: Lateral Load of 6-inch Model in Cemented Siliceous Sand (2°, 3 sec)

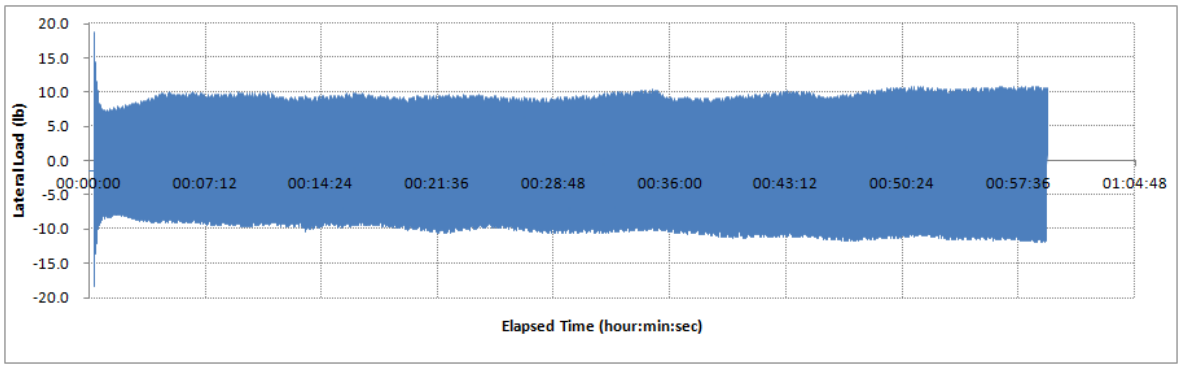

Figure 9.12: Lateral Load of 6-inch Model in Cemented Siliceous Sand (5°, 3 sec)

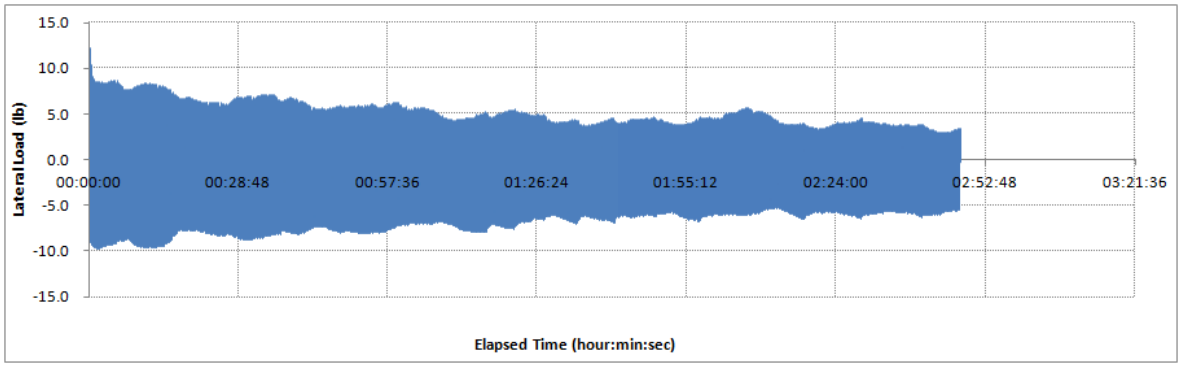

Figure 9.13: Lateral Load of 6-inch Model in Cemented Siliceous Sand (5°, 10 sec)

In general, the lateral resistance of the foundation increases with increasing rotation angle of the model in cemented siliceous sand. However, the difference of the lateral load for different loading period is not significant. This observation is similar to those from the tests in clay and in loose siliceous sand. However, the measured lateral loads (or lateral resistance) are higher in cemented siliceous sand than in the loose siliceous sand and in clay.

The excess pore water pressures for the 2-degree rotation and 5-second period lateral load test are shown in Figure 9.14 and 9.15. The excess pore water pressures are calculated by subtracting the hydrostatic pressures from the corresponding measured pore water pressures. The pressure at Tip has a slightly larger range of fluctuation; however, the excess pore water pressures are relatively uniform inside the suction can in the cemented siliceous sand comparing to the tests in clay. The excess pore water pressure redistribute much more quickly inside the suction can in sand because of its higher permeability. Similar to the tests in loose siliceous sand, pore water pressures increase whether the model tilts to either direction and subsequently decreases when the model is changing its tilting direction due to the cyclic loads. This can also be attributed to the high permeability of sand.

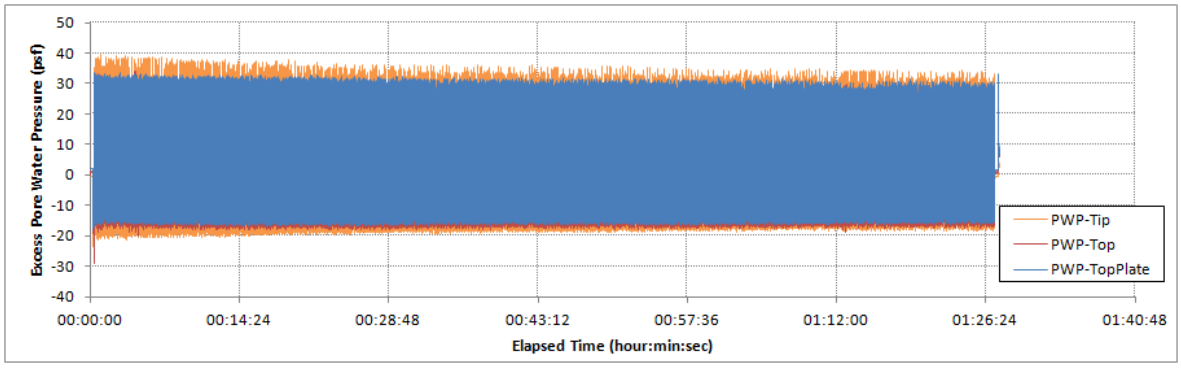

Figure 9.14: Excess Pore Water Pressure of 6-inch Model in Cemented Siliceous Sand (2° rotation, 5-sec period)

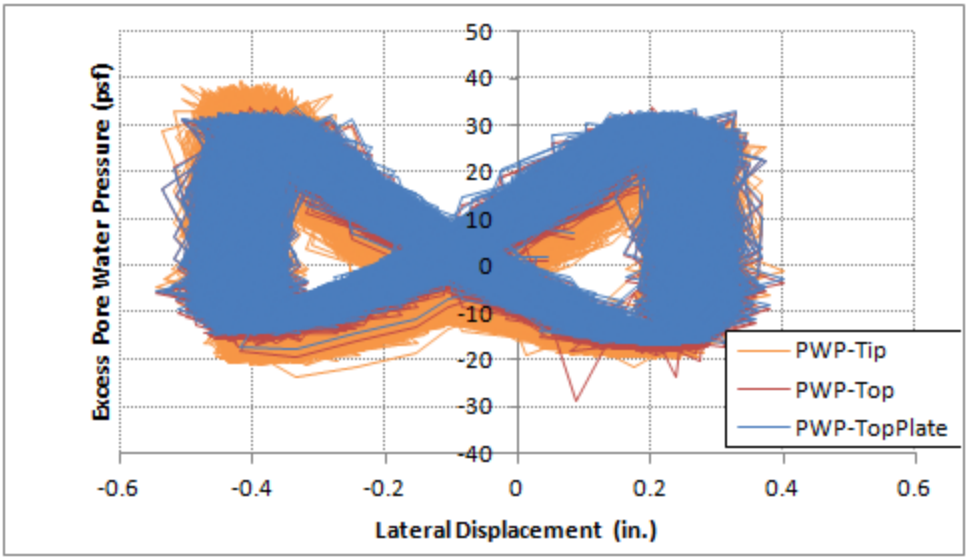

Figure 9.15: Excess Pore Water Pressure versus Lateral Displacement of 6-inch Model in Cemented Siliceous Sand (2° rotation, 5-sec period)

The tilt angles for the 2-degree rotation and 5-second period lateral load test are shown in Figure 9.16 and 9.17. The tilt angle in the direction perpendicular to loading is close to zero degree as expected. The tilt angle in the loading direction goes between +/- 0.8 degree, where the positive angle indicates that model tilts to the left and negative angle indicates right-tilting movement.

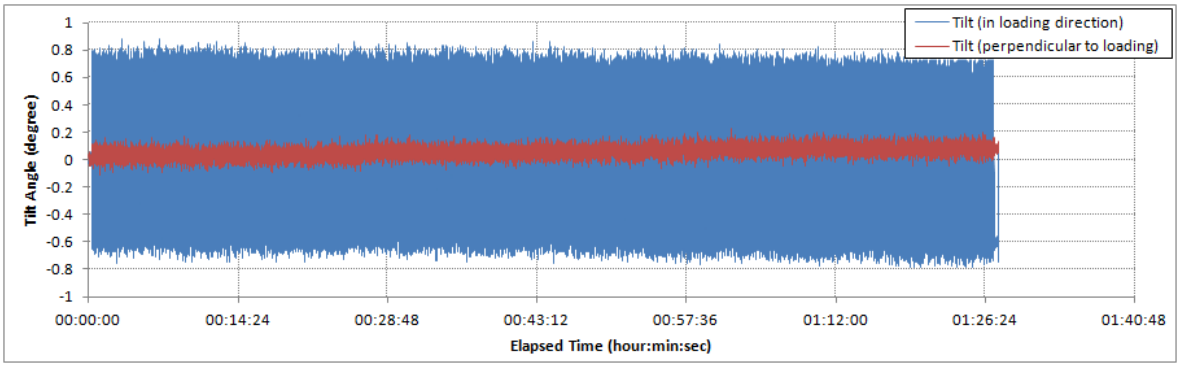

Figure 9.16: Tilt Angles of 1-foot Model in Cemented Siliceous Sand (2° rotation, 5-sec period)

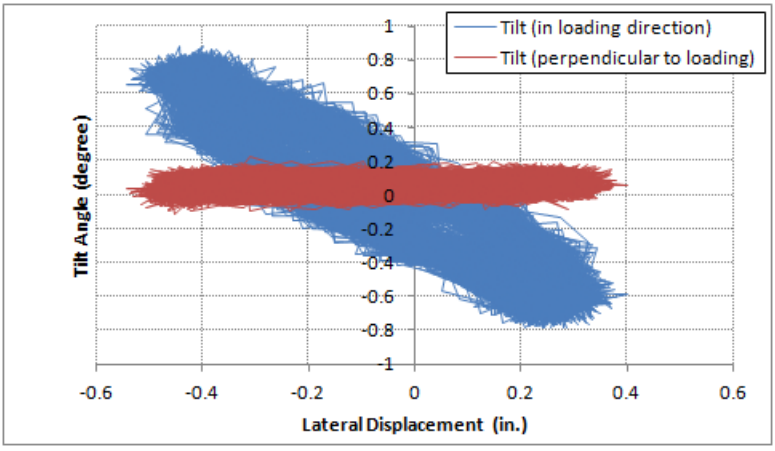

Figure 9.17: Excess Pore Water Pressure versus Lateral Displacement of 1-foot Model in Cemented Siliceous Sand (2° rotation, 5-sec period)

9.3 Axial Load Tests

Axial load tests on the 6-inch diameter model in cemented siliceous sand were conducted by placing several 5-lb weights on the model in steps. The weights were placed on the model (see Figure 9.18) in steps to apply approximately 10, 20, and 30 lb of load with around 30 seconds for each step. The vertical displacement of the model was monitored using a dial gauge. Figure 9.19 shows the load-displacement curves of three loading-unloading cycles. Since the weights were placed on top of the extended arm and the dial gauge also measured the displacement at the top of the extended arm, the displacements in Figure 9.19 include the deformation of the extended arm.

The excess pore water pressures of the three cycles of axial load tests are shown in Figure 9.20 to 9.22. The theoretical excess pore water pressure is assumed to be zero because the high permeability of the sand and the loading is under a drained condition. The measured excess pore water pressures are essentially zero, which match well with the assumed drained condition.

Figure 9.18: Axial Load Test in Cemented Siliceous Sand

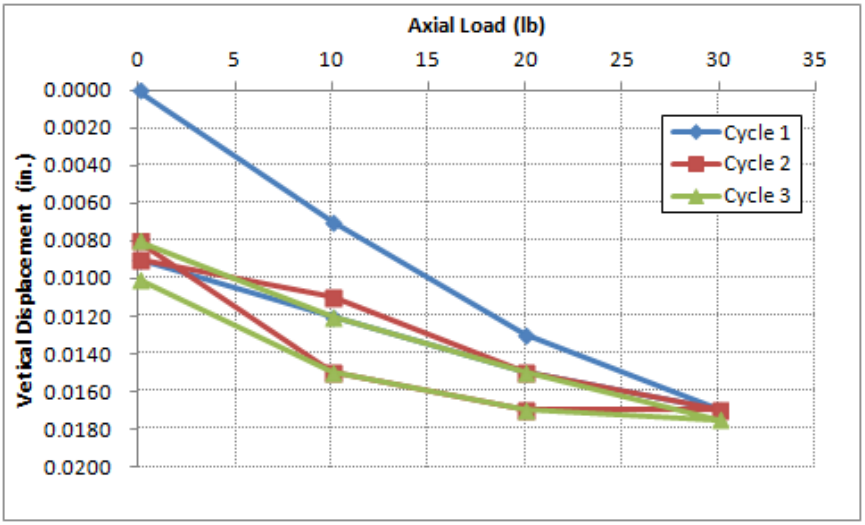

Figure 9.19: Load-Displacement Curve from Axial Load Tests

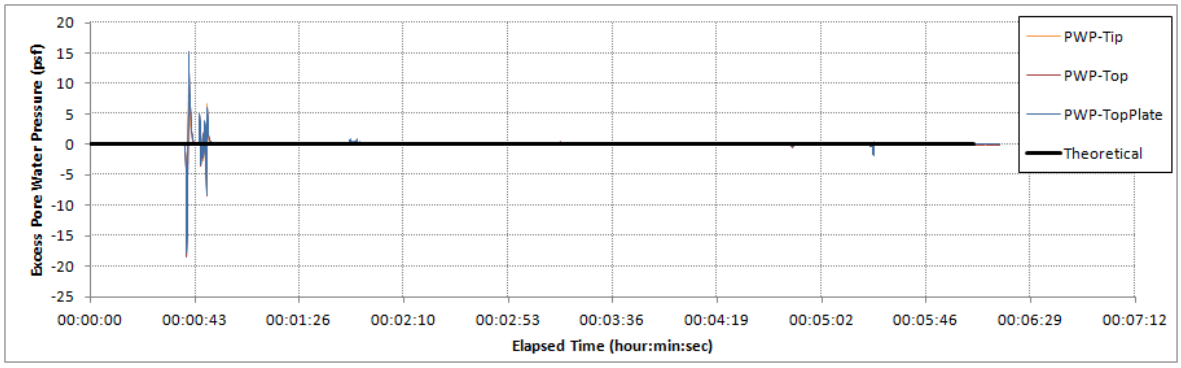

Figure 9.20: Excess Pore Water Pressure from Axial Load Test (Cycle 1)

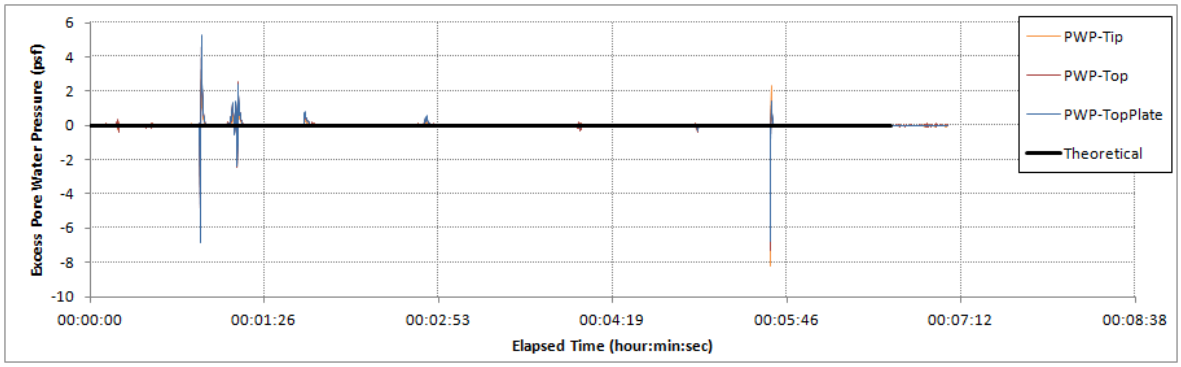

Figure 9.21: Excess Pore Water Pressure from Axial Load Test (Cycle 2)

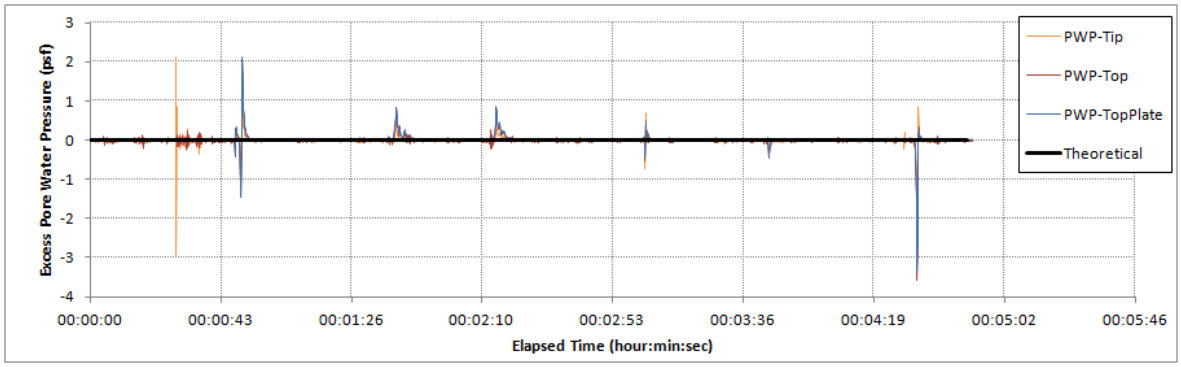

Figure 9.22: Excess Pore Water Pressure from Axial Load Test (Cycle 3)

9.4 PROOF LOAD TESTS

Proof load tests were conducted instead of ultimate axial capacity test because the load required to failure the model foundation in sand exceeds the capacity our loading system. The proof load tests were conducted after all the axial and lateral load tests were completed. The axial proof load was applied by stacking weights on the model in steps (see Figure 9.23), and the vertical displacement of the model was measured on top of the extended arm by a dial gauge.

The model was loaded up to 292 lb and then uploaded for two cycles. The load-displacement curves from the two proof tests are shown in Figure 9.24. The maximum vertical displacement of around 0.005 diameter of the model (0.005 D) was measured under the 292 lb proof load in the first cycle. Note that the axial load does not include the weight of the model. Unlike the previous axial load test, the weights are placed near mudline directly on top of the suction can; therefore, the displacement in Figure 9.24 does not include the deformation of the extended arm.

Figure 9.23: Proof Load Tests in Cemented Siliceous Sand

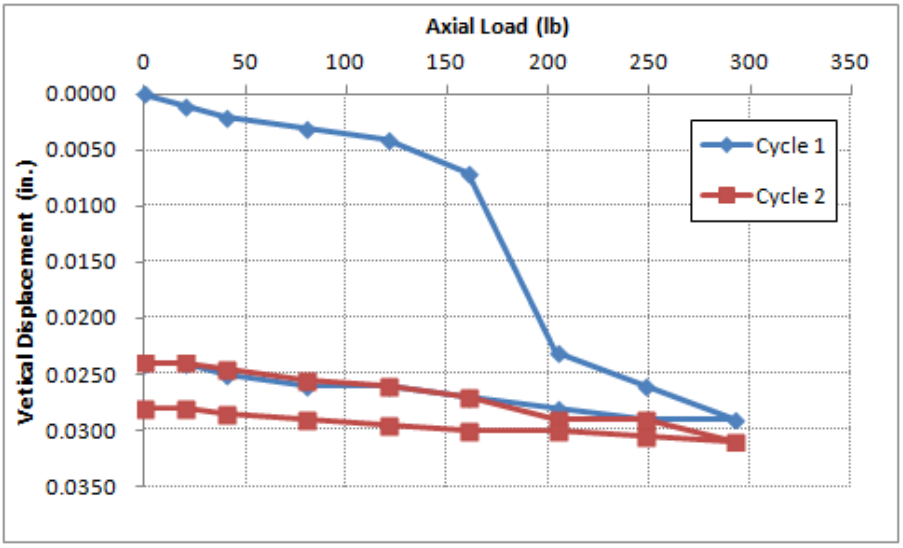

Figure 9.24: Load-Displacement Curve from Proof Load Tests

The excess pore water pressures from the proof load tests are shown in Figure 9.25 and 9.26. The theoretical excess pore water pressure is assumed to be zero because the high permeability of the sand and the loading is under a drained condition. The spikes in Figure 9.25 and 9.26 occurred when the weights were placed on the model or when the tubes for pore water pressure measurement were disturbed accidentally while placing the weights.

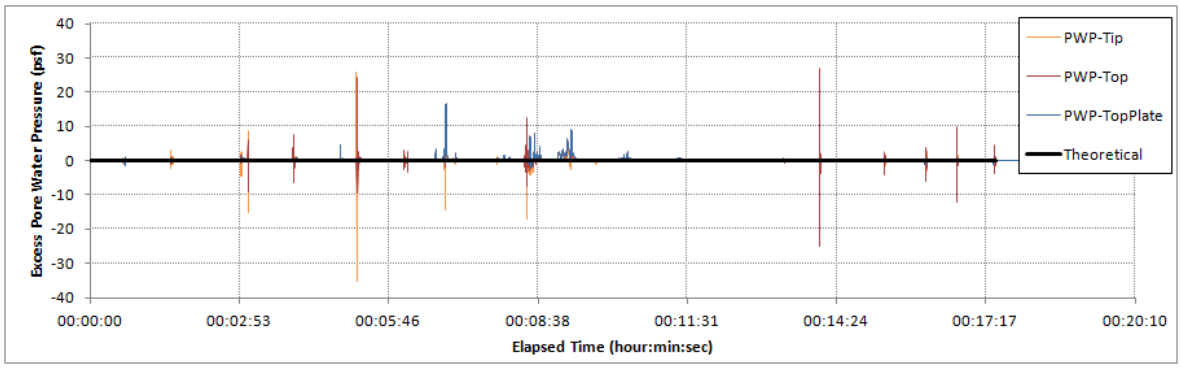

Figure 9.25: Excess Pore Water Pressure from Proof Load Test (Cycle 1)

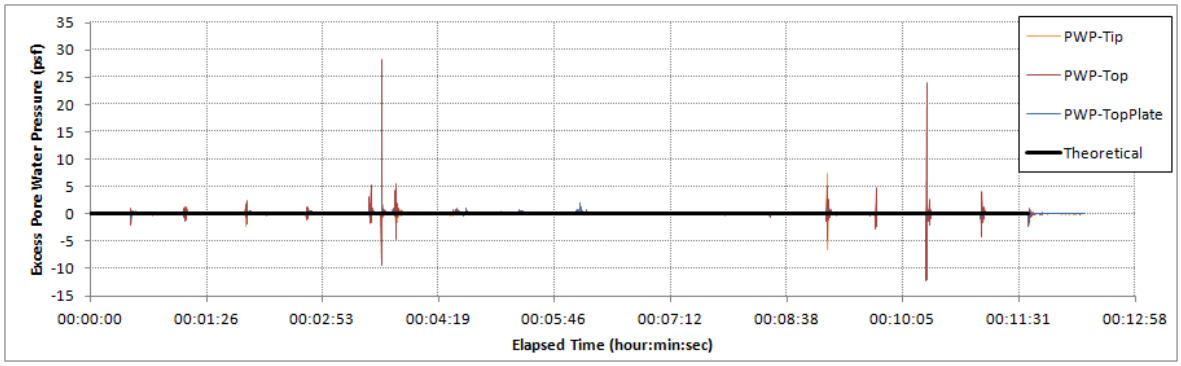

Figure 9.26: Excess Pore Water Pressure from Proof Load Test (Cycle 2)

9.5 PULLOUT

The 6-inch diameter SCF model was pulled out of the cemented siliceous sand manually after all the tests were completed. The load cell and the linear displacement

transducer were attached to the model to measure the load and vertical displacement, respectively. The suction can was plugged by the cemented siliceous sand when it was pulled out as shown in Figure 9.27.

Figure 9.27: 6-inch Diameter SCF Model after Pullout from Cemented Siliceous Sand

Figure 9.28 to 9.30 show the measured vertical load and displacement during the pullout process. A peak load of 99 lb was measured at 0.47 inch of vertical displacement. The measured pore water pressures during pullout are presented in Figure 9.31 and 9.32. Negative pore water pressures in the figures indicate suction was developed inside the suction can to provide resistance to pullout. When suction in the suction can decreases, the measured vertical load also drops significantly.

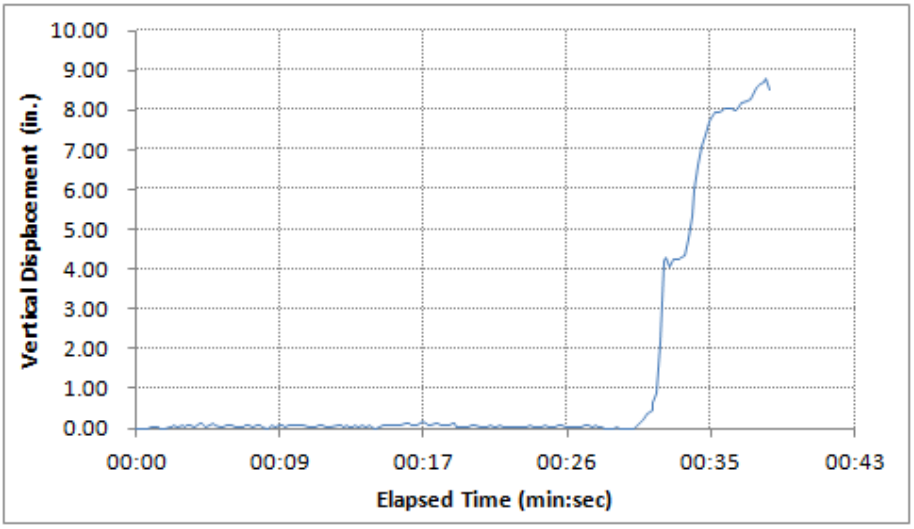

Figure 9.28: Vertical Displacement of 6-inch SCF Model Pullout Test in Cemented Siliceous Sand

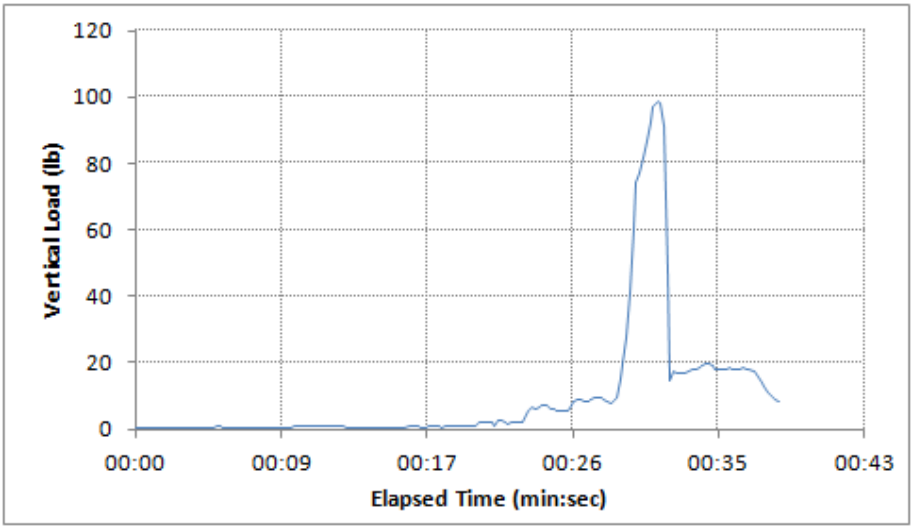

Figure 9.29: Vertical Load of 6-inch SCF Model Pullout Test in Cemented Siliceous Sand

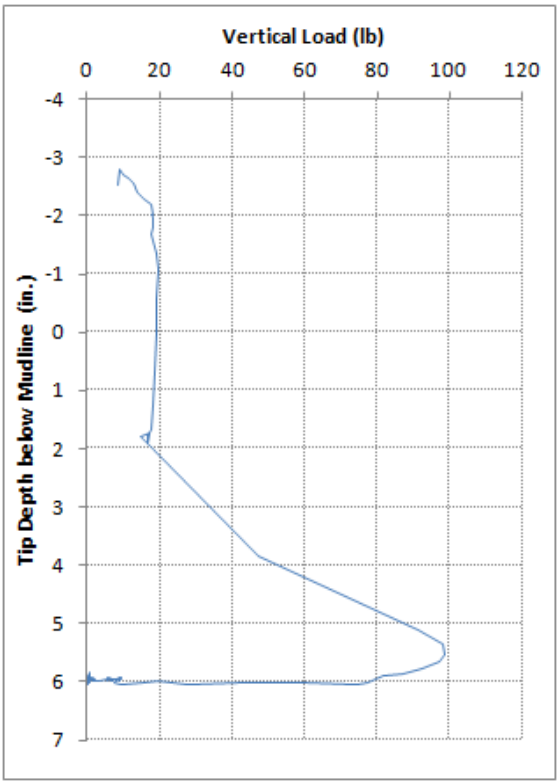

Figure 9.30: Load-Displacement Curve of 6-inch SCF Model Pullout Test in Cemented Siliceous Sand

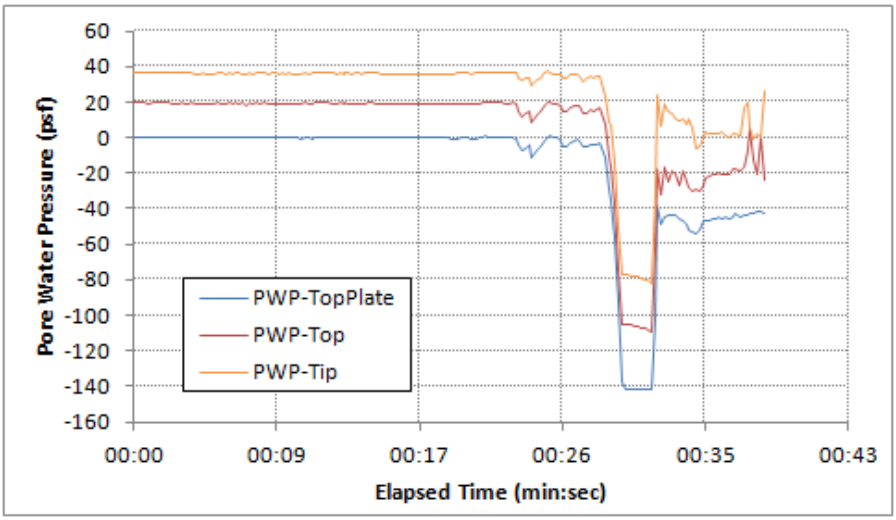

Figure 9.31: Pore Water Pressures of 6-inch SCF Model Pullout Test in Cemented Siliceous Sand

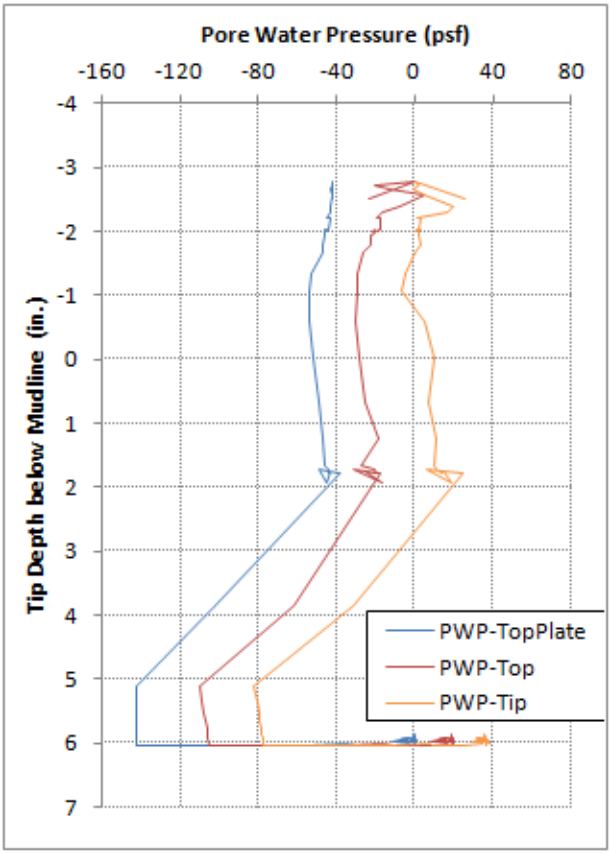

Figure 9.32: Pore Water Pressures versus Displacement of 6-inch SCF Model Pullout Test in Cemented Siliceous Sand

9.6 Summary for Tests in Cemented Siliceous Sand

The poorly graded siliceous sand used in the cement siliceous sand test bed had a mean grain size of 0.4 mm (same as the loose siliceous sand test bed). The siliceous sand was mixed with 1% type I Portland cement to create the cementation between sand particles. The unconfined compression strength of the cemented sand was around 346 psf. The estimated saturated unit weight of the cemented siliceous sand test bed was 126 pcf. The cone tip resistance at 6 inches deep was approximately 28 ksf at 3.5 to 5.5 inches deep according to 1.05-inch diameter cone penetrometer tests. The 6-inch diameter SCF

model was installed in the cemented siliceous sand by carefully placing the suction can in the test bed before the initial set of the cement to represent a "wish in place" condition.

For the 1000-cycle lateral load tests, walking of the suction can in cemented siliceous sand is not significant (less than 0.04 D) for all the applied 1, 2, and 5-degree (±0.5, ±1, and ±2.5 degrees) rations and 3, 5, and 10-second loading periods. No significant settlement (less than 0.01 D) occurs with 1 and 2-degree rotations. However, the suction can may have more significant settlements or upward movements (up to 0.1 D) with 5-degree rotation. Fissures and cracks in the cemented siliceous sand around the suction can formed right after the tests were started. The cementation near the foundation was broken after cycles of load and turned the cemented sand into loosed sand. During the lateral tests, it was observed that the sand flowed around the cyclically loaded foundation. This localized liquefaction of the loose sand around the suction can was caused by the increase in pore water pressure during cyclic loading. After cycles of lateral load, a cone-shape depression formed around the suction can on the surface of the sand deposit. The cone-shape depression and fissured zone extended to approximately one diameter out from the suction can. Measured lateral loads (or lateral resistance) are relatively stable without significant stiffening or softening effects in most of the tests in cemented siliceous sand. However, softening behavior occurs at the beginning of the first test with the same magnitude of rotation because the cementation was being broken in the first couple of cycles. For 5-degree rotation tests, stiffening or softening behavior may also occur due to the settlements or upward movements of the suction can.

The difference in the measured lateral load for different loading period (3, 5, and 10 seconds) is not significant which indicates that there is little stain rate effect in this range of loading periods. This observation is consistent with previous tests in this study.

However, the measured lateral loads (or lateral resistance) are higher in cemented siliceous sand than in the loose siliceous sand and in clay.

During cyclic lateral load tests, the pressure in the soil plug near the tip of the suction can has a slightly larger range of cyclic fluctuation comparing to that under the top pate; however, the excess pore water pressures are relatively uniform inside the suction can in the cemented siliceous sand comparing to the tests in clay. The excess pore water pressure redistribute much more quickly inside the suction can in sand because of its higher permeability.

Proof load tests were conducted instead of ultimate axial capacity test because the load required to fail the model foundation in sand exceeds the capacity our loading system. The suction can was loaded up to approximately 15% of its ultimate capacity and then uploaded for two cycles. A maximum vertical displacement of around 0.005 diameter of the suction can was measured under the maximum proof load in the first cycle. No significant excess pore water pressure builds up throughout the proof load tests. During the pullout test, a peak load of approximately 5% of the estimated ultimate capacity in compression was measured at 0.08 diameter of vertical displacement. Negative pore water pressure (suction) was developed inside the suction can which provides a large proportion of pullout resistance. The suction can was plugged by the cemented siliceous sand when it was pulled out.

Chapter 10: Tests in Cemented Calcareous Sand Test Bed

The 6-inch diameter SCF model was used for the scale model tests in the cemented calcareous sand test bed. The properties of the cemented calcareous sand test bed and the oyster shell meal can be found in Section 2.5. The scale model tests conducted in this test bed includes: lateral load tests, axial load tests, and proof load test. The test procedure and the summary of test results are presented in the following sections.

10.1 INSTALLATION

The 6-inch diameter SCF model was placed in the test bed while preparing the cemented calcareous deposit that represents a "wish in place" condition. The model was carefully twisted into the oyster shell meal and cement mixture before the initial set of cement. The test bed was allowed to cure for 40 hours before any test was conducted. Figure 10.1 shows the 6-inch model installed in the cemented calcareous sand test bed.

Figure 10.1: 6-inch Diameter SCF Model in Cemented Calcareous Sand

10.2 LATERAL LOAD TESTS

Two-way, displacement controlled, cyclic lateral load tests for 6-inch diameter SCF model were conducted in the cemented calcareous sand test bed. The lateral tests are similar to those presented in Section 6.2 for 6-inch diameter SCF model in overconsolidated clay. The lateral resistance, the walking displacement (translational permanent displacement), and the settlement were measured under 1000 cycles of lateral load in these tests.

10.2.1 Walking and Settlement

Table 10.1 shows the walking displacement and the settlements of the 6-inch diameter SCF model after 1000 cycles of lateral load in the cemented calcareous sand test bed. For the 5-degree rotation tests, the walking displacement of 0.40 inch shown in Table 10.1 is the accumulated walking for 3, 5, and 10-second tests. The measurements in between these tests are not available because the line connecting to linear displacement transducer dislocated. The 5-degree rotation tests were later re-conducted. However, a gap of 2 inches wide and 4 inches deep formed on the opposite side of the mean load after the first 5-degree tests (see Figure 10.6), and therefore, the repeated tests were conducted with the gap. The walking displacement and settlement of the model for all the lateral load tests are illustrated in Figure 10.2 and 10.3, respectively except the tests without lateral displacement measurements.

Figure 10.2 shows that, in general, walking of the model in cemented siliceous sand is not very significant; however, sometimes the walking displacement can be up to 0.09 diameter of the model (0.09 D), which is more significant than previous tests in loose and cemented siliceous sand. Figure 10.3 shows no significant settlement for all rotation angles and loading periods. The settlements or upward movements are all less than 0.02 D after 1000 cycles of lateral load.

Soil Type	SCF Model	Rotation (degrees)	Period (seconds)	Mean Load (lbs)	Walking Displ. (inches)	Settlement (inches)	Test Date
Cemented Calcareous Sand	6-inch Diameter Model	1	3	0.25	-0.12	0.053	11/21/2012
			5	0.25	0.25	0.011	11/21/2012
			10	0.25	-0.29	0.010	11/21/2012
		2	3	0.50	-0.02	-0.031	11/26/2012
			5	0.50	0.00	0.000	11/26/2012
			10	0.50	0.19	0.013	11/26/2012
		5*	3	1.25	0.40*	-0.061	11/27/2012
			5	1.25		-1.806	11/27/2012
			10	1.25		-0.927	11/27/2012
		5	3	1.25	0.54	-0.114	11/28/2012
			5	1.25	0.12	-0.082	11/28/2012
			10	1.25	-0.16	0.067	11/28/2012

* The walking displacement of 0.40 inch is the accumulated walking for 3, 5, and 10-second tests. The measurements in between these tests are not available because the line connecting to linear displacement transducer dislocated. A gap of 2 inches wide and 4 inches deep formed on the opposite side of the mean load at the end of the tests.

- Note: negative values of walking displacement indicate that the model walks in the opposite direction of the mean load; negative values of settlement indicate that the model moves upward.

Table 10.1: Walking and Settlement of 6-inch Diameter SCF Model after 1000 Cycles of Lateral Load in Cemented Calcareous Sand

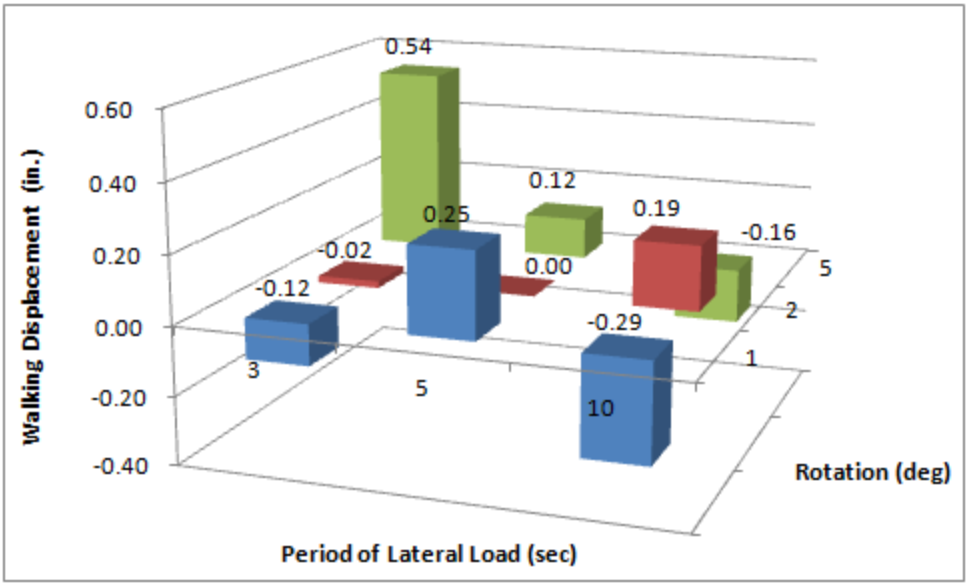

Figure 10.2: Walking of 6-inch Diameter SCF Model in Cemented Calcareous Sand

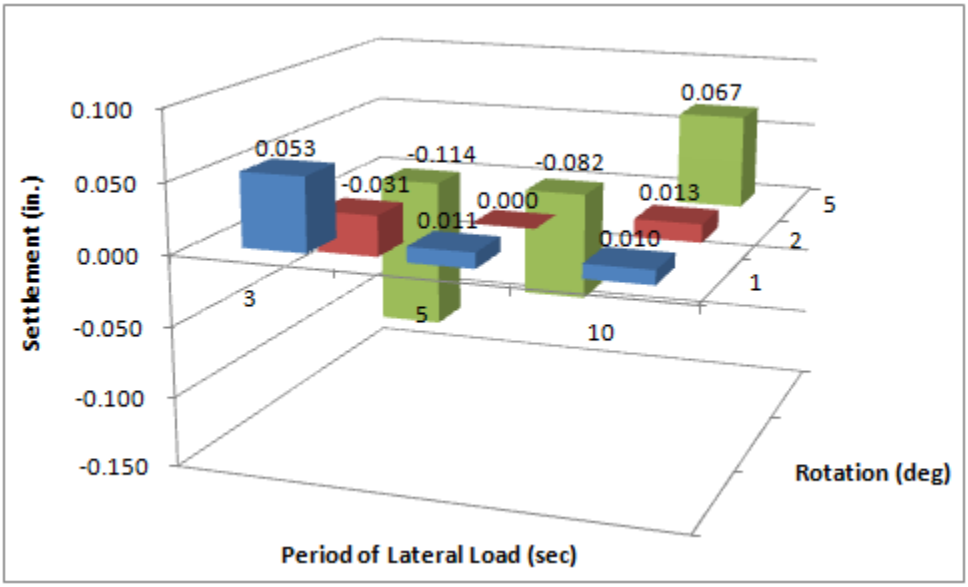

Figure 10.3: Settlement of 6-inch Diameter SCF Model in Cemented Calcareous Sand

Pictures of the 6-inch SCF model after lateral load tests in cemented calcareous sand are shown in Figure 10.4 to 10.7. No significant fissures and cracks in the cemented calcareous sand around the model were observed after the tests were started because the

cemented calcareous sand was more ductile (see the unconfined compression tests in Section 2.5). However, a gap around the model opened up after cycles of load. The gap on right side (opposite to the mean load side) got wider throughout the tests and was measured 2 inches wide and 4 inches deep after the 5-degree rotation tests. Unlike the siliceous sand tends to fill the gap around the model, the gap in cemented calcareous sand stayed open throughout the tests. This can be attributed to the higher strength of the cemented calcareous sand due to the angular shape of the oyster shell particles. This gap also causes the model in the cemented calcareous sand to have a lower lateral resistance (or lower measured lateral loads) as shown in the next section comparing to previous tests in siliceous sands.

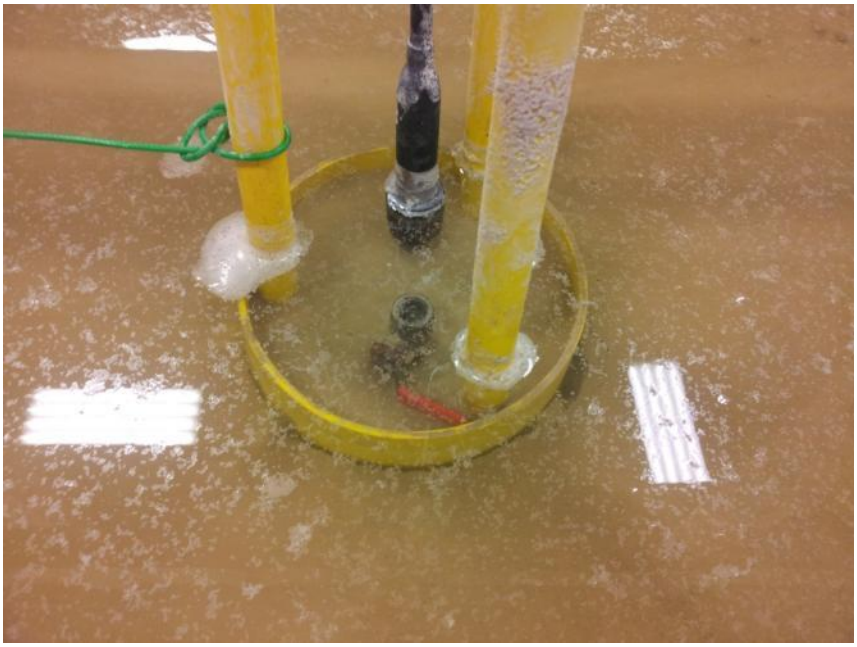

Figure 10.4: SCF Model after 1-degree Lateral Load Tests in Cemented Calcareous Sand

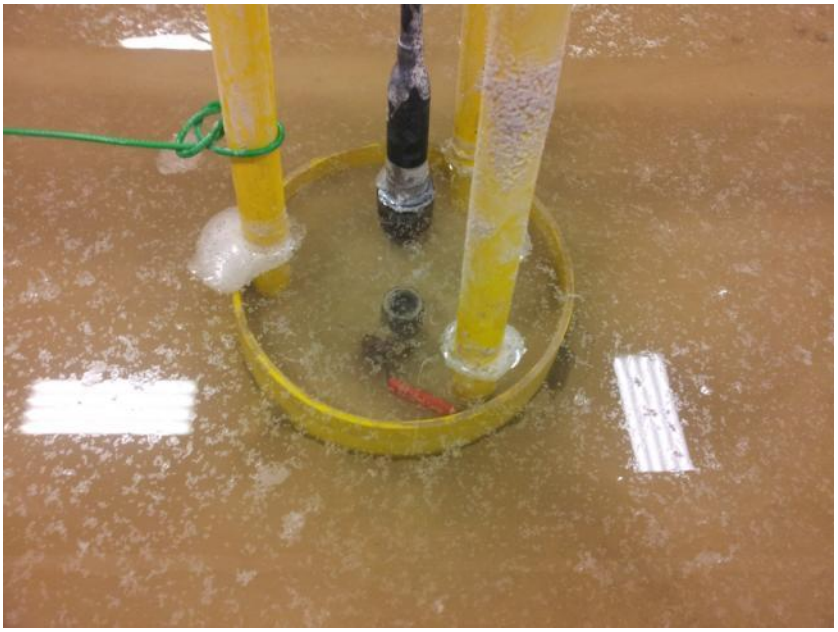

Figure 10.5: SCF Model after 2-degree Lateral Load Tests in Cemented Calcareous Sand

Figure 10.6: SCF Model after 5-degree Lateral Load Tests in Cemented Calcareous Sand

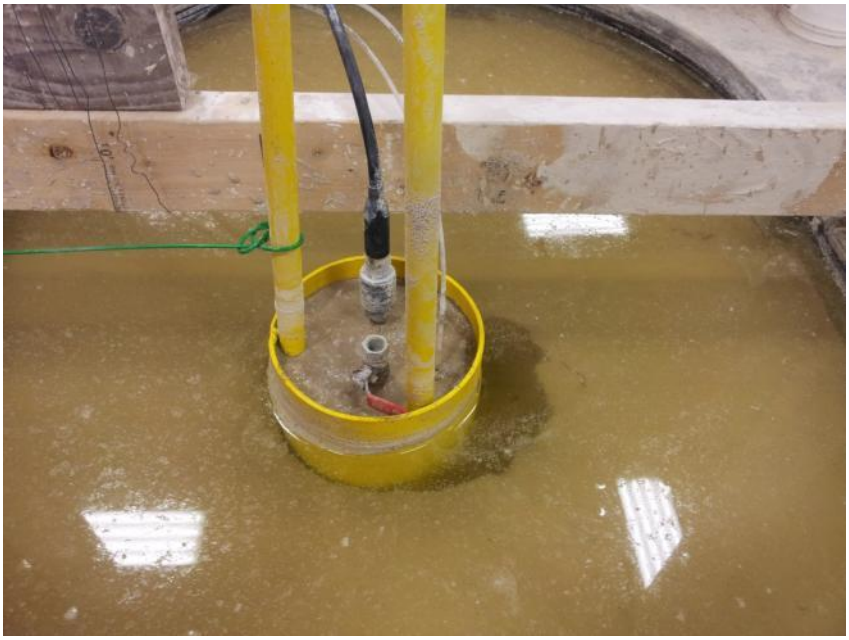

Figure 10.7: SCF Model after the Repeated 5-degree Lateral Load Tests in Cemented Calcareous Sand

10.2.2 Lateral Load, Displacement, Pore Water Pressure, and Tilt Angle

In terms of the lateral load, lateral displacement, pore water pressure, and tilt angle measurements, the 2-degree rotation and 5-second period test is taken as an example for the lateral tests in cemented calcareous sand.

The time history of the 1000-cycle lateral load and lateral displacement are presented in Figure 10.8 and 10.10. The lateral load and displacement are both measured at 3 ft above the top plate of the model (or 3 ft above the mudline) as shown in Figure 6.4. The hysteresis loops of later load versus lateral displacement are shown in Figure 10.10

In Figure 10.8, positive lateral displacement indicates that the model tilts to the right while negative displacement indicates left tilting movement. The lateral displacement fluctuates within a stable range and shows no sign of shifting which indicates that the model has no significant walk. The load shown in Figure 10.9 and 10.10

are obtained by subtracting the weight of counter weights (see Figure 6.4) from the lateral load measured by the load cell. The load cell registers positive loads when the model tilts to the left and negative loads when it moves to the right. The lateral load shifted slightly to the negative side because of the presence of the mean load as discussed in Section 6.2.2.

In Figure 10.9, the measured lateral load (or lateral resistance) fluctuates in a relatively stable range. No significant stiffening or softening effects occurred in the 2-degree rotation, 5-second period test. However, softening behavior was observed for most of the 3-second and 5-second period tests for all ration angles (see Figure 10.11 to 10.13). The softening behavior can be attributed to the broken down of the cementation between oyster shell particles. Since the 10-second period tests were conducted after 1 and 2-second period tests (after 2000 cycles of lateral displacement at the same magnitude), the 10-seond period tests show no significant softening effect because the cemented calcareous sand was already degraded. For the repeated 5-degree rotation tests, the measured lateral loads are the lowest (see Figure 10.14), because the first 5-degree tests degradation (3000 cycles of load in total) already degraded the cemented calcareous sand and created the gap.

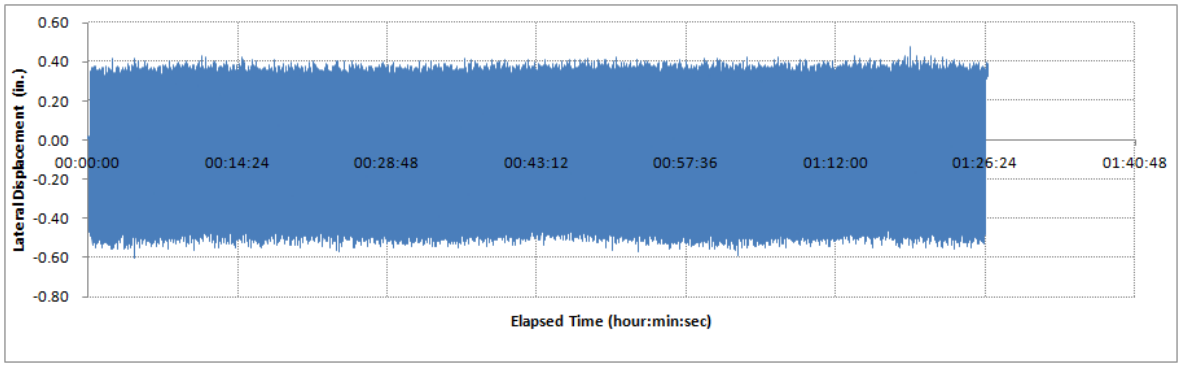

Figure 10.8: Lateral Displacement of 6-inch Model in Cemented Calcareous Sand (2°, 5 sec)

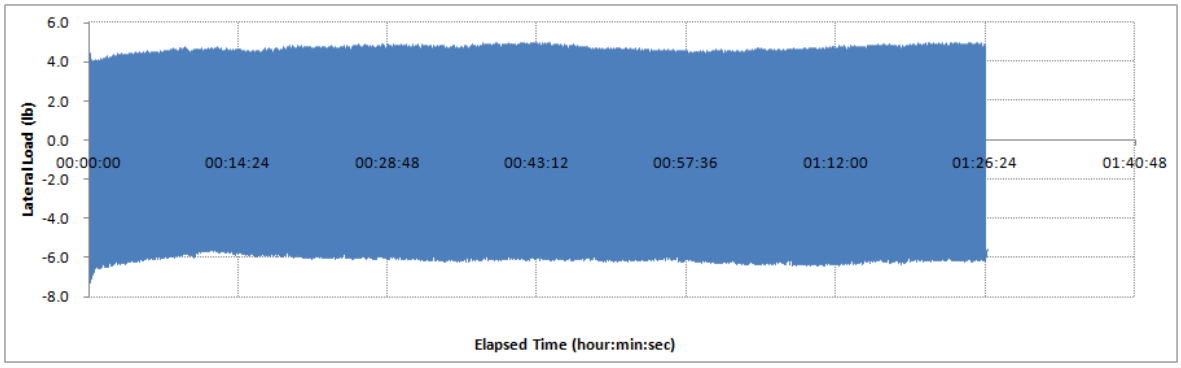

Figure 10.9: Lateral Load of 6-inch Model in Cemented Calcareous Sand (2°, 5 sec)

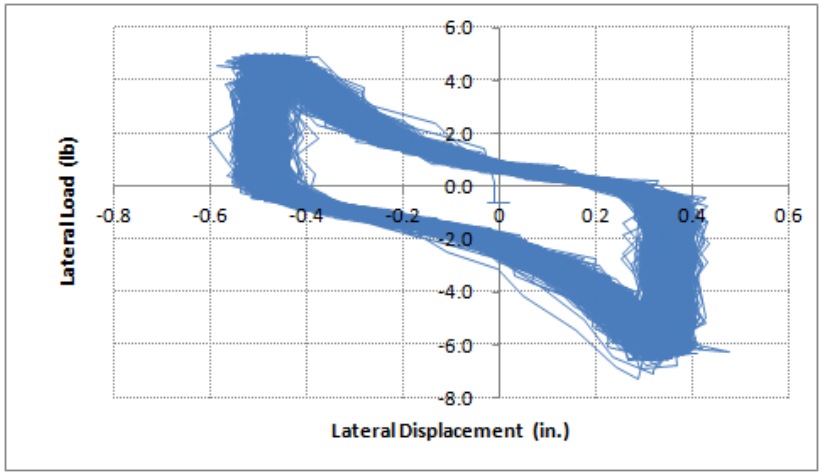

Figure 10.10: Lateral Load versus Lateral Displacement of 6-inch Model in Cemented Calcareous Sand (2°, 5 sec)

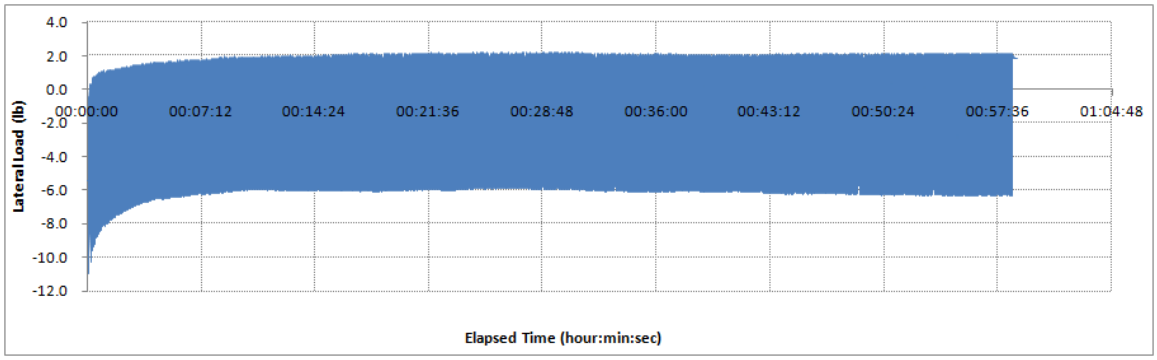

Figure 10.11: Lateral Load of 6-inch Model in Cemented Calcareous Sand (1°, 3 sec)

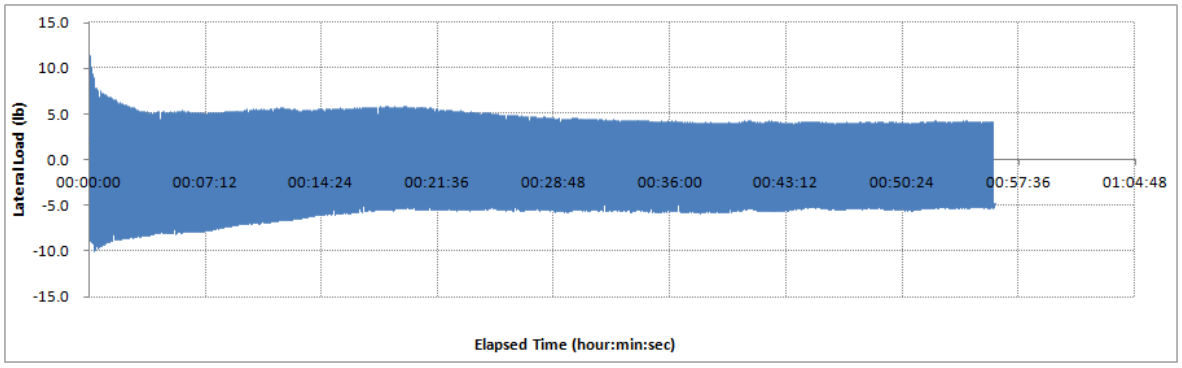

Figure 10.12: Lateral Load of 6-inch Model in Cemented Calcareous Sand (2°, 3 sec)

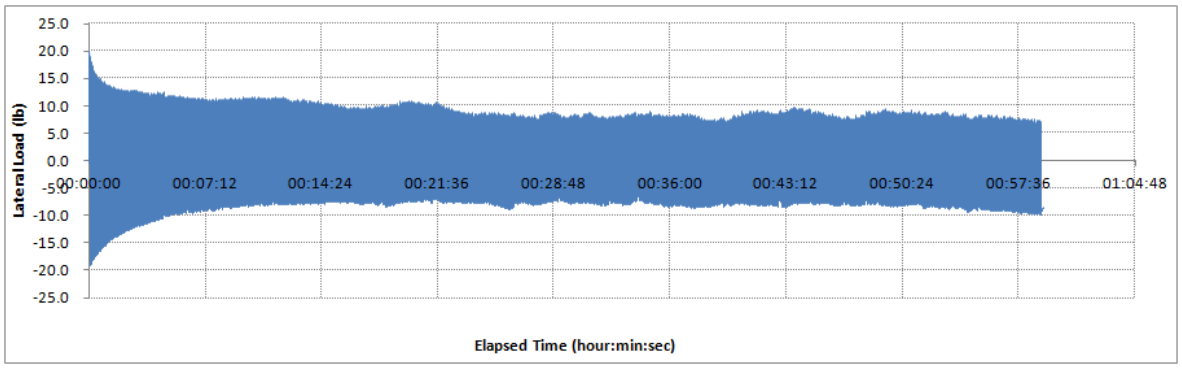

Figure 10.13: Lateral Load of 6-inch Model in Cemented Calcareous Sand (5°, 3 sec)

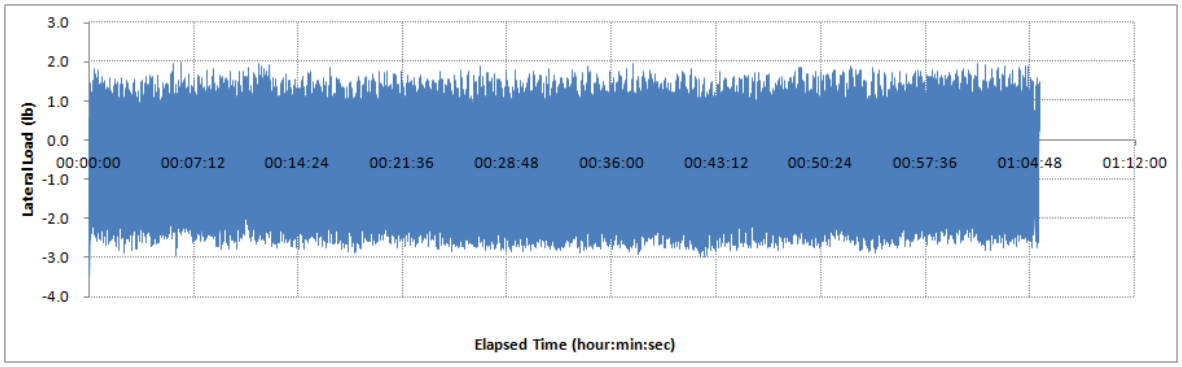

Figure 10.14: Lateral Load of 6-inch Model in Cemented Calcareous Sand (Repeated 5°, 3 sec)

In general, the lateral resistance of the foundation increases with increasing rotation angle of the model in cemented calcareous sand. However, the difference of the lateral load for different loading period is not significant. Lateral resistance of the model in cemented calcareous sand depends heavily on number of load cycles and magnitude of displacement the foundation previously experienced. The lateral resistance decreases with increasing lateral load cycles and increasing size of the gap in the cemented calcareous sand.

The excess pore water pressures for the 2-degree rotation and 5-second period lateral load test are shown in Figure 10.15 and 10.16. The excess pore water pressures are calculated by subtracting the hydrostatic pressures from the corresponding measured pore water pressures. The excess pore water pressures inside the suction can in cemented calcareous sand are not as uniform as those in cemented siliceous sand; the excess pore water pressure at Tip has a larger range of fluctuation. This can be attributed to the higher proportion of fine grain particles in the oyster shell meal comparing to the more uniform siliceous sand (see Figure 2.20). As a result, the permeability of the cemented calcareous sand is lower than the cemented siliceous sand, and the excess pore water pressure builds up near the tip cannot redistribute as easily.

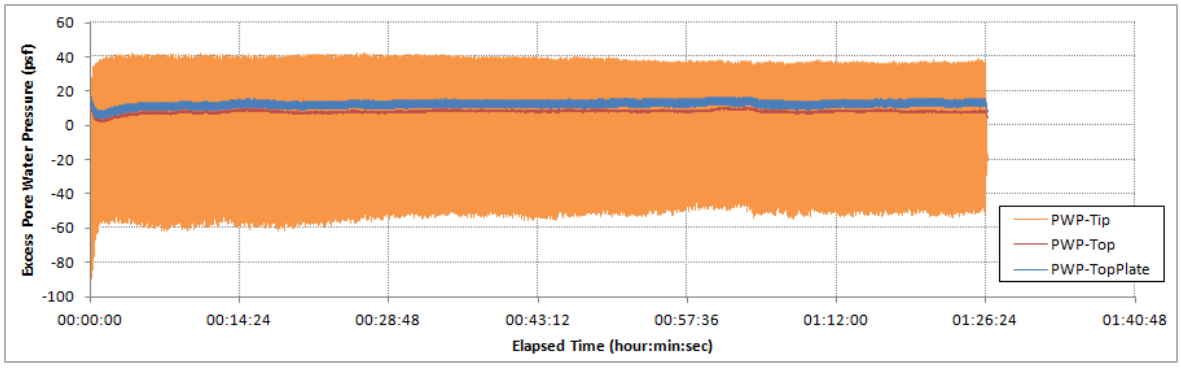

Figure 10.15: Excess Pore Water Pressure of 6-inch Model in Cemented Calcareous Sand (2° rotation, 5-sec period)

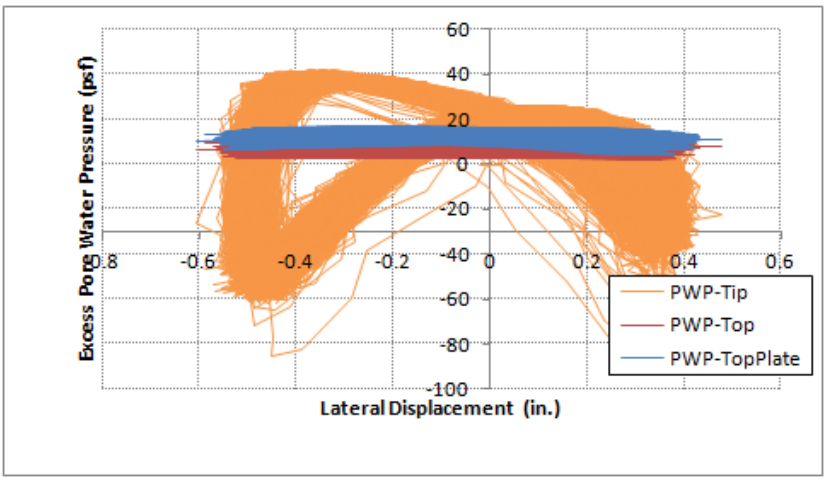

Figure 10.16: Excess Pore Water Pressure versus Lateral Displacement of 6-inch Model in Cemented Calcareous Sand (2° rotation, 5-sec period)

The tilt angles for the 2-degree rotation and 5-second period lateral load test are shown in Figure 10.17 and 10.18. The tilt angle in the direction perpendicular to loading is close to zero degree as expected. The tilt angle in the loading direction goes between +/-1 degree, where the positive angle indicates that model tilts to the left and negative angle indicates right-tilting movement.

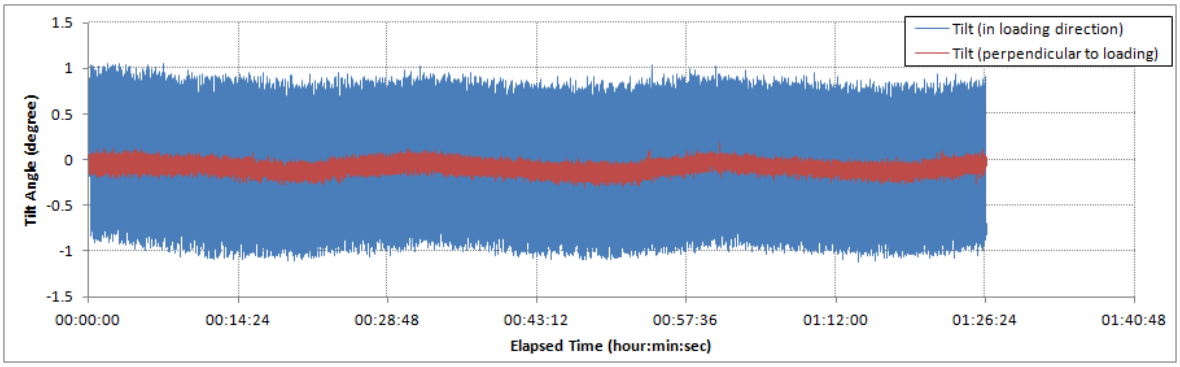

Figure 10.17: Tilt Angles of 1-foot Model in Cemented Calcareous Sand (2° rotation, 5-sec period)

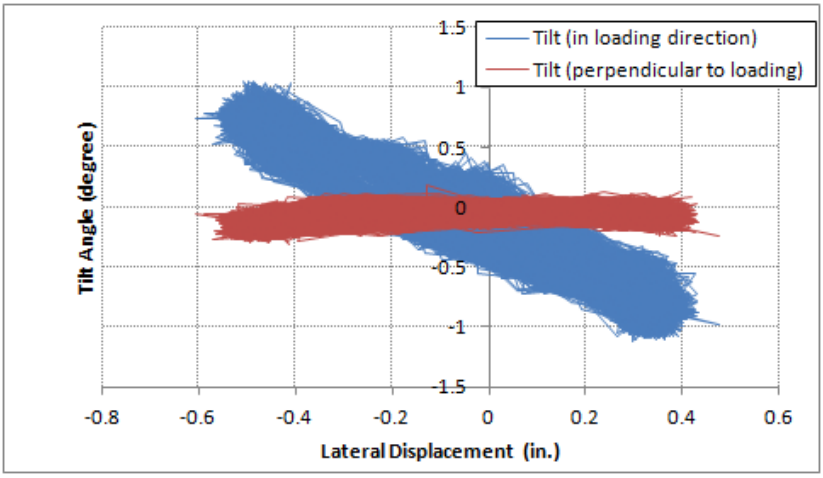

Figure 10.18: Excess Pore Water Pressure versus Lateral Displacement of 1-foot Model in Cemented Calcareous Sand (2° rotation, 5-sec period)

10.3 AXIAL LOAD TESTS

Axial load tests on the 6-inch diameter model in cemented calcareous sand were conducted by placing several 5-lb weights on the model in steps. The weights were placed on the model in steps to apply approximately 10, 20, and 30 lb of load with around 30 seconds for each step. The vertical displacement of the model was monitored using a dial gauge. Figure 10.19 shows the load-displacement curves of three loading-unloading cycles.

The excess pore water pressures of the three cycles of axial load tests are shown in Figure 10.20 to 10.22. The theoretical excess pore water pressure is assumed to be zero because the high permeability of the sand and the loading is under a drained condition. The measured excess pore water pressures are essentially zero except some spikes and very little excess pore water pressure occurred when the weights were placed or removed from the model.

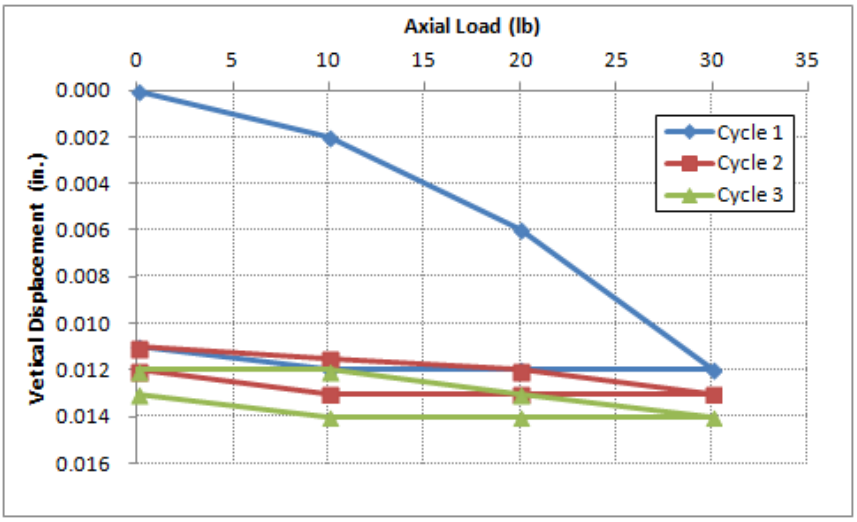

Figure 10.19: Load-Displacement Curve from Axial Load Tests

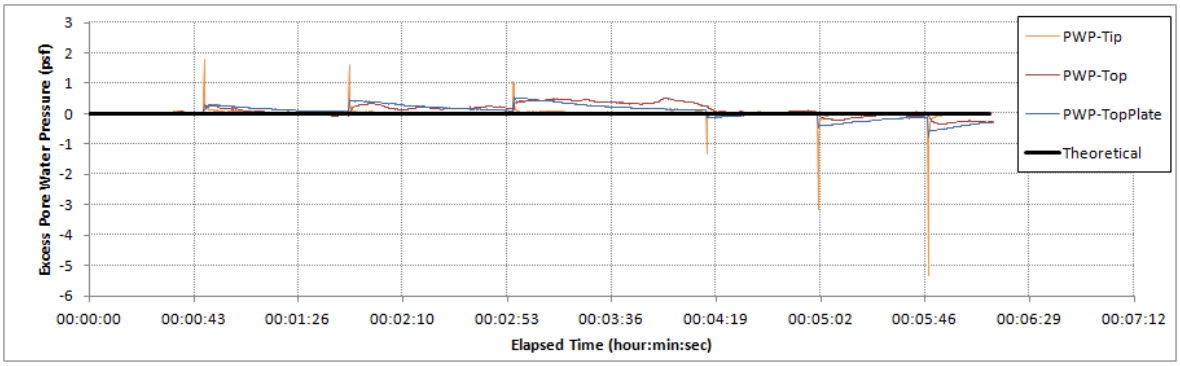

Figure 10.20: Excess Pore Water Pressure from Axial Load Test (Cycle 1)

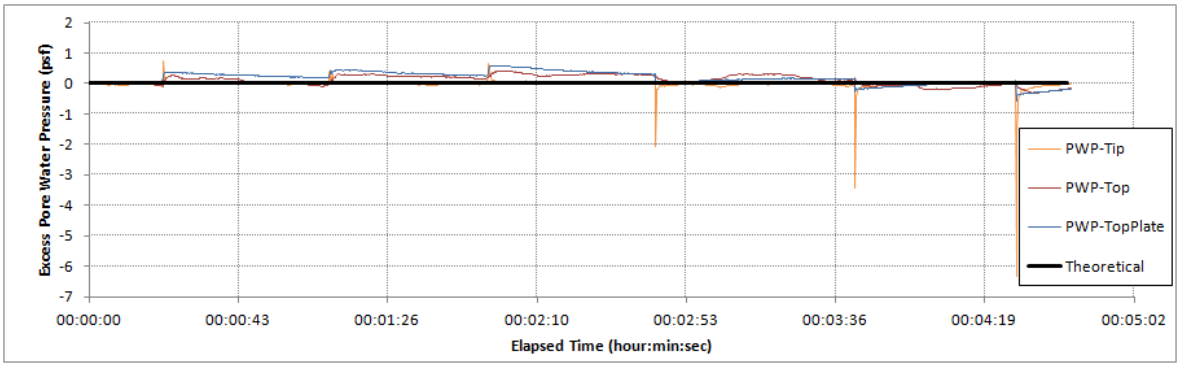

Figure 10.21: Excess Pore Water Pressure from Axial Load Test (Cycle 2)

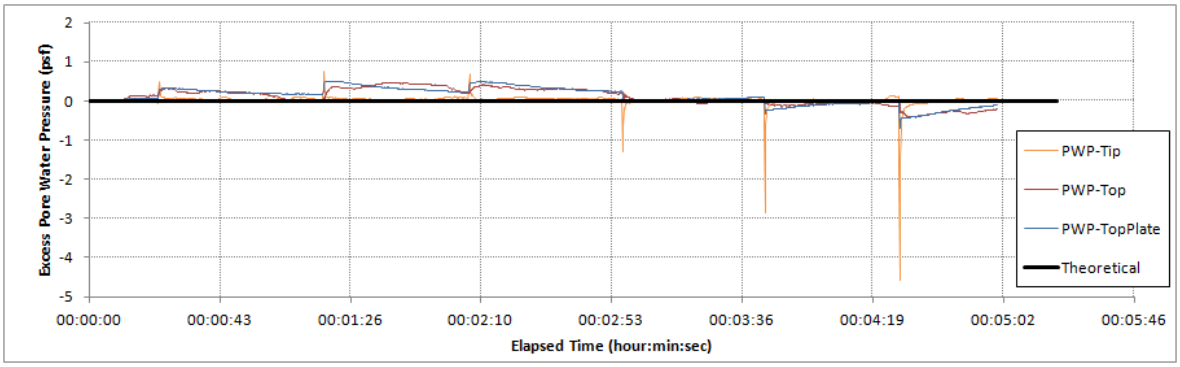

Figure 10.22: Excess Pore Water Pressure from Axial Load Test (Cycle 3)

10.4 PROOF LOAD TESTS

Proof load tests were conducted instead of ultimate axial capacity test because the load required to failure the model foundation in calcareous exceeds the capacity of our loading system. The proof load tests were conducted after all the axial and lateral load tests were completed. The axial proof load was applied by stacking weights on the model in steps, and the vertical displacement of the model was measured on top of the extended arm by a dial gauge. The model was loaded up to 292 lb and then uploaded for two cycles. The load-displacement curves from the two proof tests are shown in Figure 10.23. The maximum vertical displacement of around 0.006 diameter of the model (0.006 D) was measured under the 292 lb proof load in the first cycle. Note that the axial load does not include the weight of the model.

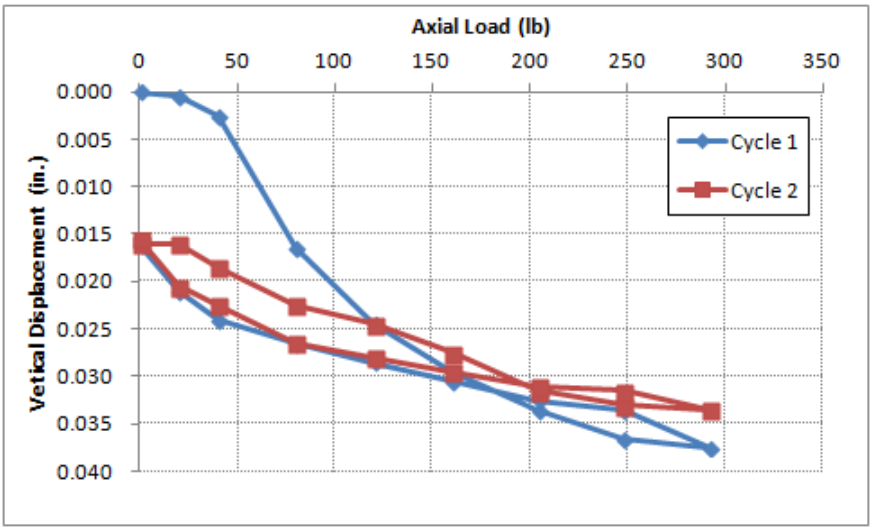

Figure 10.23: Load-Displacement Curve from Proof Load Tests

The excess pore water pressures from the proof load tests are shown in Figure 10.24 and 10.25. The theoretical excess pore water pressure is assumed to be zero because the relatively high permeability of the cemented calcareous sand and the loading is under a drained condition. In Figure 10.24 and 10.25, the spikes and little excess pore water pressure occurred when the weights were placed on the model or when the tubes for pore water pressure measurement were disturbed accidentally while placing the weights.

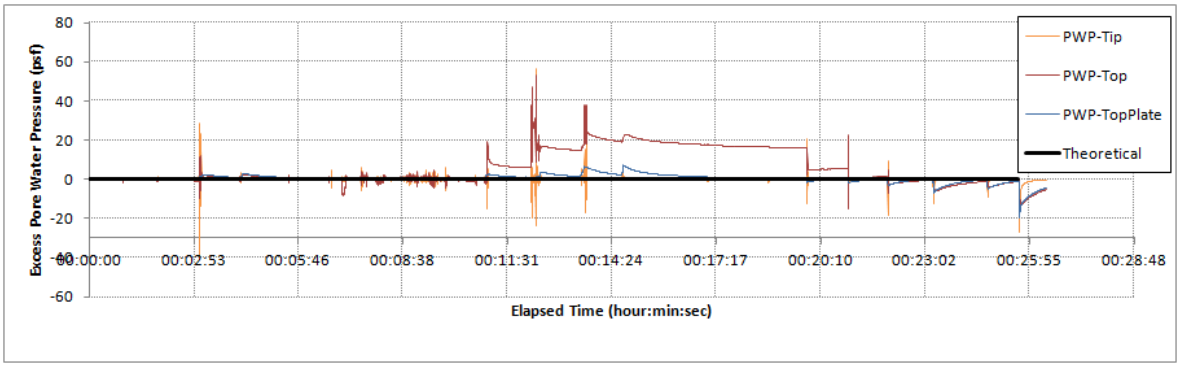

Figure 10.24: Excess Pore Water Pressure from Proof Load Test (Cycle 1)

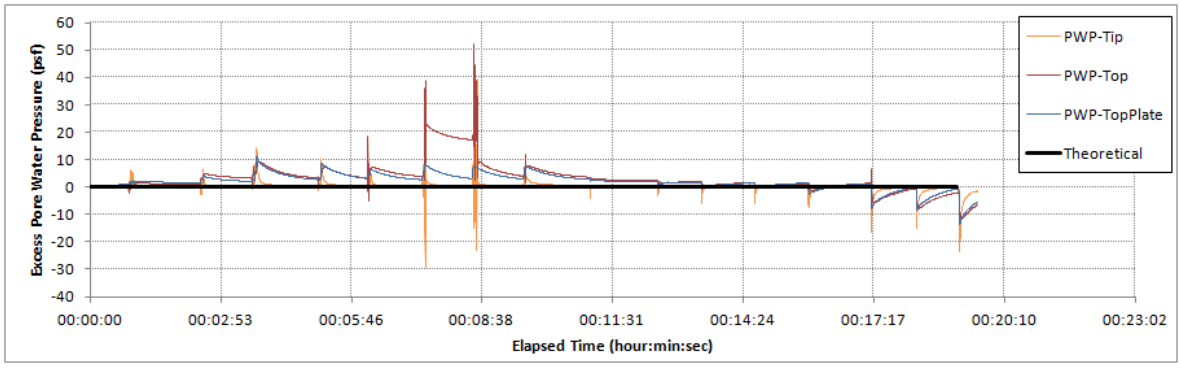

Figure 10.25: Excess Pore Water Pressure from Proof Load Test (Cycle 2)

10.5 PULLOUT

Pullout test was not conducted for the 6-inch SCF model in cemented calcareous sand because there was essentially no resistance between the model and the soil due to the gap and degradation after thousands of cyclic loading.

10.6 SUMMARY FOR TESTS IN CEMENTED CALCAREOUS SAND

The cemented calcareous sand test bed was prepared by mixing 1% of Type I Portland cement with oyster shell meal. The oyster shell meal had angular particles with a mean grain size of 0.3 mm and 8% of fine particles. The unconfined compression strength of the cemented calcareous sand was between 800 to 1200 psf, which is stronger but more ductile than the cemented calcareous sand used in this study. The cone tip resistance was between 28 to 34 ksf at 3 to 4 inches deep. The saturated unit weight of the cemented calcareous sand was 117 pcf. The 6-inch diameter SCF model was installed in the cemented calcareous sand by carefully placing the suction can in the test bed before the initial set of the cement to represent a “wish in place” condition.

For the 1000-cycle lateral load tests, in general, walking of the suction can in cemented calcareous sand was not very significant; however, occasionally the walking displacement can be up to 0.09 D. No significant settlement occurs for all the applied 1,

2, and 5-degree (±0.5, ±1, and ±2.5 degrees) rotation and loading periods. The settlements or upward movements were all less than 0.02 D. In the first couple of lateral tests, no significant fissures and cracks in the cemented calcareous sand around the suction can were observed because the cemented calcareous sand was more ductile. However, a gap around the suction can opened up after few thousands of accumulated load cycles. After the 5-degree rotation tests, the gap on the side opposite to the mean load was measured at 2 inches wide and 4 inches deep. Unlike the siliceous sand tends to fill the gap around the suction can, the gap in cemented calcareous sand stayed open throughout the tests. Because of the presence of the gap, the suction can had a significant lower lateral resistance in cemented calcareous sand comparing to previous tests in siliceous sands. The lateral resistance of the suction can showed softening behavior in most of the tests conducted. The softening behavior can be attributed to the broken down of the cementation between oyster shell particles. However, the 10-second period tests usually have no significant softening effect because the cemented calcareous sand was already degraded in the 3 and 5-second period tests which were conducted before the 10-second tests. The difference in the measured lateral load for different loading period (3, 5, and 10 seconds) is not significant which indicates that there is little stain rate effect in this range of loading periods. This observation is consistent with previous tests in clay and sand. Lateral resistance of the suction can in cemented calcareous sand depends heavily on number of load cycles and magnitude of displacement that the foundation previously experienced. The lateral resistance decreases with increasing lateral load cycles and increasing size of the gap in the cemented calcareous sand.

During cyclic lateral load tests, the excess pore water pressures inside the suction can in cemented calcareous sand are not as uniform as those in cemented siliceous sand; the excess pore water pressure in the soil plug near the tip of the suction can has a larger

range of cyclic fluctuation comparing to that under the top plate. This can be attributed to the higher proportion of fine grain particles in the oyster shell meal comparing to the more uniform siliceous sand, and as a result, a lower permeability of the cemented calcareous sand.

Proof load tests were conducted instead of ultimate axial capacity test because the load required to fail the model foundation in calcareous sand exceeds the capacity our loading system. The suction can was loaded up to less than 15% of its estimated ultimate axial capacity and then uploaded for two cycles. A maximum vertical displacement of around 0.006D was measured under the 292 lb proof load in the first cycle. No significant excess pore water pressure builds up throughout the proof load test. The pullout test was not conducted for the 6-inch SCF model in cemented calcareous sand because there was essentially no resistance between the suction can and the soil due to the large gap and degradation of cemented calcareous sand after thousands of cyclic loading.

Chapter 11: Analysis of Cyclic Lateral Load Tests in Clay

Since cyclic lateral loading is one of the most important aspects for the design of rigid foundations with small length to diameter ratios, more detailed analyses on cyclic loading tests are presented in this chapter. Analyses in this chapter focus on the cyclic loading tests in normally consolidated and overconsolidated clays because they are two common soil profiles in offshore environments.

In this chapter, the lateral load versus lateral displacement loops obtained in cyclic lateral load tests in normally consolidated and overconsolidated clays are first transformed to pseudo-static load-displacement curves. These load-displacement curves are then used to compare with plastic limit analysis and finite element analysis results. Finally, static and cyclic p-y analysis for foundations with small length to diameter ratios are developed by fitting these experimental load-displacement curves.

11.1 Experimental Lateral Load-Displacement Curves

The cyclic lateral loading test results show softening behaviors in the first couple cycles in some tests and, in some cases, followed by stiffening behaviors to the end of 1000 load cycles (see Section 6.2.2 and 7.2.2). It is not practical and feasible to simulate the whole dynamic loading process using available analysis techniques. Therefore, plastic limit analyses, static finite element analyses and pseudo-static p-y analyses are conducted to capture some of the important characteristics of the cyclic lateral load-displacement relationship.

As shown in Section 6.2.2 and 7.2.2, the measured lateral loads tend to be higher in the first couple cycles and subsequently stabilized to lower lateral loads within the first 100 cycles. In some cases, the measured lateral loads increase again showing stiffening

behavior still the end of the tests because of the increased lateral resistance due to foundation settlement and maybe partially drain loading condition. However, this stiffening behavior only occurs in normally consolidated clay with larger rotation of the foundation and can be simulated by increase the penetration (or length) of the foundation. Therefore, this study focuses on the load-displacement behavior in the first 10 cycles and also the stabilized behavior from cycle 100 to 200 before the stiffening behavior occurs.

Figure 11.1 and 11.2 show an example of the process to establish a point in the pseudo-static load-displacement relationship (or backbone curve) using the hysteresis loop of the 2-degree rotation, 10-second period lateral test in overconsolidated clay. Note that the lateral loads and lateral displacements are measured at 3 ft above the mudline as shown in Figure 6.6 and 6.7.

Figure 11.1(a) shows the original load-displacement hysteresis loops of the first 10 cycles and Figure 11.1(b) shows the loops of Cycle 100 to 200. Note that instead of centering about the origin (or having lateral loads with a mean of zero pound) the loops shifted to the negative load side because of the presence of the static mean current load acting on the foundation in the tests (see Section 6.2.2 and 7.2.2). This static mean current load increase the measured lateral load when the foundation tilts to the opposite direction of the mean current load and decrease the same amount of load when the foundation tilts to the same direction with the mean current load. In order to minimize this effect by the additional mean current load and obtain information from a pure two-way cyclic lateral loading condition, the loops are shifted to the positive and centered about the origin as shown in Figure 11.2. Control points are then selected for the loops of the first 10 cycles (see Figure 11.2a) and those of cycle 100 to 200 (see Figure 11.2b) to represent data points in the pseudo-static load displacement relationship. This process is then repeated for all the cyclic lateral load tests in overconsolidated clay and normally

consolidated clay. For overconsolidated clay, the loops and the corresponding control points of the first 10 cycles and cycle 100 to 200 are presented in Figure 11.3 and 11.4, respectively. Similarly, the results for normally consolidated clay are shown in Figure 11.5 and 11.6.

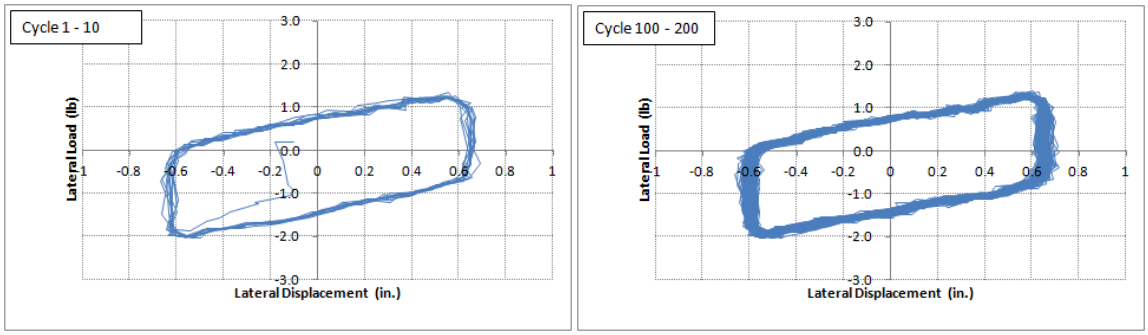

Figure 11.1: Original Lateral Load versus Lateral Displacement Hysteresis Loop in OC Clay with Additional Static Mean Load Acting on the Foundation

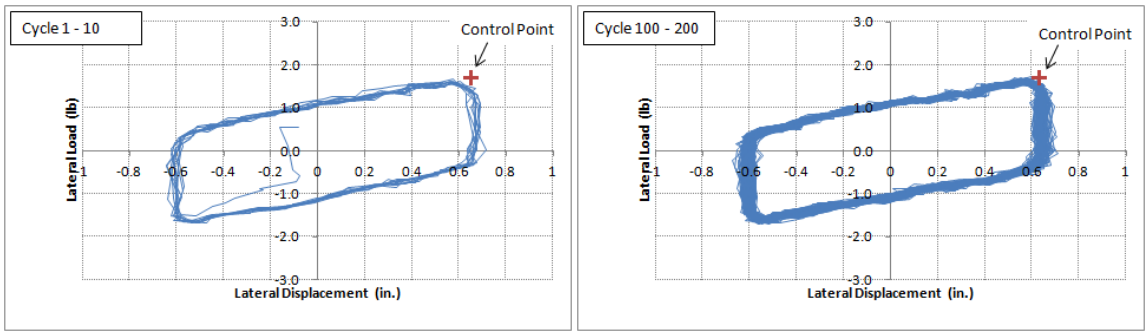

Figure 11.2: Control Points and Centered Lateral Load-Displacement Hysteresis Loops in OC Clay (Removing Effects from Static Mean Current Load Acting on the Foundation)

In Figure 11.3 to 11.6, the loops with different rotation angles and the corresponding control points are plotted in the same chart for each of the loading periods. The control points in each of the chart represent the "backbone" pseudo-static lateral load-displacement relationship at 3 ft above the mudline for each loading period in either

normally consolidated clay or overconsolidated clay. Note that, in Figure 11.5, the loops of first 10 cycles of 5-degree, 10 second test is not shown because of its unusually low load measurements possibly due to a leak in the soil plug.

Finally, the lateral load-displacement relations (control points or backbone curves) in Figure 11.3 to 11.6 are compiled in Figure 11.7 and 11.8 for overconsolidated clay and normally consolidated clay, respectively.

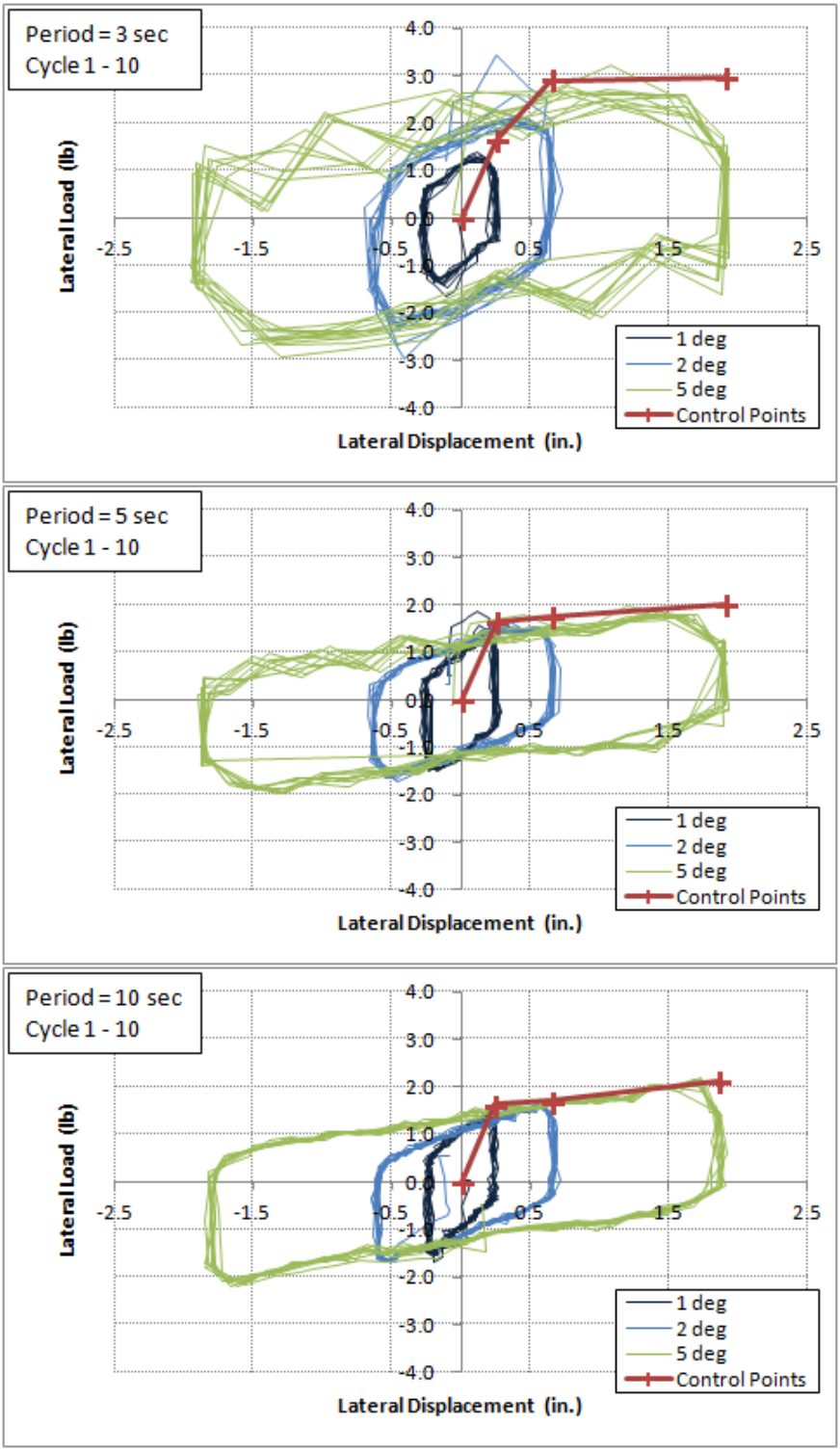

Figure 11.3: Lateral Load versus Lateral Displacement in OC Clay (Cycle 1 to 10)

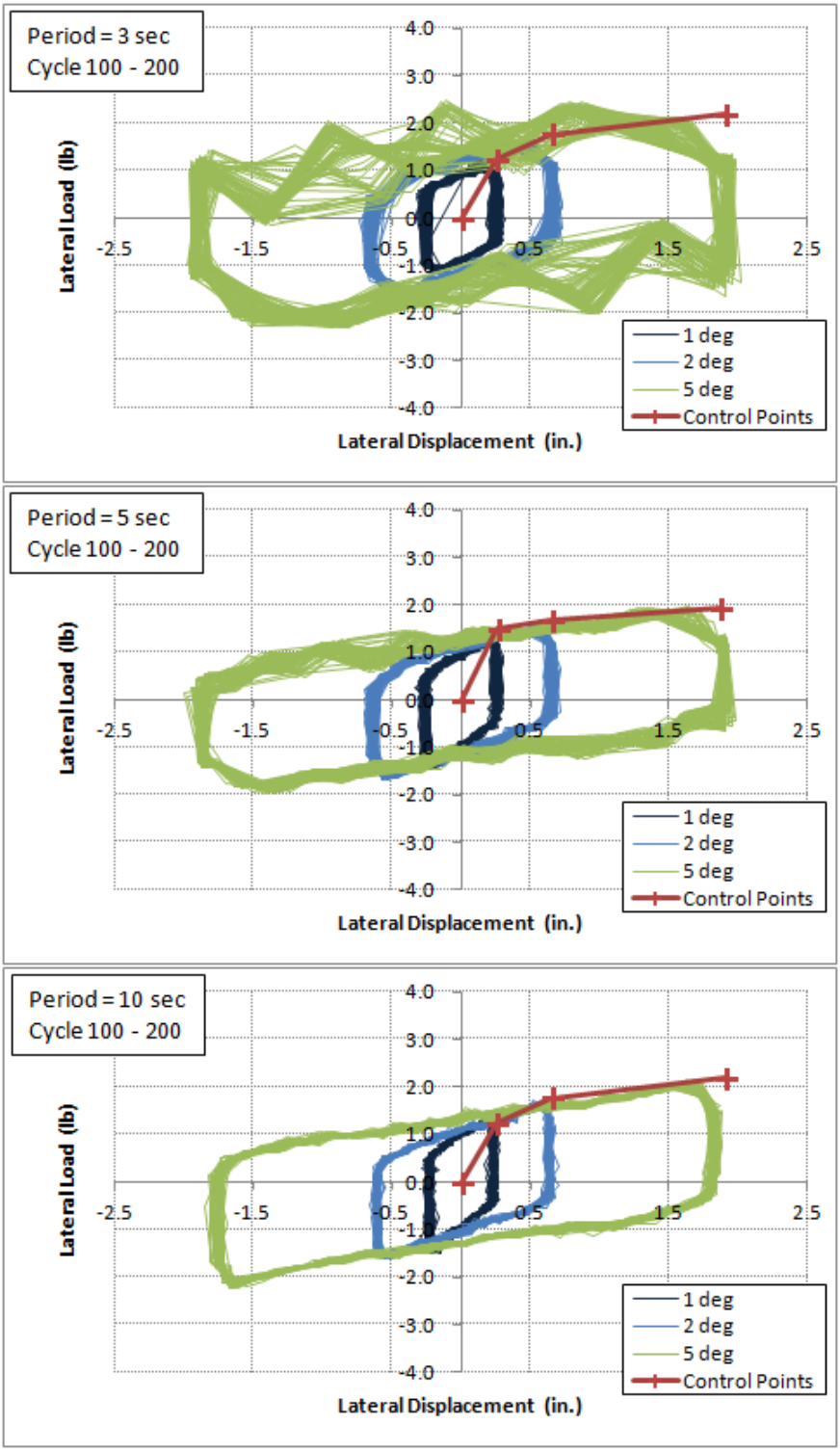

Figure 11.4: Lateral Load versus Lateral Displacement in OC Clay (Cycle 100 to 200)

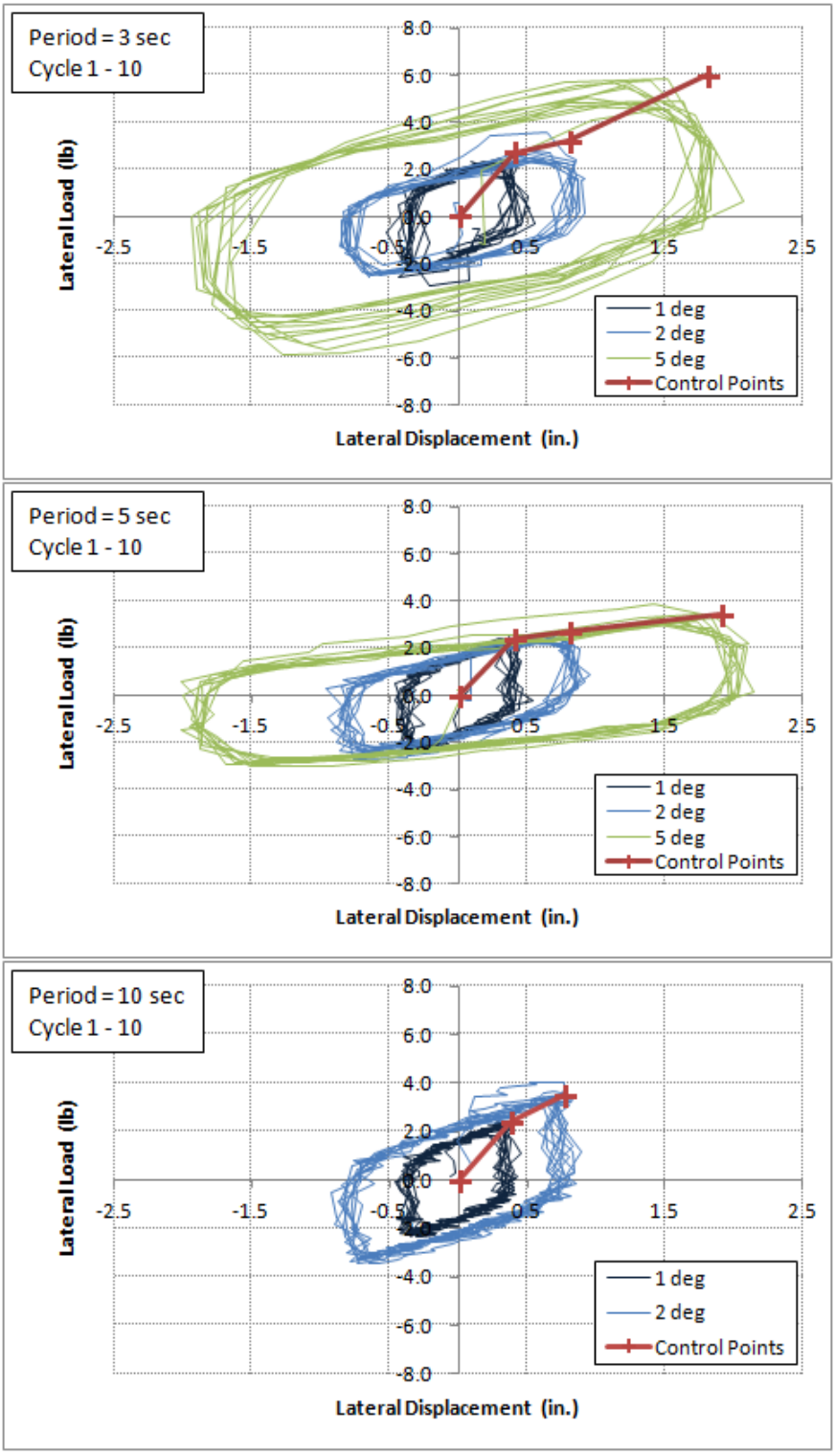

Figure 11.5: Lateral Load versus Lateral Displacement in NC Clay (Cycle 1 to 10)

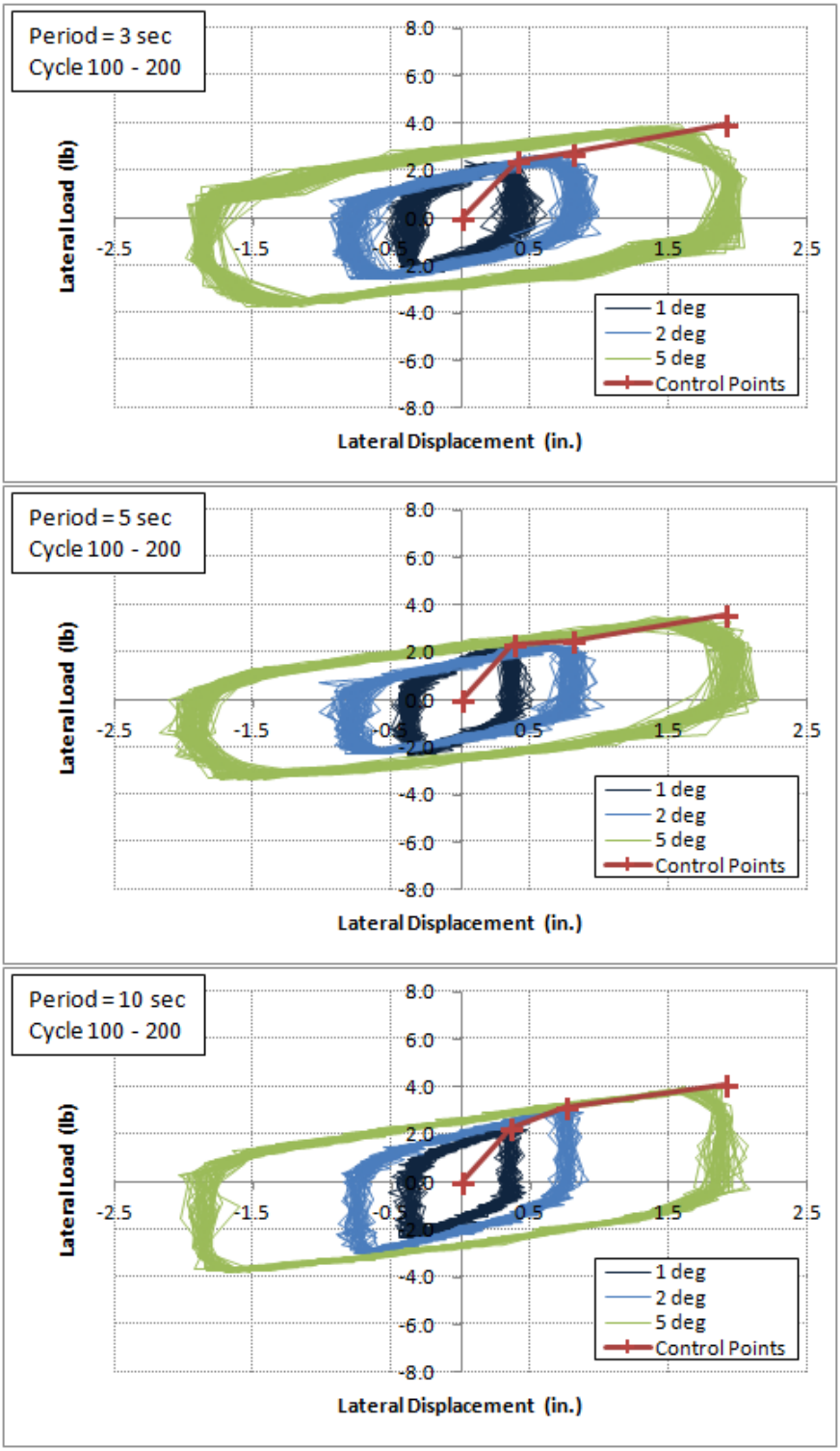

Figure 11.6: Lateral Load versus Lateral Displacement in NC Clay (Cycle 100 to 200)

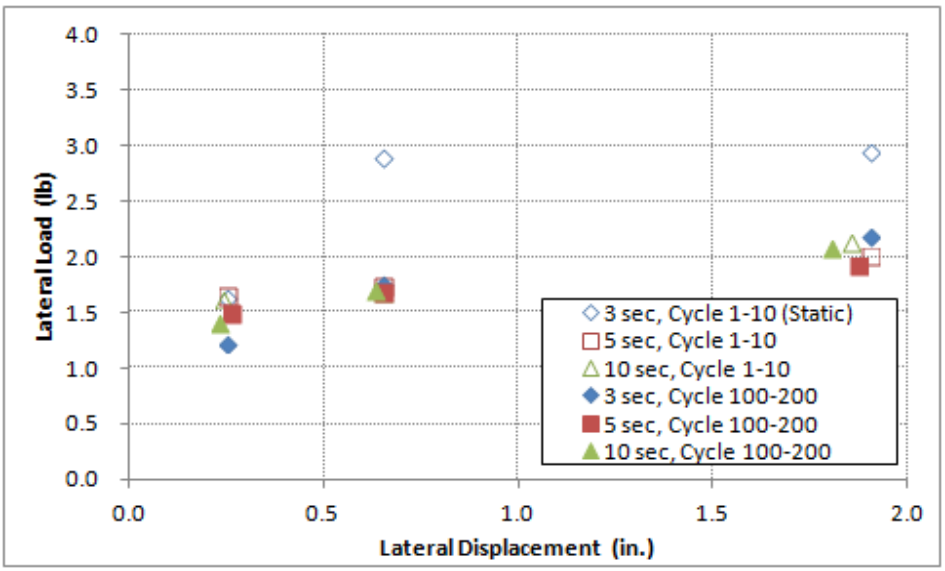

Figure 11.7: Experimental Lateral Load-Displacement in OC Clay

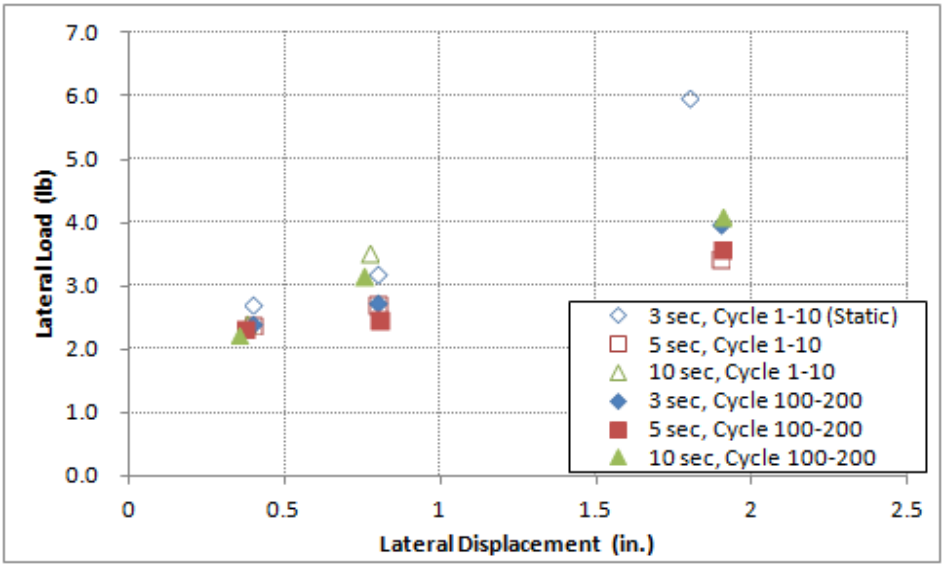

Figure 11.8: Experimental Lateral Load-Displacement in NC Clay

Both Figure 11.7 and Figure 11.8 show that the first 10 cycles of 3-second period tests have higher lateral (or rotational) resistance and stiffness than the other tests.

However, the lateral resistance of the first 10 cycles of 5- and 10-second period tests is lower and similar to that of cycle 100 to 200 in all tests. The resistance in the first 10 cycles of 3-second period tests is higher because all the cyclic lateral load tests were performed in the sequence of 3, 5, and then 10 second period. The 3-second period tests are the first tests for each rotation angle. In other words, it was the first time that the soil around the foundation was displaced that much for a given rotation angle in the first couple cycles of the 3-second period tests. Therefore, the lateral load-displacement relationships from the first 10 cycles of 3-second period are the virgin lateral load-displacement curves or can be refer to "static" loading curve (Matlock 1970). If the foundation is subjected to further cyclic loading, the lateral resistance will decrease and stabilize in most cases as shown in the rest of the tests in Figure 11.7 and 11.8. These cyclically degraded responses can be referred to "cyclic" loading curves (Matlock 1970). Note that, however, the differences in lateral resistance between static and cyclic loading curves are less significant with smaller lateral displacements (or rotation).

By comparing the lateral load-displacement curves in normally consolidated clay (Figure 11.8) and in oversonsolidated clay (Figure 11.7), the foundation in overconsolidated clay tends to reach its ultimate capacity (or the load-displacement curve reaches a plateau) at a smaller rotation angle comparing to that in normally consolidated clay. In other words, suction can foundations have more ductile behavior in normally consolidated clay. Note that the strain rate (loading rate) effects are not significant within the load periods (3, 5, and 10 seconds) used in this study.

The experimental static and cyclic lateral loading curves shown in Figure 11.7 and 11.8 will be used to compare with plastic limit analyses and finite element analyses and to construction the p-y analysis model in the following sections.

11.2 PLASTIC LIMIT ANALYSIS

The plastic limit analysis program, FALL16, was used to estimate the ultimate lateral capacity of the suction can foundation in overconsolidated clay and normally consolidated clay test beds. FALL16 was developed by Don Murff, Chuck Aubeny, Seungwoon Han, and Yuqing Wu based on a simplified plastic limit analysis for more slender suction caissons (Aubeny and Murff 2003). Plastic limit analysis can be used to estimate the ultimate capacity of the foundation. However, it cannot provide the information on the load-displacement response.

Table 11.1 and Table 11.2 show the FALL16 input parameters that were used to calaculate the suction can lateral capacities in overconsolidated clay and normally consolidated clay, respectively. The lateral loads were applied at 3 ft above the mudline, and therefore, the calculated capacities will be comparable to the measured loads in the experiments. Separate analyses were conducted using the undisturbed and remolded undrained shear strengths of the test beds measured by T-bar. Since a gap between the foundation and surrounding soil was observed in the lateral load tests in overconsolidated clay, it was assume that there is no backside suction acting on the foundation. However, no significant gap was observed in the lateral load tests in normally consolidated clay. Therefore, backside suction was applied on the foundation for the analyses for the foundation in normally consolidated clay.

Caisson Diameter	Caisson Length	Load Application point	Soil Strength at Mudline	Soil Strength Gradient	Soil Unit Weight	Interface Friction Coeff. α	Caisson Backside Suction
0.5 ft	0.5 ft	-3 ft	Undisturbed: 45 psf Remolded: 22 psf	0 psf/ft	40 pcf	1.0	No

Table 11.1: FALL16 Input Parameters for Calculating Lateral Capacity in OC Clay

Caisson Diameter	Caisson Length	Load Application point	Soil Strength at Mudline	Soil Strength Gradient	Soil Unit Weight	Interface Friction Coeff. α	Caisson Backside Suction
1 ft	1 ft	-3 ft	0 psf	Undisturbed: 14 psf/ft Remolded: 7 psf/ft	40 pcf	1.0	Yes

Table 11.2: FALL16 Input Parameters for Calculating Lateral Capacity in NC Clay

The lateral capacity and the depth to center of rotation predicted by FALL16 are presented in Table 11.3 and 11.4 for overconsolidated clay and normally consolidated clay, respectively. The calculated lateral capacities were also compared with the experimental load-displacement data in Figure 11.9 and 11.10. In these two figures, the filled circles are the test data for the "static" loading conditions or the virgin load-displacement relationships from the first tests for a given rotation angle (see Section 11.1). The circles represent "cyclic" loading conditions that are from the tests experience cyclic degradation.

	Lateral Capacity	Depth to Center of Rotation
Undistrubed s_u	3.03 lb	3.60 in.
Remolded s_u	1.52 lb	3.60 in.

Table 11.3: FALL16 Input Parameters for Calculating Lateral Capacity in OC Clay

	Lateral Capacity	Depth to Center of Rotation
Undistrubed s_u	5.55 lb	9.20 in.
Remolded s_u	2.77 lb	9.20 in.

Table 11.4: FALL16 Input Parameters for Calculating Lateral Capacity in NC Clay

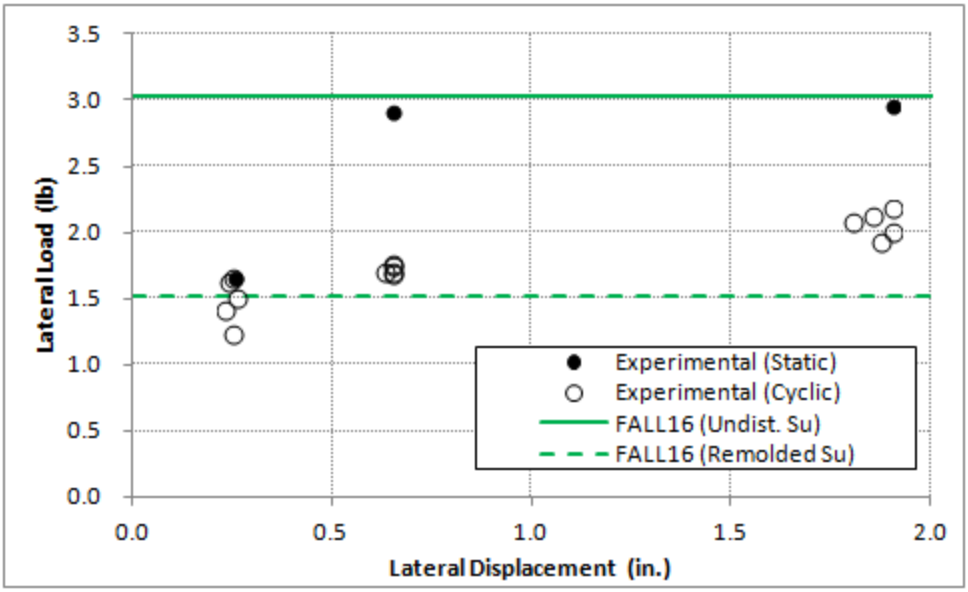

Figure 11.9: FALL16 versus Experimental Lateral Resistance in OC Clay

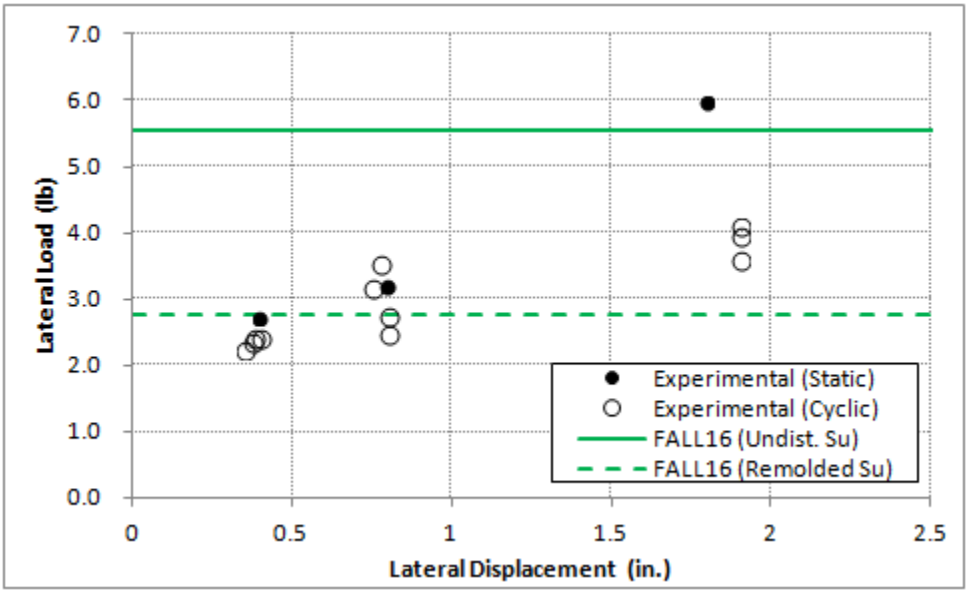

Figure 11.10: FALL16 versus Experimental Lateral Resistance in NC Clay

Figure 11.9 shows that, in overconsolidated clay, FALL16 predicts an ultimate lateral capacity that is close to the experimental "static" capacity if the undisturbed

undrained shear strength of the soil is used in the analysis. However, it overestimates the "cyclic" lateral resistance by approximately 50%. This can be attributed to that the soil at the slip surfaces is disturbed and loaded back and forth during cyclic loading condition. Therefore, the soil resistance decreases from the original static loading. If the remolded undrained shear strength of the soil is used for the analysis, FALL16 predicts a lower lateral capacity which underestimates the cyclic lateral resistance by approximately 25%.

Figure 11.10 shows similar trends in normally consolidated clay. Using the undisturbed undrained shear strength of the soil, FALL16 predicts a lateral capacity close to the experimental resistance for "static" loading. However, it overestimates the "cyclic" loading resistance by approximately 40%. If the remolded undrained shear strength of the soil is used, FALL16 predicts a lateral capacity that is approximately 30% lower than the experimental cyclic resistance.

In general, using the undisturbed undrained shear strength of the soil, FALL16 predicts a lateral capacity close to the "static" experimental lateral resistance, but overestimate the cyclic lateral resistance. If the remolded undrained shear strength is used, FALL16 predicts a lateral resistance underestimates the cyclic lateral resistance. Note that FALL16 was originally developed for more slender suction caissons and predicted capacity closer to finite element analysis with an aspect ratio greater than 6 (Aubeny et al, 2003). Therefore, FALL16 may not be the most appropriate tool for predicting the lateral resistance of a stubbier suction caisson. In order to better characterize the lateral load-displacement response of the stubby suction caissons, finite element analysis and p-y analysis model are developed and compared with the experimental data in the following sections.

11.3 FINITE ELEMENT ANALYSIS

In order to have a better understanding of the lateral load-displacement response and the failure mechanism of the stubby suction caisson, finite element analyses were conducted by using the commercial package Abaqus under an undrained static loading condition. The finite element model constructed for this study consists of a steel 6-inch diameter suction can in homogeneous soil with a constant undrained shear strength. Because of the symmetry of the laterally loaded suction can, only half of the model was analyzed as shown in Figure 11.11. The element used in this model is predominately C3D20R, a 20-node quadratic brick continuum element with reduced integration (Simulia, 2012).

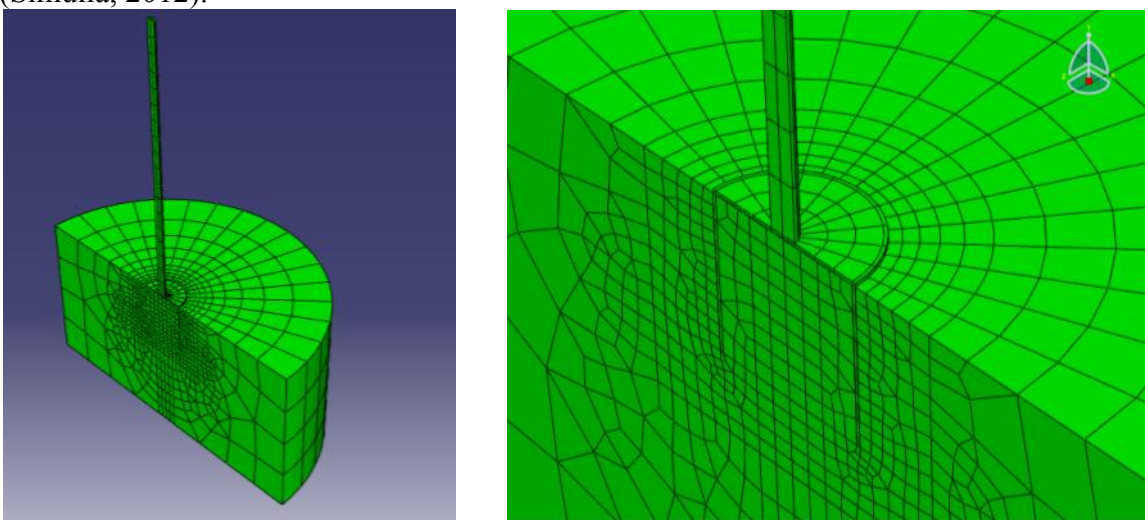

(a) Whole FEM Model (b) Detailed Mesh around Foundation

Figure 11.11: Finite Element Mesh Used in Abaqus

The steel suction can in the finite element model has the same dimensions as the 6-inch diameter scale model, which is 6 inches in diameter and 6-inch in length with a wall thickness of 1/8 inch and a 3 ft long extended arm. The steel is assumed to have an elastic modulus (E) of 29,000,000 psi, a Poisson's ratio of 0.26, and a yield strength of 36,000 psi. The clay is modeled as an elastic-perfectly plastic material using Mohr-

Coulomb yielding criterion. The clay is assumed to be saturated and, therefore, has a cohesion equals to the undrained shear strength of soil (s_u) and a friction angle of zero. The elastic modulus (E) of clay was determined by assuming a constant $E/s_u = 300$, and the Poisson's ratio was assumed to be 0.495. Separate analyses were conducted by using an undisturbed undrained shear strength of 45 psf and a remolded undrained shear strength of 22 psf which were measured in the overconsolidated clay test bed.

Boundary condition at the symmetry plane was set up that all the nodes in the plane have only in-plane movements. Fixed boundary was assumed at the bottom of the soil and the nodes on the vertical side of the soil boundary were only allow to move in the vertical direction. The lateral load was applied by prescribing a lateral displacement of 3 inches at the top of the 3-ft long extended arm to simulate the lateral load tests. The lateral resistance then can be obtained by the reaction force at the top of the extended arm. Since this was a half model analysis, the lateral resistance calculated by Abaqus was multiply by 2 to obtain the lateral resistance of a full model.

11.3.1 Tied Soil-Foundation Wall Interface

The soil was assumed to be tied to the suction can for the first set of analyses. The magnitude of displacement and plastic strain calculated by Abaqus are shown in Figure 11.12 and 11.13, respectively. The elements of suction can are made invisible in these figures for a better view of the soil elements. The lateral load-displacement responses using undisturbed and remolded undrained shear strengths are plotted with the experimental data in Figure 11.14. The center of rotation located approximately 3.5 inches (0.58D) below the mudline can be clearly identified by the displacement magnitude in Figure 11.12. The suction can and the adjacent soil move about the center of rotation suggesting that rotation is the dominating failure mechanism. The circular

failure surface can be seen around the suction can by the plastic strain distribution in Figure 11.13 while the rest of the soil mass remains elastic or undisturbed.

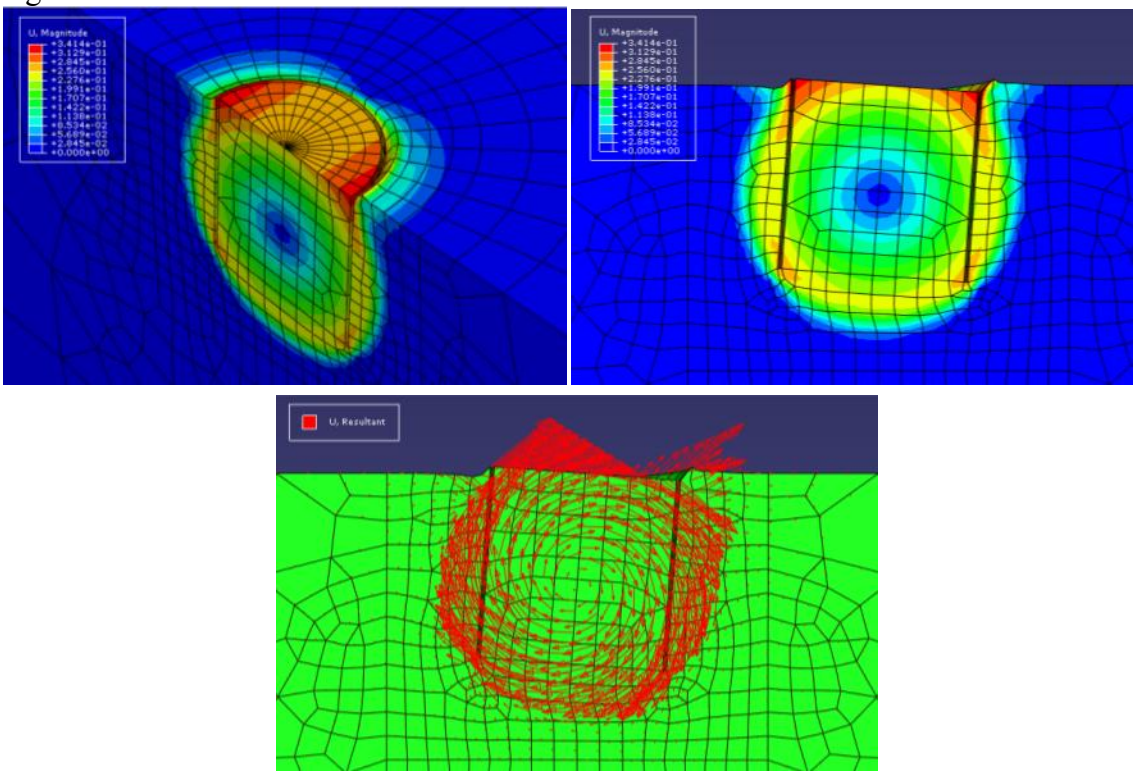

Figure 11.12: Displacement Magnitude by Abaqus with Tied Soil and Outer Wall Interface

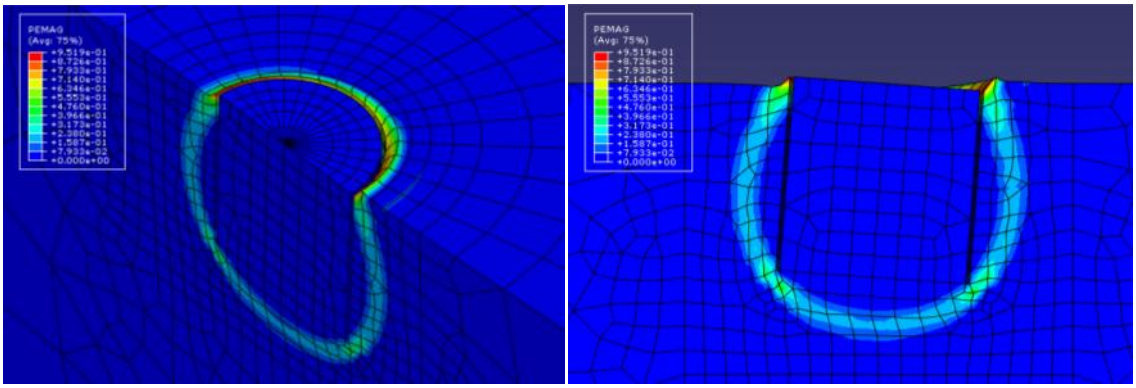

Figure 11.13: Plastic Strain Magnitude by Abaqus with Tied Soil and Outer Wall Interface

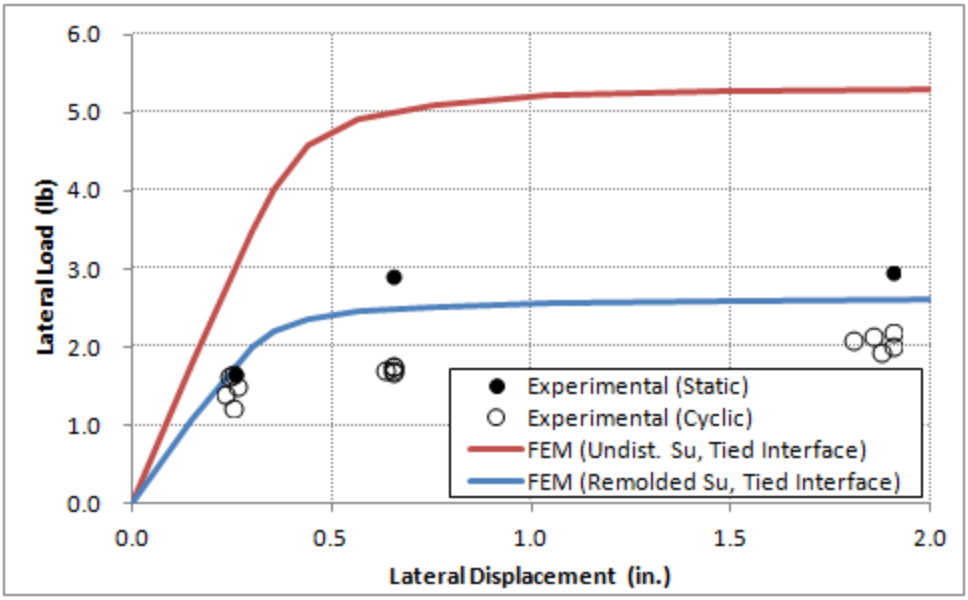

Figure 11.14: Lateral Load-Displacement Curves by Abaqus with Tied Soil and Outer Wall Interface

As shown in Figure 11.14, by using undisturbed undrained shear strength of soil and tied soil-foundation wall interface, the finite element model overestimates the "static" lateral capacity of the suction can in oversonsolidated clay by approximately 75% while overestimates the "cyclic" lateral capacity by 165%. If the remolded undrained shear strength of soil was used, the finite element model estimates a lateral capacity in between the static and cyclic lateral capacity. Since a gap between the foundation and the soil was observed during the lateral load tests, the tied soil-foundation wall interface may not be the most appropriate assumption. This is also the main reason that the finite element model overestimates the lateral capacity of the foundation.

11.3.2 Slippable Soil-Outer Wall Interface

In order to better simulate the laterally load suction can in overconsolidated clay, the finite element model was modified by defining a soil-outer wall interface that can slip

and separate. Two cases of soil-outer wall interface properties were considered to bound the problem: 1) a frictionless interface and 2) a interface with a friction coefficient of 0.8 and a maximum interface shear stress equal to the undrained shear strength of the soil. The magnitude of displacement and plastic strain calculated by this modified finite element model are shown in Figure 11.15 and 11.16, respectively.

As shown in Figure 11.15, the magnitude of displacement again suggests rotation about the center of rotation is the dominating failure mechanism. The center of rotation is located deeper at 4.3 inches below mudline in the case with a slippable interface. Instead of having the soil on the backside (opposite to the loading direction) moving with the suction can, a gap opens up with a slippable soil-outer wall interface. On the side of loading, a passive soil wedge, similar to that suggested by Murff and Hamilton (1993), is pushed upward. In Figure 11.16, the plastic strain indicates a spherical slip surface at the tip of the foundation which is similar to the assumption made by Aubeny and Murff (2003).

The lateral load-displacement curves obtained from this modified finite element model using both cases of interface settings are potted with the experimental data in Figure 11.17. The cases with frictionless interface predicts lateral capacities that are 18% lower than the cases with a friction coefficient of 0.8 and a maximum interface shear strength equal to the undrained shear strength of the soil (designated as slippable interface in this figure). When using the undisturbed undrained shear strength of the soil, the two cases of interface settings seem to bound the experimental “static” load-displacement relationship well. If the remolded undrained shear strength of the soil is used in the model, the slippable interface settings also provide a reasonable lower bound for the “cyclic” load-displacement relationship.

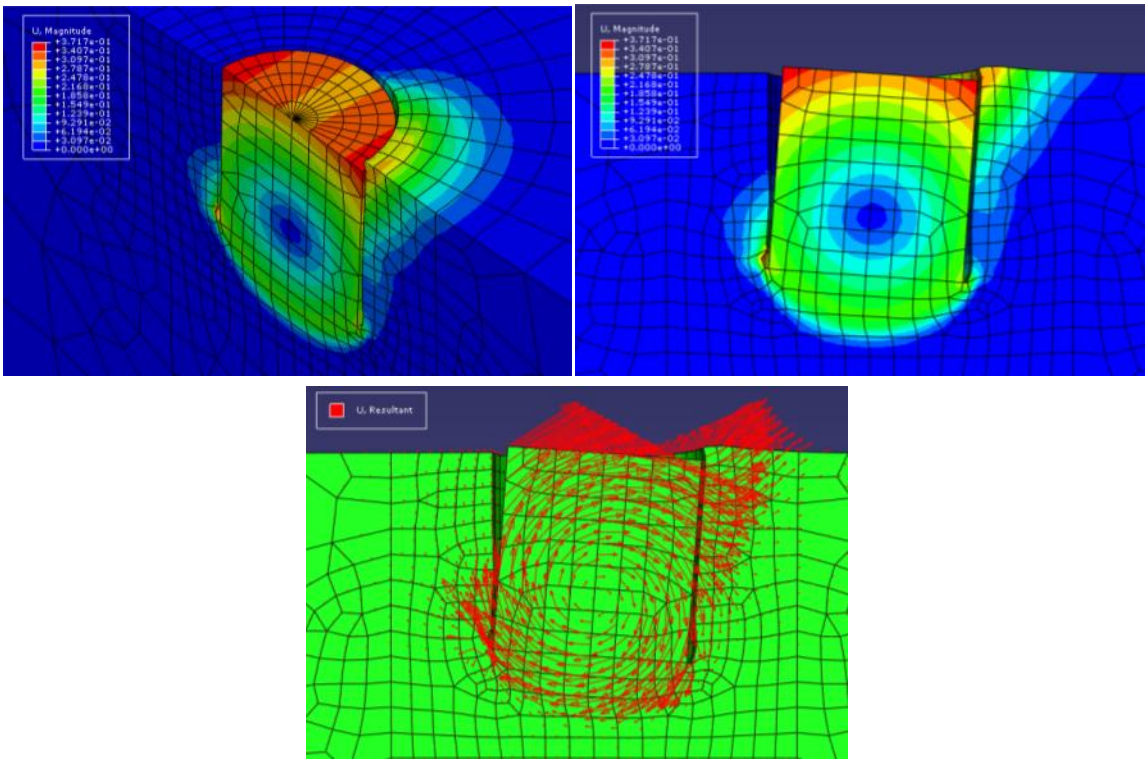

Figure 11.15: Displacement Magnitude by Abaqus with Slippable Soil and Outer Wall Interface

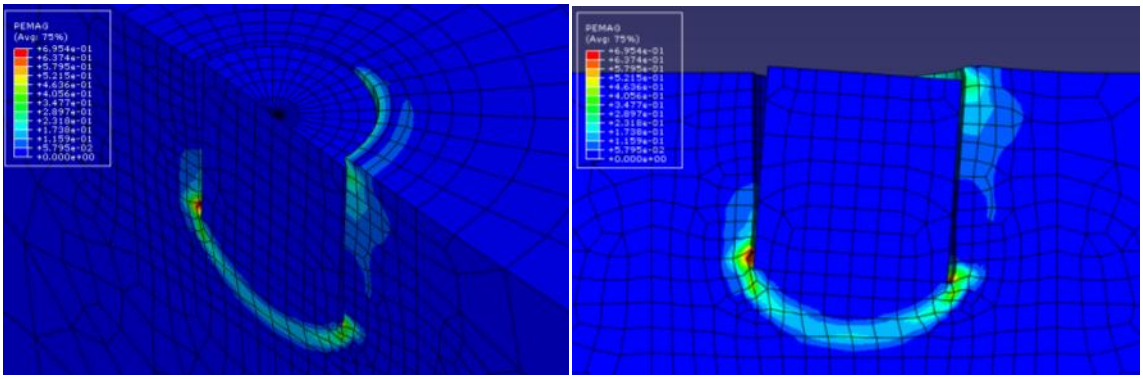

Figure 11.16: Plastic Strain Magnitude by Abaqus with Slippable Soil and Outer Wall Interface

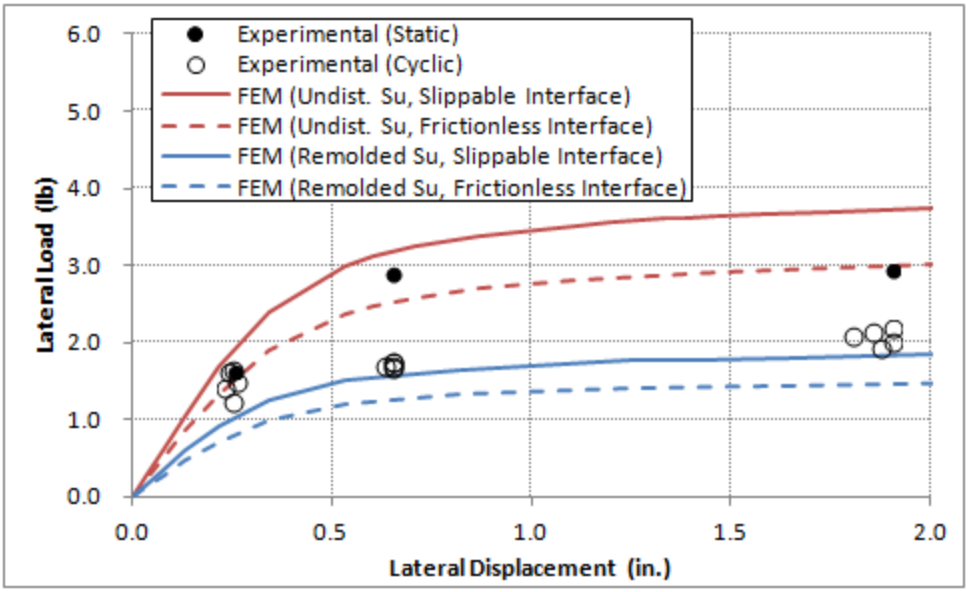

Figure 11.17: Lateral Load-Displacement Curves by Abaqus with Slippable and Frictionless Soil-Outer Wall Interface.

11.4 RIGID CAISSON P-Y ANALYSIS

An Excel spreadsheet based p-y analysis model for predicting the lateral load-displacement response was developed in this study for stubby caissons by using the lateral load test results of the suction can foundation. P-y analysis can provide useful information on load-displacement response of foundations and require less computational effort comparing to finite element analysis. The construction, calibration, and analysis results of this p-y analysis model are presented in the following sections.

11.4.1 Rigid Caisson p-y Analysis Model

The stubby suction caisson is assumed to be a rigid short cylinder in this p-y analysis model because of its higher stiffness comparing to a slender pile. However, it should be noted that stubby suctions may deforms when they are loaded in the field. A

rotational failure mechanism (see Figure 11.18a) is assumed to be the dominating failure mode of the laterally loaded caisson according to previous studies (Murff and Hamilton 1993, Aubeny and Murff 2003) and the finite element analyses in the previous section. This failure mechanism consist of a shallow failure (a soil wedge and/or a gap), flow-around failure at depth, and a spherical slip surface at the tip of the caisson. According to the failure mechanism, the soil resistance acting on the caisson can be simplified as two components (see Figure 11.18b): side resistance on the side of the caisson and the resisting moment from the shear stress acting on the spherical slip surface at the tip. The soil resistance on the side is a function of depth that accounts for the lower resistance due to the upward soil wedge near the surface as well as the higher flow-around resistance at depth. Consequently, the two resistance components can be discretized and represented by the mathematical model as shown in Figure 11.19. The side resistance is discretized into 40 translational nonlinear springs attached along the wall of the caisson and the end resisting moment is idealized as a rotational spring at the center of rotation.

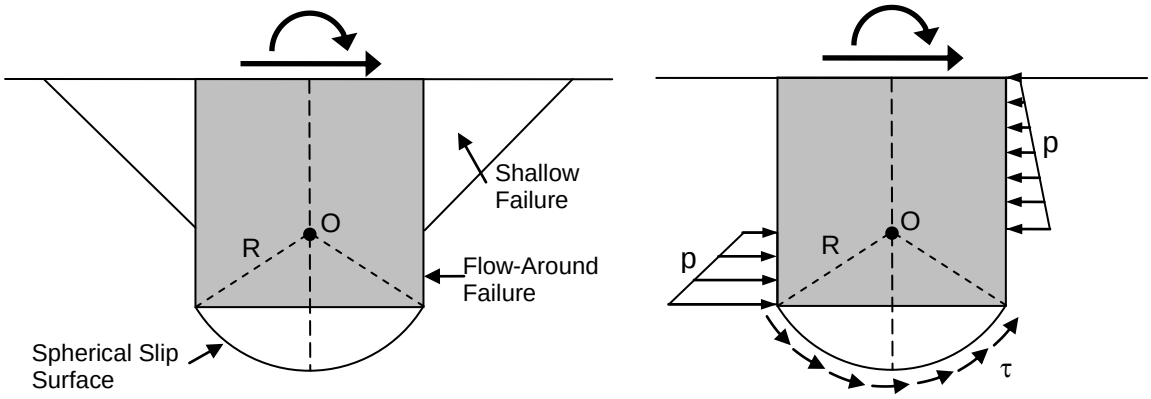

(a) Failure Mechanism (b) Soil Resistance on Caisson

* Note that the flow-around failure may not be fully mobilized.

Figure 11.18: Failure Mechanism and Soil Resistance on Rigid Caisson.

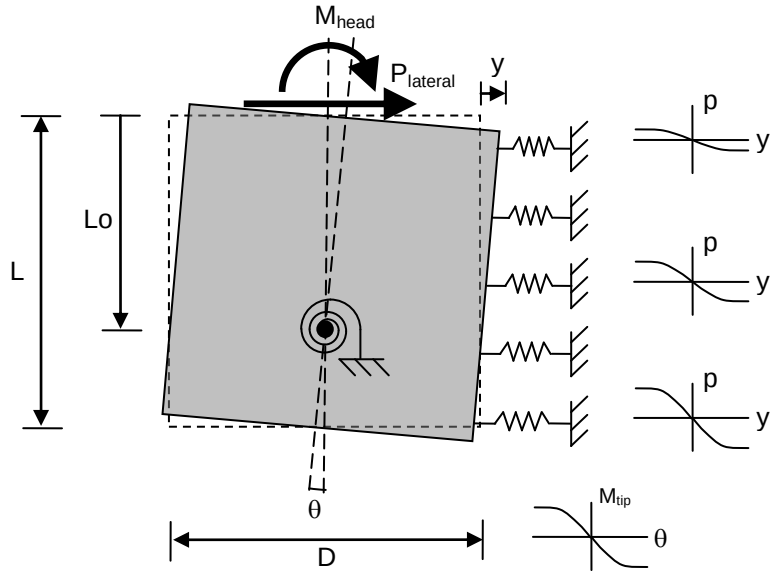

Figure 11.19: Mathematical Model for Rigid Caisson p-y Analysis.

The side resistance component is similar to the p-y analysis model developed by Matlock (1970) and Reese (1975) for conventional pile foundations. The relation between the unit lateral resistance (p, lateral resistance per unit length of the foundation) and lateral displacement (y) is provided by the nonlinear p-y curves. Details on the side resistance are presented in Section 11.4.2. The end resisting moment is to account for the resistance from the spherical slip surface as presented by Aubeny and Murff (2003) and in Figure 11.16. The relation between end resisting moment (M_{tip}) and rotation angle (θ) is provided by a nonlinear M_{tip}-θ curve as presented in Section 11.4.3.

This rigid caisson p-y analysis model solves the corresponding rotation angle (and accordingly lateral displacement) of a give lateral load and moment acting on top of the caisson by optimizing the depth to center of rotation to satisfy both force and moment equilibrium. The solving procedure can be broken down to the following steps:

1. Given a lateral load, $P_{lateral}$, and moment, M_{head}, acting on the top of the caisson.
2. Assume a trial depth to the center of rotation, Lo.
3. Assume a trial rotation angle, θ.
4. Calculated the end resisting moment by using the M_{tip}-θ curve.
5. Calculate the lateral displacements, y, at the depths of each lateral resistance spring using the assumed center of rotation and the assumed rotation angle.
6. Use the lateral displacement, y, of each spring to find the corresponding lateral resistance of the 40 springs by the p-y curves.
7. Sum moment about the center of rotation and check if the moment equilibrium is satisfied. If not, assume a new rotation angle, θ, and repeat the procedure from Step 4.
8. Sum the lateral forces and check if force equilibrium is satisfied. If not, assume a new depth to the center of rotation, Lo, and repeat the procedure from Step 3.
9. If both force and moment equilibrium are satisfied. The assumed Lo and θ are the solutions of the depth to the center of rotaion and the rotation angle for the given $P_{lateral}$ and M_{head} acting on the caisson.

More details on the side resistance, the end resistance, and the results of the rigid caisson p-y analysis model are shown in the following sections.

11.4.2 Side Resistance (p-y Curves)

To construct the p-y curves for side resistance springs, we first need to determine the ultimate resistance per unit length, which defines the ultimate resistance of the springs. The ultimate resistance per unit length, p_u, can be expressed as:

$$p_u = N_p s_u D \quad \text{(Equation 11.1)}$$

where

N_p = bearing capacity factor for laterally loaded pile (dimensionless),

s_u = undrained shear strength of soil,

D = diameter of caisson.

The value of N_p at depths where the full flow-around failure occurs is selected to be 12 in this study instead of 9 recommended by API RP 2GEO (2011) and Matlock (1970). This value is determined by fitting the rigid caisson p-y analysis results to the experimental lateral load-displacement responses. The N_p value of 12 also agrees with the full flow-around N_p of 12 recommended by Stevens and Audibert (1979) as well as Murff and Hamilton (1993), the analytical solution of 11.94 for rough piles by Randolph and Houlsby (1984), and 12.7 to 13.4 reported by Jeanjean (2009). At shallower depths where shallow failures (such as soil wedge and gapping) can occur due to the lower overburden stress, the reduced N_p can be expressed as Equation 11.2 suggested by Matlock (1970).

$$N_p = 3 + \frac{\gamma' z}{s_u} + J\frac{z}{D} \leq 12 \quad \text{(Equation 11.2)}$$

where

γ' = submerged unit weight of soil,

z = depth below mudline,

J = dimensionless constant.

In this study, the value of J was determined to be 5 by fitting the experimental lateral load-displacement response of the suction can in kaolinite. Using a greater *J* of 5 is

consistent with the suggestions of previous studies by Reese et al. (1975), Stevens and Audibert (1979), and Murff and Hamilton (1993) which indicated that the J = 0.5 suggested by Matlock (1970) is too low and overestimated the depth where N_p is fully mobilized (see Section 2.2.2).

If γ' = 40 pcf, the N_p profile obtained using Equation 11.2 can be plotted as Figure 11.20 for the suction can in overconsolidated clay test bed and in normally consolidated clay test bed. Note that a s_u of 45 psf was used for the overconsolidated clay and a s_u gradient of 14 psf/ft with s_u = 0 psf at mudline was used for the normally consolidated clay. When the N_p profile is expressed in terms of normalized depth, z/D, a diameter of 6 inches and a diameter of 12 inches based on the scale model tests were used for overconsolidated clay and normally consolidated clay, respectively.

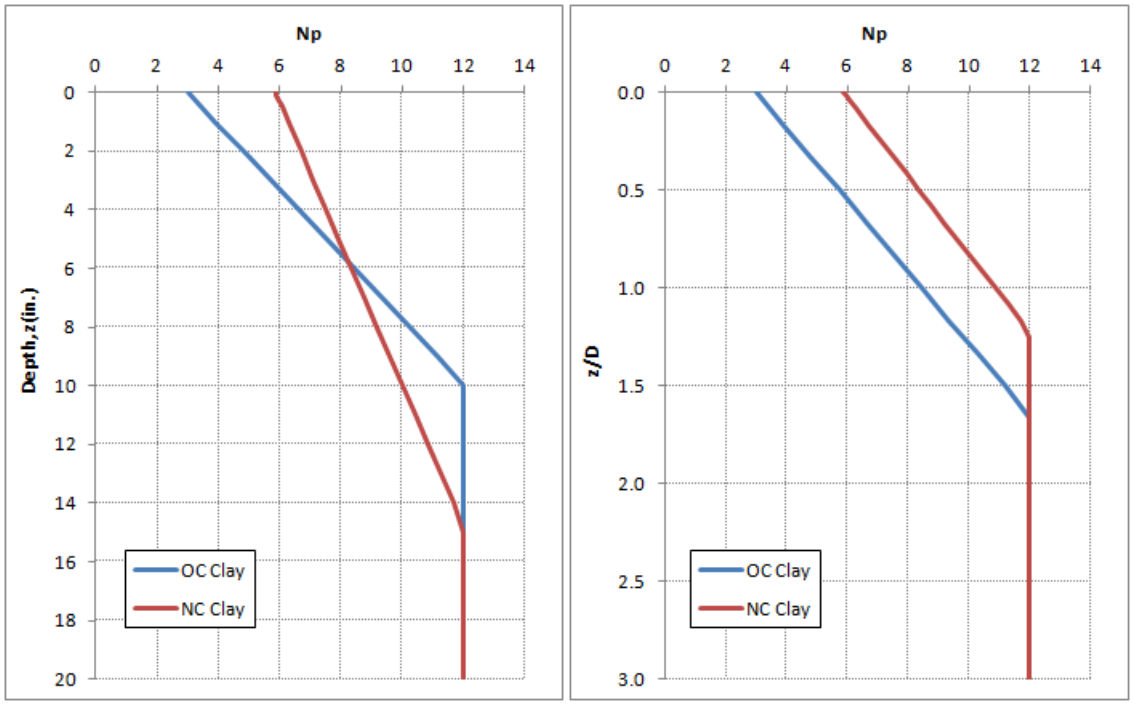

Figure 11.20: Bearing Capacity Factor N_p versus Depth

In Figure 11.20, N_p of overconsolidated clay approaches a lower value of 3 at the mudline which implicitly takes the upward soil wedge and the observed gap into account. For normally consolidated clay with s_u = 0 psf at the mudline and a gradient s_u1 = 14 psf/ft, N_p approaches $3 + \frac{\gamma'}{s_u 1} = 5.86$ which is higher than that in the overconsolidated clay. This fits well with that there was no significant gap formed around the suction can in the normally consolidated clay. Note that N_p does not reach the full flow-around value of 12 within the length of the suction can (z/D = 1) in both clay profiles.

In order to construct the p-y curves for stubby caissons, we also need to determine another important parameter y_{50}, which is the lateral displacement that $0.5p_u$ is mobilized. It can be calculated by Equation 11.3, which was obtained by fitting the suction can lateral load test data.

$$y_{50} = \frac{1}{6}\varepsilon_{50} D \qquad \text{(Equation 11.3)}$$

In the above equation, ε_{50} is the axial strain corresponds to half of the ultimate shear strength of the soil. It typically ranges from 0.005 to 0.02 with brittle or stiff clay close to the low end and soft clay close to the high end of this range. For the suction can lateral load tests in oversonsolidated clay and normally consolidated clay, $\varepsilon_{50} = 0.008$ provides a good fit to the experimental load-displacement data when the Matlock's p-y curves are used. When elastic-perfectly plastic p-y curves are used, $\varepsilon_{50} = 0.01$ provides a better fit to the experimental data. The Matlock's and the elastic-perfectly plastic p-y curves are presented in the rest of this section. Note that the y_{50} calculated by Equation 11.3 is less than the $y_{50} = 2.5\varepsilon_{50} D$ suggested by Matlock (1970). Therefore, the p-y curves used in this rigid caisson p-y analysis model have stiffer lateral load-displacement

response than that suggested by Matlock (1970) and API RP 2GEO (2011). The proposed stiffer p-y curves are aligned with previous studies by Stevens and Audibert (1979) and Jeanjean (2009) which suggested the stiffness of the p-y curves recommended by API are too low comparing to field and scale model test results (see Section 2.2.2).

Two sets of p-y curves are used for the rigid caisson p-y analysis model: 1) the p-y curves suggested by Matlock (1970) and 2) elastic-perfectly plastic p-y curves. In both sets, the p-y curves for both static loading condition and cyclic loading condition are provided. The static loading condition refers to the lateral loading events that reach a lateral displacement the foundation never experienced before and no cyclic degradation occurs. The lateral resistance decreases if the foundation is loaded cyclically and the soil is loaded back-and-forth. These p-y curves are shown in Figure 11.21 to 11.24.

Matlock's p-y curves for static loading condition can be expressed in a non-dimensional form as shown in Equation 11.4 and Figure 11.21 while the curves for cyclic loading condition can be expressed in Equation 11.5 and Figure 11.22. Note that the limiting value of 0.63 for cyclically degraded $\frac{p}{p_u}$ was determined by fitting the lateral load tests of suction can in clay.

$$\frac{p}{p_u} = 0.5\left(\frac{y}{y_{50}}\right)^{1/3} \leq 1.0 \quad , for\ static\ loading \qquad \text{(Equation 11.4)}$$

$$\frac{p}{p_u} = 0.5\left(\frac{y}{y_{50}}\right)^{1/3} \leq 0.63 \ , for\ cyclic\ loading \qquad \text{(Equation 11.5)}$$

Similarly, the simpler elastic-perfectly plastic non-dimensional p-y curves for static loading condition can be expressed by Equation 11.6 and Figure 11.23 while the curves for cyclic loading condition can be expressed in Equation 11.7 and Figure 11.24.

$$\frac{p}{p_u} = 0.5\left(\frac{y}{y_{50}}\right) \leq 1.0 \quad , for\ static\ loading \qquad \text{(Equation 11.6)}$$

$$\frac{p}{p_u} = 0.5\left(\frac{y}{y_{50}}\right) \leq 0.63 \ , for\ cyclic\ loading \qquad \text{(Equation 11.7)}$$

Finally, a family of p-y curves can be obtained by using Equations 11.4 to 11.7 with the same y_{50} calculated by using Equation 11.3 but a increasing p_u with depth obtained from Equations 11.1 and 11.2. The families of Matlock's and Elastic-Perfectly Plastic p-y curves are plotted in Figures 11.25 to 11.28 for overconsolidated clay and normally consolidated clay.

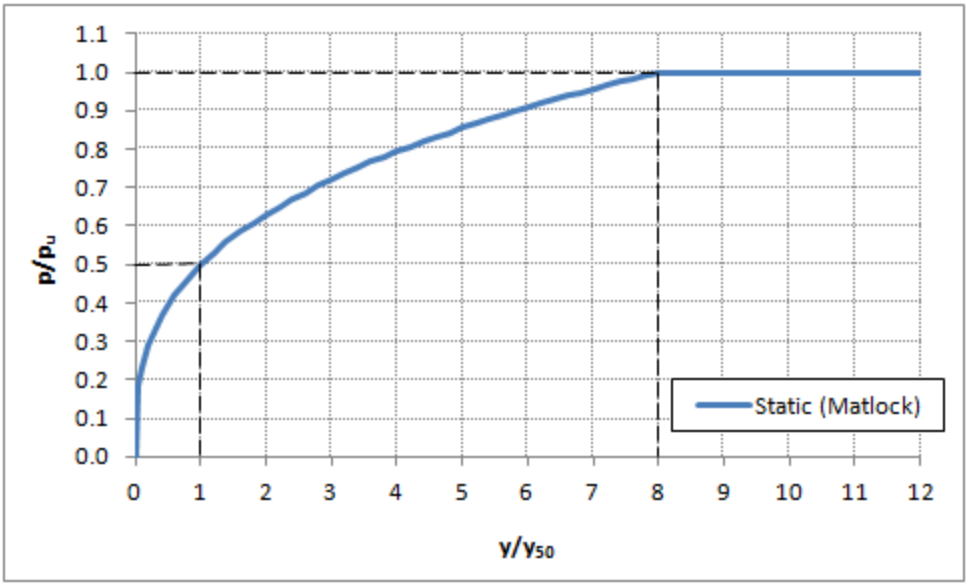

Figure 11.21: Static p-y Curve (Matlock)

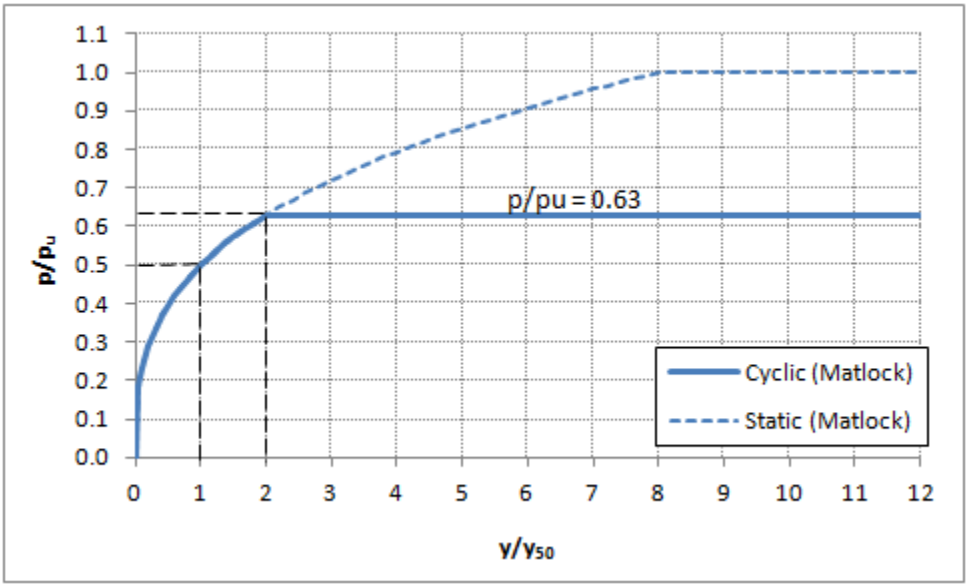

Figure 11.22: Cyclic p-y Curve (Matlock)

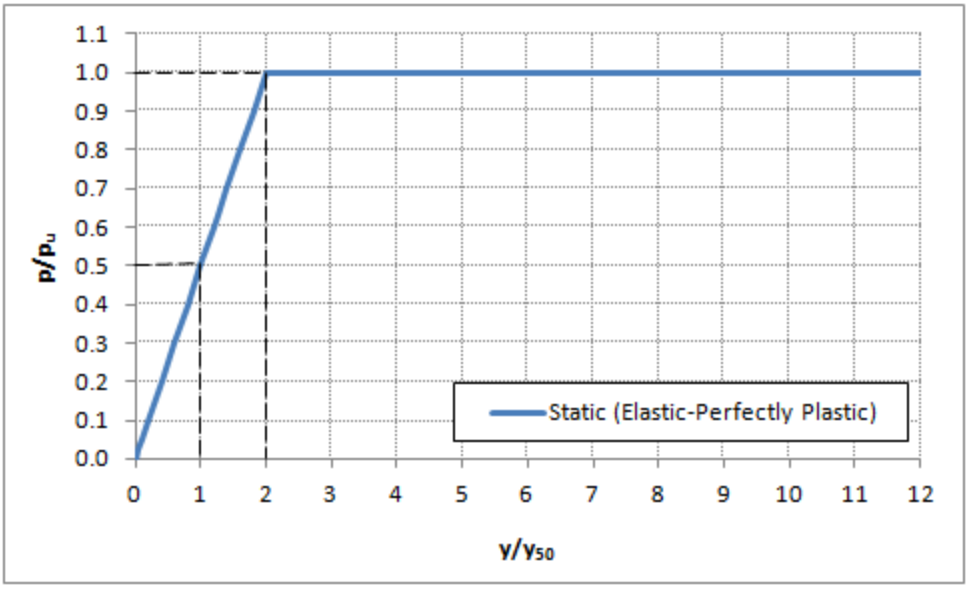

Figure 11.23: Static p-y Curve (Elastic-Perfectly Plastic)

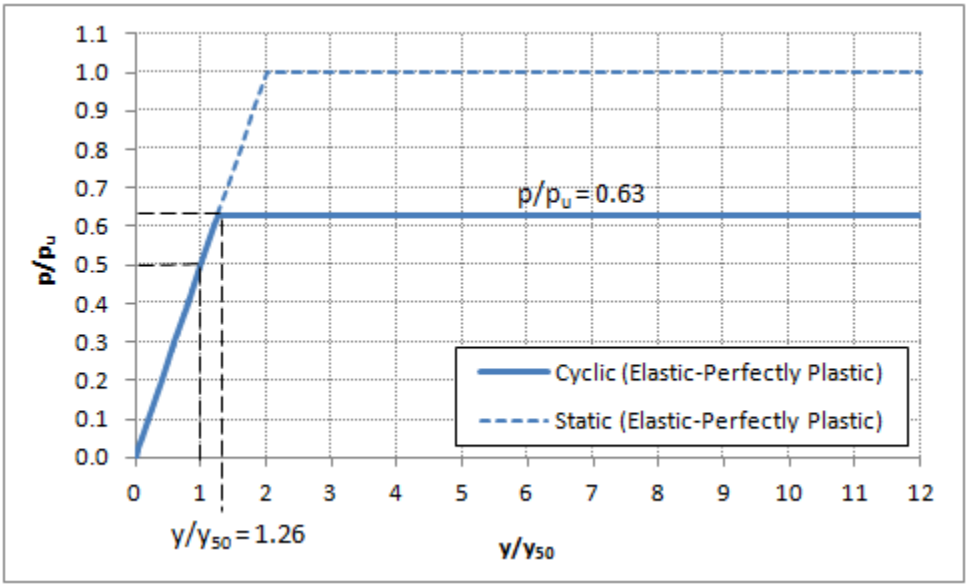

Figure 11.24: Cyclic p-y Curve (Elastic-Perfectly Plastic)

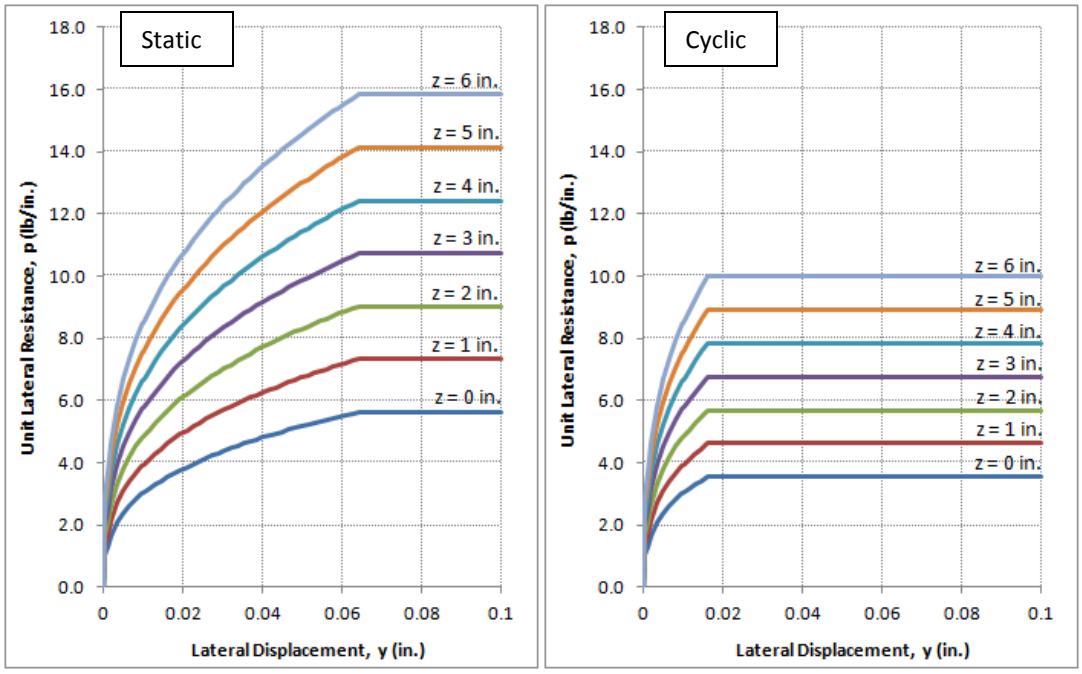

Figure 11.25: Family of p-y Curves (Matlock) for Suction Can in OC Clay

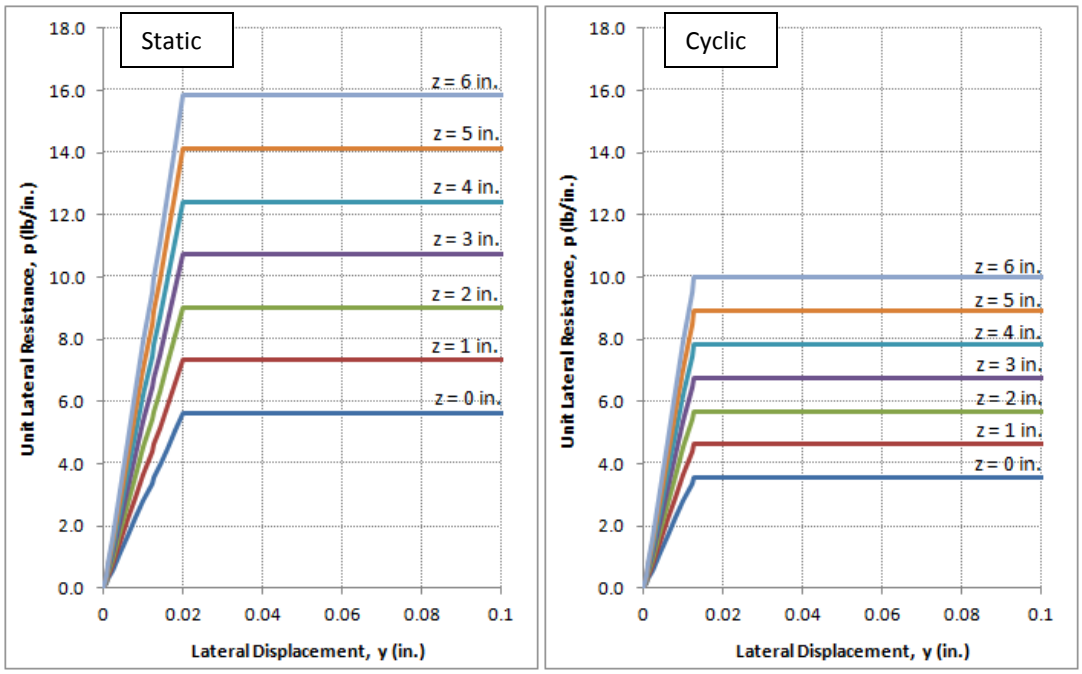

Figure 11.26: Family of p-y Curves (Elastic-Perfectly Plastic) for Suction Can in OC Clay

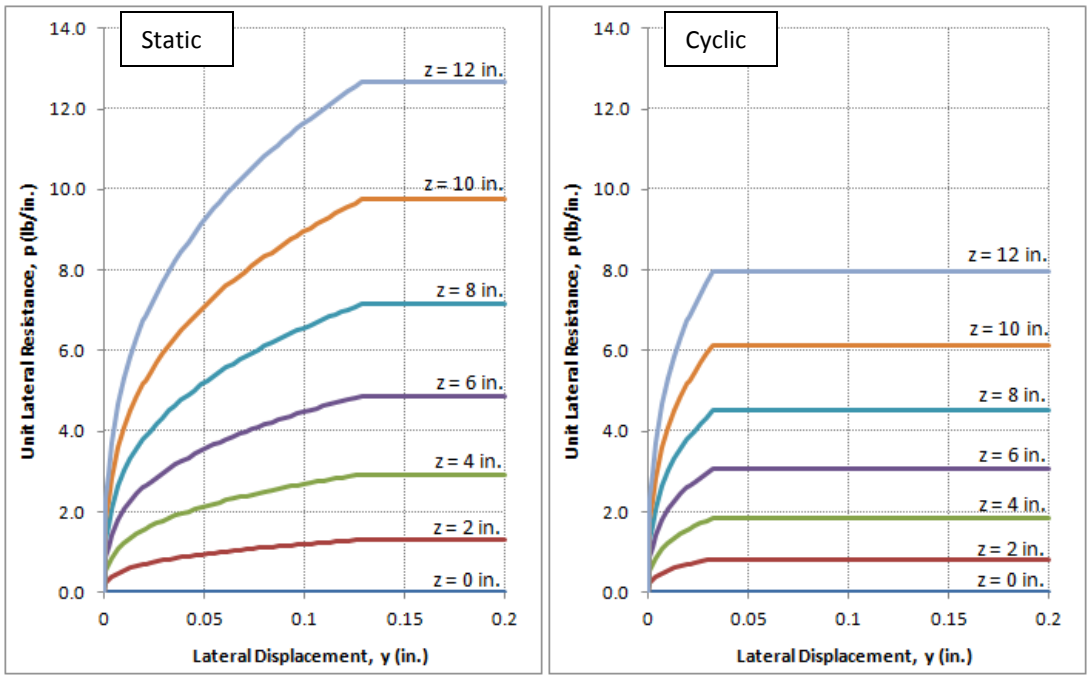

Figure 11.27: Family of p-y Curves (Matlock) for Suction Can in NC Clay

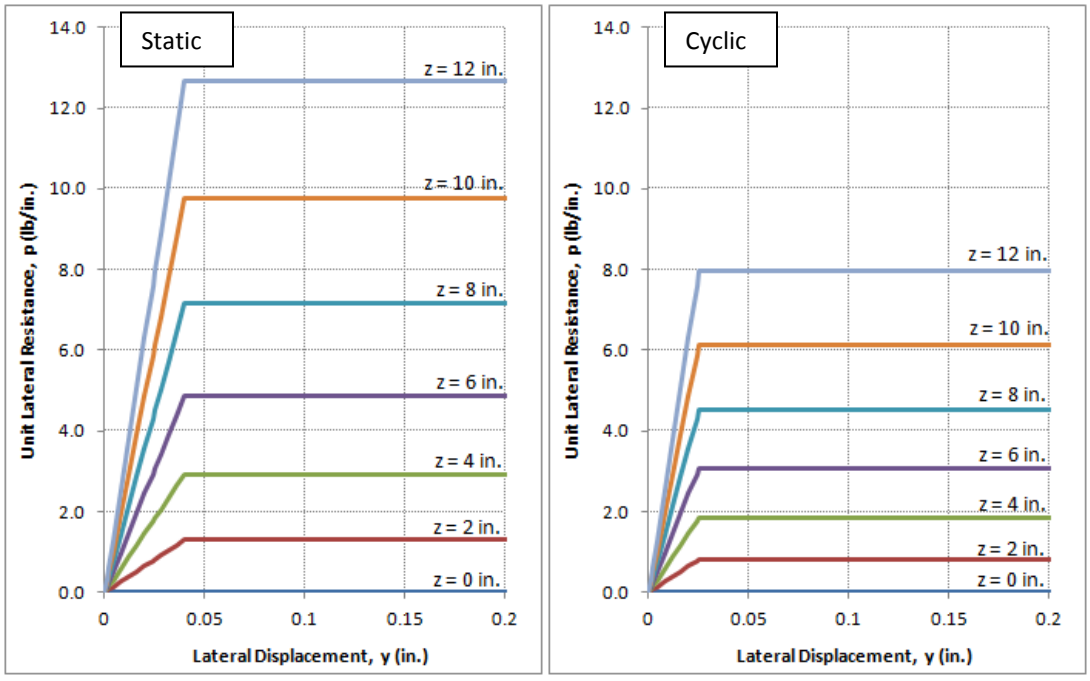

Figure 11.28: Family of p-y Curves (Elastic-Perfectly Plastic) for Suction Can in NC Clay

11.4.3 Resisting Moment from Spherical End Cap (M_{tip}-θ Curves)

Different from flexible piles, the end resistance contributes a significant portion of the total lateral resistance of a stubby caisson. Therefore, it is crucial to properly model this end resistance in the rigid caisson p-y analysis. In this study, the end resistance is assumed to be the total resisting moment about the center of rotation from the shear stresses acting along the spherical soil slip surface as shown in Figure 11.28. This end resisting moment is modeled by an elastic-perfectly plastic rotational spring at the center of rotation with an ultimate resisting moment, M_u, when the undrained shear strength of soil is fully mobilized along the spherical slip surface. The end resisting moment versus rotation angle are defined by the M_{tip}-θ curves. In order to calculate the ultimate resisting moment, the caisson and spherical soil end cap are divided into n slices (n = 40 in this study) parallel to the direction of loading as shown in Figure 11.29. The total resisting moment can be obtained by summing the moment for each slice as shown in Figure 11.30.

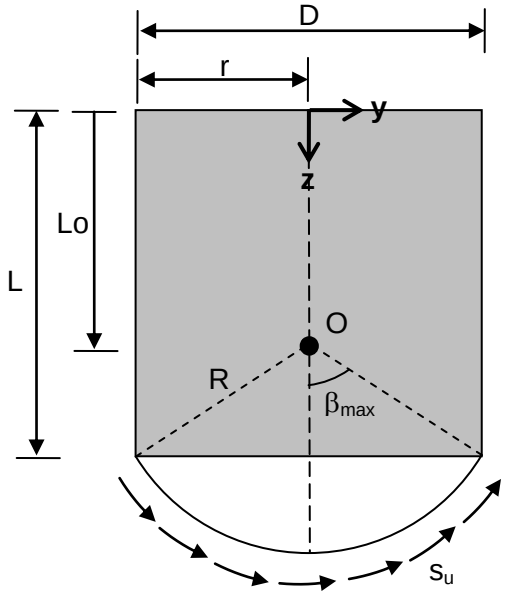

Figure 11.28: Spherical Slip Surface and End Resisting Moment

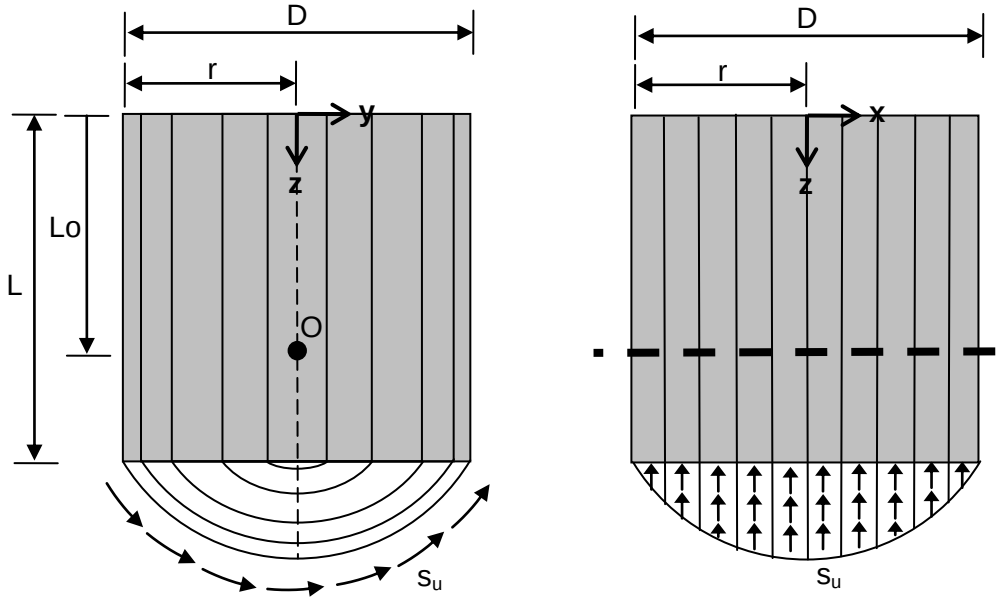

(a) Side View (b) Front View

Figure 11.29: Schematic of Slices for Calculating End Resisting Moment

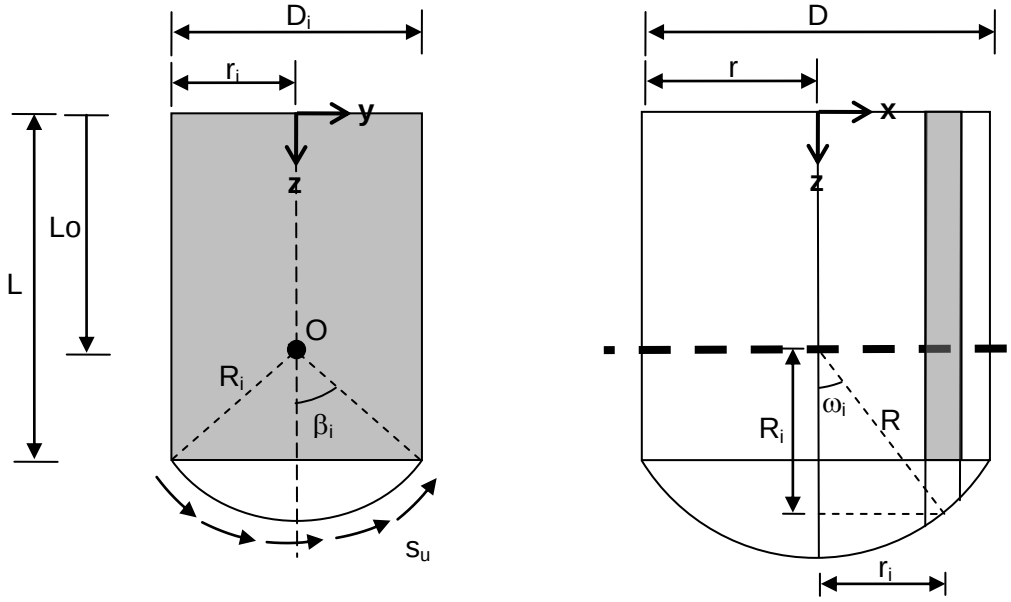

(a) Side View of Slice i (b) Front View of Slice i

Figure 11.30: Schematic of Slice i for Calculating End Resisting Moment

If the undrained shear strength is not constant along the spherical slip surface, each slice can be further divided into m segments (m = 40 in this study) along the arc of the slip surface as shown in Figure 11.30. Therefore, the ultimate end resisting moment of Slice i, $M_{u,i}$, can be calculated using Equation 11.8.

$$M_{u,i} = R_i \sum_{j=1}^{m} s_{u,j} A_j \qquad \text{(Equation 11.8)}$$

where

R_i = moment arm of Slice i = $\sqrt{R^2 - r_i{}^2}$, see Figure 11.30 (b),

A_j = spherical surface area of Segment j.

Finally, the total ultimate end resisting moment, M_u, can be obtained by summing all the resisting moment on all the n slices using Equation 11.9.

$$M_u = \sum_{i=1}^{n} M_{u,i} = \sum_{i=1}^{n} \left(R_i \sum_{j=1}^{m} s_{u,j} A_j \right) \qquad \text{(Equation 11.9)}$$

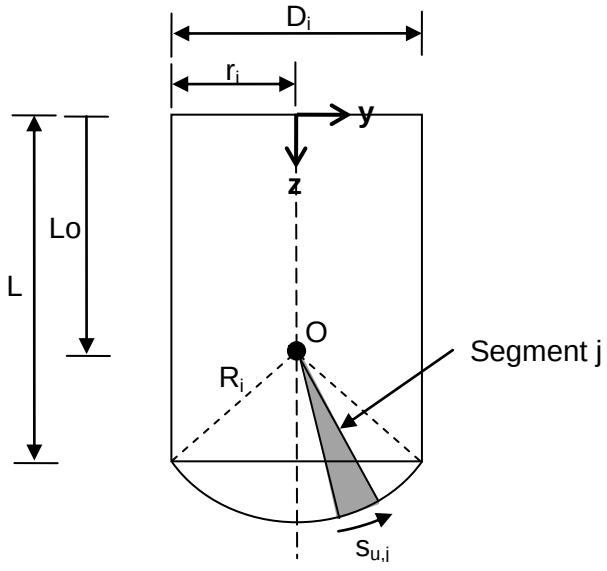

Figure 11.30: Schematic of Segment j of Slice i for Calculating End Resisting Moment

To construct the M_{tip}-θ curve for end resisting moment, we also need to determine the θ_{50}, which is the rotation such that $0.5M_u$ is mobilized. It can be calculated by Equation 11.10, which was obtained by fitting the suction can lateral load test data.

$$\theta_{50} = \sqrt{2}\varepsilon_{50}\beta_{max} \quad \text{(Equation 11.10)}$$

where

$\beta_{max} = \sin^{-1}\left(\frac{D/2}{R}\right)$, in radians, see Figure 11.28.

In the above equation, ε_{50} is the same as that used for the p-y curves in Section 11.4.2. In this study, $\varepsilon_{50} = 0.008$ was used if the Matlock's p-y curves are applied to the side resistance, while $\varepsilon_{50} = 0.01$ was used if elastic-perfectly plastic p-y curves are applied in the model.

With the above calculated M_u and θ_{50}, the elastic-perfectly plastic M_{tip}-θ curve for static loading condition can be expressed in a non-dimensional form as shown in Equation 11.11 and Figure 11.32. The M_{tip}-θ curve for cyclic loading condition can be expressed in Equation 11.12 and Figure 11.33. Note that the limiting value of 0.63 for cyclically degraded resisting moment was the same as that for p-y curves. These static and cyclic M_{tip}-θ curves fit well with the lateral load test data of suction can in clay test beds.

$$\frac{M_{tip}}{M_u} = 0.5\left(\frac{\theta}{\theta_{50}}\right) \leq 1.0 \quad , for\ static\ loading \quad \text{(Equation 11.11)}$$

$$\frac{M_{tip}}{M_u} = 0.5\left(\frac{\theta}{\theta_{50}}\right) \leq 0.63 \ , for\ cyclic\ loading \quad \text{(Equation 11.12)}$$

Using the M_{tip}-θ curves for end resisting moment along with either the Matlock's or the elastic perfectly plastic p-y curves for side resistance, the lateral load-displacement

response of a stubby caisson can be solved by this rigid caisson p-y analysis model following the procedure in Section 11.4.1.

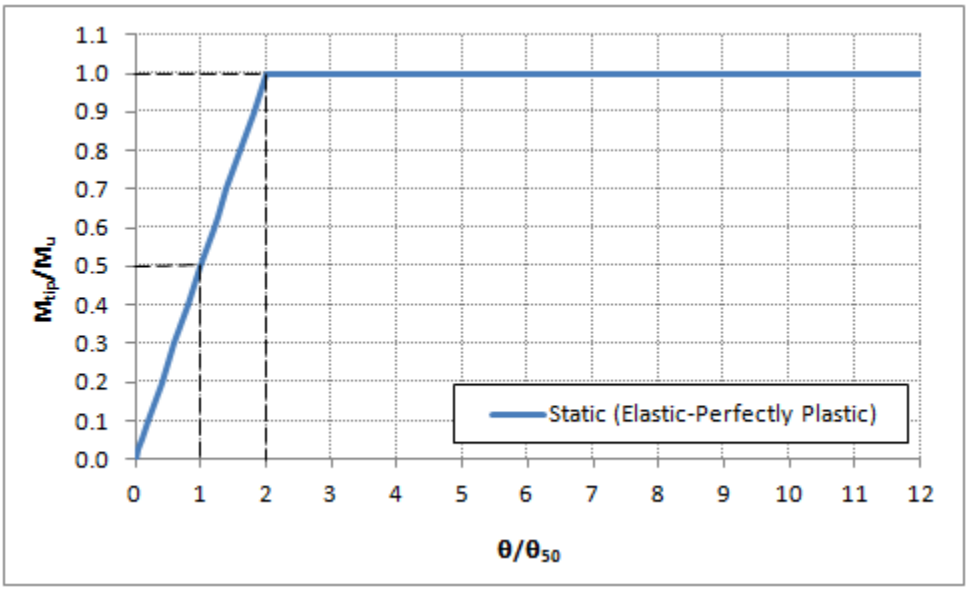

Figure 11.32: Static M_{tip}-θ Curve (Elastic-Perfectly Plastic)

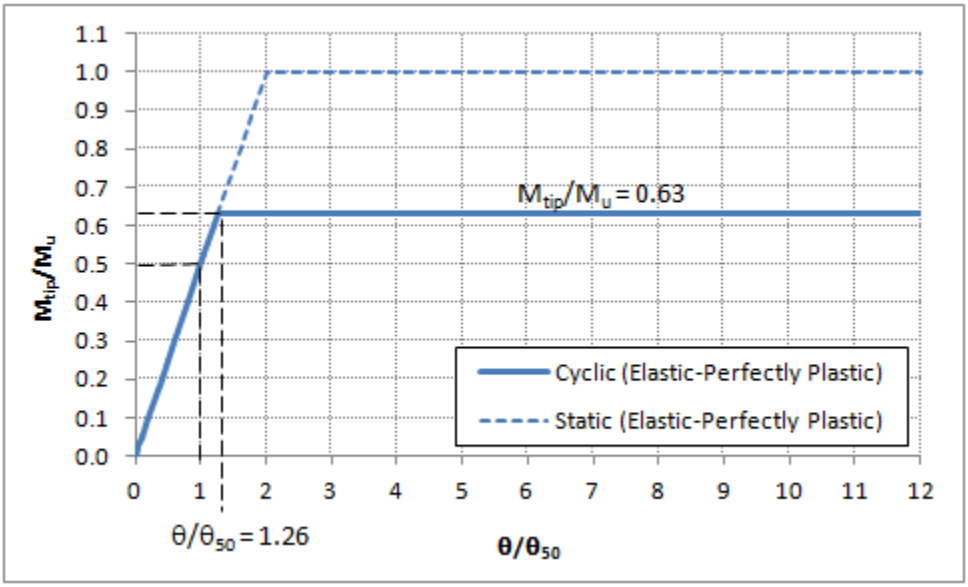

Figure 11.33: Cyclic M_{tip}-θ Curve (Elastic-Perfectly Plastic)

11.4.4 Results of Rigid Caisson p-y Analysis

The lateral load-displacement responses calculated by the rigid caisson p-y analysis model are compared with the suction can lateral load tests in overconsolidated and normally consolidated clay. In order to compare with the experiments, the lateral load acting at 3 ft above the mudline was applied in the model by a lateral load, $P_{lateral}$, and a corresponding moment, M_{head} = (3 ft)×$P_{lateral}$, acting on top of the caisson. The lateral displacement at 3 ft above mudline was calculated using geometry with the calculated depth to center of rotation and the rotation angle of the caisson.

For the suction can in overconsolidated clay, the lateral load-displacement curves obtained by the rigid caisson p-y analysis model are plotted in Figure 11.34 and compared with the experiment data. The cases using Matlock's p-y curves along with the elastic-perfectly plastic M_{tip}-θ curve are designated as Static p-y and Cyclic p-y for static and cyclic loading conditions, respectively. The cases using elastic-perfectly plastic p-y curves along with elastic-perfectly plastic M_{tip}-θ curve are designated as Static p-y and Cyclic p-y. Figure 11.34 shows that the load-displacement curves predicted by the model fit well with the experimental data for both the cases of using Matlock's and elastic-perfectly plastic p-y curves.

Example lateral displacement (y), normalized unit lateral resistance (p/p_u), and unit lateral resistance (p) profiles calculated by the model for suction can in overconsolidated clay are plotted in Figure 11.35. Matlock's static p-y curves were used to produce these example profiles. The profiles are calculated for lateral loads of 1, 2, and 3.2 lb applied at 3 ft above the mudline. Figure 11.35 shows that the center of rotation is located at 3.6, 3.7, and 3.8 inches deep under the 1-, 2-, and 3.2-lb lateral load. Rotation (or displacement) of the foundation is relatively small until the applied lateral load approaches the ultimate capacity (3.2 lb) where the foundation starts to rotate

significantly. The p/p_u profiles show that the ultimate side resistance is mobilized from close to the top and the tip of the caisson as lateral load increases. However, the ultimate side resistance may never be mobilized in the region adjacent to the center of rotation. The unit lateral resistance profile shows that the ultimate lateral resistance is lower near the mudline because of the upward soil wedge and gapping reduces the bearing capacity factor, N_p.

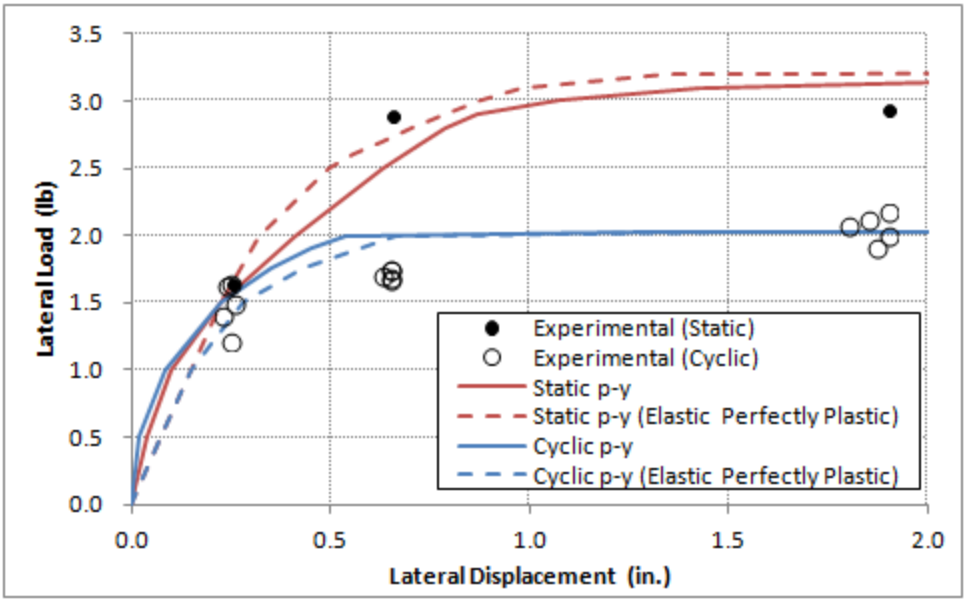

Figure 11.34: Lateral Load-Displacement Curves for Suction Can in OC Clay by Rigid Caisson p-y Analysis Model

Examples of mobilized end resisting Moment, M_{tip}, for suction can in overconsolidated clay calculated by the rigid caisson p-y analysis model is shown in Figure 11.36. The end resisting moment is fully mobilized when the foundation is loaded close to its lateral capacity (3.2 lb) as shown in Figure 11.36(a). Figure 11.36(b) shows that, in overconsolidated clay, the end moment resistance may contribute approximately

30% of the total resisting moment of the stubby caisson when it reaches its ultimate lateral load capacity.

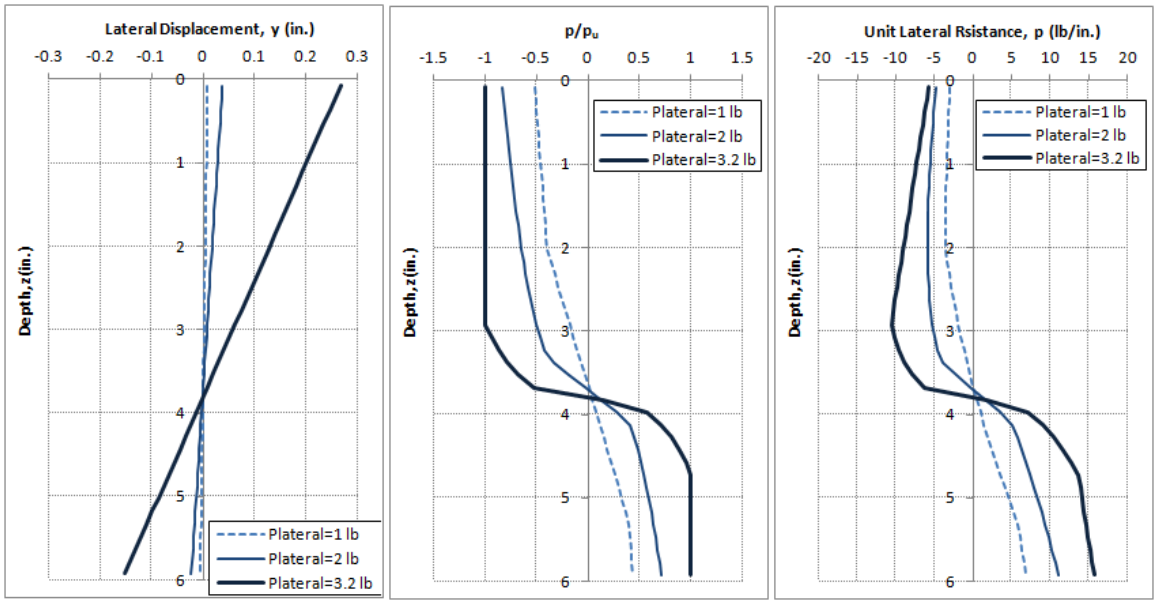

Figure 11.35: Example Displacement and Mobilized Resistance Profiles for Suction Can in OC Clay by Rigid Caisson p-y Analysis Model

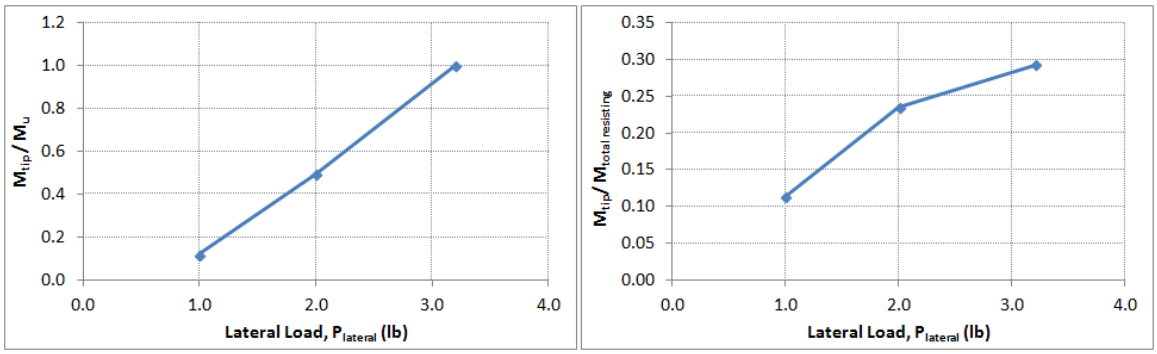

(a) M_{tip}/M_u vs. Lateral Load (b) $M_{tip}/M_{total\ resisting}$ vs. Lateral Load

Figure 11.36: Example Mobilized End Resisting Moment, M_{tip}, for Suction Can in OC Clay by Rigid Caisson p-y Analysis Model

For the suction can in normally consolidated clay, the lateral load-displacement curves obtained by the rigid caisson p-y analysis model are plotted in Figure 11.37 with the experiment data. Figure 11.34 shows that the load-displacement curves predicted by the model fit well with the experimental data for both the cases of using Matlock's and elastic-perfectly plastic p-y curves except when the applied lateral load is close to the ultimate capacity. By examining the experiment data, it is found that the foundation settled 0.3 to 0.5 inches when these data points with lateral displacement around 1.8 inches (or 5-degree rotation) were taken. This means that the suction can penetrated an extra 0.3 to 0.5 inches into the soil. In order to take these settlements into account, the length of the foundation was increased from 12 inches to 12.5 inches in the rigid caisson p-y analysis model. Figure 11.38 shows that if the settlements are taken into account, the static load-displacement curves matches well with experiment data close to the ultimate capacity. Similar results are shown in Figure 11.39 for cyclic loading condition.

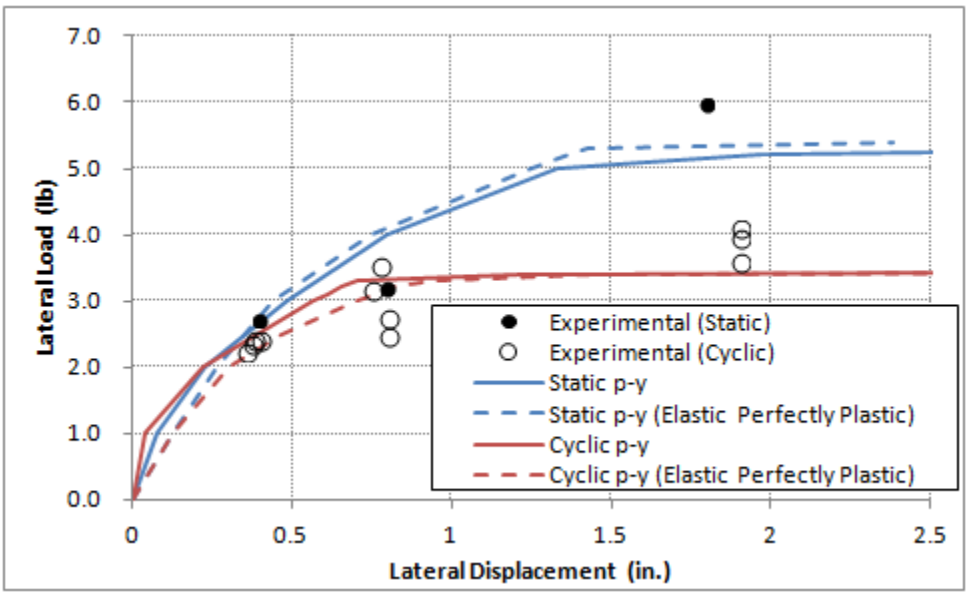

Figure 11.37: Lateral Load-Displacement Curves for Suction Can in NC Clay by Rigid Caisson p-y Analysis Model

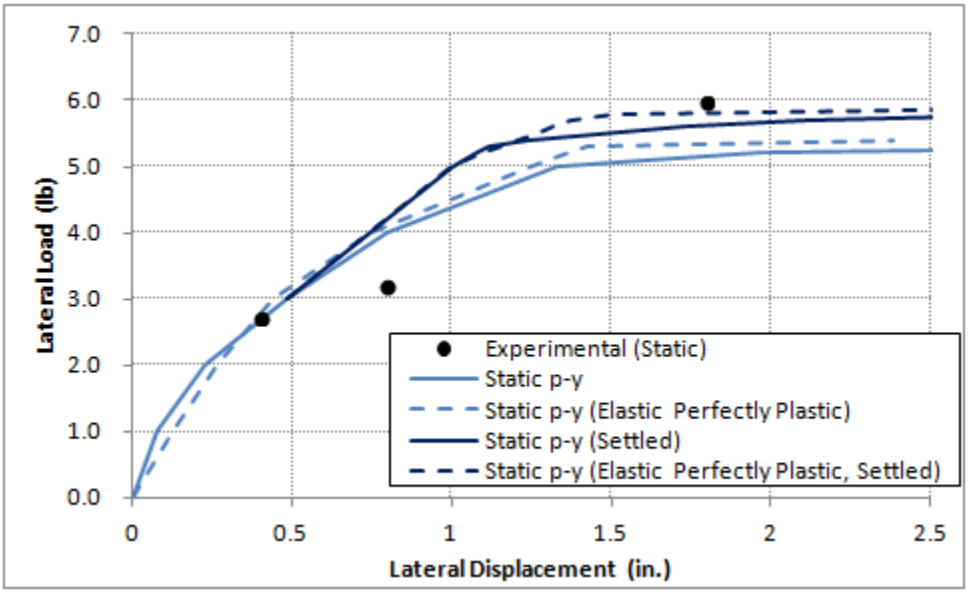

Figure 11.38: Static Lateral Load-Displacement Curves for Suction Can in NC Clay by Rigid Caisson p-y Analysis Model (Consider 0.5-inch Settlement)

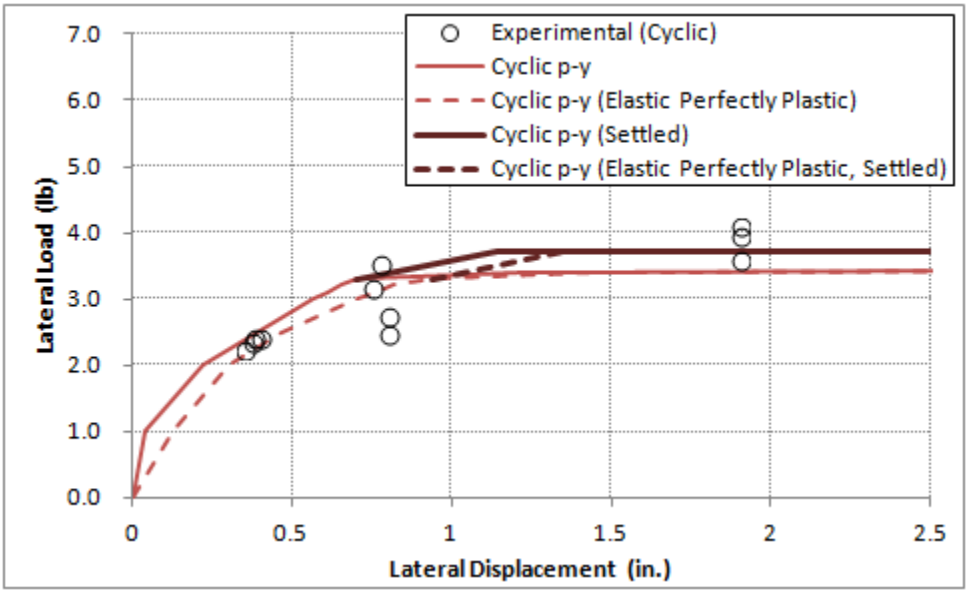

Figure 11.39: Cyclic Lateral Load-Displacement Curves for Suction Can in NC Clay by Rigid Caisson p-y Analysis Model (Consider 0.5-inch Settlement)

Figure 11.40 shows example lateral displacement (y), normalized unit lateral resistance (p/p_u), and unit lateral resistance (p) profiles calculated by the model for suction can in normally consolidated clay. Matlock's static p-y curves were used to produce these example profiles. The profiles are calculated for lateral loads of 2, 4, and 5.4 lb applied at 3 ft above the mudline. Figure 11.40 shows that the center of rotation is located at 8.9, 9.0, and 9.2 inches deep under the 2-, 4-, and 5.4-lb lateral load. Similar to the results in overconsolidated clay, rotation of the foundation is relatively small until the applied lateral load approaches the ultimate capacity (5.4 lb) where the foundation starts to rotate significantly. The p/p_u profiles show that the ultimate side resistance is mobilized from close to the top and the tip of the caisson as lateral load increases while the side resistance close to the center of rotation is never fully mobilized. The unit lateral resistance profile shows that the ultimate lateral resistance approaches zero near the mudline because the s_u is close to zero.

Examples of mobilized end resisting Moment, M_{tip}, for suction can in normally consolidated clay calculated by the rigid caisson p-y analysis model are shown in Figure 11.41. The end resisting moment is fully mobilized when the foundation is loaded close to its lateral capacity (5.4 lb) as shown in Figure 11.41(a). Figure 11.41(b) shows that the end moment resistance may contribute more than 40% of the total resisting moment of the stubby caisson in normally consolidated clay comparing to 30% in overconsolidated clay. This implies that the end resistance for stubby caisson is even more important in normally consolidated clay because of the increasing undrained shear strength with depth.

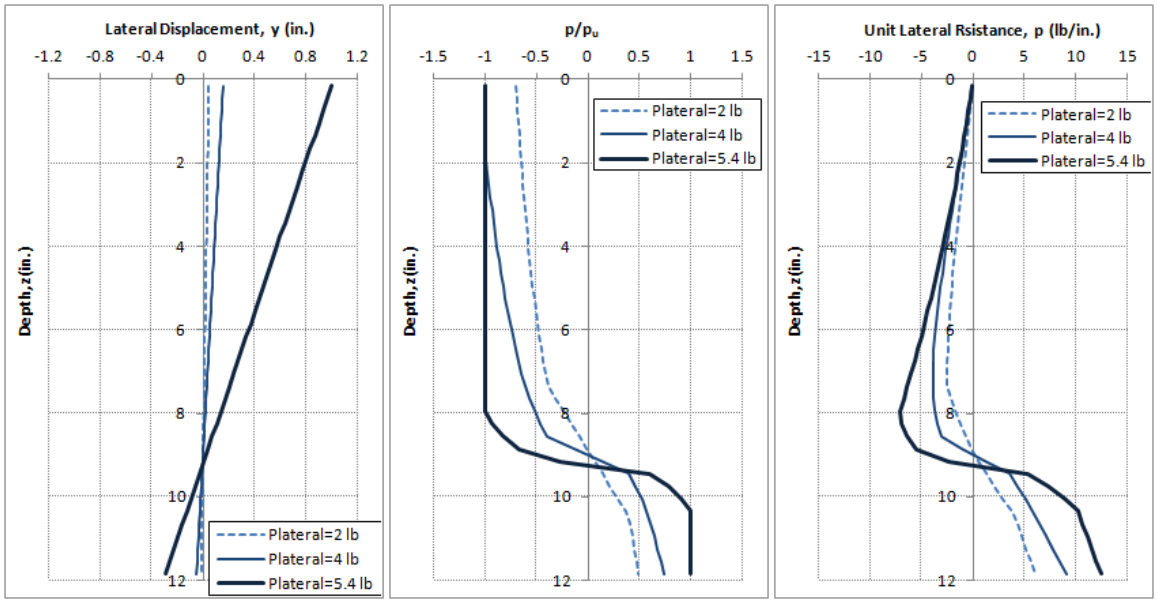

Figure 11.40: Example Displacement and Mobilized Resistance Profiles for Suction Can in NC Clay by Rigid Caisson p-y Analysis Model

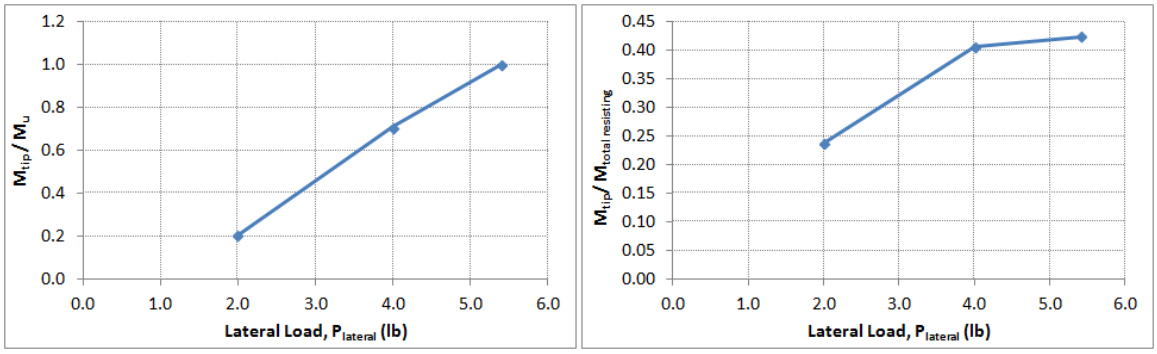

(a) M_{tip}/M_u vs. Lateral Load (b) $M_{tip}/M_{total\ resisting}$ vs. Lateral Load

Figure 11.41: Example Mobilized End Resisting Moment, M_{tip}, for Suction Can in NC Clay by Rigid Caisson p-y Analysis Model

11.4.5 Comparison of API p-y Analysis and Rigid Caisson p-y Analysis Model

Figure 11.42 and 11.43 compare the predicted lateral resistance on the suction can in overconsolidated clay by using API p-y analysis (or Matlock 1970) and rigid caisson

p-y analysis. Figure 11.42a shows that the flow-around N_p recommended by API is 9 while the value of the proposed rigid caisson p-y analysis model is 12. The N_p reach the flow around value deeper into the soil according to API and p-y curves recommend by API are compared with the proposed curves that are used in rigid caisson p-y analysis model. As a result, in Figure 11.42b, the ultimate unit lateral resistance at a given depth according to API p-y curves is much lower than that according to the proposed p-y curves for rigid caissons. Also shown in Figure 11.42b, the $y_{50} = 2.5\varepsilon_{50}D$ recommended by API results in a much less stiff p-y curve than the proposed model. These effects are all reflected. Another difference is that the API p-y analysis does not include the end resistance of the caisson. As a result of all the above differences, in Figure 11.43, the caisson lateral capacity and lateral stiffness predicted by the p-y analysis recommended by API is much lower than the test data and those predicted by rigid caisson p-y analysis.

Similar results are shown in Figure 11.44 and 11.45 for the suction can in normally consolidated clay. These comparisons indicate that the lateral capacity and stiffness of the caisson may be significantly underestimated if the p-y curves recommended by API are used. This underestimation of stiffness and resistance using API p-y curves is consistent with those reported by Stevens and Audibert (1979) and Jeanjean (2009) for flexible piles. Note that the y_{50} modification recommended by Stevens and Audibert (1979) does not help in this case because the 12-inch diameter suction can used in normally consolidated clay test bed is close to the 12.75-inch diameter pile used for developing the API p-y curves (see Section 2.2). For the 6-inch diameter suction can used in the overconsolidated clay, the y_{50} modification by Stevens and Audibert (1979) makes the p-y curves even softer.

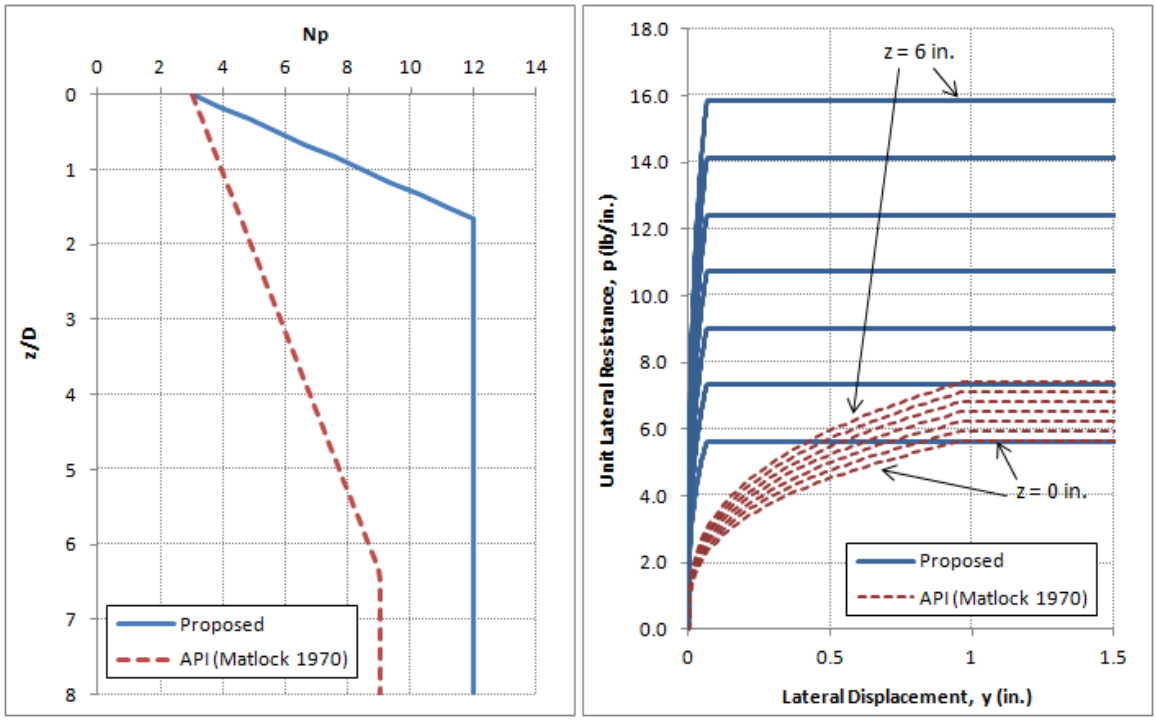

(a) N_p versus z/D (b) Family of p-y curves

Figure 11.42: Comparison of API and Rigid Caisson Static p-y Curves in OC Clay

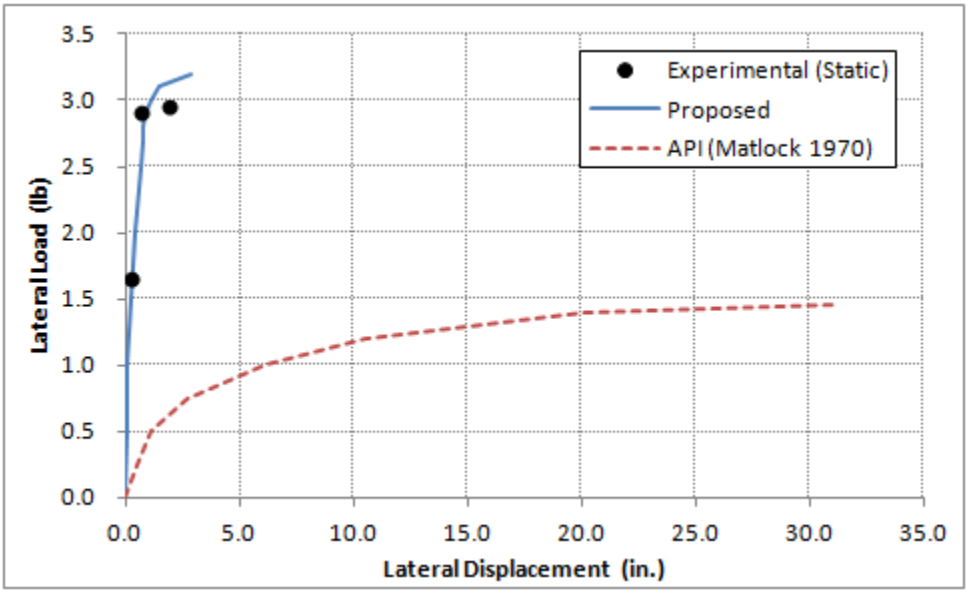

Figure 11.43: Lateral Load-Displacement Predictions using API and Rigid Caisson Static p-y Curves in OC Clay

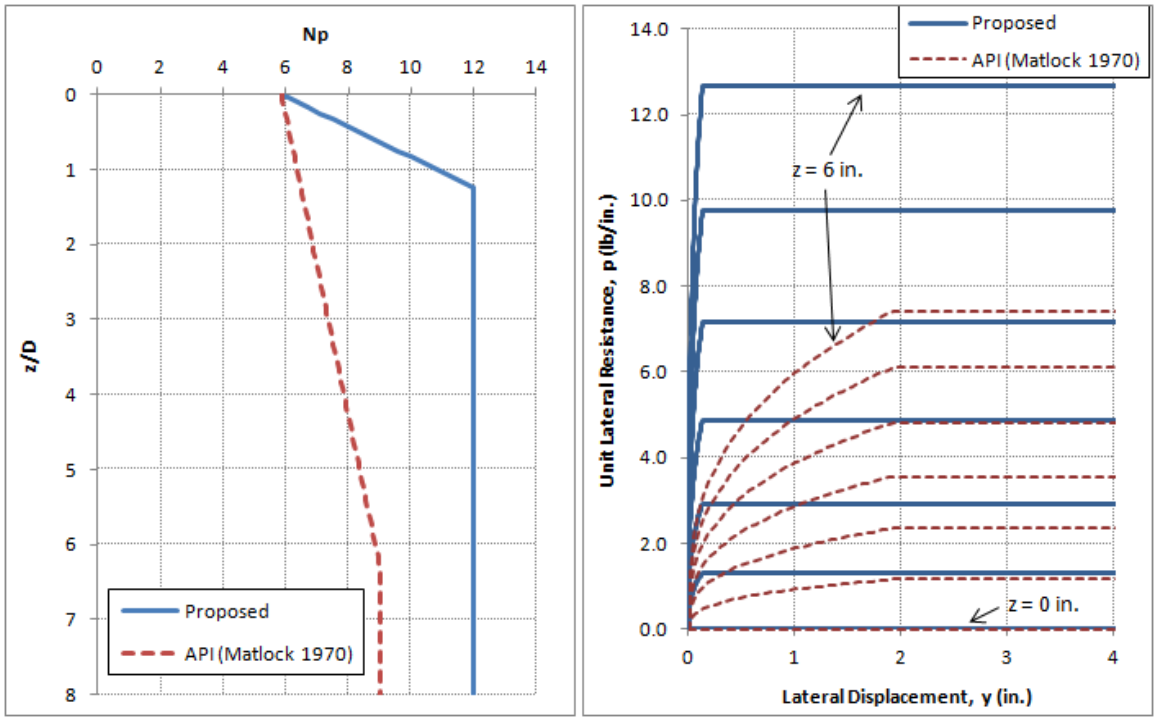

(a) N_p versus z/D (b) Family of p-y curves

Figure 11.44: Comparison of API and Rigid Caisson Static p-y Curves in NC Clay

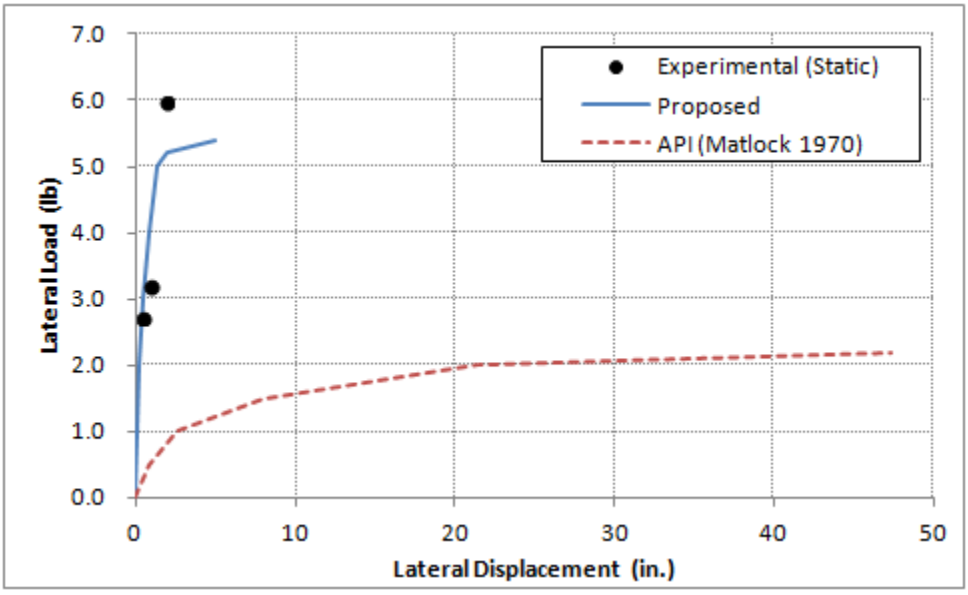

Figure 11.44: Lateral Load-Displacement Predictions using API and Rigid Caisson Static p-y Curves in OC Clay

11.4.6 Analysis of Bothkennar Field Lateral Load Test (Houlsby et al. 2005) Using Rigid Caisson p-y Analysis Model

The prediction by the rigid caisson p-y analysis is compared with larger scale field tests results reported by Houlsby et al. (2005). The field suction caisson moment resistance tests were conducted in a clay test pit using load controlled cyclic load tests. One set of the published moment-rotation curves from a large amplitude cyclic moment test with moment increased with cycles is used for this comparison. This test was used to evaluate the moment resistance of caisson under extreme loading condition. The parameters used for rigid caisson analysis is summarized in Table 11.5. Details about the parameters and the field test can be found in Section 2.3.1.

Caisson Diameter	Caisson Length	Height of Lateral Load Applied above Cap	Undrained Shear Strength at Surface	Undrained Shear Strength Gardient	Soil Submerged Density (Unit Weight)
3 m (118 in.)	1.5 m (59 in.)	4.23 m (166.5 in.)	11.43 kPa (238.7 psf)	1.9 kPa/m (12.1 psf/ft)	680 kg/m^3 (42.5 pcf)

Table 11.5: Input Parameters for Rigid Caisson p-y Analysis

For the ε_{50} of 0.005, the predicted moment-rotation curve by rigid caisson p-y analysis model under extreme static loading condition is plotted with the experimental curves in Figure 11.45. As shown in Figure 11.45, the stiffness predicted by the model is close to the measured stiffness. However, the model overpredicts the moment capacity by 25%. This discrepancy may be attributed to the uncertainty of the undrained shear strength of the clay at the site. The undrained shear strength was measured more than 10 years (in 1992) before the suction caisson experiments. A relatively small difference in the undrained shear strength of soil near the surface can make significant difference in the lateral capacity of foundations. The smaller aspect ratio of 0.5 for the suction caisson

used in the field tests may also contribute to the discrepancy of model prediction and field test results. More field and laboratory tests may be required to validate the proposed rigid caisson p-y analysis model.

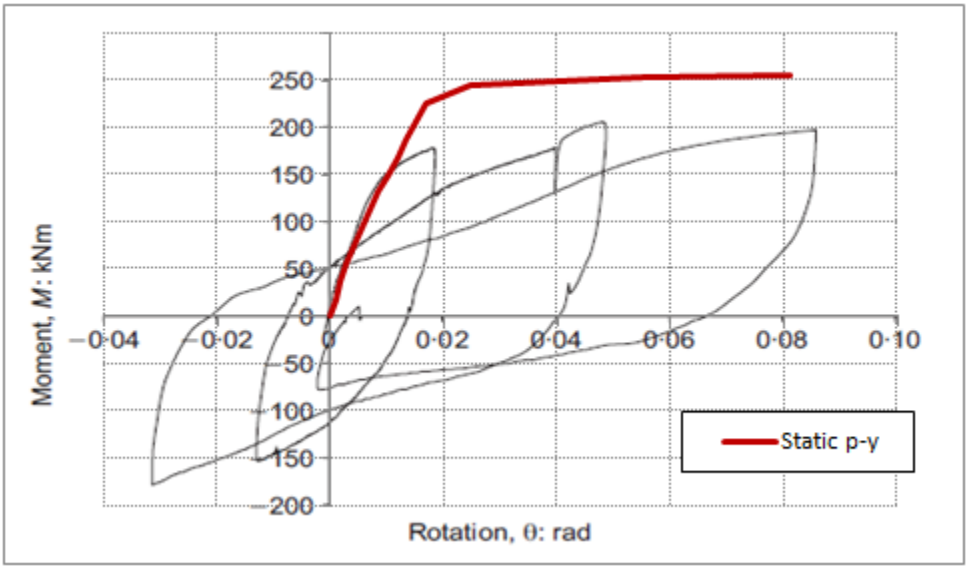

Figure 11.45: Comparison of Field Lateral Load Test (Houlsby et al., 2006) and Rigid Caisson p-y Analysis for Static Loading Condition (edited after Houlsby et al., 2006)

11.5 SUMMARY

Pseudo-static lateral load displacement relationships (backbone curves) of suction can in clay are constructed for the first 10 cycles and cycle 100 to 200. The lateral load-displacement relationships from the first 10 cycles of 3-second period are the virgin lateral load-displacement curves or can be refer to the "static" loading curves. If the foundation is subjected to further cyclic loading, the lateral resistance decreases (cyclically degraded) to "cyclic" loading curves. However, the differences in lateral resistance between static and cyclic loading curves are less significant with smaller lateral

displacements (or rotations). The suction can in overconsolidated clay tends to reach its ultimate capacity at a smaller lateral displacement (or rotation) comparing to that in normally consolidated clay. According to the complied experimental lateral load-displacement relationships, the strain rate (loading rate) effects are not significant within the load periods (3, 5, and 10 seconds) used for cyclic lateral load tests in this study.

The plastic limit analysis program FALL16, which was originally developed for more slender suction caissons, is used to estimate the ultimate lateral capacity of the suction can foundation in clay. FALL16 predicts an ultimate lateral capacity that is close to the experimental "static" capacity if the undisturbed undrained shear strength of the soil is used in the analysis. However, it overestimates the "cyclic" lateral resistance by 40% to 50%. If the remolded undrained shear strength of the soil is used for the analysis, FALL16 predicts a lower lateral capacity which underestimates the cyclic lateral resistance by approximately 25% to 30%.

Finite element analyses are conducted to simulate the laterally loaded suction can under undrained condition. If the soil-outer wall interface is allowed to separate and slip, a gap forms on the backside of the foundation which reproduces the gap observed in the experiments. In this case, the lateral load-displacement curve by the finite element model matches well with the experimental "static" response when the undisturbed undrained shear strength of the soil is used while it matches well with the experimental "cyclic" response when the remolded undrained shear strength is used.

An Excel spreadsheet based p-y analysis model is developed for caissons with small aspect ratio. In this model, the caisson is assumed to be rigid with p-y springs provide side resistance and a rotational spring at the center of rotation to simulate the resisting moment from the shear stresses on the spherical slip surface at the end of the caisson. The p-y curves were calibrated using the experimental "static" and "cyclic"

lateral load-displacement response of suction can in clay. The calibrated p-y curves are significantly stiffer and have higher ultimate resistance than the p-y curves recommended by API. The finding that the API p-y curves underestimate the stiffness and ultimate soil resistance is consistent with previous research by Stevens and Audibert (1979) and Jeanjean (2009) for flexible piles. This rigid caisson p-y analysis model can efficiently predicts the lateral load-displacement response of caisson in clay under both static and cyclic loading conditions. This model shows that the end resisting moment, which consists of 30% to 40% of total resisting moment, is an important component of the total lateral resistance of less slender caisson. The rigid caisson p-y analysis model is compared with the results from larger scale field tests. The stiffness predicted by the model is close to the measured stiffness in the field. However, the model overpredicts the moment capacity by 25%. This discrepancy may be attributed to the uncertainty of the undrained shear strength of the clay at the site and also the smaller aspect ratio of 0.5 for the suction caisson used in the field tests. More field and laboratory tests may be required to validate the proposed rigid caisson p-y analysis model.

Chapter 12: Conclusions

Suction can foundation (SCF) model tests using 1-foot diameter and 6-inch diameter scale models with an aspect ratio of one are performed in five different soil profiles: normally consolidated clay, overconsolidated clay, loose siliceous sand, cemented siliceous sand, and cemented calcareous sand. Tests were conducted in order to evaluate the performance of this stubby suction caisson under axial and lateral loads in these five different soil profiles. The test program involves monitoring settlements, lateral displacements (walking), tilt, lateral load and pore water pressures in the suction can during cyclic lateral loading at one, three and five degrees of rotation. The model foundations are also monitored during installation, axial load tests, and pullout tests.

In general, for two-way cyclic lateral load tests, the SCF model in 1 and 2-degree (±0.5 and ±1 degree) rotation tests in all the five soil profiles has no significant walking or settlement after 1000 cycles of load. However, more significant walking or settlement may occur at extreme conditions such as the 5-degree rotation tests. Larger gaps between the foundation wall and the soil may also form in these extreme conditions in overconsolidated clay, cemented siliceous sand, and cemented calcareous sand. The gaps may reduce the lateral resistance of the foundation especially in cemented calcareous sand. The load period (in a range between 3 to 10 seconds) does not have a significant effect on the lateral resistance of the foundation.

Since cyclic lateral loading is one of the most important aspects for the design of rigid foundations with small aspect ratios, more detailed analyses on cyclic loading tests are conducted for the foundation in clay. Plastic limit analysis, finite element analysis, and a finite difference model with translational and rotational springs developed in this research were used to evaluate the laterally loaded suction can in clay.

Conclusions on the performance of suction can in clay test beds (normally consolidated clay and overconsolidated clay) are summarized in Section 12.1 while Section 12.2 presents the conclusions on suction can performance in sand test beds (loose siliceous sand, cemented siliceous sand, and cemented calcareous sand).

12.1 PERFORMANCE OF SUCTION CAN IN CLAYS

The properties of normally consolidated and overconsolidated clay test beds are summarized in Section 12.1.1. The conclusions on installation, performance under cyclic lateral loadings, and ultimate axial capacity of suction can in both clay test beds are presented in Section 12.1.2, 12.1.3, and 12.1.4, respectively.

12.1.1 Properties of Normally Consolidated and Overconsolidated Clay Test Beds

- The undrained shear strength increased linearly with depth in normally consolidated kaolinite test bed. The undrained shear strength at mudline was approximately 0 psf with a gradient of 14 psf/ft measured by a T-bar penetrometer. The measured undrained shear strength gradient decreased to 7 psf/ft after remolding the soil by penetrating and pulling out the T-bar for 6 cycles.
- The overconsolidated kaolinite test bed had a nearly constant undrained shear strength profile. The undrained shear strength was approximately 45 psf measured by a T-bar penetrometer. This undrained shear strength corresponds to a c/p ratio of approximately 4.0 at the mid-depth of the 6-inch suction can. The measured undrained shear strength decreased to 22 psf after remolding the soil by penetrating and pulling out the T-bar for 6 cycles.

12.1.2 Installation of Suction Can in Clays

- The 1-foot diameter SCF model was installed in the normally consolidated clay by penetrating under its own weight. The weight of the suction can was greater than the penetration resistance calculated by the limit analysis method recommend by API RP 2SK (A 2008) with α equal to the inverse of sensitivity and $N_c = 7.5$ for the tip area of the wall. This calculation confirmed that the caisson can be installed by self weight.
- The 6-inch diameter SCF model was installed in the overconsolidated clay by pushing in with dead weights in addition to self-weight. The penetration resistance was consistent with the calculation recommend by API RP 2SK (A 2008) with α equal to the inverse of sensitivity and $N_c = 7.5$ for the tip area of the wall.

12.1.3 Performance of Suction Can under Cyclic Lateral Loadings in Clays

- For the 1000-cycle lateral load tests in normally consolidated clay, walking and settlements of the suction can are not significant (less than 0.01 diameter of the suction can or 0.01 D) with 1-dregree (±0.5 degree) rotation. More significant settlements (up to 0.11 D) may occur with 2-degree (±1 degree) rotation under the weight of the steel model. With 5-degree (±2.5 degrees) rotation, the walking displacement and settlement may go up to 0.17 D and 0.24 D, respectively. After the cyclic lateral tests, a circular zone of disturbed soil on the surface extended to approximately 0.8 diameter out from the suction can. No significant gap formed between the foundation and the soil during the lateral tests except a small gap opened up during 5-degree rotation tests.

- In normally consolidated clay, the cyclic lateral resistance is higher in the first couple cycles because of the effect of setup and, subsequently, the measured lateral load decreases in a couple of cycles due to the soil disturbance. In the tests with larger rotations (2- and 5-degree tests), the lateral resistance increases with the number of loading cycle; this "stiffening" behavior may be attributed to the settlement of the foundation because it penetrates deeper into the soil. The overconsolidation of soil around the wall of the foundation due to cyclic loading may also contribute to this stiffening effect.
- For the 1000-cycle lateral load tests in overconsolidated clay, walking of the suction can in overconsolidated clay is not significant (less than 0.03 diameter of the suction can or 0.03 D) for all the 1-, 2-, and 5-degree rations (±0.5, ±1, and ±2.5 degrees) and all the 2-, 5-, and 10-second loading periods. The settlements of the suction can are not significant (less than 0.02 D). Settlement increases with increasing rotation of the foundation and seems to increase with decreasing loading period. The increase in settlement is more prominent when the rotation increases from 2 degrees to 5 degrees. Fissures and cracks formed in the clay around the suction can after cyclic lateral loadings. The circular zone of disturbed soil on the surface extended to approximately 0.6 diameters out from the foundation. A gap (less than 1/4 inch wide) was opened up around the foundation under cyclic lateral loading and was filled with slurry quickly after few hundred cycles of loading.
- In coverconsolidated clay, the cyclic lateral resistance is relatively stable without significant stiffening or softening effects in most of the tests. However, softening behavior usually occurs within the first 100 cycles in the first tests at the same rotation angle, because the overconsolidated clay is being remolded. If the suction

can is loaded laterally with a pre-existing gap between the wall and soil, the measured lateral resistance is stable from the first cycle throughout the test. If the foundation is loaded without the presence of a gap, the lateral resistance tends to be higher in the first couple of the loading cycles and then drop to approximately the same magnitude as the test conducted with a pre-existing gap.

- For the cyclic lateral load test in both clay test beds, the difference in the measured lateral load for different loading period (3, 5, and 10 seconds) is not significant which indicates that there is little stain rate effect in this range of loading periods.
- During cyclic lateral load tests in both clay test beds, the excess pore water pressure in the soil plug has larger cyclic fluctuations near the tip of the suction can comparing to that under the top plate because it is closer to the failure plane under the suction can. After installation, the excess pore water pressure built up due to the weight of the suction can never fully dissipated during the period of tests (10 days in normally consolidated clay and 25 days in overconsolidated clay).
- Pseudo-static lateral load displacement relationships (backbone curves) of suction can in overconsolidated and normally consolidated clay are constructed by selecting control points for the measured lateral load-placement hysteresis loops of the first 10 cycles and those of cycle 100 to 200.
- The experimental lateral load-displacement relationships (backbone curves) show that, for a given foundation rotation, the first 10 load cycles have higher lateral resistance than subsequent loading cycles. During the first couple of load cycles, it is the first time that the soil around the foundation experienced such displacement. Therefore, the lateral load-displacement relationships from the first

10 cycles of 3-second period are the virgin lateral load-displacement curves or can be refer to the short-term "static" loading curves.

- If the foundation is subjected to further cyclic loading, the lateral resistance decreases (cyclically degraded) to the long-term "cyclic" loading curves. However, the differences in lateral resistance between static and cyclic loading curves are less significant with smaller rotations (or lateral displacements measured at 3 ft above mudline).
- The suction can in overconsolidated clay tends to reach its ultimate capacity at a smaller lateral displacement (or rotation angle) comparing to that in normally consolidated clay. In other words, suction can foundations have more ductile behavior in normally consolidated clay while they have lateral stiffness in overconsolidated clay.
- According to the complied experimental lateral load-displacement relationships, the strain rate (loading rate) effects are not significant within the load periods (3, 5, and 10 seconds) used for cyclic lateral load tests in this study.
- The plastic limit analysis program FALL16, which was originally developed for more slender suction caissons, is used to estimate the ultimate lateral capacity of the suction can foundation in clay. FALL16 predicts an ultimate lateral capacity that is close to the experimental "static" capacity if the undisturbed undrained shear strength of the soil is used in the analysis. However, it overestimates the "cyclic" lateral resistance by 40% to 50%. If the remolded undrained shear strength of the soil is used for the analysis, FALL16 predicts a lower lateral capacity that underestimates the cyclic lateral resistance by approximately 25% to 30%.

- Finite element analyses are conducted by using the commercial package, Abaqus, to simulate the laterally loaded suction can under undrained condition in overconsolidated clay. The overconsolidated clay is modeled as an elastic-perfectly plastic material using Mohr-Coulomb yielding criterion. If the soil-suction can interface is assumed to be a tied interface, the finite element model overestimates the lateral capacity of the suction can. If the soil-outer wall interface is allowed to separate and slip, a gap forms on the backside of the foundation which reproduces the gap observed in the experiments. In this case, the lateral load-displacement curve by the finite element model matches well with the experimental "static" response when the undisturbed undrained shear strength of the soil is used while it matches well with the experimental "cyclic" response when the remolded undrained shear strength is used.
- An Excel spreadsheet based p-y analysis model is developed for caissons with small aspect ratio. In this model, the caisson is assumed to be rigid with p-y springs provide side resistance and a rotational spring at the center of rotation to simulate the resisting moment from the shear stresses on the spherical slip surface at the end of the caisson. Two sets of p-y curves were used along with the elastic-perfectly plastic rotational spring: 1) the curves similar to Matlock's p-y curves and 2) the elastic-perfectly plastic p-y curves. Both cases were calibrated using the experimental "static" and "cyclic" lateral load-displacement response of suction can in clay. The calibrated p-y curves for rigid caisson are significantly stiffer and have higher ultimate resistance than the p-y curves recommended by API. The finding that the API p-y curves underestimate the stiffness and ultimate soil resistance is consistent with previous research by Stevens and Audibert (1979) and Jeanjean (2009) for flexible piles. This rigid caisson p-y analysis

model can efficiently predicts the lateral load-displacement response of caisson in normally conconsolidated and overconsolidated clay under both static and cyclic loading conditions. This model shows that the end resisting moment, which consists of 30% to 40% of total resisting moment, is an important component of the total lateral resistance of less slender caisson.

- The rigid caisson p-y analysis model is compared with the results from larger scale field tests conducted by Houlsby et al. (2005b). The stiffness predicted by the model is close to the measured stiffness in the field. However, the model overpredicts the moment capacity by 25%. This discrepancy may be attributed to the uncertainty of the undrained shear strength of the clay at the site and also the smaller aspect ratio of 0.5 for the suction caisson used in the field tests. More field and laboratory tests may be required to validate the proposed rigid caisson p-y analysis model.

12.1.4 Ultimate Axial Capacity of Suction Can in Clays

- In the normally consolidated clay test bed, the ultimate axial capacity in compression for the 1-foot diameter SCF model is close to the axial capacity calculated by the limit analysis recommended by API with $N_c = 7.2$ for bearing (corrected for embedment by the method suggested by Skempton, 1951) and $\alpha = 0.8$ for side shear. During the pullout test, a peak load was measured at 0.08 diameter of vertical displacement. Negative pore water pressure (suction) was developed inside the suction can which provides a large proportion of pullout resistance in terms of reversed end bearing. A layer of clay (less than 1/4 inch thick) sticks on the wall of the suction can indicate that it was under undrained

loading condition during pullout. The suction can was plugged when it was pulled out, but the soil plug fell off within one minute.

- In overconsolidated clay, there was no clear failure based on the load-displacement curve when the suction can is loaded in compression. Therefore, failure is defined by reaching a displacement of 0.1 diameter of the suction can (0.6 inch). The ultimate axial capacity in compression for the 6-inch diameter SCF model is close to the calculated axial capacity using the method recommended by API with $N_c = 7.2$ (corrected for embedment using the method suggested by Skepmton, 1951) and assuming the presence of a gap ($\alpha = 0$). During the pullout test, a peak load was measured at 0.41 diameter of vertical displacement. Negative pore water pressure (suction) was developed inside the suction can which provides a large proportion of pullout resistance in terms of reverse end bearing. A layer of clay (less than 1/4 inch thick) sticks on the wall of the suction can indicates that it was under undrained loading condition during pullout. The suction can was plugged when it was pulled out, but the soil plug fell off within one minute.

12.2 PERFORMANCE OF SUCTION CAN IN SANDS

The properties of loose siliceous sand, cemented siliceous sand, and cemented calcareous sand test beds are summarized in Section 12.1.1. The conclusions on the performance of suction can under cyclic lateral loadings and under axial loadings in sand test beds are presented in Section 12.1.2 and 12.1.3, respectively.

12.2.1 Properties of Sand Test Beds

- The poorly graded siliceous sand in the loose siliceous sand test bed had a mean grain size of 0.4 mm with an estimated saturated unit weight of 113 pcf. The cone tip resistance at 6 inches deep was between 400 to 1200 psf according to cone penetrometer tests.
- In the cemented siliceous sand, the poorly graded siliceous sand was mixed with 1% type I Portland cement to create the cementation between sand particles. The unconfined compression strength of the cemented sand was around 346 psf. The estimated saturated unit weight of the cemented siliceous sand test bed was 126 pcf. The cone tip resistance at 6 inches deep was approximately 28 ksf at 3.5 to 5.5 inches deep according to 1.05-inch diameter cone penetrometer tests.
- The cemented calcareous sand test bed was prepared by mixing 1% of Type I Portland cement with oyster shell meal. The oyster shell meal had angular particles with a mean grain size of 0.3 mm and 8% of fine particles. The unconfined compression strength of the cemented calcareous sand was between 800 to 1200 psf, which is stronger but more ductile than the cemented calcareous sand used in this study. The cone tip resistance was between 28 to 34 ksf at 3 to 4 inches deep. The saturated unit weight of the cemented calcareous sand was 117 pcf.

12.2.2 Performance of Suction Can under Cyclic Lateral Loadings in Sands

- For all the sand test beds, the 6-inch diameter SCF model was installed by carefully placing the suction can in the test beds while preparing the sand deposits to represent a "wish in place" condition.
- For the 1000-cycle lateral load tests in all of the three sand test beds, walking and settlement of the suction can were not significant (usually less than 0.02 D) for most of the applied 1-, 2-, and 5-degree (±0.5, ±1, and ±2.5) rations and 3-, 5-, and 10-second loading periods. However, the suction can in sands may have more significant settlements or upward movements (up to 0.18 D) with 5-degree rotation. In cemented calcareous sand, occasionally the walking of the foundation can be up to 0.09 D.
- During the lateral tests in loose siliceous sand, it was observed that the sand flowed around the cyclically loaded foundation. This localized liquefaction of the loose sand around the suction can was caused by the increase in pore water pressure during cyclic loading. After cycles of lateral loading, a cone-shape depression formed around the suction can on the surface of the sand deposit. The cone-shape depression extended to approximately 0.5 diameters out from the suction can.
- In the cemented siliceous sand, fissures and cracks around the suction can formed right after cyclic lateral loads were applied to the suction can. The cementation between sand particles near the foundation was broken after cycles of load and turned the cemented sand into loosed sand. Localized liquefaction of the loosed sand around the suction can similar to tests in loose sand was observed. A cone-shape depression also formed in the loosed sand around the suction can. The

cone-shape depression and fissured zone extended to approximately one diameter out from the suction can.

- In cemented calcareous sand, no significant fissures and cracks around the suction can were observed in the first couple of lateral tests because the cemented calcareous sand was more ductile. However, a gap around the suction can opened up after few thousands of accumulated load cycles. After the 5-degree rotation tests, the gap on the side opposite to the mean load was measured at 2 inches wide and 4 inches deep. Unlike the siliceous sand tends to fill the gap around the suction can, the gap in cemented calcareous sand stayed open throughout the tests.
- In all the three sand test beds, the lateral resistance was relatively stable without significant stiffening or softening effects in most of the tests. However, in loose siliceous sand, stiffening behavior was observed in the first lateral load test in this test bed because the loose siliceous sand deposit was densified slightly under the cyclic loading. In cemented siliceous sand and cemented calcareous sand, softening behavior occurs at the beginning of the first test with the same magnitude of rotation because the cementation was being broken in the first couple of cycles. For more extreme loading conduction such as 5-degree rotation tests in sand test beds, stiffening or softening behavior may also occur due to the settlements or upward movements of the suction can which cause the increase and decrease of side resistance of suction can, respectively.
- The lateral resistance of suction can is higher in cemented siliceous sand than in the loose siliceous sand and in clay. In cemented calcareous sand, the suction can had a significant lower lateral resistance because of the presence of the larger gap comparing to tests in siliceous sands. Lateral resistance of the suction can in cemented calcareous sand depends heavily on number of load cycles and

magnitude of displacement that the foundation previously experienced. The lateral resistance decreases with increasing lateral load cycles and increasing size of the gap in the cemented calcareous sand.

- For all the test in the three sand test beds, the difference in the measured lateral load for different loading period (3, 5, and 10 seconds) is not significant which indicates that there is little stain rate effect in this range of loading periods. This observation is consistent with the tests in clays.
- During cyclic lateral load tests in sands, the pressure in the soil plug near the tip of the suction can has a larger range of cyclic fluctuation comparing to that under the top plate; however, the excess pore water pressures are more uniform inside the suction can in sands comparing to the tests in clay. The excess pore water pressures redistribute much more quickly inside the suction can in sands because of its higher permeability. However, the excess pore water pressures inside the suction can in cemented calcareous sand are not as uniform as those in siliceous sands; the excess pore water pressure in the soil plug near the tip of the suction can has a larger range of cyclic fluctuation comparing to that under the top plate. The less uniform excess pore water pressures can be attributed to the higher proportion of fine grain particles and the more tortuous flow path in the oyster shell meal comparing to the more uniform and rounded siliceous sand.

12.2.3 Performance of Suction Can under Axial Loadings in Sands

- Proof load tests were conducted instead of ultimate axial capacity test because the load required to fail the model foundation in sand exceeds the capacity our loading system. In loose siliceous sand, the suction can was loaded up to approximately 85% of its estimated ultimate capacity and then uploaded for two

cycles. A maximum vertical displacement of around 0.06 D was measured under the maximum proof load in the first cycle. No significant excess pore water pressure builds up during the test until the foundation starts to move more significantly when the axial load was close to the maximum proof load. During the pullout test, a peak load of approximately 15% of the axial capacity in compression was measured at 0.08 diameter of vertical displacement. Negative pore water pressure (suction) was developed inside the suction can while the suction was loaded in tension. The suction can was plugged when it was pulled out, but the soil plug fell off within seconds.

- In cemented siliceous sand, a proof load of approximately 15% of its ultimate capacity was applied on the suction can and then uploaded for two cycles. A maximum vertical displacement of around 0.005 diameter of the suction can was measured under the maximum proof load in the first cycle. No significant excess pore water pressure builds up throughout the proof load tests. During the pullout test, a peak load of approximately 5% of the estimated ultimate capacity in compression was measured at 0.08 diameter of vertical displacement. Negative pore water pressure (suction) was developed inside the suction can which provides a large proportion of pullout resistance. The suction can was plugged by the cemented siliceous sand when it was pulled out.
- In cemented siliceous sand, a proof load of less than 15% of its ultimate capacity was applied on the suction can and then uploaded for two cycles. A maximum vertical displacement of around 0.006 D was measured under the 292 lb proof load in the first cycle. No significant excess pore water pressure builds up throughout the proof load test. The pullout test was not conducted for the 6-inch SCF model in cemented calcareous sand because there was essentially no

resistance between the suction can and the soil due to the large gap and degradation of cemented calcareous sand after thousands of cyclic loading.

References

Allersma, H.G.B., Kirstein,A.A.R.B., and Brinkgreve, T.S. (1999). "Centrifuge and Numerical Modeling of Laterally Loaded Suction Piles," Proceedings of the Ninth International Offshore and Polar Engineering Conference, Brest, France, vol.1, pp. 711–717.

API RP 2GEO. (2011). "Geotechnical and Foundation Design Considerations," ANSI/API Recommended Practice 2GEO, First Edition, American Petroleum Institute, April 2011.

API RP 2SK. (A 2008). "Design and Analysis of Stationkeeping Systems for Floating Structures," API Recommended Practice 2SK, Third Edition, American Petroleum Institute, Addendum May 2008.

ASTM D2166 – 06. (2006). "Standard Test Method for Unconfined Compressive Strength of Cohesive Soil," ASTM International.

ASTM D 2573 – 01. (2002). "Standard Test Method for Field Vane Shear Test in Cohesive Soil." ASTM International.

ASTM D 4253 – 00 (Reapproved 2006) "Standard Test Methods for Maximum Index Density and Unit Weight of Soils Using a Vibratory Table," ASTM International.

ASTM D 4254 – 00 (Reapproved 2006) "Standard Test Methods for Minimum Index Density and Unit Weight of Soils and Calculation of Relative Density," ASTM International.

Aubeny, C.P., Han, S.W., and Murff, J.D. (2003a). "Inclined Load Capacity of Suction Caissons," International Journal of Numerical and Analytical Methods in Geomechanics, Vol. 27, No. 14, pp. 1235-1254.

Aubeny, C.P. and Murff, J.D. (2003), "Simplified Limit Solutions for Undrained Capacity of Suction Anchors," Int. Symposium on Deepwater Mooring Systems, Houston, Proc., ASCE, pp. 76-90.

Aubeny, C.P.; Gilbert, R.B.; Lee, C.H.; Lupulescu C.; Murff J.D.; and Yang M. (2008). "Out of Plane Loading of Plate Anchors Analytical and Experimental Modeling." Offshore Technology Reach Center. November 2008.

Aubeny, C.P., Gilbert R.B., Randall, R., Zimmerman, E., McCarthy, K., Chen, C.-H., Drake A., Yeh, P., Chi, C.-M., and Beemer, R. (2011). "The Performance of Drag Embedment Anchors (DEA)," Final Report, Prepared for MMS, Contract Number M09PC00028, MMS Project Number 645, Offshore Technology Research Center Project 32558-A6960.

Audibert, J.M., Morvant, M.N., Won, J.Y., Gilbert, R.P. (2006) “Torpedo Piles – Laboratory and Field Research,” International Society of Offshore and Polar Engineers, San Francisco, June 2006, Paper No. 2006-PCW-03.

Barari, A. and Ibsen, L.B. (2012). “Undrained Response of Bucket Foundations to Moment Loading,” Applied Ocean Research, Vol. 36 (2012), pp. 12-21.

Bransby, M. F. & Yun, G.-J. (2009). “The Undrained Capacity of Skirted Strip Foundations under Combined Loading,” Géotechnique, Vol. 59, No. 2, pp.115–125.

Byrne B.W. and Houlsby G.T. (2004). “Experimental Investigations of the Response of Suction Caissons to Transient Combined Loading,” Journal of Geotechnical and Geoenvironmental Engineering, Vol. 130, No. 3, March 1, 2004.

Byrne B.W. and Houlsby G.T. (2006). “Assessing novel foundation options for offshore wind turbines,” World Maritime Technology Conference, London.

Cao, J.C. (2003). "Centrifuge Modeling and Numerical Analysis of the Behavior of Suction Caissons in Clay," Ph.D. Thesis, Memorial University of Newfoundland, Canada.

Cao, J., Phillips, R., Popescu, R., Audibert, J.M.E., and Al-Khafaji, Z. (2003). “Numerical Analysis of the Behavior of Suction Caissons in Clay,” International Journal of Offshore and Polar Engineering, Vol. 13, No. 2, pp 154-159.

Cassidy, M.J., Randolph, M.F., and B.W. Byrne (2006). “A Plasticity Model Describing Caisson Behaviour in Clay,” Applied Ocean Research, Vol. 28, pp. 345–358.

Clukey, E.C., Aubeny, C., and Murff,J.D. (2004). "Comparison of Analytical and Centrifuge Model Tests for Suction Caissons Subjected to Combined loads," Journal of Offshore Mechanics and Arctic Engineering—Transactions of the ASME126(4),364–367.

Clukey, E.C., and Morrison,M.J. (1995). The Response of Suction Caissons in Normally Consolidated Clays to Cyclic TLP Loading Conditions," Proceedings of the Offshore Technology Conference, Houston, TX, pp.909–915.

Dendani, H., and Colliat, J-L. (2002). “Girassol: Design Analysis and Installation of the Suction Anchors,” Proceedings of the 34th Annual Offshore Technology Conference, Houston, Texas, OTC 14209, May 6-9.

Deng, W., and Carter, J.P. (2002). “A theoretical study of the vertical uplift capacity of suction caissons,” International Journal of Offshore and Polar Engineering, Vol. 12, No. 2, pp. 89-97.

El-Gharbawy, S.L. (1998). “The Pullout Capacity of Suction Caisson Foundations for Tension Leg Platforms,” Ph.D. Dissertation, The University of Texas at Austin.

El-Gharbawy, S., and Olson, R. (1999). “Suction Caisson Foundations in the Gulf of Mexico,” Proceedings of the OTRC '99 Conference, Austin, Texas, April 29-30, pp. 281-295.

El-Sherbiny, R. (2005). “Performance of Suction Caisson Anchors in Normally Consolidated Clay,” Ph.D. Dissertation, The University of Texas at Austin.

Finn, L. and Hegler, R. (2013). “Buoyant Tower Design Innovation: Applying Deepwater Technology to Shallow Water Challenges,” 2013 Offshore Technology Conference, May 06 - 09, 2013, Houston, TX, USA.

Fuglsang, L.D., and Steensen-Bach, J.O. (1991). "Breakout Resistance of Suction Piles in Clay," Proceedings of the International Conference on Centrifuge 1991, Boulder, Colorado, pp.153–159.

Ganjoo, K. (2010). “Experimental Testing of Pure Translation and Rotation Loading of Drag Anchors.” M.S. Thesis, The University of Texas at Austin.

Gilbert, R. B., Morvant, M., and Audibert, J. (2008), “Model Torpedo Pile Tests in Kaolinite Test Beds,” Final Project Report Prepared for the Minerals Management Service.

Gilbert, R. B., Aubeny, C. P., Chen, C.-H., McCarthy, K. B., and Vilkki, J. (2012) “Experimental and Analytical Modeling for Drag Anchors,” Final Report Prepared for ABS Consulting, Project No. ABSC/1514096/DM-06, Offshore Technology Research Center Project 32558-B2930.

GMC, Inc. (2013). http://gmcltd.net/

Horton Wison Deepwater. (2013). http://www.hortonwison.com/

Houlsby, G.T., Ibsen, L. B., and Byrne, B.W. (2005a). “Suction Caissons for Wind Turbines,” Proc International Symposium on Frontiers in Offshore Geotechnics, Perth, Australia, 19-21 September, Taylor and Francis, pp. 75-94.

Houlsby, G.T., Kelly, R.B., Huxtable, J. and Byrne, B.W. (2005b) “Field Trials of Suction Caissons in Clay for Offshore Wind Turbine Foundations”, Géotechnique, Vol. 55, No. 4, May, pp 287-296.

Houlsby, G.T., Kelly, R.B., Huxtable, J. and Byrne, B.W. (2006) “Field Trials of Suction Caissons in Sand for Offshore Wind Turbine Foundations”, Géotechnique, Vol. 56, No. 1, pp. 3–10.

Huang, J., Cao, J., and Audibert, J.M.E. (2003). “Geotechnical Design of Suction Caisson in Clay,” Proceedings of the 13th International Offshore and Polar Engineering Conference, Honolulu, Hawaii, May 25-30, pp. 770-779.

Hung, L. C. and Kim, S. R. (2012). “Evaluation of Vertical and Horizontal Bearing Capacities of Bucket Foundations in Clay,” Ocean Engineering, Vol. 52 (2012) pp. 75–82.

Ibsen, L. B., Liingaard, M., and Nielsen, S. A. (2005). "Bucket Foundation, a Status" Conference Proceedings Copenhagen Offshore Wind 2005, Copenhagen, DK.

Iskander, M. (1995). "An Experimental Facility to Model the Behavior of Steel Pipe Piles in Sand," Ph.D. Dissertation, The University of Texas at Austin.

Iskander, M. (2010). "Behavior of Pipe Piles in Sand—Plugging and Pore-Water Pressure Generation During Installation and Loading," Springer Series in Geomechanics and Geoengineering, Springer-Verlag Berlin Heidelberg.

Jeanjean, P. (2009). "Re-Assessment of P-Y Curves for Soft Clays from Centrifuge Testing and Finite Element Modeling," 2009 Offshore Technology Conference, Houston, Texas, USA.

Kelly, R.B., Houlsby, G.T., and Byrne, B.W. (2006). "A Comparison of Field and Laboratory Tests of Caisson Foundations in Sand and Clay", Géotechnique, Vol. 56, No. 9, pp. 617–626.

Kroncke, M.W. (2009) "Experimental modeling for in-plane and out-of-plane loading of scaled model drag embedment anchors," M.S. Thesis, The University of Texas at Austin.

LeBlanc, C. (2009). "Design of Offshore Wind Turbine Support Structures," Ph.D. Thesis, Aalborg University, Denmark.

Lee, C. H. (2008). "Constructing Test Beds of Clay with a Specified Profile of Undrained Shear Strength versus Depth," M.S. Thesis, The University of Texas at Austin.

Long, M. and Gudjonsson, G.T. (2004). "T-bar testing in Irish soils," Proc. of 2nd Int. Conference on Geotechnical and Geophysical Site Characterization, ISC'2, Porto. Vol. 1.pp719–726. Millpress

Lu, Q., Randolph, M.F., Hu, Y., and Bugarski, I.C. (2004), "A numerical study of cone penetration in clay," Geotechnique, Vol. 54.

Luke, A.M. (2002). "Axial Capacity of Suction Caissons in Normally Consolidated Kaolinite," M.S. Thesis, The University of Texas at Austin.

Luke, A.M., Rauch, A.F., Olson, R.E., and Mecham, E.C. (2005). "Components of Suction Caisson Capacity Measured in Axial Pullout Tests," Ocean Engineering Vol. 32, pp. 878–891.

Lam, N.-S. (2005). "The Theoretical Modelling of Circular Shallow Foundation for Offshore Wind Turbines," Ph.D. Thesis, University of Oxford.

Matlock, Hudson (1970). "Correlations for Design of Laterally Loaded Piles in Soft Clay," Second Annual Offshore Technology Conference, Houston, Texas.

Maniar, D.R. and Tassoulas, J.L. (2002). "Nonlinear Finite Element Simulation of Suction Caissons," Proceedings of the 15th ASCE Engineering Mechanics Conference, Colombia University, New York, June 2-5.

Maniar, D.R., Vasquez, L.F.G., and Tassoulas, J.L. (2003). “Installation and Pullout of Suction Caissons: Finite-element simulation," Proceedings of the 22nd International Conference on Offshore Mechanics and Arctic Engineering, OMAE2003-37501, Cancun, Mexico, June 8-13.

McCarthy, K.B. (2011). “Experimental In-Plane Behavior of a Generic Scale Model Drag Embedment Anchor in Kaolinite Test Beds.” M.S. Thesis, The University of Texas at Austin.

Miller, Jaime. (2009). “Model Torpedo Pile Tests in Reconstituted Normally Consolidated Clay.” M.S. Thesis, The University of Texas at Austin.

Murff, J. D. and Hamilton, J. M. (1993). “P-ultimate for Undrained Analysis of Laterally Loaded Piles.” J. Geotechnical Engineering, ASCE, 119(1), 95-107.

Raines, R.D., and Garnier,J. (2004). Physical Modeling of Suction Piles in Clay," Proceedings of the International Conference on Offshore Mechanics and Arctic Engineering—OMAE, pp.621–631.

Randolph, M. F., and Houlsby, G. T. (1984). "The Limiting Pressure on a Circular Pile Loaded Laterally in Cohesive Soil." Geotechnique, London, England, 34(4), 613-623.

Randolph, M.F., and Puzrin,A.M. (2003). "Upper Bound Limit Analysis of Circular Foundations on Clay under General Loading," Geotechnique53(9),785–796.

Randolph, M.F. (2004). “Characterization of soft sediments for offshore applications,” Proceedings ISC-2 on Geotechnical and Geophysical Site Characterization, pp. 209-232.

Reese, L. C., Cox, W. R., and Koop, F. D. (1975). "Field Testing and Analysis of Laterally Loaded Piles in Stiff Clay," Proceedings of Seventh Annual Offshore Technology Conference, Houston, Texas.

Renzi, R., Maggioni,W., Smith,F. (1991). "A Centrifugal Study on the Behavior of Suction Piles," Proceedings of the International Conference on Centrifuge 1991, Boulder, Colorado, pp.169–176.

Simulia (2012). “Abaqus 6.12 Analysis User’s Manual,” Dassault Systèmes Simulia Corp., Providence, RI, USA.

Skempton, A.W. (1951). “The bearing capacity of clays,” Proceedings, Building Research Congress, London, pp. 180-189.

Sparrevik, P. (2002). "Suction Pile Technology and Installation in deepwaters," Proceedings of the Offshore Technology Conference, Houston, TX, USA, Paper OTC 14241.

Stevens, J.B. and Audibert, J.M.E. (1979) “Re-examination of P-y Curve Formulations,” Proceedings of the Offshore Technology Conference, Houston, TX, USA, Paper #3402.

Stewart, D.P, and M.F. Randolph. (1994). “T-Bar Penetration Testing in Soft Clay,” Journal of Geotechnical Engineering, 1994: 2230-2235.

Sukumaran, B., and McCarron, W. (1999). “Total and Effective Stress Analysis of Suction Caissons for Gulf of Mexico Conditions,” Proceedings of the OTRC '99 Conference, Austin, Texas, April 29-30, Geotechnical Special Publication No. 88, pp. 247-260.

Sukumaran, B., McCarron, W.O., Jeanjean, P., and Abouseeda, H. (1999). “Efficient finite element techniques for limit analysis of suction caissons under lateral loads,” Computers and Geotechnics, Vol. 24, No. 2, pp. 89-107.

Templeton, J.S. III (2002). "The Role of Finite Elements in Suction Foundation Design Analysis," Proceedings of the Offshore Technology Conference, Houston, TX, USA, Paper OTC14235.

Templeton, J.S. III (2012). “Finite Element Analysis in Offshore Geotechnics – A Thirty-Year Retrospective,” 2012 SIMULIA Customer Conference.

Tran, M.N., Randolph, M.F., and Airey, D.W. (2005). "Study of Seepage Flow and Sand Plug Loosening in Installation of Suction Caissons in Sand," International Offshore and Polar Engineering Conference, Seoul, Korea, June 2005, pp. 516–521.

Vanka, S. K. R. (2004). “Laboratory Tests to Estimate Strength Profile of Normally Consolidated Kaolinite,” M.S. Thesis, The University of Texas at Austin.

Vásquez, L. F. G., Maniar, D. R., and Tassoulas, J. L. (2010). “Installation and Axial Pullout of Suction Caissons: Numerical Modeling,” Journal of Geotechnical and Geoenvironmental Engineering, Vol. 136, No. 8, August 1, 2010.

Waston, P.G., and Randolph,M.F. (1997). "Vertical Capacity of Caisson Foundations in calcareous sediments," Proceedings of the Seventh International Offshore and Polar Engineering Conference, Honolulu, USA, pp.784–790.

Watson, P.G., and Randolph, M.F. (1998). “Failure Envelopes for Caisson Foundations in Calcareous Sediments,” Applied Ocean Research, Vol. 20 (1998), pp. 83-94.

Yoon, G.-L., Kim, B.-T., Kim, B.-O., and Han, S.-H. (2003). “Chemical–Mechanical Characteristics of Crushed Oyster-Shell,” Waste Management, Vol. 23, 2003, pp. 825–834.

Zdravkovic, L., Potts,D.M., and Jardine, R.J. (2001). "A Parametric Study of the Pull-out Capacity of Bucket Foundations in Soft Clay," Geotechnique51(1), 55–67.

Zhan, Y.-G., and Liu, F.-C. (2010). "Numerical Analysis of Bearing Capacity of Suction Bucket Foundation for Offshore Wind Turbines," Electronic Journal of Geotechnical Engineering, Volume 15 [2010] Bundle F.

Zhang, J.H., Yan, D., Sun, G.L., and Li,W.X. (2003). Development of a Dynamic Loading Device for Suction Pile in Centrifuge," Proceedings of the BGA International Conference on Foundations: Innovations, Observations, Design and Practice, University of Dundee, Scotland, pp.985–990.

Zhang, J.H., Zhang, L.M., and Lu, X.B., (2007). "Centrifuge Modeling of Suction Bucket Foundations under Ice-sheet Induced Cyclic Lateral Loadings," Ocean Engineering 34 (8–9),1069–1079.

Zhang, J.H., Chen, Z.Y., and Li, F. (2010). "Three Dimensional Limit Analysis of Suction Bucket Foundations," Ocean Engineering 37 (2010), pp.790–799.

Zhu, B., Byrne; B. W., and Houlsby, G. T. (2013). "Long-Term Lateral Cyclic Response of Suction Caisson Foundations in Sand," Journal of Geotechnical and Geoenvironmental Engineering, Vol. 139, No. 1, January 1, 2013.

Vita

Ching-Hsiang Chen was born in Taipei, Taiwan. He earned his bachelor's degree in Civil Engineering from National Cheng Kung University in Taiwan in 2004. In fall 2004, he enrolled in the graduate program in Transportation Engineering at National Taiwan University and graduated with a master's degree in 2006. After 13 months of military service, he worked as a pavement engineer at Integrated Engineering Evaluations, Corp. in Taiwan for 16 months. In August 2009, he entered the Ph.D. program in Geotechnical Engineering at The University of Texas at Austin.

Permanent email: shanechen@utexas.edu

This dissertation was typed by Ching-Hsiang Chen.